https://doi.org/10.15388/vu.thesis.120
https://orcid.org/0000-0001-7606-6493

VILNIUS UNIVERSITY
CENTER FOR PHYSICAL SCIENCES AND TECHNOLOGY

Rokas
SKAISGIRIS

Optimization of donor-acceptor based Thermally Activated Delayed Fluorescence emitters

DOCTORAL DISSERTATION

Natural Sciences,
Physics (N 002)

VILNIUS 2020

This dissertation was written between 2016 and 2020 at Institute of Photonics and Nanotechnology, Vilnius University.
The research was supported by the Research Council of Lithuania: scholarship for academical accomplishments and grant no. S-MIP-17-73 and the European Social Fund project SMART no. 09.3.3-LMT-K-718-01-0026.

Academic supervisor:
Prof. Habil. Dr. Saulius Juršėnas (Vilnius University, Natural Sciences, Physics – N 002)

Dissertation Defense Panel:

Chairman – Prof. Habil. Dr. Gintaras Valušis (Center for Physical Sciences and Technology, Natural sciences, Physics – N 002)

Members:
Prof. Habil. Dr. Vidmantas Gulbinas (Center for Physical Sciences and Technology, Natural sciences, Physics – N 002)
Dr. Tadas Malinauskas (Kaunas University of Technology, Natural Sciences, Chemistry – N 003)
Prof. Dr. Edvinas Orentas (Vilnius University, Natural Sciences, Chemistry – N 003)
Dr. Arvydas Ruseckas (University of St Andrews, Scotland, Natural sciences, Physics – N 002)

The dissertation shall be defended at a public meeting of the Dissertation Defense Panel at 15:00 on 14 December 2020 in Room A101 of the Center for Physical Sciences and Technology.
Address: Saulėtekio av. 3, NFTMC, Room A101, Vilnius, Lithuania.
Tel. +370 5 264 8884; email: office@ftmc.lt.

The text of this dissertation can be accessed at the Vilnius University Library, as well as on the website of Vilnius University: www.vu.lt/naujienos/ivykiu-kalendorius.

https://doi.org/10.15388/vu.thesis.120
https://orcid.org/0000-0001-7606-6493

VILNIAUS UNIVERSITETAS
FIZINIŲ IR TECHNOLOGIJOS MOKSLŲ CENTRAS

Rokas
SKAISGIRIS

Termiškai aktyvuotos uždelstosios fluorescencijos donor–akceptorinių spinduolių optimizavimas

DAKTARO DISERTACIJA

Gamtos mokslai,
Fizika (N 002)

VILNIUS 2020

Disertacija rengta 2016–2020 metais Vilniaus universiteto Fotonikos ir nanotechnologijų institute. Mokslinius tyrimus rėmė Lietuvos mokslo taryba: stipendija už akademinius pasiekimus ir projektas nr. S-MIP-17-73 ir ES SF projektas SMART nr. 09.3.3-LMT-K-718-01-0026.

Mokslinis vadovas:
Prof. Habil. Dr. Saulius Juršėnas (Vilniaus universitetas, gamtos mokslai, fizika – N 002)

Gynimo taryba:

Pirmininkas – prof. habil. dr. Gintaras Valušis (Fizinių ir technologijos mokslų centras, gamtos mokslai, fizika – N 002)

Nariai:
prof. habil. dr. Vidmantas Gulbinas (Fizinių ir technologijos mokslų centras, gamtos mokslai, fizika – N 002)
dr. Tadas Malinauskas (Kauno technologijos universitetas, gamtos mokslai, chemija – N 003)
prof. dr. Edvinas Orentas (Vilniaus universitetas, gamtos mokslai, chemija – N 003)
dr. Arvydas Ruseckas (Šv. Endriu universitetas, Škotija, gamtos mokslai, fizika – N 002)

Disertacija ginama viešame Gynimo tarybos posėdyje 2020 m. gruodžio mėn. 14 d. 15:00 val. Nacionalinio fizinių ir technologijos mokslų centro A101 auditorijoje. Adresas: Saulėtekio al. 3, NFTMC, A101 aud., Vilnius, Lietuva.
Tel. +370 5 264 8884; el. paštas: office@ftmc.lt.

Disertaciją galima peržiūrėti Vilniaus universiteto bibliotekoje ir VU interneto svetainėje adresu: www.vu.lt/naujienos/ivykiu-kalendorius.

ACKNOWLEDGEMENTS

First of all, I want to thank my supervisor prof. Saulius Juršėnas for optimism and ability to easily refresh my motivation to pursue career in science. I am also very thankful to dr. Tomas Serevičius for introduction to TADF world and time-resolved spectroscopy, heads-up notifications on new scientific material and brilliant ideas and writing capabilities.

I am very happy to have such great colleagues at Institute of Photonics and Nanotechnology and especially my roommates at cabinet B 201. Thanks Justina Jovaišaitė for maintaining strict order in the lab, dr. Regimantas Komskis for philosophical conversations and dr. Gediminas Kreiza for balancing professionalism with sophisticated sense of humor.

I also wish to thank my partners Agnė, Andrius, Dovydas, Egidijus, Justinas and Simas from PLLC "Tradiciniai Gurmanai" for hard, yet productive work and maintaining professionalism and keeping traditions alive. I apologize I was unable to attend all extracurricular activities and the production yield dropped significantly, recently. With deepened knowledge and improved equipment we will soon be achieving better quality and quantity.

I am grateful to have had an opportunity to spend my summers and write this thesis in my grandparents house in Andrioniškis. I thank all my friends from there for the unforgettable memories. Furthermore, wild nature, fresh air and adorable pets proved to be a great inspiration for writing.

Exclusive gratitude goes to my lovely wife Kristina, who felt the implications of writing this thesis the most, but remained kind and supportive throughout it. Sorry for sometimes being grumpy and not spending enough time with you, I will definitely make up for that now.

Moreover, I would like to thank my sisters Eglė and Beata with their crazy little kids Rusnė, Dominic, Vėjas and Anna who can always brighten up the mood by sharing their wacky adventures.

Galiausiai, šią disertaciją skiriu savo tėvams Deimantui ir Ilonai. Ačiū, kad užauginote, rodėte pavyzdį, visada suteikėte laisvę rinktis ir palaikėte net ir netikėčiausiose situacijose. Taip pat siunčiu linkėjimus savo šauniai močiutei Bernadetai!

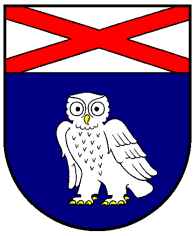

CONTENTS

LIST OF ABBREVIATIONS

A	Acceptor
Cbz	Carbazole
CCD	Charge coupled device
CT	Charge Transfer
D	Donor
DF	Delayed fluorescence
DFT	Density functional theory
DSC	Differential scanning calorimetry
ΔE_{ST}	Singlet-triplet energy gap
EQE	External quantum efficiency
Φ_{F}	Internal fluorescence quantum yield
FL	Fluorescence
FWHM	Full width at half maximum
HOMO	Highest occupied molecular orbital
IC	Internal conversion
ICT	Intramolecular charge transfer
ISC	Inter-system crossing
ITO	Indium tin oxide
^{1}LE	Singlet locally excited state
^{3}LE	Triplet locally excited state
LUMO	Lowest unoccupied molecular orbital
Nd:YAG	Neodymium doped yttrium aluminum garnet
NIR	Near-infrared
NMR	Nuclear Magnetic Resonance
$-O_2$	Oxygen deficient environment
$+O_2$	Oxygen saturated environment
OLED	Organic light emitting diode
PF	Prompt fluorescence
PH	Phosphorescence
PMMA	Poly(methyl methacrylate)
PTZ	Phenothiazine
PXA	Phenoxazine
PYR	Pyrimidine
rISC	Reverse inter-system crossing
RTP	Room temperature phosphorescence
SOC	Spin-orbit coupling
TADF	Thermally Assisted Delayed Fluorescence
TGA	Thermogravimetric analysis
TIFL	Time-integrated fluorescence
TRFL	Time-resolved fluorescence
UV	Ultraviolet

INTRODUCTION

While a direct link of computer to the brain is desired and is slowly developed [1–3], today it remains more a of a science fiction than reality. Meanwhile our gateway to the internet and interaction with technology are screens. Never before have humanity spent so much time staring at the different kind of screens whether it is used for work, relaxation, access to news and information or as a mean of communication. The things got even more escalated in the face of global pandemic this year, when social distancing became the only countermeasure against deadly virus and the screen became our only window for social interactions.

Naturally high demands are raised for screens as they are used everyday: high resolution, pure colors, high contrast and luminance, all served in compact and flexible package. Moreover, the exhausted hardware advances in smartphone market and a large number of brands together high technological cravings of consumers puts a fierce rivalry among the manufacturers as they try to seduce us with an unprecedented new features and designs . If we analyze the latest breakthrough advances of smartphones, one important thing can be noted. High contrast and definition displays with "true black" color, foldable phones, on-screen fingerprint detector, behind the screen front camera, curved displays have one thing in common – they were made possible by organic light emitting diode (OLED). The TV and monitor producers are also exploiting OLEDs as new unseen technologies emerges: wallpaper TV's, which are glued directly to the wall, a projector like rollabale TV's and even transparent TV are soon to be commercially available on consumer level. The OLED monitors, meanwhile, offer extremely fast response times with impressive color gamut. The OLED market is expected to reach $33 billion by the end of 2020 and is rapidly catching up with LCD technology in smartphone and TV categories, where the advantages of OLED shine out the most.

The organic compounds have been here for billions of years and are the main building material of nature, yet only recently they ventured into man made products. Organic materials combines electrical properties of semiconductors with chemical and mechanical advantages of organic matter such as plastic, therefore for the last century they were extensively researched [4–6]. The endless selection of compounds exhibits various interesting properties, one of them is electroluminescence – emission of light caused by passing electric current. While the first observations of blue electroluminescence from anthracene crystals was reported as early as 1963 [7], the first organic device was introduced by Tang and van Slyke in 1987 [8] followed by extensive studies and a successful commercialization in the next decade as backlight in LCD screens [9, 10]. The initial (1^{st} generation) devices were based on radiative singlet decay to

ground sate, called fluorescence (Figure: 1). However due to spin statistics electrically injected charge carriers yield 25 % singlet and 75 % non-emissive triplet states [11]. Combined with unenhanced out-coupling efficiency this lead to devices with external quantum efficiencies (EQE) comparable to those of halogen light bulb (under 5 %).

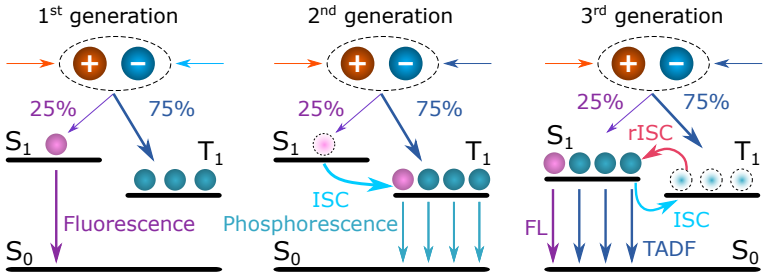

Figure 1: Principle schemes of different generations of OLED devices.

A widely-used approach to overcome this limitation was presented with the 2nd generation phosphorescence emitters (Figure 1). The emission of these devices originates from the triplet state while the singlet excitons are converted to triplets via efficient intersystem crossing (ISC). A heavy-atom is introduced into the organic compounds which mixes the singlet and triplet states due to enhanced spin-orbit coupling (SOC), enabling triplet emission and boosting ISC [11,12]. The triplet harvesting enabled internal quantum efficiencies (IQE) of unity leading to devices with EQE of 20–30 % without additional outcoupling techniques. While second generation OLEDs are successfully deployed, they suffer from poor stability, especially in the blue emission region [13]. Moreover expensive metals like iridium and platinum are typically used to induce the heavy-atom effect which also raises concerns for environmental effects. Thus an all organic approach is desirable.

In 2012 Adachi *et al.* utilised E-type delayed emission, firstly observed by Parker *et al.* [14], to harvest the "dark" triplet states in efficient emitters without the use of heavy metals and named it thermally activated delayed fluorescence (TADF), introducing the 3rd generation of organic emitters [15–17]. Here the molecular compounds are designed to have small (usually less than about 200 meV) energy gap between lowest singlet and lowest triplet states ΔE_{ST}, so that reverse intersystem crossing (rISC) can be initiated by ambient thermal energy. All of TADF triplet states can be harvested by efficient rISC producing IQE values of up to 100 % [18,19].

The TADF emitters offer the same high performance as commercially available phosphorescence emitters in a more elegant, all organic, package. Yet only now we are witnessing the dawn of TADF commercialization era from companies like Kyulux and Cynora. However, unsolved problems such as low external quantum efficiency (EQE) of deep-blue emitters, high efficiency roll-

off at higher luminance values and fast degradation of devices still plagues the TADF emitters, slowing down their applicability.

Aim and novelty

While TADF emitters are one of the heavily researched branch of organic semiconductors some effects like conformational disorder impact on emission properties remain rather unexplored. Moreover, the design strategies of third generation emitters are not, yet, clear enough as the science behind the conditions for efficient TADF and required molecular structure is still at its young age. The aim of this work was to explore how molecular modifications impact TADF properties of donor–acceptor compounds and suggest optimization pathways to improve TADF properties, especially in the blue region of emission.

To achieve this aim several tasks were set:

- Utilize time-resolved spectra measurements to perform in-depth analysis of thermally assisted delayed fluorescence in differently modified compounds containing pyrimidine acceptor and carbazole, phenothiazine or phenoxazine donor moieties.
- Investigate solid-state TADF emission and decay transients of molecules possessing different core rigidity, yet similar photophysical properties in dilute solutions, to assess effects of conformational disorder.
- Reveal the origin of fast dual delayed fluorescence in compounds were donor and acceptor moieties are bound by non-conjugated σ-bridge and evaluate their performance as TADF emitters.
- Assess how small modifications of phenyl-pyrimidine acceptor core with methyl groups or linking pattern of carbazole donor units affect TADF emission properties and decay lifetimes.
- Prepare OLED devices with optimized donor-acceptor compounds as TADF emitters and evaluate their electroluminance properties together with external quantum efficiencies.

Statements to be defended

1. Some of the undesirable solid-state conformational disorder effects in donor-acceptor TADF compounds can be prevented by designing a rigid molecular core or accelerating reverse intersystem crossing rate.
2. TADF donor–acceptor molecules with hyperconjugated spacer (D–σ–A) should be designed with great care as weak coupling between donor and acceptor results in extremely low radiative decay rate which can hardly compete with various non-radiative decay pathways.

3. High emission yield in carbazole–pyrimidine TADF compounds can be achieved by selective optimization of linking pattern of donor units and enhancing prompt fluorescence yield rather than delocalizing the π–electron system.

4. Phenoxazine–pyrimidine D–A–D molecular structure shows remarkable submicrosecond TADF decay time-constant in solid-state, achieved by selective structural modifications by methyl units, minimizing the singlet-triplet energy gaps.

Layout of the dissertation

The dissertation is presented as a collection of articles with chapters 1–3 summarizing the findings in papers [**A1**–**A6**]. The papers are numbered in chronological order of their publish date.

In the first chapter based on papers [**A1, A3**] the effects of conformational disorder in solid-state are explored in several TADF compounds exhibiting similar emissions, but possessing different molecular structure. In the second chapter, based on [**A2**] the in–depth property analysis of donor–acceptor compounds joined by hyperconjugated σ bridge is presented. Here several donor units were bound to triazine acceptor fragment by hexafluoroisopropylidene spacer unit. Though initial investigation of the compounds suggested extremely fast TADF lifetime, the time-resolved analysis revealed interplay of intra-/intermolecular charge transfer states with exceptionally long prompt fluorescence. In the final chapter based on articles [**A4, A5, A6**] different molecule structure optimization strategies are employed on compounds possessing pyrimidine acceptor and carbazole or phenoxazine donor moietes, to create efficiently performing OLEDs. Devices exhibiting relatively efficient deep-blue, very efficient blue and extremely efficient green electroluminescence are presented. Also TADF decay lifetime of 860 ns was achieved which is amongst the lowest values reported for TADF emitters.

Contribution of the author

The author performed all photophysical characterization, steady-state and time-resolved spectroscopy experiments, processed and analysed the obtained data. The author also contributed to preparation and participated in discussions of all manuscripts.

The synthesis of most of the molecules presented in this work were carried out by organic chemistry group led by prof. Sigitas Tumkevičius (Vilnius University). Other compounds were synthesized by prof. Vytautas Getautis group (Kaunas University of Technology) and OPERA group led by prof. Chihaya Adachi (Kyushu University, Japan). DFT modeling was performed by dr.

Tomas Serevičius (Vilnius University) and dr. Alytis Gruodis (Vilnius University). DSC measurements and analysis was carried out by dr. Regimantas Komskis (Vilnius University). All OLED devices were prepared and analysed by Dovydas Banevičius (Vilnius University). The author is honored to work alongside these great people and thanks them for contributing to this work!

LIST OF PUBLICATIONS

On the dissertation topic

[A1] T. Serevičius, **R. Skaisgiris**, J. Dodonova, L. Jagintavičius, J. Bucevičius, K. Kazlauskas, S. Juršėnas, S.Tumkevičius, Emission wavelength dependence on the rISC rate in TADF compounds with large conformational disorder, Chem. Comm. **55**(13), 1975–1978 (2019).

[A2] **R. Skaisgiris**, T. Serevičius, K. Kazlauskas, Y. Geng, C. Adachi, S. Juršėnas, Origin of dual emission in σ-bridged donor–acceptor TADF compounds, J. Mater. Chem. C. **7**(40), 12601–12609 (2019).

[A3] T. Serevičius, **R. Skaisgiris**, J. Dodonova, K. Kazlauskas, S. Juršėnas, S. Tumkevičius, Minimization of solid-state conformational disorder in donor–acceptor TADF compounds, Phys. Chem. Chem. Phys. **22**(1), 265–272 (2020).

[A4] T. Serevičius, **R. Skaisgiris**, J. Dodonova, L. Jagintavičius, D. Banevičius, K. Kazlauskas, S. Tumkevičius, S. Juršėnas, Achieving Submicrosecond Thermally Activated Delayed Fluorescence Lifetime and Highly Efficient Electroluminescence by Fine-Tuning of the Phenoxazine-Pyrimidine Structure, ACS Appl. Mater. Interfaces **12**(9), 10727–10736 (2020).

[A5] T. Serevičius, **R. Skaisgiris**, I. Fiodorova, V. Steckis, J. Dodonova, D. Banevičius, K. Kazlauskas, S. Juršėnas S. Tumkevičius, Achieving efficient deep-blue TADF in carbazole-pyrimidine compounds, Org. Electon. **82**, 105723 (2020).

[A6] T. Serevičius, J. Dodonova, **R. Skaisgiris**, D. Banevičius, K. Kazlauskas, S. Juršėnas and S. Tumkevičius, Optimization of the carbazole–pyrimidine linking pattern for achieving efficient TADF, J. Mater. Chem. C **8**(32), 11192–11200 (2020).

Conference presentations

[C1] **R. Skaisgiris**, T. Serevičius, J. Dodonova, L. Jagintavičius, J. Bucevičius, K. Kazlauskas, S. Juršėnas, S. Tumkevičius. The impact of conformational disorder on the stability of tadf wavelength, Optical Probes 2019, Vilnius, 2019.

[C2] I. Fiodorova, **R. Skaisgiris**, V. Steckis, J. Dodonova, T. Serevičius, S. Juršėnas, S. Tumkevičius. Synthesis and photophysical properties of pyrimidine-carbazole based fluorophores, Open Readings 2019, Vilnius, 2019.

[C3] **R. Skaisgiris**, A. Miasojedovas, A. Gruodis, D. Gudeika, J. V. Gražulevičius, S. Juršėnas. Organic colorimetric sensors for biological applications based on dimethylaminobenzene moiety, Open Readings 2017, Vilnius, 2017.

BRIEF INTRODUCTION OF TADF

This chapter will introduce the reader to the basics of thermally activated delayed fluorescence, needed to comprehend this thesis.

Harvesting "dark" triplet states

Several approaches for upconverting non-emissive triplet states to emissive singlet states are known: TADF, hot exciton and triplet-triplet annihilation (TTA) (Figure 2). In case of hot exciton process, the excitons are converted in high-lying (called hot) triplet states (T_n) whose energy is close to high-lying singlet state (S_n). The rISC should be fast enough to compete with internal conversion to lower-lying triplet states [20–22]. While IQE of 100 % is theoretically possible, efficient devices realizing hot exciton triplet extraction are yet to be demonstrated. Meanwhile, TTA method involves a collision between two triplet excitons. In the process one of the excitons annihilates surrendering its energy to upconvert the other exciton into a higher lying state. However, as one exciton is lost for every singlet generated, the maximum internal efficiency is limited to $25\,\% + 75\,\%/2 = 62.5\,\%$ [23–25].

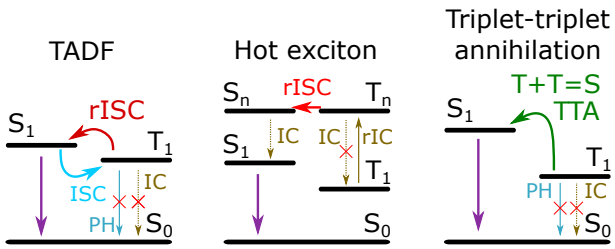

Figure 2: Multiple ways of harvesting "dark" triplet states.

Thermally Activated Delayed Fluorescence

The TADF, on the other hand, can achieve 100 % internal quantum efficiency (IQE), however small energy difference between lowest lying singlet (S_1) and lowest lying triplet (T_1) states (ΔE_{ST}) are required, together with minimized radiative and non-radiative pathways of triplet state relaxation. The TADF is deemed as the most promising mechanism therefore this work focuses on it. Like the name suggest TADF, is a temperature sensitive process, as the thermal energy is needed to overcome the ΔE_{ST} barrier, and its main parameter – reverse intersystem crossing rate (k_{rISC}) can be expressed in a Boltzmann distribution relation:

$$k_{\mathrm{rISC}} = A \exp\left\{-\frac{\Delta E_{\mathrm{ST}}}{kT}\right\}. \tag{1}$$

It appears that to achieve efficient reverse intersystem crossing the energy gap between S_1 and T_1 should not exceed room temperature energy ($kT \approx 25\,\mathrm{meV}$) by much (usually $\Delta E_{\mathrm{ST}} < 200\,\mathrm{meV}$). The lowest singlet and triplet states energies can be expressed by orbital energy (E_{orb}), Coulomb repulsion energy (K) and exchange energy (J) of two unpaired electrons lying in highest occupied molecular orbital (HOMO) and lowest unoccupied molecular orbital (LUMO) as defined by formulas (2) and (3) [26, 27]:

$$E_{\mathrm{S1}} = E_{\mathrm{orb}} + K + J, \tag{2}$$

$$E_{\mathrm{T1}} = E_{\mathrm{orb}} + K - J. \tag{3}$$

As the singlet and triplet states have the same electron arrangement the energies E_{orb}, K and J remain the same for both states. However the exchange energy decreases the energy of triplet state as both unpaired electrons have the same spin while increasing it for singlet state with opposite spin electrons. Therefore the triplet state is always of lower energy than the singlet and the difference is defined by double exchange energy (4):

$$\Delta E_{\mathrm{ST}} = E_{\mathrm{S1}} - E_{\mathrm{T1}} = 2J. \tag{4}$$

The exchange energy can be evaluated by equation (5), where the ϕ and ψ represents the HOMO and LUMO wavefunctions, respectively, e is electron charge and r_1, r_2 denotes to electron coordinates:

$$J = \iint \phi(r_1)\psi(r_2)\left(\frac{e^2}{r_1 - r_2}\right)\phi(r_2)\psi(r_1)\,\mathrm{d}r_1\,\mathrm{d}r_2\,, \tag{5}$$

Apparently the exchange energy (in conjunction with ΔE_{ST}) depends inversely on the HOMO–LUMO orbital coupling therefore small overlap of the orbitals is required to minimize singlet–triplet energy band gap and subsequently increase k_{rISC}. However, the oscillator strength (f), which is dimensionless property that defines the probability of absorption and emission of the photon, depends directly on the same HOMO–LUMO overlap. Therefore high orbital overlap of HOMO–LUMO will result in efficient fluorescence emission but will prohibit rISC of triplet states due to high ΔE_{ST}. On the other hand minimized coupling of HOMO–LUMO will effectively promote excitations from triplet states to singlet states, however the emission will be suppressed by inefficient radiative decay (k_{r}) and the excitation will be quenched non-radioactively after several ISC-rISC cycles. It is important to highlight, that in order to achieve efficient TADF emission the HOMO–LUMO overlap must be tuned to balance

the contradicting k_{rISC} and k_{r} rates. While other approaches like multiple resonance effect can be employed to minimize the overlap [28, 29], the spatial separation in donor(D) – acceptor(A) compounds is usually favored. Here the overlap of HOMO and LUMO orbitals is reduced by sterically hindered spiro structures [30–32] or separation of the D and A fragments with large, twisted spacers [33–35].

While rISC values of efficient TADF compounds usually range in 10^5–$10^6\,\mathrm{s}^{-1}$, the breakthrough the 7^{th} order of magnitude $k_{\mathrm{rISC}} > 10^7\,\mathrm{s}^{-1}$ was recently reported [36, 37].

TADF emission from exciplex

Another approach to minimizing the ΔE_{ST} can be achieved by utilizing exciplex emitters [15, 38, 39]. An exciplex is a bimolecular complex which can be formed by spatially close excited and ground state molecules. A low energy gap is easily realized due to the intermolecular nature of charge transfer in exciplexes as the exchange energy is inversely dependant on the distance between HOMO and LUMO orbitals (5). This allowed to design highly efficient exciplex emitters with EQE of up to 20 % [40, 41]. However, the TADF properties and efficiency are strongly dependant on the distance between the donor and acceptor fragments [42–44]. In dilute solutions the formation of exciplex is completely diffusion driven and is susceptible to viscosity and concentration variations, while in solid-state the D and A are locked in uncontrollable geometries and are sensitive to doping concentrations. The shortcomings of exciplex design can be dealt with in a controlled manner by bounding D and A fragments with conjugated [45] or non-conjugated [46, 47] spacer in close proximity of several Å. High efficiencies up to EQE = 18 % were reported for such geometries [48].

Understanding TADF mechanism

Initially the minimization of ΔE_{ST} was the main aspiration in designing efficient TADF emitters, as the equation (1) suggested it is a direct way of increasing rISC. It was assumed that rISC happened from lowest triplet charge transfer state ^{3}CT to lowest singlet charge transfer state ^{1}CT. However that is strictly forbidden, because spin-orbit (SOC) operator acts on both angular momentum and spin, consequently any change to spin must be followed by a change in angular momentum [49, 50]. Therefore the SOC is basically zero between two states with same spatial orbitals and different spins. The direct transition from ^{3}CT to ^{1}CT can still be mediated by hyperfine coupling when the the energy-gap between them is low (less than 1 meV) [51], however it accounts only for a minuscule amount of k_{rISC} and can be neglected [52]. Observations of molecules with similar ΔE_{ST} values and vastly different k_{rISC}

in different environment suggested that singlet and triplet states are of different character [53, 54], most probably charge transfer ^{1}CT and locally excited ^{3}LE. Moreover Ward *et al.* [55] showed that by sterically hindering the molecular core of D–A, the emission can be switched from TADF to RTP.

A novel model backed by experimental [56] and quantum dynamic [52,57,58] studies proposed that the rISC from ^{3}CT to ^{1}CT is a second order process (equation (6)) mediated by vibronic coupling of ^{3}CT to ^{3}LE and SOC of ^{3}LE to ^{1}CT state:

$$k_{\mathrm{rISC}} = \frac{2\pi}{\hbar} \left| \frac{\left\langle {}^1\Psi_{\mathrm{CT}} \middle| \hat{H}_{\mathrm{SOC}} \middle| {}^3\Psi_{\mathrm{LE}} \right\rangle \left\langle {}^3\Psi_{\mathrm{LE}} \middle| \hat{H}_{\mathrm{vib}} \middle| {}^3\Psi_{\mathrm{CT}} \right\rangle}{\delta\left({}^3E_{\mathrm{LE}} - {}^3E_{\mathrm{CT}}\right)} \right|^2 \delta\left({}^3E_{\mathrm{LE}} - {}^1E_{\mathrm{CT}}\right), \quad (6)$$

here the $\hbar$ is Planck's constant; $^1\Psi_{\mathrm{CT}}$, $^3\Psi_{\mathrm{LE}}$, $^3\Psi_{\mathrm{CT}}$ are charge transfer singlet, locally excited triplet and charge transfer triplet wavefunctions respectively; $\hat{H}_{\mathrm{SOC}}$ and $\hat{H}_{\mathrm{vib}}$ are spin-orbit and vibronic coupling Hamiltonians; $\delta\left({}^3E_{\mathrm{LE}} - {}^1E_{\mathrm{CT}}\right)$ and $\delta\left({}^3E_{\mathrm{LE}} - {}^3E_{\mathrm{CT}}\right)$ are Kronecker deltas of the two equations. Therefore both energy gaps between ^{3}CT-^{3}LE and ^{3}LE-^{1}CT play a crucial role in TADF efficiency and some lability of D–A compound is needed to facilitate vibronic coupling of ^{3}CT and ^{3}LE states [52, 57, 59–61].

The transition from ^{3}CT to ^{1}CT state is a two step process. Initially a large vibronic coupling between ^{3}LE and ^{3}CT is necessary to form an equilibrium between two states on a scale much faster than rISC (reverse internal conversion rate $k_{\mathrm{rIC}} \gg k_{\mathrm{rISC}}$). Then a the ^{3}CT is mediated to ^{1}CT via ^{3}LE in a very efficient way as ^{3}CT and ^{1}CT have good overlap and therefore strong vibronic coupling. A simplified representation of full Hamiltonian model is represented in Figure 3.

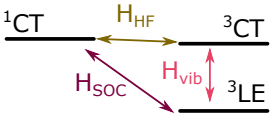

Figure 3: Simplified representation of full Hamiltonian model. The hyperfine coupling (H_{HF}) between ^{1}CT and ^{3}CT states is active when the energy gap between them is very small [51]. Vibronic coupling (H_{vib}) between ^{3}CT and ^{3}LE is crucial to enable rISC via spin-orbit coupling (H_{SOC}) from ^{3}LE to ^{1}CT. Adapted from [59].

Three TADF types can now be discerned (Figure 4): 1) the one discussed above - lowest triplet state is locally excited ^{3}LE therefore a first step of populating ^{3}CT is required through rIC and then a second order coupling is realized through the initial ^{3}LE state; 2) ^{3}LE and ^{3}CT are degenerate and 3) where ^{3}CT is initially populated. For the last two types efficient rISC can proceed through second order coupling without first step [52].

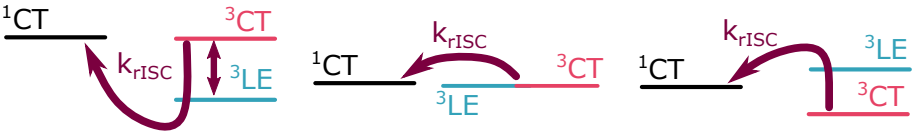

Figure 4: Three types of TADF mechanisms. Adapted from [52].

Conformational disorder of TADF emitters in solid-state

With availability of time-resolved spectroscopy a strange phenomena was noted: the emission in solid-state was initially redshifted and then subsequently blueshifted in the later times producing broadened emission spectra, while the emission of the same D–A TADF compounds in diluted solutions was stable [62–66]. What is more, the decay transients in solid-state were elongated with multiexponential profile prohibiting from approximating the decay lifetime (Figure 5).

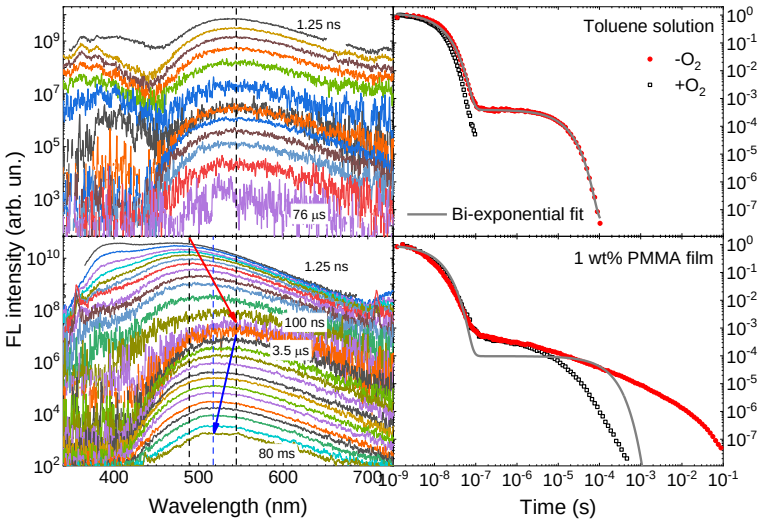

Figure 5: Conformational disorder effects on TADF time-resolved spectra and transient decay in solid-state. The red and blue arrows denote to initial redshift of prompt emission and later blueshift of delayed emission, respectively. The grey solid line in decay transients is bi-exponential fit of the data.

Méhes *et al.* proposed the origin of such gradual shifts is mediated by slowly shifting CT states of singlet and triplet due to dipole interactions between guest an hosts [65]. Another explanation, presented in more detail below, by Northey *et al.* suggested the conformational disorder in solid state as the origin of the shifts [67, 68].

In order to achieve efficient rISC, separation of HOMO–LUMO orbitals is important according to equation (5), which is easily achievable by bounding

donor and acceptor units in orthogonal geometry. However some rotational flexibility is needed to facilitate vibronic coupling between ^{3}CT and ^{3}LE states (6). In dilute solutions the molecules are free to rotate therefore they can relax to geometry with lowest energy. When embedded in solid-state matrix, on the other hand, the molecule rotations are impeded by rigid surrounding and they are frozen at different geometries with dispersion of D–A angles.

The molecules with the most planar structure show largest HOMO–LUMO overlap. This increases the energy of lowest singlet state (S_1) in the process producing bluest LE type emission due to largest bandgap, also ensuring fastest k_r due to enhanced oscillator strength (Figure 6 leftmost case). The ΔE_ST however, will be large due to large exchange energy J. On the other hand the molecules with near orthogonal twist angles, having negligible HOMO–LUMO overlap, will have their S_1 band stabilized at lower energies with negligible f due to the CT nature of $S_0 \rightarrow S_1$ transition (Figure 6 rightmost case). Such conformers will have efficient rISC due to small ΔE_ST gap, yet small k_r value. In solid-state films, we will have a dispersion of conformers with different D–A angles, therefore different k_r and k_rISC rates somewhere in between these two extreme conditions (Figure 6 case in the center).

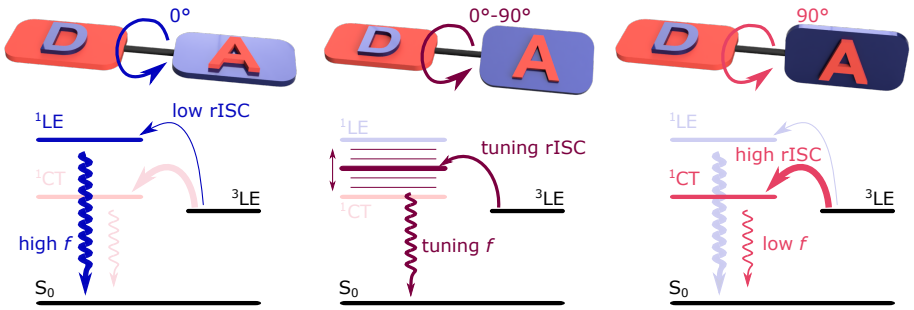

Figure 6: The influence of different diheadral angles between donor and acceptor units on rISC rate and oscillator strength.

Just after the excitation the most planar conformers with fastest radiative decay and bluest emission will emit first, followed by conformers with progressively larger twist angles and therefore redshifted emission. The last of prompt fluorescence will be radiated by most orthogonal conformers. On the other hand, the delayed emission will be promoted by minimized ΔE_ST gap of the most twisted conformers producing the initial delayed emission at the long-wavelength end of the spectra. The TADF emission will then be blueshifted as the conformers with larger ΔE_ST undergo rISC. The sum of dispersed k_r and k_TADF rates will produce multiexponential decay transients.

EXPERIMENTAL DETAILS

This chapter describes the measurement equipment and methods used to characterise researched compounds in this work.

Quantum chemical simulations

Quantum chemical simulations were used to assess structural and electronic properties of molecules before financially demanding and labour intensive synthesis of compounds were initiated. The calculations were performed by using density functional theory (DFT) as implemented in the Gaussian 09 software package at the B3LYP/6-31G(d) level [69]. Polarizable Continuum Model (PCM) was used to estimate the solvation behaviour of toluene surrounding in geometry optimization. Tomas Serevičius was the mastermind behind simulations used in this work.

Synthesis of compounds

The synthesis of researched molecules in papers **[A1, A3, A4, A5, A6]** were performed by organic chemistry group led by prof. Sigitas Tumkevičius at Vilnius University. The synthetic details and molecular characterizations are presented in corresponding papers and their supporting information. The compound **4CzPN** in **[A3]** was synthesized by prof. Vytautas Getautis group at Kaunas University of Technology according to Uoyama *et al.* [16]. The donor-σ-acceptor molecules researched in **[A2]** were synthesized at Center for Organic Photonics and Electronics Research (OPERA) group led by Chihaya Adachi at Kyushu University and are detailed in work by Geng *et al.* [70].

Preparation of dissolved samples

All measurements in solutions were performed after dissolving compounds in spectroscopic toluene (Sigma-Aldrich) solvent at concentration 10^{-5} M, unless stated otherwise. Toluene solvent was chosen due to its similar polarity to popular TADF hosts as CT emission is strongly dependant on media polarity. All researched molecules displayed relatively good solubility in toluene. A low concentration of 10^{-5} M was chosen to avoid molecule to molecule interactions, contrary a larger concentration of 10^{-4} M was used in paper **[A2]** to observe concentration induced effects in solutions. Measurements were taken in both oxygen sutured and oxygen deficient environments in quartz cuvettes. Oxygen removal was achieved by 5 repetitive freeze-pump-thaw cycles using cuvette with attached Schlenk type valve.

Preparation of solid–state samples

To restrict molecular liability of the compounds, the samples were impeded in poly(methylmethacrylate) (PMMA) films. Usually a low doping concentration of 1 % was used in order to observe single molecule emission properties, while a variety of doping concentrations (1–100 %) were used in article **[A2]** to investigate effects of molecular aggregation. In OLED devices the emissive layer is usually constructed of emitter molecules (guest) incorporated into host material, to reduce molecular aggregation induced quenching [71, 72]. Photophysical evaluation of samples in different host materials were performed in this work, generally a commercially available hosts: DPEPO (Bis[2-(diphenylphosphino)phenyl]ether oxide), CBP (4,4'-Bis(N-carbazolyl)-1,1'-biphenyl), mCP (1,3-Bis(N-carbazolyl)benzene) and TSPO1 (diphenyl[4-(triphenylsilyl)phenyl]phosphine oxide) were used, while the optimal concentrations were determined experimentally by performing quantum yield measurements at different concentrations. The host selection was limited to materials with higher triplet energies than guest material, in order to avoid quenching of the emitter triplet state [65, 73]. Moreover a good exciton transfer from host to guest is crucial and ambipolar hosts are desired to promote exciton formation in emitting layer [27, 74]. The solid–state samples were prepared by dissolving the compounds and polymer or host material at appropriate ratios in toluene or chloroform solutions (45 mg/ml) and when wet–casting or spin–coating for 1 min at 1000 rpm on quartz substrates.

To conduct experiments in oxygen-saturated or oxygen–deficient environments at different temperature, the solid–state samples were mounted in a closed cycle He cryostat (Cryo Industries 204N). To eliminate oxygen the ambient pressure was reduced to 10^{-4} torr. For temperature dependant measurements the atmosphere in cryostat was replaced with He and the temperature was controlled in the range of 10–300 K.

Variation of solvent viscosity

The viscosity of environment in work **[A2]** was varied by diluting PMMA polymer in toluene at different proportions [35]. Even though PMMA is less polar media than toluene, the differences are slight enough not to play a major role. The concentration of polymer was increased from 0 mg/ml to 250 mg/ml to realize surroundings with different viscosity. The change of viscosity was clearly observed visually, however precise values of viscosity were not measured due to lack of equipment and having negligible importance for the experiment.

Steady-state absorption

A photon passing through material has a probability to be absorbed by a molecule in the process exciting it to a higher state. The probability of absorption remains the same throughout the sample. The remaining intensity of incident light at specified depth of material is defined by Beers-Lambert law [75]:

$$I = I_0 \times 10^{\varepsilon c l}, \tag{7}$$

where I is light intensity at at depth l of sample, I_0 – initial light intensity, c – concentration of the sample and ε is molar extinction coefficient. The extinction coefficient is a unique property of material which is strongly dependant on the photon wavelength and defines its probability of being absorbed. This dependence is called absorption spectrum.

The absorption spectra in this work were recorded using UV-vis-NIR spectrophotometer Lambda 950 (Perkin Elmer) using a reference (pure solvent for solutions or empty polymer matrix for solid-state). The equipment provides absorption spectra in optical density (OD) units which are later converted to extinction coefficient, by using equation (7). The OD is a logarithmic intensity ratio of the incident light and the light transmited through the sample:

$$OD = -\lg \frac{I_0}{I}. \tag{8}$$

Photoluminescence measurements

When molecule is excited to a higher state, over time it will decay radiatively or non-radiatively to its ground state. In the former case a photon of specific wavelength is emitted. Intensities of emitted photons at specific wavelengths are called photoluminescence spectra and can be recorded by spectrometer. In this work, the steady state emission was measured using a CCD spectrometer PMA-12 (Hamamatsu). The samples were excited using a CW xenon lamp and a computer controlled monochromator (FWHM $< 10\,\mathrm{nm}$). The excitation wavelength was usually selected to be coincident with absorption peak, unless stated otherwise.

Determining Quantum Yield

The quantum yield (Φ_F) is the ratio between the number of absorbed and emitted photons and is an intrinsic property of molecule:

$$\Phi_\mathrm{F} = \frac{\text{Ph. emitted}}{\text{Ph. absorbed}}. \tag{9}$$

The quantum yields were determined by integrating sphere (Sphere Optics) in two configuration measurement mode [76]. Two spectra were recorded with PMA-12 (Hamamatsu) connected via optical fiber to integrating sphere for each quantum yield measurement: configuration A – with a reference sample inside integrating sphere and configuration C – with the investigated sample in the same position. The spectra are divided into to regions L – incident light region and P – emission region. After integrating the regions in both A and C configurations we can calculate the observed quantum yield [76]:

$$\Phi^{\text{obs}} = \frac{P_c - P_a}{L_a - L_c}. \tag{10}$$

To correct for re-absorption a method described in FLS980 Series Reference Guide by Edinburgh Instruments [77] was employed. A very low concentration sample emission is measured without integrating sphere to record "true" emission spectra. The long wavelength tail of this spectra is then matched with emission spectra tail observed in integrating sphere. The difference in two areas correspond to re-absorbed area a_{reab}. Then the "true" quantum yield Φ_{F} can be determined:

$$\Phi_{\text{F}} = \frac{\Phi^{\text{obs}}}{1 - a_{\text{reab}} + a_{\text{reab}} * \Phi^{\text{obs}}}. \tag{11}$$

Time–resolved spectroscopy

Time-resolved fluorescence spectra, fluorescence decay transients and phosphorescence spectra were obtained by time-gated intensified CCD camera iStar DH340T (Andor) with a spectrograph SR-303i (Shamrock). The camera is synchronized with nanosecond YAG:Nd^{3+} laser NT 242 with an optical parametric generator (Ekspla, pulse duration 7 ns) used to excite the samples. The synchronization of laser and camera allow us to integrate the emission spectra for desired duration (integration time) (from 2 ns to 10 s with resolution of 10 ps) at a specified time after sample excitation (delay) (resolution 10 ps).

Time–resolved fluorescence spectra were recorded by exponentially increasing the delay and integration time of gated iCCD camera [78], which allow us to detect up to 10 orders of magnitude in time and intensity. The time and intensity value correction is then performed according to integration times using software package *Matlab*. The fluorescence decay transients can be acquired by integrating emission spectra at wavelength range specific for desired emission peak and approximated by bi–exponential decay profiles (if possible). For measurements of phosphorescence spectra the samples were cooled to 10 K temperature in order to suppress riSC and observe triplet emission. The low temperature of 10 K was chosen as some thermally activated emission is still observable for the most efficient TADF emitters at higher temperatures. Phosphorescence spectra were usually recorded after a 100 µs delay with a 89 ms

integration time. A low energy laser fluence (20–200 nJ) was generally used in order to minimize the degradation of studied compounds. The repetition rate of laser was selected in range from 10 Hz to 1 kHz individually for different samples according to the delay of their latest detectable emission.

Characterising TADF emitters

Energy gap ΔE_{ST} between lowest singlet state (S_1) and lowest triplet state (T_1) was assessed by determining energies associated with each state from the onset of fluorescence and phosphorescence spectra respectively. The onset energy of emission was used instead of peak as the charge transfer (CT) state, which is dominant in donor–acceptor emitters, is broad and structureless [75]. While the phosphorescence usually originates from ^{3}LE state and vibronic structure is often exposed, the energy level of triplet can then be assessed form the peak of the 0-0 transition. If vibronic structure is missing, the energy is determined from onset of emission.

Another important parameter of TADF emitters valuable for determining k_{rISC} and Φ_{ISC} is the ratio between delayed Φ_{DF} and prompt emissions Φ_{DF}. A simple way of determining this factor is based on the observation that long living triplet states are strongly quenched by molecular oxygen whose ground state is also triplet $^3O_2$ [79,80]. As the DF portion of emission is long-lived and originates from these same triplet states, it is usually suppressed in the presence of oxygen. Therefore the integrated steady-state emission in oxygen-rich

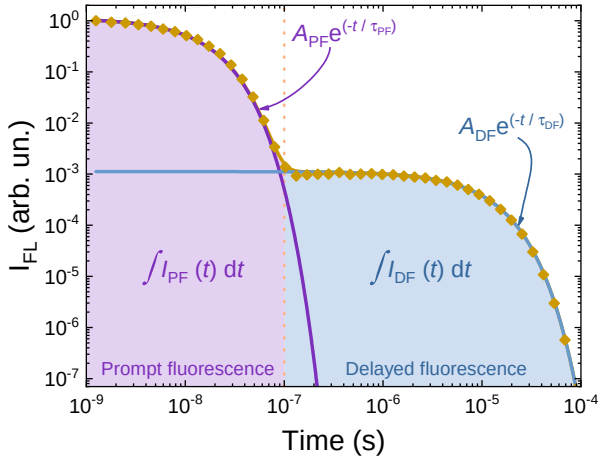

Figure 7: An example of typical decay transients of TADF emitter in the absence of ambient oxygen. The dark orange diamonds represent integrated emission from time-resolved spectra at specific time delays. The data can be partitioned into prompt (purple) and delayed (blue) portions which both can be fitted by exponential decay profiles.

environment will correspond to Φ_{PF}, while in oxygen-deficient conditions the same region of steady-state emission will be supplemented by excited states, upconverted from triplet state, leading to integral value of $\Phi_{PF}+\Phi_{DF}$. It is easy to calculate Φ_{DF}/Φ_{PF} ratio by assessing steady-state emission integrals in both air-equilibrated and degassed conditions, however this method was avoided in this work due to several reasons. First of all, the rISC of the best TADF emitters can sometimes outperform quenching by molecular oxygen while extremely long-lived fluorescence can also be effectively quenched by it [81,82]. Moreover some hosts have low oxygen permeability resulting in reduced quenching even in oxygen-rich surrounding.

Another approach of evaluating Φ_{DF}/Φ_{PF} includes analyzing decay kinetics in oxygen-deficient surroundings. In typical TADF decay transient two regions can be discerned: the initial PF and slower DF (Figure 7). Both of these regions can be fitted by individual exponents whose sum approximates the whole decay kinetic:

$$I_{FL}(t) = A_{PF}e^{-t/\tau_{PF}} + A_{DF}e^{-t/\tau_{DF}}. \tag{12}$$

Then the ratio Φ_{DF}/Φ_{PF} can then be evaluated either by using parameters of the fitted decay transients or by integrating PF and DF regions of kinetics [27]:

$$\Phi_{DF}/\Phi_{PF} = \frac{A_{DF}\tau_{DF}}{A_{PF}\tau_{PF}} \approx \int I_{DF}(t)\,\mathrm{d}t \,/ \int I_{PF}(t)\,\mathrm{d}t\,. \tag{13}$$

The estimation of reverse intersystem crossing rate is of extreme importance as it is one of the main parameter determining the efficiency of TADF process (Figure 8). k_{rISC} can be determined by using prompt, delayed and rISC

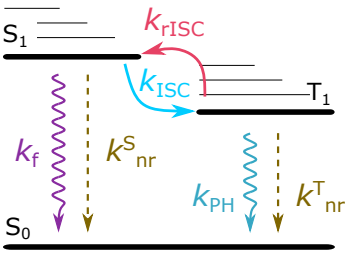

Figure 8: Visualization of competing processes in TADF emitter.

efficiencies and lifetime of delayed emission from the relationship [27]:

$$k_{rISC} = \frac{\Phi_{rISC}}{\tau_{DF}}\left(\frac{\Phi_{PF}+\Phi_{DF}}{\Phi_{PF}}\right). \tag{14}$$

The efficiencies Φ_{PF} and Φ_{DF} are estimated from decay transient proportions depicted in Figure 7 and absolute quantum yield, while τ_{DF} is estimated by fitting the slow component of decay transient. The rISC efficiency can be

approximated to $\Phi_{\mathrm{rISC}} \approx 1$ in case of $\Phi_{\mathrm{DF}}/\Phi_{\mathrm{PF}} \geqslant 4$, as such high DF/PF ratios mean that k_{rISC} is the dominant decay pathway for triplet states, which simplifies equation (14) greatly [27]. However in case the DF/PF ratio is lower than 4, Φ_{rISC} must be evaluated by:

$$\Phi_{\mathrm{rISC}} = \frac{\Phi_{\mathrm{DF}}}{\Phi_{\mathrm{F}}\Phi_{\mathrm{ISC}}}. \tag{15}$$

Two concurring non-radiative decay pathways of singlet state (S_1) are: deactivation through vibrations of molecular core or intersystem crossing to triplet state (Figure 8). If compounds exhibit similar non-radiative decay rates in both loose and rigid environments of dilute solution and polymer matrix, respectively, the former can be neglected, making the ISC the dominant pathway. Its efficiency can then be defined by [83]:

$$\Phi_{\mathrm{ISC}} = 1 - \Phi_{\mathrm{F}}. \tag{16}$$

In case of an active non-radiative quenching of singlet states by vibrations the ISC efficiency should be evaluated by [84]:

$$\tau_{\mathrm{DF}} = \tau_{\mathrm{PH}} - \left(\frac{1}{\Phi_{\mathrm{ISC}}} - 1\right)\tau_{\mathrm{PH}}\frac{\Phi_{\mathrm{DF}}}{\Phi_{\mathrm{PF}}}, \tag{17}$$

here τ_{PH} – is lifetime of phosphorescence when the rISC is not active. It is determined by exponentially fitting low temperature (10 K) decay transient of phosphorescence spectra.

The ISC rate is then determined by:

$$k_{\mathrm{ISC}} = \frac{\Phi_{\mathrm{ISC}}}{\tau_{\mathrm{PF}}}, \tag{18}$$

while the non-radiative decay rates for singlet and triplet states are estimated according to [27, 83]:

$$k_{\mathrm{nr}}^{\mathrm{S}} = \frac{1}{\tau_{\mathrm{PF}}} - \left(k_{\mathrm{f}} + k_{\mathrm{ISC}}\right), \tag{19}$$

$$k_{\mathrm{nr}}^{\mathrm{T}} = \frac{k_{\mathrm{rISC}}}{\Phi_{\mathrm{rISC}}} - k_{\mathrm{rISC}}. \tag{20}$$

Another approach to evaluate k_{rISC} by kinetic modeling of transient photoluminescence was suggested by Hasse *et al.* [85]. Here a TADF model is simplified to one mixed triplet state (T_1) while phosphorescence and non–radiative pathways are ignored (equivalent to $\Phi_{\mathrm{rISC}} \approx 1$). Then the model can be described by linear differential equations:

$$\frac{\mathrm{d}[S_1]}{\mathrm{d}t} = -(k_\mathrm{F} + k_\mathrm{ISC})[S_1] + k_\mathrm{rISC}[T_1],$$
$$\frac{\mathrm{d}[T_1]}{\mathrm{d}t} = k_\mathrm{ISC}[S_1] - k_\mathrm{rISC}[T_1]. \tag{21}$$

The initial singlet $[S_1], (t = 0)$ state is depleted by radiative decay (k_F) and intersystem crossing to triplet states (k_ISC) and is populatetd by the upconverted triplet states via TADF (k_rISC). Meanwhile the initial triplet state is $[T_1] = 0, (t = 0)$ repleted by intersystem crossing from singlet states (k_ISC) and depleted by rISC to singlet state (k_rISC) (Figure 8). By numerically modeling these equations the specific values of $k_\mathrm{F}, k_\mathrm{ISC}, k_\mathrm{rISC}$ can be estimated without partitioning the decay transients into regions of prompt and delayed emissions. Using this method the triplet population at any given moment can also be evaluated.

Production and characterization of OLED devices

The OLED devices were fabricated on precleaned indium-tin oxide (ITO)–coated glass substrates. The small-molecule and cathode layers were thermally evaporated using vacuum evaporation apparatus (Vacuum Systems and Technologies Ltd) at $< 6 \times 10^{-6}$ Torr pressure and deposition rate of about 1 Å/s. OLED devices were encapsulated with a clear glass cover to prevent the interaction with ambient.

A typical device structure of OLEDs produced in papers **[A4, A5, A6]** was: indium tin oxide (ITO)/ 1,1-bis[(di-4-tolylamino)phenyl]-cyclohexane (TAPC) (30 nm)/ 4,4',4"-tri(N-carbazolyl)triphenylamine (TCTA) (5 nm)/ (10 wt%) TADF emitter:DPEPO (bis(2-(diphenylphosphino)phenyl) ether oxide) (15 nm)/ 1,3,5-tri(m-pyridin-3-yl-phenyl)benzene (TmPyPB) (65 nm)/lithium fluoride (LiF) (0.8 nm)/Al (100 nm). Though exact layer arrangement and thickness varies for specific devices and will be specified individually. ITO and Al acted as anode and cathode, the TCTA and TAPC were used as hole injection and transport layers, respectively, while LiF with TmPyPB as electron injection and transport layers, respectively.

Device current-voltage (I-V) characteristics and electroluminescence properties were measured using calibrated integrating sphere (Orb Optronics) and CCD spectrometer PMA-11 (Hamamatsu), powered by 2601A power supply unit (Keithley) The production and charachterization of OLED devices were performed by Dovydas Banevičius.

1. CONFORMATIONAL DISORDER IN DONOR–ACCEPTOR TADF MOLECULES

In this chapter, the results of papers **[A1, A3]**, discussing the impact of conformational disorder in solid-state and suggesting two different strategies for minimizing its effects, are presented.

Motivation

In one of the most widely used TADF emitter architecture, fast rISC is achieved by sterically fixing electron-donor and electron-acceptor moieties at near orthogonal angles, ensuring small singlet–triplet energy splitting and minimization of non-radiative effects [86,87]. However, the efficient rISC also requires vibronic coupling between ^{3}LE and ^{3}CT states, which usually is achieved through torsion of D–A angle [52, 57, 59–61]. When embedded in solid-state host, the lability of molecular core translates into dispersion of conformers – molecules frozen with a variety of different angles between donor and acceptor – possessing different prompt and TADF emission properties [55, 66, 67]. It was noticed that dispersion of ^{1}CT and ΔE_{ST} energies due to different D–A angles lead to temporal spectral shifts of prompt and delayed emission as well as prolonged and multi-exponential decay profiles [62, 65, 68, 88]. This translates into several undesirable effects: the broadening of emission spectra due to spectral shifts, which is contrary to the desire of pure color OLED's, and roll-off of device performance at higher currents as longer decay times allows quenching of excitons by triplet-triplet (TTA), singlet-triplet (STA) and other annihilations [89]. Despite its influence on crucial TADF parameters, the conformational disorder effects are still scarcely studied. In this chapter, the effects of molecular rigidity and rISC rate on conformational disorder in solid state are investigated.

1.1. The effects of conformational disorder on molecules with different rigidity

To emphasize the role of molecular core rigidity two typical donor-acceptor compounds were selected displaying similar photophysical properties in dilute solutions but completely different molecular structures, geometries and stiffness. The 4,6-Bis(2-methyl-4-(10H-phenothiazin-10-yl)phenyl)pyrimidine (**PTZ-mPYR**) comprises of diphenyl-pyrimidine (PYR) acceptor unit and two phenothiazine (PTZ) donor fragments with non-planar geometry. While 1,2,3,4-tetrakis(carbazol-9-yl)-5,6-dicyanobenzene (**4CzPN**) is composed of dicyanophenyl acceptor decorated with four adjacent carbazole (Cbz) donor units (Figure 1.1). Both investigated molecules utilize a single bond to link donor and acceptor fragments which provides a rotational freedom.

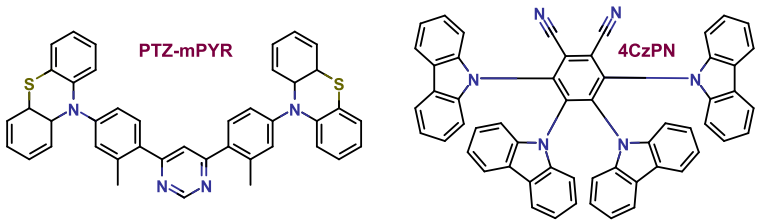

Figure 1.1: Molecular structures of two TADF emitters investigated in this work with completely different molecular structures, yet exhibiting similar emission properties in dilute solutions.

The optimized geometries (by DFT calculations) revealed that the phenothiazine moiety in the **PTZ-mPYR** compound is almost perpendicular (88.9°) to the phenyl fragment. Moreover the PTZ units are also bent along the C-N bonds [90] allowing a larger rotational flexibility compared to planar donor moieties [91]. For **4CzPN** the donor carbazole units are twisted by 62–67° in respect to central phenyl ring. Tight spatial crowding of carbazole units lead to large steric hindrance and rigidity of molecular core. Here the molecular rigidity is defined as the rotational stiffness of angle between donor and acceptor units, therefore flexible molecules will have a large D–A angle dispersion, while the rigid ones will have a small dispersion.

The flexibility of **PTZ-mPYR** together with steric hindrance of **4CzPN** was supported by estimating vibrational frequencies of the lowest vibrational modes in the harmonic approach in ground state. For **PTZ-mPYR** the lowest vibrational mode was the twisting motion of donor unit at only $6\,\mathrm{cm}^{-1}$, while the same motion in **4CzPN** was represented by higher vibration mode at $45\,\mathrm{cm}^{-1}$ due to the steric hindrance between donor units. Supposedly, larger energetic barriers for the twisting motion of donor units should result in lower ΔE_{ST} dispersion and lower conformational disorder in solid-state [92, 93].

It should be stressed that despite completely different molecular structures both **PTZ-mPYR** and **4CzPN** demonstrate very similar emissions peaking at 535 and 525 nm, respectively (Figure 1.2). Even the decay times are comparable, with prompt fluorescence decay lifetime of 10 and 14 ns and delayed fluorescence lifetimes of 11 and 15.5 µs for **PTZ-mPYR** and **4CzPN**, respectively (Figure 1.4). While ΔE_{ST} were also comparable with values of 25 and 10 meV for **PTZ-mPYR** and **4CzPN** respectively, the quantum yields of prompt and delayed emission decreased for **PTZ-mPYR** (0.04 and 0.04 *vs.* 0.09 and 0.61, respectively) as the more flexible core promoted non-radiative decay through internal conversion.

Despite comparable photophysical properties in diluted solutions substantial differences between **PTZ-mPYR** and **4CzPN** were observed when embedded in 1 wt% PMMA solid films. First of all, the quantum yield of delayed

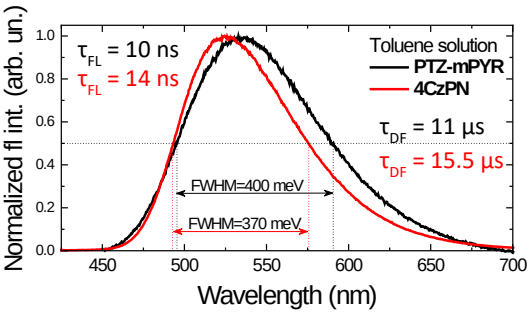

Figure 1.2: Emission of **PTZ-mPYR** and **4CzPN** in 10^{-5} M toluene solution, with decay lifetimes and spectra FWHM depicted inset.

component (Φ_{DF}) increased drastically from 0.04 to 0.32 in rigid surrounding for **PTZ-mPYR** while it remained relatively the same (0.61 and 0.54) for the **4CzPN**. The increase in emission yield was determined by restriction of molecular movement, which in turn minimized the decay through internal conversion. Secondly, both materials exhibited temporary spectral shifts inherent to conformational disorder in solid state. The initial red shift of prompt emission was observed for the first 100 ns as the fluorescence wavelength stabilised up to 10 µs, then a blueshift of delayed emission was observed (Figure 1.3a).

Obvious differences of spectral shifts were observed for **PTZ-mPYR** and **4CzPN**. At first, the **PTZ-mPYR** prompt emission is redshifted by about 340 meV indicating a large distribution of ^{1}CT energies, followed by blueshift of 80 meV. The smaller blueshift of delayed emission, compared to initial redshift, is a consequence of wide variety of ΔE_{ST} energies, as the highest energy states possesses low k_{rISC}, susceptible to quenching by various quenchers even in the oxygen-free environment. As the latest, bluest, delayed fluorescence is quenched, the integrated delayed emission experiences a redshift (Figure 1.3b) compared to integrated prompt fluorescence. Meanwhile, the rigid **4CzPN** has a superior emission wavelength stability as the redshift and blueshift for the **4CzPN** are both 100 meV, therefore all conformers with dispersed properties are emissive and both integrated prompt and delayed fluorescence share the same spectra (Figure 1.3b).

The advantage of small dispersion of ^{1}CT energies are apparent in time integrated spectra of oxygen-deficient ($-O_2$) and oxygen-rich ($+O_2$) 1 wt% PMMA films (Figure 1.3 b and c). As the oxygen is introduced it quenches more of the latest delayed states with higher ΔE_{ST} values leading to a redshift of integrated delayed emission. However the emission peak is blueshifted by 150 meV as prompt emission from a wide dispersion of ^{1}CT states dominates over the long-wavelenght delayed emission. On the other hand, the emission wavelength of **4CzPN** is stable in both conditions, due to low dispersion of conformations, as the latest delayed fluorescence originates from similar conformer states with

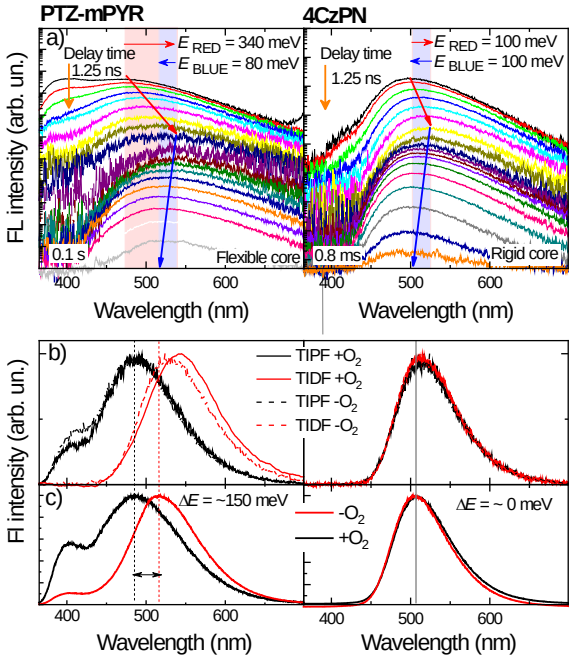

Figure 1.3: a) Time resolved spectra of **PTZ-mPYR** and **4CzPN** indicating the initial redshift and following blueshift by arrows; b) corresponding time-integrated prompt fluorescence (TIPF) and time-integrated delayed fluorescence (TIDF) spectra with and c) time-integrated spectra of emission in oxygen-rich ($+O_2$) and oxygen-free ($-O_2$) environments with peak emission wavelength marked by dashed lines.

rather low ΔE_{ST} and rapid k_{rISC}, even in the oxygen-saturated ambient. It is important to note here, that the emission wavelength can be influenced by such unexpected parameters as TADF lifetime.

A small, conformational disorder led, dispersion of ^{1}CT energies in solid state, for compound **4CzPN**, is confirmed by only a slight increase of FWHM of emission spectra from 370 meV in toluene solution to 400 meV in both oxygen-rich and oxygen-free PMMA films. Meanwhile, for flexible cored **PTZ-mPYR**, a 15 % increase from 400 meV in toluene solution to 460 meV in oxygen-deficient PMMA films was recorded. The widening of emission spectra is initiated by large dispersion of ^{1}CT energies and quenching of the latest emission. The effect is exaggerated in oxygen-saturated ambient where even more of delayed emission is quenched, leading to FWHM increase of 46 % from $-O_2$ to $+O_2$ in PMMA films (460 and 670 meV, respectively).

The presence of conformational disorder and lower polarity of solid PMMA surrounding increased ΔE_{ST}, which represents the average gap of all conformers, for both **PTZ-mPYR** and **4CzPN** compared to toluene solutions (from 25 meV to 187 meV and from 10 meV to 140 meV, respectively).

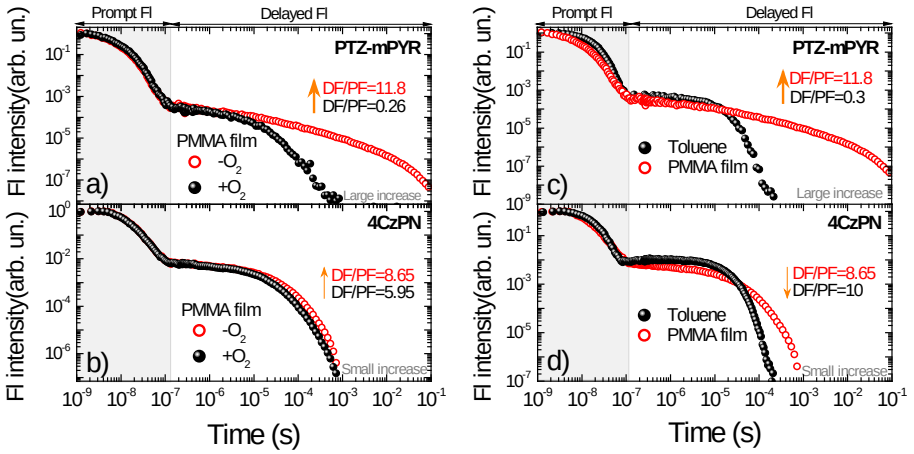

Figure 1.4: Fluorescence transients of **PTZ-mPYR** and **4CzPN** compared in oxygen-saturated $+O_2$ and oxygen-deficient $-O_2$ 1 wt% PMMA films (on the left). On the right: transients of same compounds in 10^{-5} M toluene solution and 1 wt% PMMA film in oxygen-deficient ambient.

Major influence of molecular rigidity is revealed in decay transients of flexible and rigid core compounds in toluene solutions and oxygen-deficient, oxygen-rich 1 wt% PMMA films (Figure 1.4). Presence of conformational disorder results in large dispersion of ΔE_{ST} values and in turn – large dispersion of decay lifetimes. The sum of all conformations produce prolonged and multi-exponential TADF decay kinetics in solid surroundings with the effect remarkably stronger for flexible **PTZ-mPYR** molecule. Strong enhancement of delayed emission is observed with removal of oxygen for flexible molecule **PTZ-mPYR** (DF/PF ratio increase from 0.26 to 11.8 was recorded) as the long living triplet states (longer than 10 µs) are easily quenched by oxygen (Figure 1.4a). Meanwhile, the rapid k_{rISC}, even for conformers with highest ΔE_{ST}, of rigid **4CzPN** compound ensures that most of delayed emission is unquenched, resulting in only a slight increase of DF/PF (from 5.95 to 8.65) when oxygen is removed (Figure 1.4b).

In an ideal case, similar properties of emission should be observed in dilute solutions and solid-state, as was shown by **4CzPN**, where only a minor decrease of TADF lifetime in PMMA films was attributed to increased polarity of PMMA (Figure 1.4d). The small disorder allowed to estimate the average decay lifetime with a three-exponential fit for **4CzPN**, while multi-exponential nature of **PTZ-mPYR** decay prevented the approximation of decay component (Figure 1.4c). A modest, three fold, increase of TADF lifetime was estimated for **4CzPN** from 15.5 µs to 46 µs which is favorable as low TADF decay lifetime ensures lower EQE roll-off of OLED. While it was hard to estimate the TADF lifetime for flexible **PTZ-mPYR** a large increase of a lifetime is ap-

parent visually (Figure 1.4c) and is supported by a 40 fold increase of DF/PF ratio.

Here it was shown, that TADF emitter with a rigid molecular core can benefit from reduced conformational disorder effects in solid-state. Moreover, a faster rISC rate should prevent the quenching of the latest, bluest delayed emission.

1.2. Two strategies for minimizing the disorder

To test or findings in a more similar molecular structures, another series based on pyrimidine acceptor were designed (Figure 1.5). To reduce lability of the

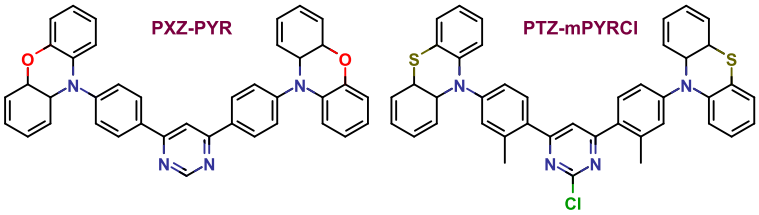

Figure 1.5: Molecular structures of **PXZ-PYR** and **PTZ-mPYRCl**.

donor unit, phenothiazine (PTZ) donor was exchanged for more sterically fixed planar phenoxazine (PXZ) donor [94, 95] in **PXZ-PYR** compound (Figure 1.6a). While the Cl atom was introduced to pyrimidine acceptor of **PTZ-mPYR** to utilize heavy atom effect [96], increasing the ISC and, in conjunction, rISC rates in **PTZ-mPYRCl**.

Despite the different donors of **PTZ-mPYR** and **PXZ-PYR**, both compounds showed relatively similar emission wavelength in toluene. Though prompt (Φ_{PF}) and delayed (Φ_{DF}) efficiencies were lower for more loosely constrained **PTZ-mPYR**(0.04 and 0.04 *vs.* 0.15 and 0.27 for **PTZ-mPYR** and **PXZ-PYR**, respectively), together with slower TADF decay (11 and 1.6 µs, respectively.).

It is apparent from time-resolved measurements (Figure 1.6b), that the **PXZ-PYR** follows the same trend when initial redshift of 160 meV is followed by a blueshift of 100 meV. However the temporal shifts are remarkably lower compared with more sterically strained **PTZ-mPYR**. Even though the blueshift is not equal to the initial redshift for **PXZ-PYR** (specifying that a portion of the latest delayed emission is still quenched) the difference is remarkably lower and therefore the emission wavelength remained stable in both oxygen-deficient and oxygen-rich surrounding. The more rigid structure of **PXZ-PYR** clearly benefited from lower TADF lifetime enhancement (Figure 1.6 c). Even though its hard to approximate the exact delayed fluorescence lifetimes due to prolonged decay, a lower (33 %) increase in DF/PF ratio indicates a low TADF lifetime enhancement. It is again confirmed, that prosperous

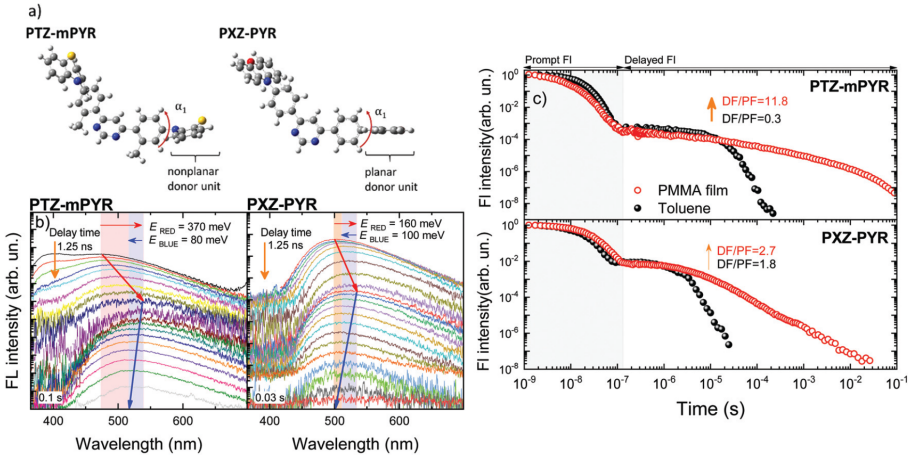

Figure 1.6: a) Optimized geometries of compounds **PTZ-mPYR** and **PXZ-PYR**, with twist angle of D–A highlighted. b) Time-resolved spectra of both compounds with temporal spectral shifts marked by red and blue arrows. c) Decay transients in oxygen-free toluene and PMMA ambients.

TADF properties in solid-state can be gained by constructing more rigid molecular core due to minimization of conformational disorder.

The second strategy of improving rISC rate to evade conformational disorder also showed promising results. The introduction of Cl atom in **PTZ-mPYRCl** redshifted the emission peak by 170 meV up to 575 nm in dilute toluene solutions, while ΔE_{ST} remained relatively similar (a known effect of heavy atom [96, 97]). Time-integrated measurements revealed that the emission energy of compound with Cl atom remained unchanged in oxygenated and oxygen-free environments (Figure 1.7b). Time-resolved spectra analysis showed that emission of **PTZ-mPYRCl** sustains a redshift of 280 meV followed by a comparable blueshift of 130 meV in $-O_2$ conditions (and 80 meV in the presence of oxygen) (Figure 1.7d). Even though the blueshift is not equal to the initial redshift, as it was in the case of **4CzPN**, it is enough to sustain stable emission wavelength.

To investigate the reason behind stable emission, decay transients were analyzed in dilute solutions (Figure 1.7c). The TADF decay lifetime was 10 times smaller for compound with Cl atom (11 and 1.1 µs, respectively). Such short TADF lifetime is comparable to benchmark values [98]. An increase in lifetime was followed by a 4 fold increase in DF/PF ratio (1.2 *vs.* 0.3) despite the similar ΔE_{ST} allowing the TADF to dominate emission. The improvement of TADF properties was mediated by internal heavy atom effect, enhancing spin-orbit coupling, crucial for ISC and rISC.

The decay kinetics in PMMA film (Figure 1.7c) are similar to those in dilute solution, thought the delayed transients are prolongued and multiexponential

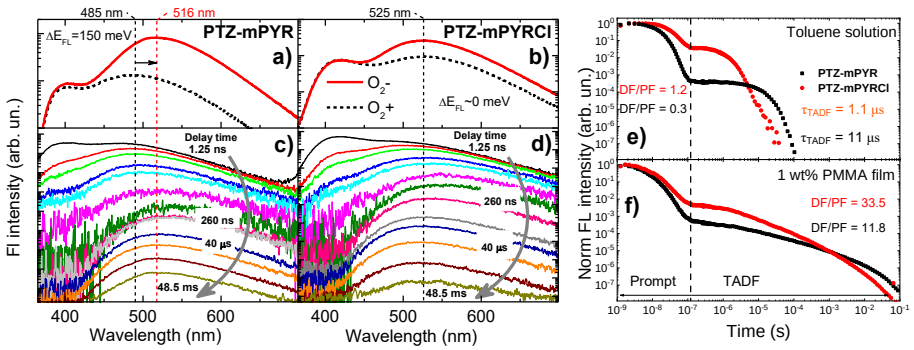

Figure 1.7: Time integrated emission spectra in 1 wt% PMMA films in oxygen-rich ($+O_2$) and oxygen-free ($-O_2$) conditions of **PTZ-mPYR** and **PTZ-mPYRCl** (a and b, respectively); Time resolved spectra in $-O_2$ of the same compounds. Decay transients of compounds in 10^{-5} M toluene solution (e) and in PMMA films (f).

due to presence of conformational disorder. Even though the decay lifetime can hardly be evaluated, it is clear that **PTZ-mPYRCl** possess a faster TADF. As both materials contain donor units which can freely rotate, the conformational disorder effects are overwhelming, however reduction of k_{rISC} allowed for the conformers with largest ΔE_{ST} to emit, stabilizing emission wavelength and shortening TADF lifetime.

Therefore minimizing the rISC rate serves as another measure to counteract some of the negative effects caused by conformational disorder.

Summary of the results

Multiple unfavorable effects on solid-state TADF properties were observed for compound **PTZ-mPYR** with flexible molecular core. A large dispersion of torsion angles between D–A produced conformers with large ΔE_{ST} energies in solid-state, prolonging TADF lifetime. The long lifetimes can hardly be approximated due to the multiexponential nature and is usually a cause of large efficiency roll-offs in OLED devices. Moreover, the conformers with slowest rISC rates were quenched even in oxygen-free ambient resulting in emission wavelength shift and broadening of spectra in solid state. All of these drawbacks were minimized by selecting a molecule with sterically hindered donor fragments (**4CzPN** and **PXZ-PYR**). Minor dispersion of ΔE_{ST} energies led to stable emission color and only a slight increase of TADF lifetime in solid-state, compared to that in a dilute solution. Similar effect of stabilising emission wavelength can be achieved by enhancing rISC rate in compound with same molecular lability.

2. BOUNDING DONOR AND ACCEPTOR BY HYPERCONJUGATED BRIDGE

This chapter summarizes the research published in paper **[A2]** and presents a deeper insight in intricate photophysical properties of several D-σ-A compounds initially studied by Geng *et al.* [70].

Motivation

While decoupling of HOMO and LUMO is commonly accomplished by twisting donor and acceptor fragments in single molecule, it can also be realized by breaking the bond between D an A moieties and relying on intermolecular charge transfer in exciplex [40]. The TADF properties, in this case, is strongly dependant on distance between D and A, which can hardly be controlled [42–44]. Recently, Geng *et al.* [70] suggested a novel strategy to utilize hyperconjugated bridge to bound donor and acceptor in a non-conjugated controlled manner. Hyperconjugation, first introduced by Mulliken *et al.* [99], describes interaction of electrons in σ orbital with an adjacent π–orbital providing somewhat weak electron delocalization between them [100, 101]. It was utilized, when several donor units were bound to triazine acceptor fragment by hexafluoroisopropylidene spacer unit [70]. The compounds displayed intermolecular charge transfer emission with negligible ΔE_{ST}. DFT-estimated oscillator strengths were very low (in the range of 0.0008–0.0054), typical for weakly interacting donor and acceptor systems. Two TADF decays were observed, one of which was very rapid with lifetime of only 200–400 ns which is one of the lowest reported [102].

In this chapter, time-resolved spectroscopy is exploited, to gain deeper insight into intriguing properties of D–σ–A compounds. Analysis of these molecules in various concentrations, temperatures and solution viscosities revealed the origin of dual emission.

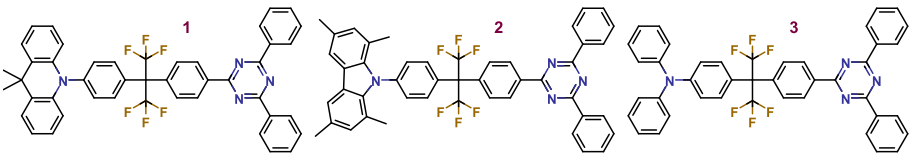

Figure 2.1: Molecular structures of D-σ-A compounds presented in [70] and investigated in this work.

Three TADF donor-σ-acceptor compounds were studied (Figure 2.1). All molecules contain planar triphenyltriazine acceptor bounded to donors of different strength: 1 - dihydroacridine, 2- tetramethylcarbazole, 3 - triphenylamine

by hexafluoroisopropylidine σ bridge.

2.1. Excited state relaxation of D–σ–A in diluted solutions

The decay transients in oxygen deficient toluene followed bi-exponential decay profiles (Figure 2.2). The first decay component had a lifetime in the range of 37–470 ns (τ_{FL1}) while the lifetime of second component was 0.45–10 µs (τ_{FL2}). Both of these decays were quenched by oxygen. Initially [70], this, along with activation by temperature, was used to evidence that both states are thermally activated delayed fluorescence. The TADF emission lifetime should become

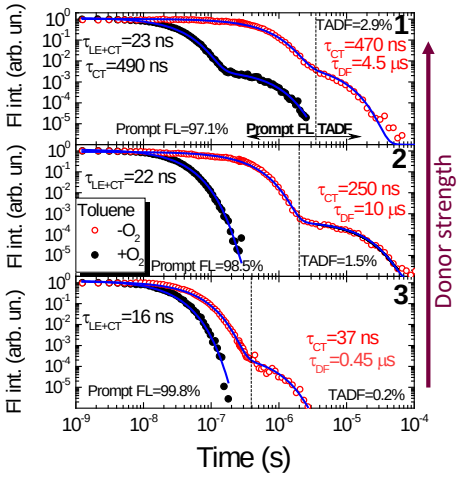

Figure 2.2: Decay transients of molecules **1**–**3** in 1.2×10^{-5} M toluene solution in the presence and absence of oxygen.

more rapid with reduced ΔE_{ST} as the rISC rate is directly dependant on the gap. However, an opposite trend can be seen from the table 2.1 for τ_{FL1}. The lifetime of first fluorescence is decreasing as the ΔE_{ST} increases, but is smaller for larger oscillator strength (f). This is expected for prompt fluorescence - the molecules with the strongest donor and largest HOMO–LUMO decoupling has the longest decay lifetime and vice-versa. On the other hand, the decay lifetime of the second fluorescence τ_{FL2} (4.5, 10 and 0.45 µs) increases with increasing ΔE_{ST} (60, 70 and 180 meV for compounds **1** and **2**, which is inline with TADF emission. The small lifetime τ_{FL2} of compound **3** can be explained by vastly larger ΔE_{ST}, which makes TADF emission very weak. Moreover the DF/PF ratios are also inline with the energy gap ΔE_{ST}, if we consider FL1 as prompt fluorescence and FL2 as delayed emission.

The increase of τ_{FL1} in low temperatures was used as a proof of TADF nature for initial decay [70]. However, the low temperature measurements were carried out in toluene solutions, above toluene freezing point, and the variation

Table 2.1: Emission properties of D-σ-A compounds in oxygen-free 1.2×10^{-5} M toluene solution.

	τ_{FL} (ns)	τ_{TADF} (µs)	DF/PF	f	ΔE_{ST} (meV)
1	470	4.5	0.03	0.0008	60
2	250	10	0.015	0.0012	70
3	37	0.45	0.002	0.0054	180

of non-radiative recombination rate was not neglected. Contrary, after performing temperature dependence measurements in rigid PMMA matrix where non-radiative pathways are mostly impeded – no temperature activation was observed.

All the evidence are implying that the first emission τ_{FL1} is prompt fluorescence and the second emission τ_{FL2} is of TADF nature. The long decay times of τ_{FL1} and susceptibility to quenching by oxygen are not typical for prompt emission. However the minuscule oscillator strengths prolongs the fluorescence lifetime enough to be quenched by oxygen [103, 104].

2.2. Dual emission in solutions

Even though a single emission band was observed in time-integrated spectra, time-resolved analyses revealed a more complex picture.

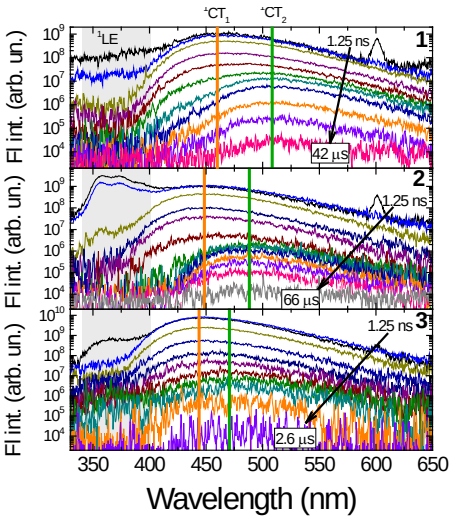

Figure 2.3: Time resolved spectra of compounds **1**–**3** in oxygen free toluene at concentraion of 1.2×10^{-5} M. The numbers denote to initial and last delay times.

Two different CT bands can be depicted at different time scales in figure

2.3. The initial CT fluorescence band $^1CT_1$ is observed at about 445–465 nm up to about 4, 2 and 0.5 µs for compounds **1**–**3**, respectively. Then later, a second $^1CT_2$ band emerges at 475–505 nm. Though a clear second band is observed only at later times, a long-wavelength shoulder is visible at all delay times, suggesting that the $^1CT_2$ is present from the beginning, however it is overwhelmed by a stronger $^1CT_1$ emission.

While both bands are clearly CT emission, as the peak wavelength depends on the strength of donor (the emission is redshifted with stronger donors), the nature of second band is not clear. Several possibilities can be considered: dynamic molecular conformer states, emerging after reorganization of molecular structure [105], or diffusion led, intermolecular interaction of donor and acceptor units [40].

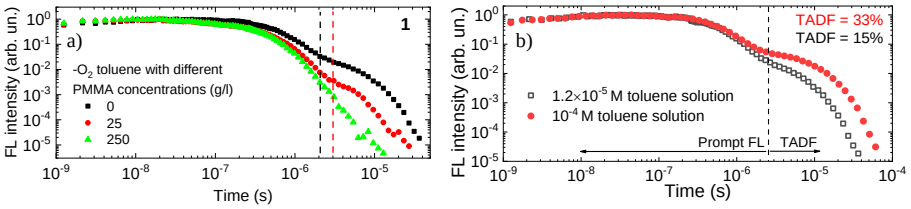

Figure 2.4: Decay transients of compound **1** in oxygen-free: a) toluene solutions of different viscosity (the viscosity was increased by introducing PMMA polymer at different concentrations); b) toluene solutions at different concentrations of 1.2×10^{-5} and 10^{-4} M.

The nature of the second $^1CT_2$ component was investigated by obtaining fluorescence decay transients in toluene solutions with varied viscosity (Figure 2.4a). The increased ambient viscosity reduced the τ_{FL} slightly from 470 to 280 ns, which can be attributed to impeded non-radiative decay. However, the TADF emission was almost completely suppressed in viscous solution, reducing DF/PF ratio from 0.15 to 0.003 (measured at peak wavelength of $^1CT_2$ band).

Moreover, the decay kinetics of compound **1** in different concentrations of 1.2×10^{-5} and 10^{-4} M of toluene solution were compared (Figure 2.4b). While the prompt fluorescence remained relatively the same, the TADF part was clearly enhanced as the DF/PF ratio increased from 0.18 in lower concentration to 0.49 in higher concentration. The emission wavelength was also shifted from 475 to 485 nm for increased concentration as the fraction of $^1CT_2$ increased.

Strong dependence on the concentration and viscosity suggest that the process in question is diffusion determined, therefore the nature of the second band was attributed to delayed fluorescence from exciplex. Formation of dimers was neglected as were no changes present in absorption spectra.

To fully quench the exciplex emission the compounds were incorporated into rigid PMMA polymer matrix, where diffusion is suppressed. Emission from isolated molecules were ensured by low concentration of 1 wt%.

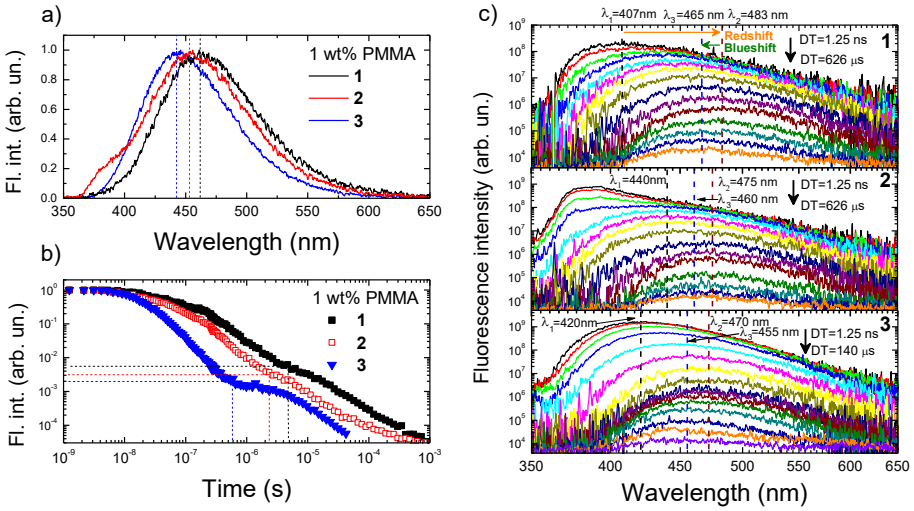

Figure 2.5: a) Integrated fluorescence spectra; b) decay transients; c) time-resolved spectra of compounds **1**–**3** in oxygen deficient 1 wt% PMMA films.

The fluorescence spectra, as in dilute solutions, exhibited intramolecular CT emission which peaked at 460, 455 and 445 ns for compounds **1**–**3**, respectively (Figure 2.5a). The decay transients in thin films were also similar to those in dilute solutions with bi-exponential decay profile, however they were greatly disfigured due to the presence of conformational disorder (Figure 2.5b). Though approximating the decay lifetimes was obstructed by multiexponential profile, the same pattern as for diluted solutions were observed for prompt fluorescence – its lifetime increased with increasing donor strength. The prompt fluorescence was also unaffected by low temperatures as expected for prompt emission. The second component was quenched by oxygen and was activated by temperature therefore was attributed to TADF. The DF/PF ratios of 1.08, 0.92 and 0.6 for compounds **1**–**3**, respectively, showed increased intensity of TADF emission, due to impeded non-radiative decay in rigid surrounding.

Large temporal shifts, discussed in the previous chapter, are observed in time-resolved spectra of PMMA films (Figure 2.5c). The smallest redshift was observed for the **2** compound as it possess the most sterically hindered tetramethyl-carbazole donor unit. As expected, the $^1CT_2$ band was absent in thin films – confirming their exciplex nature. As the non-radiative decay and diffusion are suppressed in rigid polymer matrix, both prompt and delayed emissions originate from the same intramolecular charge transfer state.

To thoroughly investigate the exciplex emission, neat films of compounds **1**–**3** were analyzed. The fluorescence spectra were of charge transfer nature, but redshifted by about 140–200 meV compared to both thin films and dilute solutions, peaking at 495, 482 and 470 nm for compounds **1**–**3**, respectively. The redshift is not unusual in neat films and is mainly caused by intermolecular interactions [106–109]. In our case, the integrated fluorescence spectra of neat film almost perfectly coincides with $^1CT_2$ band observed in toluene solution and, therefore, is attributed to exciplex formation (Figure 2.6 a,b and c). Unsurprisingly, the exciplex emission dominates in tightly-packed molecular environment of in neat film.

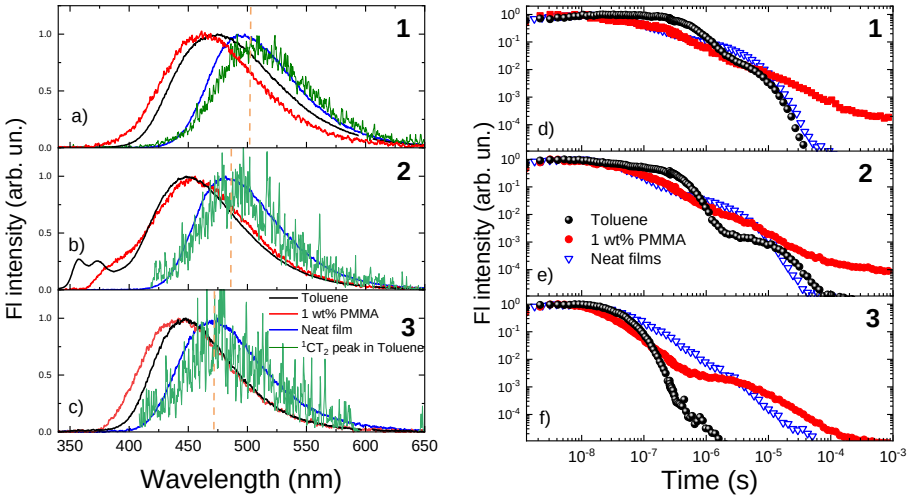

Figure 2.6: Integrated emission spectra (a-c) and decay transients (d-f) of compounds **1**–**3** in neat film, 1.2×10^{-5} M toluene solution and 1 wt% PMMA film. Time resolved spectra of $^1CT_2$ state in toluene solution is also presented in (a-c).

The decay transients of compounds **1**–**3** in neat films are depicted in figures 2.6 d, e, and f along the decay kinetics in 1.2×10^{-5} M toluene solutions and 1 wt% PMMA film. Interestingly, the initial prompt fluorescence closely resembles the decay kinetic in thin film (except compound **3**) – lowered τ_{FL} perturbed by conformational disorder is observed. Meanwhile, the second (TADF) component is very similar to that of the dilute solution. It is not disturbed by conformational disorder and even shows comparable decay lifetime, supporting the assumption that they both arise from exciplexes. There was no TADF emission present in compound **3**, as the weak delayed fluorescence, observed in toluene solutions, was probably quenched at defect sites. The TADF emission in neat films was greatly enhanced compared to toluene solution due to large concentration of TADF-active exciplex states with DF/PF ratios of 1.63 and 1.44 for compounds **1** and **2**, respectively. The TADF nature of the second

component was also confirmed by activation with temperature.

2.4. Optimization of intra/intermolecular TADF

As intramolecular TADF emission is dominant in diluted films and intermolecular TADF fluorescence is prevailing in neat films – a gradual interplay of these processes was observed by tuning the doping concentration (in the range 0.01–100 wt%) of PMMA films. Figure 2.7a shows how the peak wavelength shifts as the balance of intra-intermolecular TADF is shifted. At low doping concentrations (0.01–2 wt%) (when no intermolecular interactions can occur) the emission peaked at 460 nm, similarly to $^1CT_1$ emission. The wavelength is redshifted in toluene solution due to the larger ambient dipole moment. The emission wavelength peak gradually increased up to 490 nm at 30 wt%, as the portion of exciplex state rises. In the range 30–100 wt% the emission wavelength remains stable as the exciplex emission is dominant.

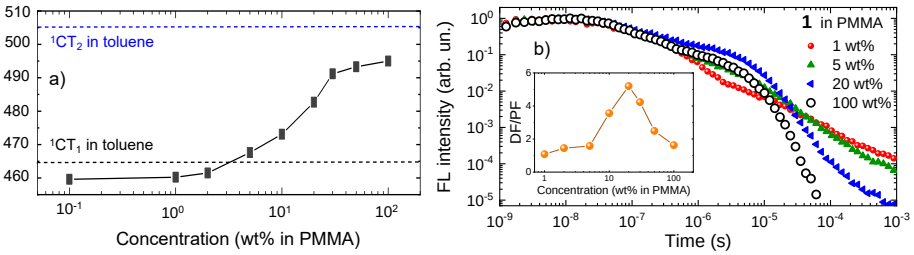

Figure 2.7: a) Integrated emission wavelength peak of compound **1** at different doping concentrations in PMMA film. Horizontal lines denote to $^1CT_1$ and $^1CT_2$ peak wavelengths. b) Normalized fluorescence decay transients of compound **1** in PMMA at different doping concentrations. Inset depicts the DF/PF ratio at different doping loads.

Similar trend was observed in fluorescence decay transients. Intramolecular TADF, highly disturbed by conformation disorder, is dominant in concentrations 1–5 wt% (Figure 2.7b). However increasing concentration give rise to undistorted and more efficient exciplex delayed fluorescence. The DF/PF ratio peaks at about 20 wt% concentration, as further increase of doping load enhance excitation mobility leading to quenching of the latest delayed emission at defect sites. The TADF lifetime also decreases at larger doping concentrations due increased quenching of the latest states. Therefore the DF/PF ratio can be tuned by selecting appropriate doping concentration in order to achieve the most efficient delayed fluorescence.

Summary of the results

A series of novel design donor-σ-acceptor TADF compounds with different donor units were analyzed. Minimization of HOMO-LUMO orbital overlap, in order achieve negligible ΔE_{ST} values, was realized through hyperconjugated hexafluoroisopropylidene spacer. This resulted in weak donor-acceptor coupling leading to several unusual effects. First, the prompt CT fluorescence outlined with a remarkably prolonged decay lifetime, which was susceptible to molecular oxygen. Due to unique characteristics it was initial misidentified as TADF emission. Second, coexisting intra- and intermolecular fluorescence of different wavelengths were observed at different timescales even in dilute solutions. The second emission was proven to originate from exciplex states. In dilute polymer films with suppressed non-radiative recombination, however, both prompt and delayed emission were of intramolecular nature. Lastly, the exciplex TADF emission dominated in neat films, however the optimal doping concentration of 20 wt% was established as further increase of doping load enabled excitation migration towards the defect sites subsequently quenching TADF emission.

The work presented in this chapter emphasises that the weak donor-acceptor coupling is not favorable for efficient intramolecular TADF and σ-bridged compounds should be designed with great care.

3. TOWARDS BLUE TADF EMITTER

This chapter summarizes the research published in papers **[A4, A5, A6]** and presents several ways of optimizing emitter structures in order to produce fast and efficient blue TADF emission.

Motivation

The recent advances in OLED technology allowed successful optimization of TADF compounds producing devices with external quantum yields approaching 40 % without applying any artificial light extraction techniques (only spontaneous molecular orientation) [30,36,110]. However, large EQE values are usually displayed only at low brightness as their yield substantially reduces at high luminance due to the pronounced quenching by triplet-triplet, singlet-triplet and similar annihilation pathways [89, 111]. Shortening the TADF lifetime has been shown to be a successful strategy for lowering EQE roll-off [89, 98, 112]. While faster rISC rate can be achieved by spatially separating HOMO and LUMO orbitals, this also leads to reduction of k_r which in turn reduces quantum yield of both prompt and delayed fluorescence. Low rate of singlet radiative decay is also harmful for lifespan of TADF devices, as the increased singlet exciton density in the light-emitting layer boosts the rate of unwanted singlet–singlet annihilation, increasing the molecular decomposition rate [113]. Moreover, TADF efficiencies are substantially lower in the deep-blue region ($CIE_y < 0.1$), desirable for colored OLED displays [114], as the EQE for such devices rarely exceeds 20 % margin [115–117]. The high requirements of short conjugation length, high triplet energy and appropriate D–A spatial structure essential for deep-blue TADF are not easily satisfied.

In this chapter several optimization strategies are employed: selectively adjusting lowest singlet energy, to achieve deep-blue emission, control of radiative and non-radiative decays through linking pattern of donor units and fine-tuning of rISC rate by small methyl modifications. Emitters with electroluminance colors ranging from green (536 nm, CIE (0.35, 0.56)) to deep-blue (441 nm, CIE (0.16, 0.12)) were produced and peak efficiency of 29.1 % with low roll-off was reached.

3.1. Achieving deep-blue emission

In order to produce deep-blue emitters, usually dihydroacridine and carbazole donors are bound to sulphone and nitrogen containing acceptor moieties [118]. However, pyrimidine-carbazole compounds are rarely being explored as TADF emitters, despite being successfully applied as high triplet energy hosts [119, 120].

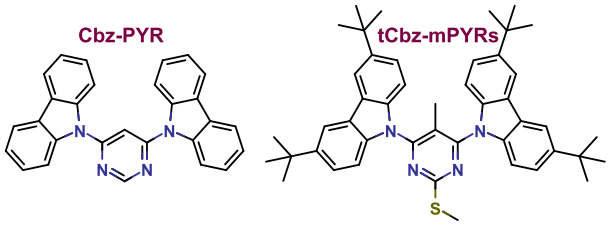

Figure 3.1: Molecular strunctures of base **Cbz-PYR** and modified version **tCbz-mPYRs**.

Seeing the potential of such compounds a carbazole-pyrimidine (**Cbz-PYR**), displaying high energy triplet and the presence of RTP, which is usually a sign of favorable energy structure for TADF [121], was selected as a candidate for molecular modifications. Based on the knowledge acquired and described in the first chapter, the following modifications were performed in order to achieve TADF while maintaining deep-blue emission (Figure 3.1). Firstly, the donor carbazole units were extended with 3,6-di-*tert*-butyl in order to increase its donor strength. Secondly, a methyl group at the 5$^{\text{th}}$ position of pyrimidine was introduced to increase steric hindrance and lower the HOMO and LUMO overlap. Finally, a heavy sulphur atom was attached to acceptor unit to enhance the ISC and rISC rates and redshift the emission peak.

3.1.1. Evaluation of emitter properties

The initial DFT calculations revealed optimistic results (Figure 3.2). The introduction of methyl group at 5$^{\text{th}}$ position of pyrimidine unit increased the twist angle between the donor and acceptor units from 37° to 48.8°. This, in conjunction with enlarged donor strength by *tert*-butyl, ensured the separation of HOMO and LUMO orbitals, confirmed by reduction of both ΔE_{ST} and oscillator strength (from 540 to 289 meV and 0.558 to 0.394, respectively). The almost two times reduction of ΔE_{ST} was achieved by selectively altering lowest singlet energy S_1 (from 3.69 to 3.43 eV), while keeping the lowest triplet energy T_1 relatively the same (from 3.15 to 3.14 eV).

The success of modifications were clearly visible in photophysical properties of the compounds. The absorption of **tCbz-mPYRs** was two folds lower compared to **Cbz-PYR** due to reduced oscillator strength, as a consequence of smaller HOMO and LUMO overlap, and peaked at wavelengths 339 and 336 nm, respectively. The fluorescence peaked at 379 and 423 nm for compounds **Cbz-PYR** and **tCbz-mPYRs**, respectively. The enlarged conjugation of donor unit together with sulphur atom redshifted the emission. In solid state, the emission peak of compound **tCbz-mPYRs** was blueshifted to 415 nm when embedded in 1 wt% PMMA film, while in 10 wt% DPEPO host, the emission was redshifted to 428 nm according to emission spectra in toluene.

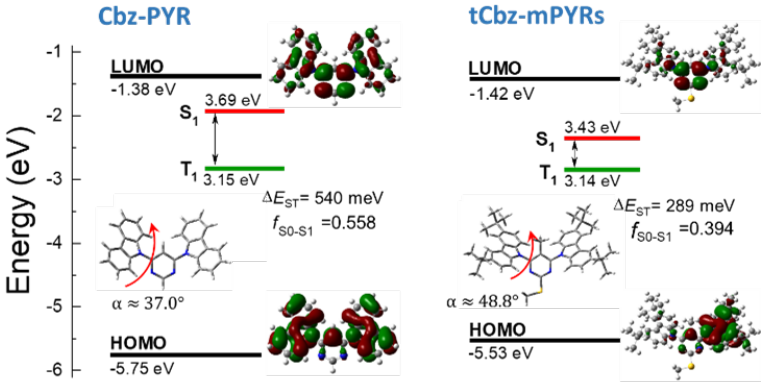

Figure 3.2: Electron densities of HOMO and LUMO, their energies, lowest singlet and lowest triplet energies, oscillator strengths and ΔE_{ST} gaps and torsion angle of D-A of compounds **Cbz-PYR** and **tCbz-mPYRs**.

These shifts were mediated by different polarity of the hosts as well as conformational disorder. The phosphorescence shows vibronic resolution due to

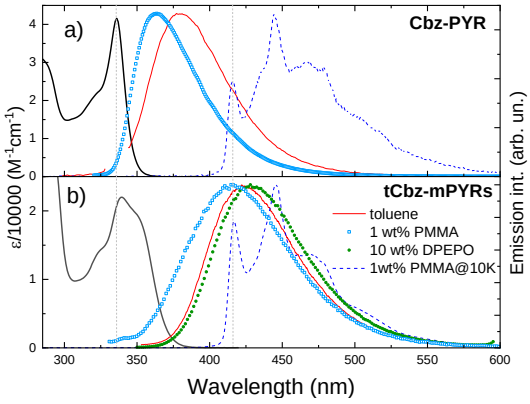

Figure 3.3: Absorbance, fluorescence emission and phosphorescence spectra of compounds **Cbz-PYR** and **tCbz-mPYRs** in 10^{-5} M toluene solution, 1 wt% PMMA films, 10 wt% DPEPO film.

originating from donor unit and being of ^{3}LE nature. The peak of 0-0 transition remains relatively unchanged in both **Cbz-PYR** and **tCbz-mPYRs** (416 and 417 nm, respectively), resulting in significantly lower ΔE_{ST} for compound **tCbz-mPYRs**, especially when embedded in DPEPO host (290 meV).

Fluorescence quantum yield (Φ_F) in dilute solutions were similar for both **Cbz-PYR** and **tCbz-mPYRs** – 0.1 and 0.07, respectively, though minor decrease of yield was attributed to changes of radiative and non-radiative decay rates. The k_r was reduced 2.6 times due to smaller f of CT emission, however it was offset by a 1.8 time slower non-radiative decay due to increase steric

hindrance of the compound **tCbz-mPYRs**.

No TADF was observed in, even oxygen-free, toluene solutions, typical for deep-blue TADF emitters [122, 123]. However strong TADF emission was observed in 1 wt% PMMA and 10 wt% DPEPO films of **tCbz-mPYRs** where non-radiative decay is remarkably impeded. The TADF nature was implied due to observed activation by temperature and susceptibility to molecular oxygen. Meanwhile, **Cbz-PYR** displayed only weak RTP as the triplet states were unable to upconvert by virtue of high ΔE_{ST} gap. Fluorescence quantum yields were enhanced to 0.44 and 0.5 in oxygen free PMMA and DPEPO films, with Φ_{TADF} amounting to 0.42 yield.

Though the TADF decay was moderately distorted by conformational disorder, a multi-exponential fit allowed to estimate the TADF lifetime of about 143 µs and rISC rate of $k_{rISC} \approx 3 \times 10^4\,s^{-1}$ of compound **tCbz-mPYRs** in 10 wt% DPEPO film, comparable to to some of the other deep-blue TADF emitters [124].

3.1.2. Deep-blue OLED device

The performance of **tCbz-mPYRs** was evaluated in the following device configuration: ITO/TAPC (30 nm)/TcTa (5 nm)/10 wt% **tCbz-mPYRs**:DPEPO (20 nm)/DPEPO (5 nm)/TmPyPb (50 nm)/LiF (0.8 nm)/Al (100 nm). The device showed deep-blue electroluminescence which peaked at 441 nm with CIE coordinates (0.16, 0.12) at luminescence of 100 cd/cm^2 (Figure 3.4). The external quantum efficiency of 8.7 % was evaluated, comparable to other efficient deep-blue OLED emitters [125–127]. However the efficiency suffered from pronounced roll-off at higher luminescence values, due to slow decay lifetime of TADF and low electroactivity of DPEPO host, though this problem is frequent with other deep-blue TADF OLEDs [128].

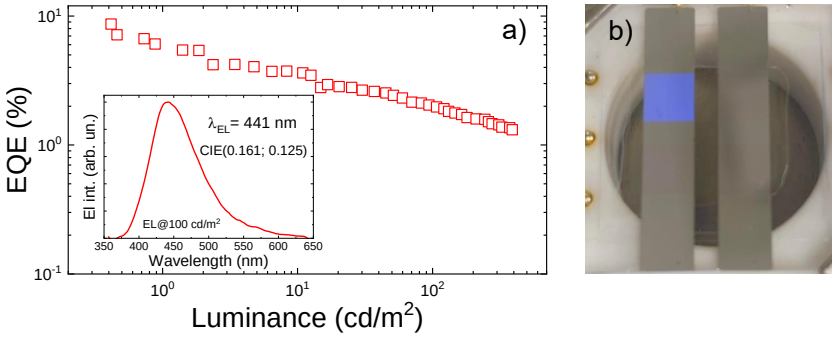

Figure 3.4: a) External quantum efficiencies of OLED devices with **tCbz-mPYRs** as emitter at different luminance values. Inset the emission spectra of the same OLED device at luminance of 100 cd/m^2. b) Photo of manufactured device.

To summarize, an approach to design deep-blue TADF emitter was presented. Carbazole–pyrimidine–carbazole compound displaying high triplet energy and RTP was modified by increasing electron donating properties of donor fragment, increasing twist angle of D-A by methyl group and enhancing ISC and rISC via heavy sulphur atom. The modifications resulted in greatly reduced ΔE_{ST} enabling efficient ($\Phi_F = 0.5$) TADF emission with an average lifetime of 147 µs in 10 wt% DPEPO film. OLED device produced with **tCbz-mPYRs** emitter exhibited deep-blue emission with CIE coordinates (0.16, 0.12) and comparable high EQE of 8.7 %. Modification of promising carbazole-pyrimidine compound proved to be a simple, yet successful strategy for designing efficient deep-blue TADF emitter.

These results are presented in more detail in paper **[A5]**.

In the next section, the deep-blue emission will be sacrificed in order to gain higher efficiency.

3.2. Control of decay rates through linking patterns

Another strategy to reduce ΔE_{ST} was deployed on **Cbz-PYR** core. Firstly, the phenyl spacer was introduced between donor and acceptor unit to decrease HOMO–LUMO overlap (**1CbzPYR**) (Figure 3.5), however the redshift of emission, due to increased conjugation, is expected. A further reduction of ΔE_{ST} was sought by altering linking pattern of carbazole donor, when two donor units were attached to acceptor core at *meta* positions of phenyl spacer to produce **2CbzPYR**. Finally, a third donor unit at *para* position was crammed in order to increase steric hindrance due to crowding effect (similarly to **4CzPN** compound discussed in chapter 1). The increased rigidity should suppress non-radiative decay pathways therefore enhancing TADF emission properties and reducing unwanted effects of conformational disorder in solid-state.

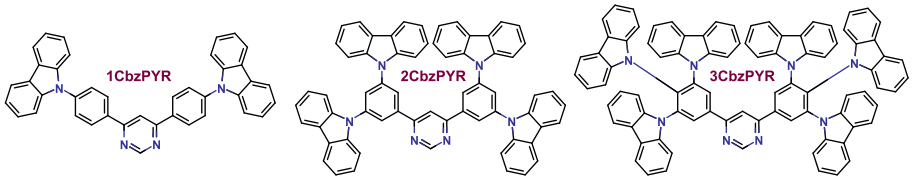

Figure 3.5: Molecular structures of phenyl-pyrimidine acceptor decorated by one (**1CbzPYR**), two (**2CbzPYR**) or three (**3CbzPYR**) carbazole donor units.

3.2.1. Quantum chemistry

The initial DFT simulations revealed that the phenyl-pyrimidine unit is rather flat in all compounds with dihedral twist angles in the range 14.5–16.5°, with the molecules containing more bulky donor fragments showing slightly lower angles (Figure 3.6). The angles between carbazole donor units and phenyl spacer were more perpendicular as they ranged from 52° for **1CbzPYR** to 56.5–67.8° for **3CbzPYR**, with the *meta* carbazole units having larger angle compared to *para* units. As expected, introduction of more carbazole units reduced LUMO

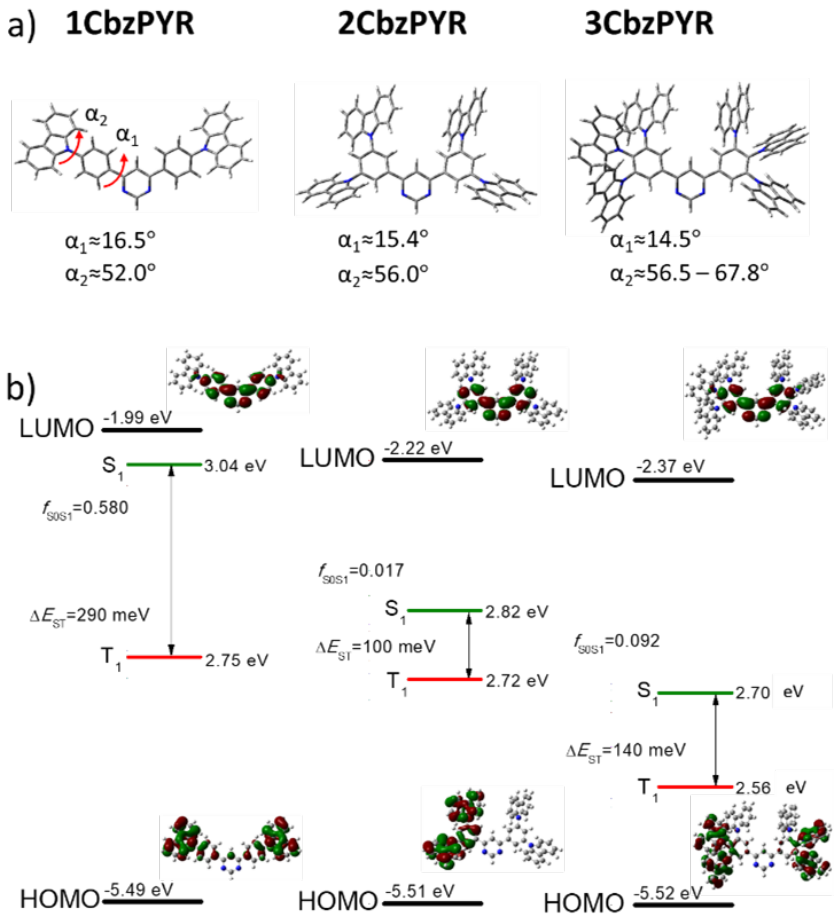

Figure 3.6: a) Optimized geometries of carbazole-pyrimidine TADF compounds and dihedral angles between phenyl-pyrimidine (α_1) and carbazole-phenyl (α_2); Energies and electron distributions of HOMO and LUMO orbitals as well as estimated oscillator strength and ΔE_{ST} values are denoted.

level (−1.99, −2.22 and −2.37 eV, respectively) while preserving same HOMO energy (from −5.49 to −5.52 eV) therefore energy bandgap was reduced due

to increased conjugation and promoted CT character. This should result in a redshift of emission for compounds with more donor untis.

The HOMO–LUMO overlap decreased due to the phenyl spacer and ΔE_{ST} was reduced for compound **1CbzPYR** compared to **Cbz-PYR** (290 and 540 meV), yet not low enough for efficient TADF. The compound with two donor units showed most decoupled HOMO–LUMO orbitals and lowest ΔE_{ST} of 100 meV with smallest oscillator strength (0.017), while introduction of *para* carbazole reinforced the HOMO–LUMO overlap leading to ΔE_{ST} of 140 meV and oscillator strength of 0.092.

3.2.2. Evaluation of emission properties

The effects of increased conjugation were evident in absorption and emission spectra of dilute toluene solutions, where direct CT absorption band peak shifted from 355 to 378 nm and the fluorescence peaked at 408, 442 and 464 nm for compounds **1CbzPYR**–**3CbzPYR**, respectively (Figure 3.7). Similar emission peak wavelengths of 408, 440 and 446 nm were observed for compounds **1CbzPYR**–**3CbzPYR** in 1 wt% PMMA films, where the slight blueshift of compound **3CbzPYR** was probably mediated by lower polarity of PMMA and small conformational disorder of more rigid molecular core. On the other hand, the blueshift of compounds **1CbzPYR** and **2CbzPYR** in lower ambient polarity, might be compensated by redshift of emission caused by conformational disorder, which is more pronounced in labile molecules. The emission of 10 wt% DPEPO film for compound **3CbzPYR** showed more CT character and larger redshift due to increased polarity of the host.

Phosphorescence spectra acquired at 10 K with 100 µs delay showed vibronic structure and was, therefore, attributed to ^{3}LE state. The evaluated ΔE_{ST} values in PMMA films were 480, 270 and 320 meV for compounds **1CbzPYR**–**3CbzPYR**, respectively. The singlet-triplet gap followed the same trend as predicted by DFT calculations: introduction of second donor unit lowered the ΔE_{ST} gap, while, for compound with three donor units, ΔE_{ST} increased due to somewhat boosted HOMO–LUMO coupling through *para*-carbazole. The ΔE_{ST} for compound **3CbzPYR** was further lowered to 110 meV when embedded in more polar 10 wt% DPEPO host.

To evaluate the effects of conformational disorder, time-resolved spectra of compounds **2CbzPYR** and **3CbzPYR** were recorded and are presented in figure 3.8. As expected a large temporal redshift of 380 meV is observed for flexible compound **2CbzPYR**, followed by a blueshift of 310 meV, therefore the latest emissive states are quenched. Meanwhile the more sterically constrained compound **3CbzPYR** showed remarkably smaller redshift of 240 meV followed by a blueshift of 190 meV. The smaller difference between shifts suggest lower quenching of the latest states. **1CbzPYR**, on the other hand, showed no delayed emission due to large ΔE_{ST}.

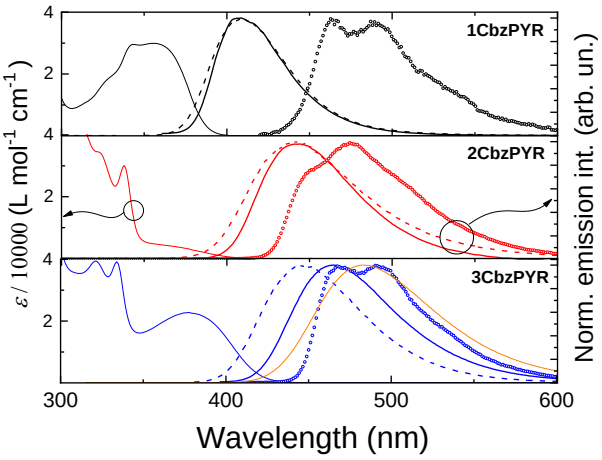

Figure 3.7: Absorption, fluorescence and phosphorescence spectra of carbazole-pyrimidine compounds acquired in: 10^{-5} M toluene solution (solid lines), 1 wt% PMMA films (dashed lines), 10 wt% DPEPO films (orange solid line for **3CbzPYR**). Phosphorescence spectra (open dots) were acquired at 10 K in PMMA films.

The decay transients for carbazole-pyrimidine compounds in 10^{-5} M toluene solutions and 1 wt% PMMA films are presented in figure 3.9. Both **2CbzPYR** and **3CbzPYR** showed bi-exponential decay of prompt and delayed emission while for compound with the largest ΔE_{ST} **1CbzPYR** only prompt emission was observed. The delayed emission was proven to be TADF due to susceptibility to molecular oxygen and activation with temperature.

The decay lifetime of prompt emission was fastest for **1CbzPYR** with strongest oscillator strength and LE type emission, while compounds with bulkier donor fragments showed remarkably slower decay in both solution and PMMA ambient. Assessed rates of prompt and delayed emission in toluene solutions, together with efficiencies are presented in table 3.1.

A remarkably low k_r of $0.7 \times 10^7\,s^{-1}$ was registered for **2CbzPYR**, with largest HOMO–LUMO decoupling. This, in conjunction with largest non-radiative decay rate of $11 \times 10^7\,s^{-1}$, resulted in lowest Φ_{PF} of 0.057. In contrast, rapid radiative decay rate ($2.9 \times 10^7\,s^{-1}$), one of the largest for TADF compounds [129], together with moderate k_{nr} ($3.8 \times 10^7\,s^{-1}$) ensured an exceptional prompt fluorescence yield of 0.43 for compound **3CbzPYR**. The Φ_{PF} and k_{fl} remained relatively the same in rigid PMMA film. This led to similar k_{nr} values in both surroundings, meaning that non-radiative decay pathway occurring through vibrations of molecular core, could be neglected and the dominating non-radiative decay could be assigned to ISC [83].

Similar trends were observed for delayed emission, the compound with larger prompt fluorescence yield, **3CbzPYR**, showed more efficient delayed fluores-

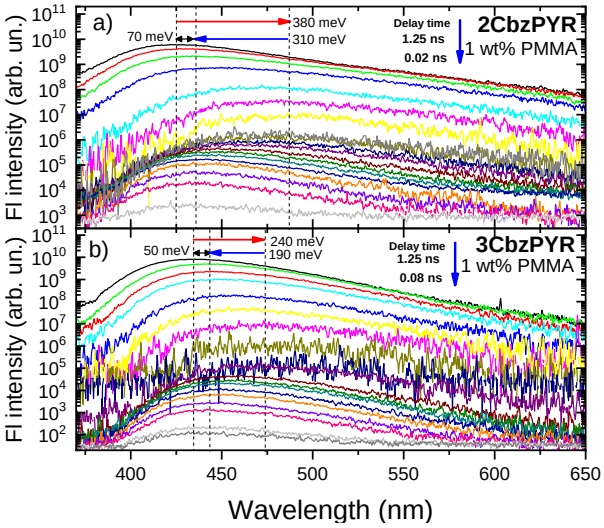

Figure 3.8: Time-resolved spectra of compounds **2CbzPYR** (a) and **3CbzPYR** (b) in 1 wt% PMMA film. Red and blue horizontal arrows depicts redshift of prompt emission and blueshift of delayed emission, respectively.

Table 3.1: Fluorescence and TADF properties for carbazole-pyrimidine compounds in 10^{-5} M toluene solutions.

	$k_{fl}/k_r/k_{nr}$ ($10^7\,s^{-1}$)	$k_{TADF}/k_{ISC}/k_{rISC}/k_{nr}^T$ ($10^7\,s^{-1}$)	$\Phi_{PF}/\Phi_{DF}/\Phi_{ISC}/\Phi_{rISC}$
1CbzPYR	26.0/22.0/3.9	–/3.9/–/–	0.85/–/0.15/–
2CbzPYR	11.0/0.7/11.0	2.2^a/11.0/1.2^b/2.2^a	0.057/0.003/0.94/0.05
3CbzPYR	7/2.9/3.8	0.7^a/3.8/1.9^b/0.6^a	0.43/0.07/0.57/0.25

$^a \times 10^5\,s^{-1}$. $^b \times 10^4\,s^{-1}$.

cence. Meanwhile **2CbzPYR**, with low molecular rigidity, displayed high non-radiative triplet quenching (k_{nr}^T) which dominated, being about 18 times higher than k_{rISC}, and resulted in negligible Φ_{DF}. Moreover, low k_r rate in conjunction with high k_{ISC} rate ($0.7 \times 10^7\,s^{-1}$ *vs.* $11 \times 10^7\,s^{-1}$, respectively) ensured that majority of upconverted excitons would cycle back to triplet states via ISC until they decay non-radiatively through k_{nr}^T. For **3CbzPYR**, however, the non-radiatively triplet pathway was suppressed by steric confinement of carbazole units. Together with high k_r, this ensured delayed fluorescence yield up to 0.07.

Further increase of Φ_{DF} was achieved in PMMA films. Here, the suppression of k_{nr}^T increased TADF yield to 0.16 and 0.33 and Φ_{PL} to 0.22 and 0.81 for compounds **2CbzPYR** and **3CbzPYR**, respectively. Despite the suppressed non-radiative decay pathway **2CbzPYR** still suffered from low k_r and, therefore, the performance of this compound was still poor.

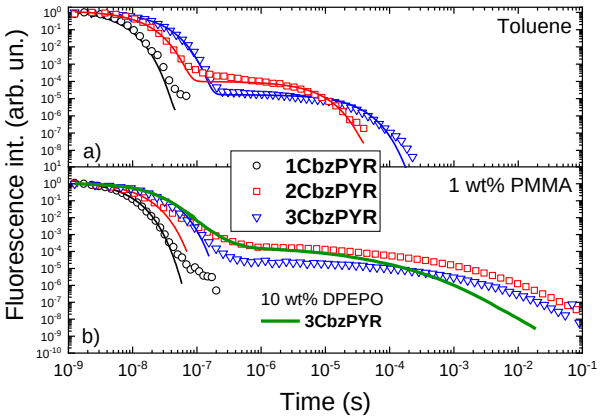

Figure 3.9: Decay transients of compounds **1CbzPYR**–**3CbzPYR**in 10^{-5} M toluene solutions (a) and 1 wt% PMMA films (b). Decay kinetic of **3CbzPYR** in 10 wt% DPEPO film is also presented as a solid green line.

3.2.3. Device performace

Due to efficient TADF and fast radiative decay, compound **3CbzPYR** was exploited as emitter. The OLED device was constructed with the following structure: ITO/TAPC (30 nm)/TCTA (5 nm)/10 wt% **3CbzPYR**:DPEPO (15 nm)/TmPyPB (65 nm)/LiF (0.8 nm)/Al (100 nm). Blue electroluminescence peaking at 473 nm with CIE coordinates of (0.16, 0.23) was observed from fabricated device. The OLED demonstrated exceptional peak external quantum efficiency of 19.7 % which is inline with large Φ_F assuming 20–30 % outcoupling efficiency. Moderate EQE roll-off was observed at larger luminance due to the average solid-state TADF lifetime of **3CbzPYR** and the weak electroactivity of the DPEPO host, though the latter issue could be solved by further optimization of the OLED architecture.

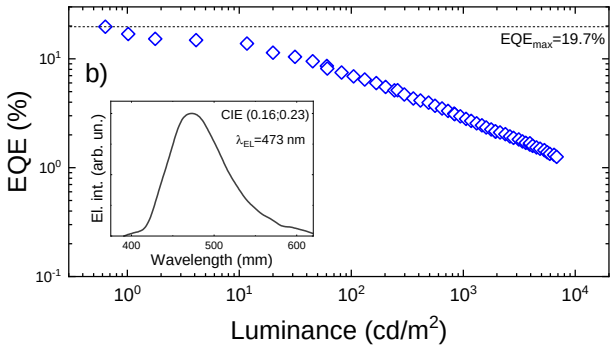

Figure 3.10: External quantum efficiency at different luminance values of OLED device with **3CbzPYR** emitter. Inset: electroluminance spectrum of device at 850 cd/m^2.

Summary of the results

To summarize, altering number and linking pattern of donor units in carbazole-phenylpyrimidine compounds proved to be an efficient way to optimize fluorescence decay rates and achieve efficient TADF emission.

The singlet energies where tuned by introducing more carbazole units without altering the triplet energies much. This enabled TADF emission in compounds with two or three carbazoles, which was absent in compound with one *para*-carbazole. Prompt and delayed fluorescence properties, on the other hand, were drastically different for both compounds. Low overlap of HOMO–LUMO orbitals, in double *meta*-carbazole substituted **2CbzPYR**, drastically lowered radiative decay rate, which was outcompeted by rapid intersystem crossing and resulted in low emission yield. Even with pronounced ISC rate, **2CbzPYR** showed low TADF yield as the majority of triplets were quenched by the rapid nonradiative decay, promoted by rather flexible molecular structure. The nonradiative singlet and triplet decays were suppressed by introducing another *para*-carbazole unit, boosting prompt and TADF emissions to 0.43 and 0.33, respectively. The stiffened core also reduced redshift induced by conformational disorder. The compound **3CbzPYR** with optimized donor-acceptor architecture was used as blue emitter in OLED device. Highly efficient electroluminescence with peak EQE of 19.7 % and colour coordinates of (0.16, 0.23) was achieved. The results are presented in more detail in paper [**A6**].

In the next section, a different molecular structure with a known fast TADF lifetime will be further improved.

3.3. Fine-tuning rISC rate by small methyl modifications

Another popular donor fragment phenoxazine (PXZ), known for its strong electron donating properties, is commonly used to construct efficient emitters in sky-blue – yellow color region [96, 130–136]. It was shown that PXZ, in conjunction with diphenyl-pyrimidine acceptor unit (**PXZ-PYR**), can exhibit fast ($\tau_{\mathrm{TADF}} = 2.56\,\mu\mathrm{s}$) which can be utilized in devices with EQE of 19.9 % [136]. Further modifications with aryl and phenyl groups on pyrimidine acceptor lowered the TADF lifetime to 1.99 µs in together enhancing the EQE up to 24.6 % [135, 136]. Another strategy of incorporating a heavy Cl or Br atom to accelerate ISC and rISC resulted in enhanced τ_{TADF} of 1.32 µs and EQE of 25.3 % [96], however the inclusion of heavy atom results in redshift of emission – an unwanted effect when aiming for blue emitters [96, 97].

Inspired by good efficiency and rapid TADF we upgraded this compound by modifying **PXZ-PYR** with either *ortho*-methyl (**PXZ-mdPYR**) or *meta*-methyl (**PXZ-muPYR**), or both *meta* and *ortho* methyl modifications (**PXZ-2mPYR**) (Figure 3.11), to increase k_{rISC} while maintaining sky-blue – green emission.

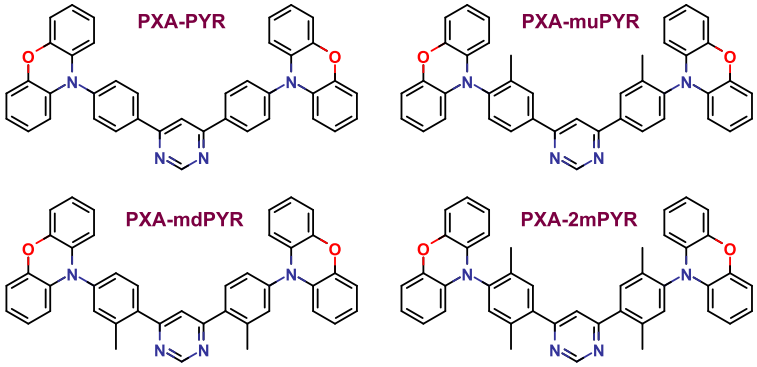

Figure 3.11: Molecular structures of compounds **PXZ-PYR**, **PXZ-muPYR**, **PXZ-mdPYR** and **PXZ-2mPYR**.

3.3.1. Tuning of decay rates

The initial DFT calculations revealed that the angle between the donor fragment and phenyl spacer was almost orthogonal with some slight variations (84.05–89.62°), for all compounds. On the other hand, the phenyl rings were only slightly twisted (19°) in respect to pyrimidine unit for both **PXZ-PYR** and **PXZ-muPYR** while introduction of *ortho*-methyl unit increased the twist angle to nearly 43° due to enhanced steric hindrance. This also led to increase of LUMO energies from −2.04 and −2.10 eV for **PXZ-PYR** and **PXZ-muPYR**, respectively, to −1.82 and −1.88 eV for **PXZ-mdPYR** and **PXZ-2mPYR**, respectively, weakening the electron-accepting ability and enlarging bandgap, while maintaining HOMO energies relatively same (from −4.79 to −4.76 eV). The enlarged badgap should result in blueshift of emission for compounds with methyl moiety. The larger twist in *ortho*-methyl modified compounds also led to reduced HOMO-LUMO overlap and reduction of oscillator strength from 0.0016 and 0.0013 for compounds **PXZ-PYR** and **PXZ-muPYR**, respectively, to 0.0002 and 0.0003 for **PXZ-mdPYR** and **PXZ-2mPYR**, respectively.

The absorption and emission spectra in 10^{-5} M toluene solution are presented in figure 3.12a. Two absorption regions can be discerned: first at about 280–350 nm, which is comprised of individual absorption of donor and acceptor fragments, and second at about 360–450 nm, attributed to charge transfer state. Fluorescence spectra of unmodified **PXZ-PYR** peaked at 543 nm, while the emission was blueshifted to 530, 528 and 519 nm for methyl modified compounds **PXZ-muPYR**, **PXZ-mdPYR**, **PXZ-2mPYR**, respectively, as predicted by DFT calculations. Therefore the introduction of methyl groups allowed us to tune CT emission wavelength for 100 meV.

The low temperature phosphorescence spectra in 1 wt% PMMA film, displayed clear vibronic progression, typical for locally excited triplet (^{3}LE) emis-

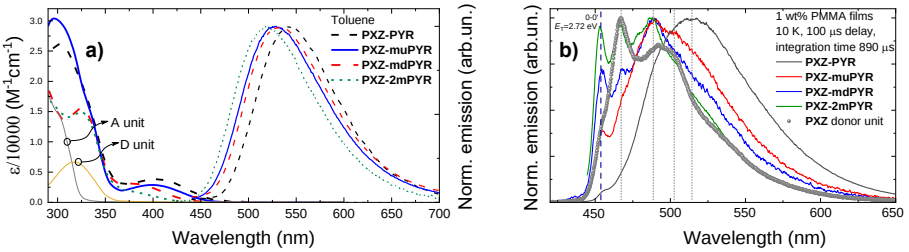

Figure 3.12: a) Absorption and emission spectra of compounds **PXZ-PYR**, **PXZ-muPYR**, **PXZ-mdPYR** and **PXZ-2mPYR** in 10^{-5} M toluene solutions together with absorption of separate pyrimidine (A) and phenoxazine (D) fragments; b) phosphorescence spectra of same compounds in 1 wt% PMMA films at 10 K temperature, measured at delay of 100 µs.

sion (Figure 3.12b). Vibronic bands of more rigid compounds **PXZ-mdPYR**, **PXZ-muPYR** and **PXZ-2mPYR** peaked at the same wavelengths as that of PXZ donor. On the other hand, the least sterically constrained **PXZ-PYR** exhibited strongly overlapped and broadened phosphorescence emission, yet weak 0^{th} vibronic band was still visible. Therefore phosphorescence of all compounds originated from the same donor fragment with the same T_1 energy of 2.72 eV. The ΔE_{ST} was estimated to be 10, 70, 150 and 130 eV for **PXZ-PYR**, **PXZ-muPYR**, **PXZ-mdPYR**and **PXZ-2mPYR**, respectively. Surprisingly, the ΔE_{ST} increased for compounds with smaller HOMO and LUMO overlap, this was made possible due to the ^{3}LE nature of the lowest triplet state.

All compounds produced bi-exponential decays in diluted toluene solutions and similar, yet multi-exponential due to conformational disorder, decay profiles in solid-state films (Figure 3.13). The origin of delayed fluorescence was attributed to TADF as it was quenched by oxygen and showed activation with temperature. The TADF lifetimes in toluene solutions were rather fast as the values ranged from 1.6 to 4.0 µs for compounds **PXZ-PYR**, **PXZ-mdPYR** and **PXZ-2mPYR**. The *meta*-methyl modified compounds **PXZ-muPYR** displayed τ_{TADF} of 0.8 µs which is among the lowest values reported for solutions [70, 97, 112, 137, 138].

TADF properties of all phenoxazine-pyrimidine are presented in table 3.2. Here, several important properties should be noted:

- The decreased TADF lifetime is related to reduced rotational flexibility of PXZ unit and the adjustment of ^{1}CT-^{3}LE energy gap by changing HOMO–LUMO overlap. The ^{3}CT-^{3}LE gap may also be altered, while spin-orbit coupling should remain relatively the same for similar molecules [139].

- The ISC and rISC rates suffered from increased ^{1}CT-^{3}LE energy gap for molecules with same flexibility of PXZ *i.e.*, the k_{rISC} decreased

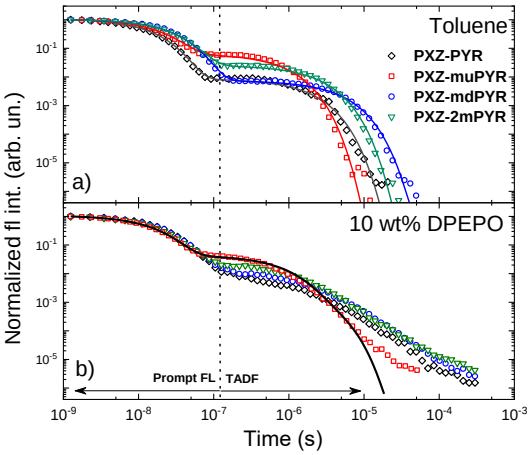

Figure 3.13: Decay transients of compounds **PXZ-PYR**, **PXZ-muPYR**, **PXZ-mdPYR** and **PXZ-2mPYR** in (a) 10^{-5} M toluene solutions and (b) 10 wt% DPEPO films.

from 1.8×10^6 to $0.7 \times 10^6\,\mathrm{s}^{-1}$ for compounds **PXZ-PYR** and **PXZ-mdPYR** with more labile donor unit and from 6.5×10^6 to $2.5 \times 10^6\,\mathrm{s}^{-1}$ for compounds **PXZ-muPYR** and **PXZ-2mPYR** with more constrained donor unit.

- Surprisingly, the increase in k_{rISC} was found for compounds with more sterically hindered PXZ units, lowered IC rates, and, supposedly, weakened vibronic coupling between ^{3}LE and ^{3}CT states (**PXZ-PYR** *vs.* **PXZ-muPYR** and **PXZ-mdPYR** *vs.* **PXZ-2mPYR**) [55]. The reduction of ^{3}LE and ^{3}CT energy gap was attributed to the cause of enhanced ISC and rISC rates for compounds with *meta*-methyl modifications (**PXZ-muPYR** and **PXZ-2mPYR**), though the mechanism is still debatable.

- Large Φ_{TADF} (0.42) of compound **PXZ-muPYR** was determined by the fastest ISC and rISC rates. However similar TADF quantum yield (0.43) was achieved by **PXZ-2mPYR** with lower rISC rate, due to reduced IC rate mediated by more rigid molecular structure.

The non-radiative pathways were suppressed even more in rigid surrounding of 1 wt% PMMA film. Here, the quantum yield was boosted to near unity for compounds **PXZ-PYR**, **PXZ-mdPYR** and **PXZ-muPYR** (0.92, 0.94 and 0.95, respectively), while for compound **PXZ-2mPYR** it remained lower at 0.72. Comparable Φ_{F} were estimated in 10 wt% DPEPO host, where increased ambient polarity redshifted emission peaks to 515–542 nm. Decay transients in DPEPO hosts were similar to those in toluene solution (Figure 3.13), however

Table 3.2: TADF properties of compounds: **PXZ-PYR**, **PXZ-muPYR**, **PXZ-mdPYR**, **PXZ-2mPYR** in oxygen-free toluene solution.

	Φ_{TADF}	ΔE_{ST} (meV)	τ_{TADF} (µs)	k_{IC} ($10^6\,s^{-1}$)	k_{ISC} ($10^7\,s^{-1}$)	k_{rISC} ($10^6\,s^{-1}$)
PXZ-PYR	0.27	10	1.6	16	4.8	1.8
PXZ-muPYR	0.42	70	0.8	5.6	4.9	6.5
PXZ-mdPYR	0.24	150	4	9.2	2.5	0.7
PXZ-2mPYR	0.43	130	2.1	3.7	3.4	2.5

the TADF decays were prolonged and multiexponential due to conformational disorder. Only the **PXZ-muPYR** with the shortest decay transient was successfully approximated with three-exponential fit. Average TADF lifetime of 860 ns was estimated, being one of the lowest among the ever reported various TADF emitters [19, 98, 138, 140].

3.3.2. Device performace

As pyrimidine–phenoxazine compounds showed promising TADF properties, OLED devices were prepared. Typical OLED structure used for similar devices [96, 135, 136] was employed, however the usual CBP host was exchanged for higher triplet energy host DPEPO, to efficiently confine triplet excitons in the emissive layer. The following structure was used: ITO/TAPC (30 nm)/TCTA (5 nm)/10 wt% TADF emitter:DPEPO (15 nm)/TmPyPB (65 nm)/LiF (0.8 nm)/Al (100 nm).

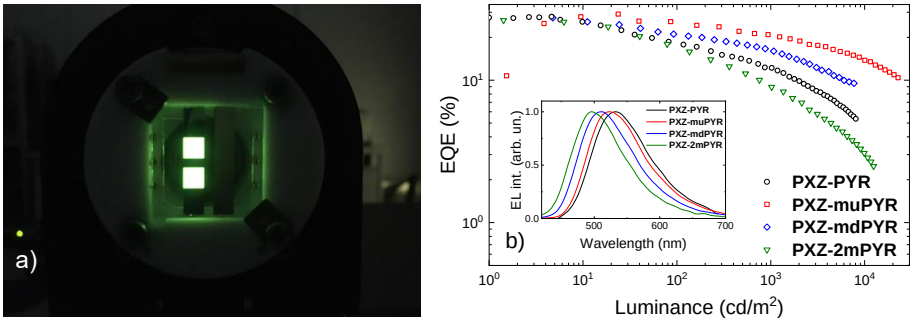

Figure 3.14: a) Prepared OLD devices with **PXZ-muPYR** used as emitter; b) External quantum efficiencies of OLED devices at different luminance values. Inset: electroluminance spectra of devices at driving voltage of 9 V.

Photo of the final device as well its EQE and electroluminance spectra are presented in figure 3.14. The EL emission color was successfully tuned from green, peaking at 536 nm for **PXZ-PYR** (CIE coordinates of (0.35.0.56)) to cyan, peaking at 502 nm for **PXZ-2mPYR** (CIE coordinates of (0.23,

0.42)). Exceptionally high EQE values of 27.9, 29.1, 27.5 and 26.3 % were obtained for compounds **PXZ-PYR**, **PXZ-muPYR**, **PXZ-mdPYR** and **PXZ-2mPYR**, respectively. These values are among the highest values reported for pyrimidine compounds without using any additional outcoupling technique (see Table S3 in the Supporting Information of [**A4**] for a comparison). The compound **PXZ-muPYR** not only showed the highest EQE of 29.1 %, but also distinguished with very low EQE roll-off as efficiency dropped to only 20.5 % at 1000 cd/m^2. A low EQE roll-off was achieved due to the short TADF lifetime of only 860 ns. The combination of submicrosecond TADF lifetime in solid-state along with EQE of nearly 30 % puts compound **PXZ-muPYR** among the best TADF emitters. Though other emitters displayed similarly high peak EQE values, the EQE roll-off was substantially worse due to longer TADF lifetimes and enhanced quenching by TTA or STA.

Summary of the results

To summarize, introduction of methyl group at phenyl spacer in pyrimidine-phenylphenoxazine compounds proved to be a powerful strategy for improving TADF properties. First, the introduction of *ortho*-methyl units were found to reduce the acceptor strength, resulting in enlarged ^{1}CT-^{3}LE gap, lowered rISC rate and TADF efficiency. Modification with *meta*-methyl fragments, on the other hand, increased the rISC rate up to $6.5 \times 10^6\,\mathrm{s}^{-1}$ producing one of shortest TADF lifetimes of 800 ns in dilute solutions. Lowering of ^{3}CT-^{3}LE gap was attributed to TADF enhancement. Introduction of both *meta*-methyl and *ortho*-methyl groups enlarged the ^{1}CT-^{3}LE energy gap, resulting in reduced rISC rate ant slowest TADF lifetime in solid-state. However, the weakened IC rate promoted radiative decay ensuring high TADF quantum yield.

The suppression of non-radiative pathways in solid-state enhanced emission quantum yield to near unity in PMMA films. Presence of conformational disorder was minimized by fast rISC rate in compound with *meta*-methyl which allowed to estimate (by three-exponential fit) one of the fastest reported TADF decay lifetime of 860 ns in 10 wt% DPEPO film. Such fast TADF resulted in high external quantum efficiency (29.1 %) device with very low EQE roll-off as efficiency dropped to only 20.5 % at 1000 cd/m^2.

Unmodified and *ortho*-methyl modified phenoxazine-pyrimidine produced efficient green OLEDs with EQE in rage of 27.5–27.9 %. Cyan EL with peak EQE of 26.3 % was obtained for compound with both *meta*-methyl and *ortho*-methyl modifications, though it suffered from large EQE roll-off due to prolonged TADF lifetime.

These results are presented in more detail in article [**A4**].

CONCLUSIONS

During this work several conclusions were drawn:

1. Requirement of twisted and somewhat liable D–A geometry for efficient TADF emission leads to several undesirable effects in solid-state, induced by conformational disorder, such as broadening and redshifting of emission spectra as well as prolonging TADF lifetime, which makes it susceptible to EQE roll-off. The disastrous effects of conformational disorder can be evaded by designing rigid molecular core or by increasing rISC rate.

2. Designing donor–acceptor molecules with hyperconjugated spacer (D–σ–A) leads to weak coupling between donor and acceptor resulting in extremely low radiative decay rate which can hardly compete with non-radiative decay pathways. This can lead to deceptive dual emission originating from intra- and intermolecular charge transfer states and is not favorable for TADF emission.

3. Molecular optimization of carbazole-pyrimidine compound by enhancing carbazole electron-donating abilities with *tert*-butyl units; sterically hindering D–A twist angle by methyl modification of pyrimidine moiety and introduction of sulphur heteroatom enabled TADF emission without disturbing lowest triplet energy. This allowed to produce a deep-blue (CIE 0.16, 0.12) and relatively efficient (EQE 8.7 %) TADF OLED device.

4. Introduction of additional carbazole donor units in carbazole-phenylpyrimidine structure decouples HOMO–LUMO orbitals reducing ΔE_{ST} gap and enables TADF emission. However double *meta*-carabazole substitute compound yields poor quantum efficiency due to both low prompt radiative and high triplet non-radiative decay rates. All of these drawbacks can be overcome by crowding with a third *para*-carbazole, which promotes radiative decay and shows good quantum yield 0.81. Blue (CIE coordinates (0.16, 0.23)) TADF OLED emitter was constructed with exceptionally high peak EQE of 19.7 %.

5. Introduction of small methyl fragments to phenyl ring of phenoxazine-phenylpyrimidine allowed manipulation of several TADF emission properties: first, the electroluminescence color was fine-tuned from green (536 nm) to cyan (502 nm); second, *meta*-methyl modification adjusted ^{1}CT-^{3}LE and ^{3}CT-^{3}LE energy gaps producing one of fastest TADF lifetime of 860 ns in solid-state. This enabled to create TADF OLED device with very high peak EQE of 29.1 % which retained efficiency of 20.5 % at high luminance of 1000 cd/m^2.

SANTRAUKA LIETUVIŲ KALBA

Įvadas

Gyvename įdomiais laikais, kuriuose sparčiai tobulėjančios technologijos nespėja tenkinti žmonių alkio naujiems technologiniams sprendimams bei patogumams. Išmani įranga tapo kasdieniu pagalbininku darbe bei buityje. Nors sparčiai plėtojamos technologijos, leisiančios tiesiogiai sujungti žmogaus smegenis su kompiuteriu [1–3], šiandiena ši galimybė labiau primena mokslinę fantastiką nei realybę. Šiuo metu ekranai išlieka pagrindine vartotojo sąsaja su prietaisais atveriančia vartus į beribes socialines platybes bei patogesnes darbo sąlygas. Šiais metais, užklupus globalinei Covid-19 pandemijai, socialinė atskirtis tapo vienintele apsisaugojimo priemone. Todėl, kaip niekada anksčiau, buvo stengtasi perkelti visą bendravimą už ekrano ribų. Nenuostabu, jog todėl reikalaujame vis geresnių vaizduoklių parametrų.

Stagnuojant išmaniųjų telefonų progresui, kiekvienas gamintojas stengiasi patraukti potencialius klientus beprecedentėmis funkcijomis ar neeiliniais dizaino sprendimais. Atkreipus dėmesį į paskutiniu metu skambiausiai reklamuojamas telefonų naujoves galime pastebėti šį tą bendro. Didelės raiškos, begalinio kontrasto („tikroji“ juoda spalva), sodrių spalvų bei lenkti vaizduokliai, sulankstomi telefonai, priekinės kameros bei pirštų antspaudo sensorius paslepimas po ekranu – visus šiuos išskirtinius ypatumus leido sukurti organinių šviestukų (OLED) ekranai. Televizorių bei monitorių gamintojai taip pat nesnaudžia. OLED technologija grįsti plonyčiai, priklijuojami prie sienos, suvyniojami ar net permatomą ekraną turintys televizoriai jau yra prieinami eiliniam vartotojui.

Nors organiniai junginiai karaliauja žemėje milijardus metų, jie visai neseniai įsiveržė į elektronikos pramonę. Puslaidininkinė organika suvienija puslaidininkių elektrines savybes su organikos plastikinėmis mechaninėmis ypatybėmis, įgalindama didelio ploto, spausdinamų bei gerais mechaniniais atsparumais pasižyminčių prietaisų realizaciją [4–6]. Dėl begalinės įvairovės organiniai junginiai pasižymi gausiu savybių spektru, viena iš jų – elektroliuminescencija – elektros srovės virtimas šviesa. Pirmą kartą elektroliuminescencija antraceno kristaluose buvo pastebėta 1963 m. [7], tačiau pirmasis organinis diodas buvo sukurtas tik 1987 m [8]. Vėlesnį dešimtmetį ši technologija buvo plėtojama ir sėkmingai komercializuota [9, 10].

Pirmosios kartos šviestukai buvo pagrįsti singletinių eksitonų fluorescencija, tačiau dėl sukinio statistikos ypatumų tik 25 % elektrinio sužadinimo yra singletinio pobūdžio, o likę 75 % injektuoto krūvio patenka į nespindulines tripletines būsenas [11]. Kartu su įprastine 20–30 % šviesos ištrūka iš prietaiso, pirmos generacijos šviestukų našumas buvo ne ką geresnis nei įprastų halogeninių lem-

pučių $< 5\,\%$.

Žemo našumo problema buvo išspęsta antros kartos fosforescenciniuose šviestukuose. Dėl įterpto sunkaus atomo juose, singletinės ir tripletinės būsenos, veikiamos stiprios sukinio–orbitos sąveikos, susimaišo, taip įgalindamos šviesos emisiją iš „tamsiųjų“ tripletinių būsenų [11, 12]. Tuo tarpu singletiniai sužadinimai yra konvertuojami į tripletinius dėl efektyvios interkombinacinės konversijos (ISC). Tokiu būdu visa emisija atsiranda iš tripletinių būsenų ir yra vadinama fosforescencija, o vidinis molekulės našumas gali siekti $100\,\%$, taigi prietaiso našumas yra ribojamas tik šviesos ištrūkos. Nors antrosios kartos šviestukai yra naudojami ligi šiol, jų gamybai reikalingi brangūs, toksiški sunkieji metalai tokie kaip iridis ar platina, taip pat jie nėra ilgaamžiški [13].

2012 m. Adachi *et al.* realizuodamas E tipo uždesltąja emisija [14] pagamino našų, visiškai organinį trečiosios kartos šviestuką [15–17]. Šiuo atveju tripletinis sužadinimas yra konvertuojamas į singletinį atgalinės interkombinacinės konversijos (rISC) metu, kurią įgalina aplinkos terminė energija molekulėse su mažu (įprastai nedidesniu nei 200 meV) energiniu tarpu tarp singletinės ir tripletinės būsenų (ΔE_{ST}). Konvertuoti sužadinimai gali relaksuoti spinduliniu būdu, todėl jų emisija yra vadinama termiškai aktyvuota uždelstąją fluorescencija (TADF). Kadangi visi elektriškai injektuoti krūvininkai turi galimybę išsispinduliuoti, tokių spinduolių vidinis našumas siekia iki $100\,\%$ [18, 19].

TADF šviestukai techninėmis charakteristikomis nenusileidžia šiuo metu plačiausiai naudojamiems fosforescenciniams šviestukams, tačiau yra kur kas paprastesnis ir elegantiškesnis, pilnai organinis sprendimas. Deja, šios kartos šviestukai dar nėra komercializuoti, nors tai įnirtingai stengiasi pasiekti kompanijos Kylux ir Cynora. Vis dėlto, išlieka keltas neišspręstų problemų, tokių kaip stiprus našumo krytis (roll-off) prie didesnių šviestuko galių, mažas sodriai mėlynų šviestukų efektyvumas ar trumpas prietaiso tarnavimo laikas.

Darbo tikslas ir naujumas

Nors termiškai aktyvuotos uždelstosios fluorescencijos (TADF) tyrimai yra viena populiariausių temų organinių šviestukų pasaulyje, tam tikri efektai, kaip konformacinės netvarkos įtaka emisijos savybėms kietame kūne, išlieka ganėtinai menkai ištirti. Taip pat, paskutiniu metu yra intensyviai siekiama komercializuoti šią technologiją, tačiau aiškių molekulinio dizaino strategijų trūkumas stabdo šį procesą.

Šio darbo tikslas yra išnagrinėti molekulinių donor–akceptorinių darinių modifikacijų įtaką termiškai aktyvuotos uždelstosios fluorescencijos savybėms bei pasiūlyti struktūrinės optimizacijos būdų siekiant sukurti našius mėlynos spalvos šviestukus.

Sprendžiami uždaviniai

Darbo tikslui įgyvendinti buvo išsikelti uždaviniai:

- Pasitelkti laike koreliuotą spektroskopiją siekiant atlikti nuodugnią termiškai aktyvuotos uždelstosios fluorescencijos analizę įvairiuose D–A organinininiuose junginiuose su pirimidino akceptoriumi bei karbazolo, fenotiazino bei fenoksazino donoriniais fragmentais.

- Išanalizuoti konformacinės netvarkos nulemtus efektus kietoje terpėje bei jų priklausomybę nuo molekulės standumo ar kitų parametrų.

- Atskleisti dvigubos, sparčios uždelstosios emisijos prigimtį dariniuose su donoras–σ–akceptorius struktūra ir įvertinti jų tinkamumą TADF šviestukams.

- Pagerinti įvairių D–A struktūros TADF spinduolių emisijos spalvą, našumą bei spartą atliekant įvairius nedidelius struktūrinius pakeitimus, kaip metilo grupės ar sunkaus atomo įterpimas.

- Pagaminti ir pademonstruoti veikiančius šviestukus panaudojant geriausias molekulines struktūras tirtas šiame darbe bei ivertinti jų elektroliuminescencines savybes.

Ginamieji teiginiai

- Kai kurie nepageidaujami šalutiniai efektai, atsirandantys dėl konformacinės netvarkos, nulemtos labilios D–A struktūros, gali būti sumažinti standinant molekulinę struktūrą ar paspartinus atgalinę interkombinacinę konversiją (rISC).

- Donoro ir akceptoriaus atskyrimas per hyperkonjuguotą σ jungtį, drastiškai sumažina spindulinės fluorescencijos spartą kartu sumažindamas ir uždelstosios emisijos efektyvumą, todėl tokia architektūra nėra lengvai pritaikoma TADF spinduoliuose.

- Gerą kvantinį našumą karbazolo–pirimidino TADF dariniuose galima pasiekti ne tik delokalizuojant π–elektronų sistemą, bet ir selektyviai optimizuojant donorinių fragmentų skaičių bei jų jungimo poziciją.

- Selektyvi fenoxazino–pirimidono D–A–D darinių modifikacija metilo pakaitais leidžia pasiekti mažesnes nei mikrosekundės TADF gesimo trukmes kietoje terpėje taip sumažinant efektyvumo krytį esant dideliam prietaiso šviesiniam skaisčiui.

Autoriaus indelis

Autorius atliko visus fotofizikinių savybių charakterizavimo bei spektroskopijos eksperimentus, susistemino ir išanalizavo rezultatus. Autorius taip pat ruošė pats bei glaudžiai bendradarbiavo su bendraautoriais rengiant publikacijas.

Didžiosios dalių junginių, analizuotų šiame darbe, sintezę atliko organinės chemijos grupė, vadovaujama prof. Sigito Tumkevičiaus (Vilniaus universitetas). Dalis kitų junginių buvo sintetintos prof. Vytauto Getaučio (Kauno technologijos universitetas) bei prof. Chihaya Adachi (Kiūšiū universitetas, Japonija) vadovaujamose grupėse. Teorinį modeliavimą atliko dr. Tomas Serevičius (Vilniaus universitetas) bei dr. Alytis Gruodis (Vilniaus universitetas). DSC eksperimentą atliko bei duomenis susistemino dr. Regimantas Komskis (Vilniaus universitetas). Visus organinių diodų prietaisus (OLED) pagamino ir ištyrė Dovydas Banevičius (Vilniaus universitetas).

Autorius džiaugiasi turėjęs galimybę bendradarbiauti su šiais puikiais žmonėmis ir dėkoja už jų indelį.

Vienoje plačiausiai naudojamų TADF spinduolių sandaroje donoro ir akceptoriaus fragmentai yra steriškai fiksuojami beveik statmenoje konfigūracijoje, taip sumažinant singleto–tripleto energijos (ΔE_{ST}) tarpą ir užtikrinant efektyvią atgalinę interkombinacinę konversiją (rISC) [86, 87]. Tačiau siekiant didelės rISC spartos taip pat svarbi ir vibroninė sąveika tarp ^{3}LE ir ^{3}CT lygmenų, kuri reikalauja šiokio tokio sukamojo laisvumo tarp donoro (D) ir akceptoriaus (A) dalių [52, 57, 59–61]. Kietoje terpėje tokios molekulės „užšąla“ skirtingose konformacijose, su įvairiais kampais tarp D ir A bei TADF emisijos savybėmis [55, 66, 67]. Ši konformacijų įvairovė sukelia keletą nepageidaujamų efektų: emisijos spektrai išplatėja (nepalanku spalvotiems ekranams siekiančiams grynų spalvų), o TADF gesimo trukmės išilgėja, taip sukeldamos šviestuko efektyvumo krytį (roll-off) prie didelių šviesių [62, 65, 68, 88, 89]. Nepaisant akivaizdaus konformacinės netvarkos poveikio TADF emisijai, šis reiškinys nėra plačiai išanalizuotas.

Siekiant gilesnės įžvalgos į konformacinės netvarkos nulemtus procesus, publikacijoje **[A3]**, pasitelkus laike–koreliuotą spektroskopiją, buvo nuodugniai ištirtos ir palygintos dvi grupės junginių, pasižyminčių panašiomis emisijos savybėmis, bet skirtingu molekuliniu kietumu. Pirmoje grupėje buvo lyginamas darinys 4,6-bis(2-metil-4-(10H-fenotiazin-10-il)fenil)pirimidinas (**PTZ-mPYR**), sudarytas iš fenil-pirimidno akceptoriaus sujungto su fenotiazino donoru per labilią metilo jungtį, su 1,2,3,4-tetrakis(karbazol-9-il)-5,6-dicianobenzenu (**4CzPN**), kuriame dicianobenzeno akceptorius sujungtas su keturiais karbazolo donorais. Dėl tankiai, šalia vienas kito, išsidėsčiusių karbazolų tarpusavio sąveikos, jų sukimasis buvo apribotas.

Minkšta **PTZ-mPYR** molekulė pasižymėjo didele įvairove konformerų su skirtingais kampais tarp donoro ir akceptoriaus, kartu ir didele įvairove TADF emisijos savybių, kurių suma nulėmė plačius emisijos spektrus (spektro pusplotis iki 670 meV) bei ilgas gesimo trukmes (trukmių įvertinti nepavyko dėl multieksponentinės prigimties) kietoje terpėje. Taip pat, buvo pastebėta, jog konformerai su didžiausiu ΔE_{ST}, kartu ir mažiausia rISC sparta ir mėlyniausia emisijos spalva buvo gesinami net bedeguonėje aplinkoje, taip sukeldami emisijos spektro poslinkį per 150 meV į raudonąją pusę. Visų šių neigiamų efektų buvo išvengta molekulėje su apribotu donorinių fragmentų sukimusi – **4CzPN**. Dėl mažos kampų bei ΔE_{ST} energijų įvairovės šio darinio emisijos spalva nekito kietoje terpėje, o TADF gesimo trukmė išaugo palyginti nedaug (nuo 15.5 µs iki 46 µs). Ta pati tendencija buvo stebima ir minkštą fenotiazino fragmentą pakeitus kietesniu fenoksazino donoru – nepageidaujami konformacinės netvarkos efektai buvo sumažinti, tačiau ne taip drastiškai kaip **4CzPN** atveju dėl palyginti minkštesnės molekulės konfiguracijos.

Kita sėkminga strategija išvengti kenksmingų konformacinės netvarkos

padarinių buvo pademonstruota publikacijoje [**A1**]. Prie to pačio **PTZ-mPYR** darinio akceptoriaus prijungus sunkų chloro atomą, dėl sukinio–orbitos sąveikos, buvo pagreitinta rISC sparta nekeičiant molekulės kietumo D–A kampo atžvilgiu. Dėl sumažėjusios TADF gesimo trukmės (nuo 11 µs iki 1.1 µs tirpale) net konformacijos su didžiausiomis ΔE_{ST} vertėmis spėdavo išsispinduliuoti, todėl raudonasis spektro poslinkis kietoje terpėje nebuvo stebimas.

Taigi, šioje disertacijos dalyje buvo pristatyti du būdai kovoti su konformacinės netvarkos nulemtais nepageidaujamais efektais: molekulės struktūros kietinimas bei rISC spartinimas.

D–σ–A konfiguracijos spinduoliai

Realizuoti mažą ΔE_{ST} tarpą galima ir atskiriant donoro bei akceptoriaus fragmentus atskirose molekulėse, taip apribojant HOMO ir LUMO orbitalių sanklotą [40]. Tačiau šiuo atveju TADF emisinės savybė stipriai priklauso nuo sunkiai kontroliuojamo atstumo tarp donoro ir akceptoriaus [42–44]. Neseniai buvo pasiūlyta D ir A sujungti per nekonjuguotą σ jungtuką, taip nutraukiant elektroninę sąveiką tarp fragmentų, tačiau tiksliai kontroliuojant atstumą tarp jų [70]. Plokščias trifeniltriazino akceptorius buvo sujungtas su įvairaus stiprumo donorais: **1** – dihidroakridinu, **2** – tetrametilkarbazolu bei **3** – trifeniaminu per hyperkonjuguotą heksafluoroisopropilidino jungtį. Šioms sistemoms buvo nustatytos labai mažos osciliatoriaus stiprio vertės (0.0008–0.0054) bei pastebėtos dvi TADF gesimo komponentės iš kurių pirmoji pasižymėjo viena greičiausių žinomų TADF trukmių 200–400 ns [102]. Publikacijose [**A2**] pateikiama nuodugni šių D–σ–A darinių neįprastų emisinių savybių, užfiksuotų laike–koreliuotos spektroskopijos būdu, analizė.

Visų pirma, buvo pastebėta, jog greitoji uždelstoji komponentė, anksčiau įvardinta kaip itin sparti TADF emisija, tebuvo įprasta krūvio pernašos (CT) fluorescencija. Neįprastai ilgos gesimo trukmės 37–470 ns buvo nulemtos itin mažų osciliatoriaus stiprio verčių ir silpnos HOMO–LUMO sąveikos, todėl jos buvo ilgesnės dariniams su stipresniais donoriniais fragmentais. Dėl lėtos gesimo spartos, pradinė fluorescencija buvo gesinama deguonies, tačiau nedemonstravo temperatūrinės aktyvacijos būdingos TADF emisijai. Tuo tarpu antroji uždelstoji komponentė spartėjo stiprėjant donorui bei mažėjant ΔE_{ST} tarpui, taip pat demonstravo temperatūrinę aktyvaciją, todėl buvo priskirta TADF uždelstajai fluorescencijai.

Plačiau išanalizavus laike išskirtus tirpalų fluorescencijos spektrus buvo pastebėta, jog pirmoji ir antroji komponentės kyla iš skirtingų būsenų su kitokiomis emisijos smailių vertėmis. Atlikus tyrimus skirtingose tirpalų koncentracijose bei klampumuose paaiškėjo, jog antroji TADF komponentė kyla iš tarpmolekulinės sąveikos – eksipleksų formavimosi.

Kietoje polimero matricoje, esant žemai molekulių koncentracijai tarp-

molekulinė sąveika buvo išjungta, tačiau sumažėjus nespindulinės rekombinacijos spartai, abi komponentės – tiek pradinė fluorescencija tiek uždelstoji TADF emisija – atsiranda iš vidujmolekulinės krūvio pernašos būsenos.

Galų gale, grynuose sluoksniuose dominavo TADF emisija iš eksipleksų. Keičiant spinduolio koncentraciją PMMA matricoje 0.1–100 wt% režiuose, buvo stebimas palaipsnis emisijos smailės slinkimas nuo būdingo vidujmolekulinei emisijai iki būdingo tarpmolekulinei emisijai. Optimaliausios TADF sąlygos buvo pasiektos 20 wt% sluoksnyje, kadangi aukštesnėse koncentracijose efektyvumas krito dėl eksitonų migravimo ir gesinimo defektuose.

Šis tyrimas parodė, jog D–σ–A architektūra nėra patraukli vidujmolekuliniams TADF spinduoliams dėl labai silpnos donoro–akceptoriaus sąveikos.

TADF spinduolių optimizacija

Paskutinėje disertacijos dalyje buvo optimizuojamos įvairios D–A spinduolių struktūros, siekiant sukurti našius TADF šviestukus. Sparčiai tobulėjanti OLED technologija jau demonstruoja šviestukus su išoriniu kvantiniu našumu (EQE) siekiančiu beveik 40 %, be specialių ištrūkos gerinimo technologijų [30, 36, 110]. Tačiau dideli efektyvumai dažniausiai pasiekiami žalios – geltonos spalvos spinduoliams. Tuo tarpu sodrios mėlynos (CIE y koordinatė < 0.1) emisijos šviestukai, geidžiami spalvotų ekranų rinkoje, retai viršija 20 % efektyvumo vertes. Nelengva išpildyti mažos konjugacijos, aukštos tripleto energijos ir tinkamos D–A struktūros reikalavimus reikalingus mėlynam spinduoliui.

Pirimidino-karbazolo dariniai yra sėkmingai naudojami kaip aukšto tripletinio lygmens matricos, tačiau retai kada taikomi kaip spinduoliai. Dėl aukšto tripleto ir demonstruojamos kambario temperatūros fosforescencijos (RTP), kuri dažnai mena apie palankią TADF energetinę struktūrą [121], buvo nuspręsta optimizuoti šį darinį, o rezultatai publikuoti straipsnyje **[A5]**.

Karbazolo donoras buvo praturtintas 3,6-di-*tert*-butilo fragmentais siekiant sustiprinti jo elektronų donoro savybes. Papildomai, pirimidino akceptorius buvo papildytas metilo grupe 5-oje pozicijoje siekiant išsukti ir sustandinti molekulę, taip sumažinant HOMO ir LUMO sanklotą. Galiausiai, sunkus sieros atomas buvo prijungtas prie akceptoriaus norint paspartinti rISC spartą, sustiprinant sukinio–orbitos sąveiką. Pradiniai DFT skaičiavimai atskleidė, jog modifikacijos sumažino ΔE_{ST} tarpą nuo 540 meV iki 289 meV, tačiau beveik nepakeitė žemiausio tripletinio lygmens energijos (nuo 3.15 eV iki 3.14 meV). Skaičiavimus patvirtino ir emisijos spektrai, kur fluorescencijos smailė pasislinko nuo 379 nm iki 423 nm, o fosforescencijos spektras išliko beveik nepakitęs, taip sumažinant ΔE_{ST} iki 290 meV 10 wt% DPEPO aplinkoje. Nors pirminis karbazolo-pirimidino darinys pasižymėjo tik silpna RTP emisija vėlesniuose laikuose, optimizacijos įgalino uždelstąją fluorescenciją modifikuotame darinyje, kurios išeiga siekė 42 %. TADF prigimtis buvo patvirtinta tempera-

tūrine aktyvacija ir jautrumu deguoniui.

Panaudojus modifikuotą karbazolo-pirimidino darinį kaip spinduolį buvo sukurtas mėlynas (CIE koordinatės (0.16, 0.12)) TADF šviestukas siekiantis 8.7 % išorinį našumą, taigi modifikacijų nauda pasitvirtino.

Dar viena optimizacijos strategija buvo pritaikyta praplėstos konjugacijos karbazolo–difenilpirimidino (**1CbzPYR**) karkasui publikacijoje [**A6**]. Energijos tarpas tarp žemiausių singleto ir tripleto lygmenų buvo sumažintas prijungiant po du karbazolo donorus prie akceptoriaus fenilo žiedų *meta* pozicijose (**2CbzPYR**). Galiausiai buvo įspraustas ir trečias karbazolas *para* padėtyje (**3CbzPYR**) kuris dėl sterinės sąveikos su gretimais donorais stipriai apribojo jų sukiojimosi laisvę, panašiai kaip ankščiau minėtame **4CzPN** darinyje.

Pradiniai DFT skaičiavimai parodė, jog dariniai su stambesniais donoriniais pakaitais pasižymėjo didesniais susisukimo kampais tarp donorų ir akceptoriaus (nuo 52° iki 67.8°). Kaip ir tikėtasi didesnis kiekis karbazolų sumažino ΔE_{ST} tarpą, nors darinyje su trimis karbazolais jis šiek tiek išaugo, lyginant su **2CbzPYR**, dėl padidėjusios HOMO–LUMO sanklotos (atitinkamai 290, 100 ir 140 meV dariniams **1CbzPYR**, **2CbzPYR**ir **3CbzPYR**).

Praplėstos konjugacijos įtaka buvo stebima emisijos spektruose, dariniuose su didesniais pakaitais emisijos smailė (1 wt% PMMA sluoksnuose) slinkosi į raudonąją pusę nuo 408 nm iki 446 nm. Eksperimentiškai įvertintas energijos tarpas tarp žemiausių singletinių ir tripletinių būsenų atitiko teorinius skaičiavimus ir buvo atitinkamai 480, 270 ir 320 meV dariniams **1CbzPYR**–**3CbzPYR**, nors **3CbzPYR** junginio ΔE_{ST} tarpą pavyko sumažinti iki 110 meV poliškesnėje DPEPO aplinkoje.

Nors molekulė su dvejais karbazolo pakaitais pasižymėjo menkiausiu ΔE_{ST} tarpu, jos našumas buvo mažiausias (**2CbzPYR** darinio $\Phi_{\mathrm{PL}} = 0.22$, tuo tarpu **1CbzPYR** ir **3CbzPYR** išeigos buvo atitinkamai 0.66 ir 0.81 1 wt% PMMA sluoksniuose). Atlikus emisijos kinetikos analizę paaiškėjo, jog žemą **2CbzPYR** darinio našumą lemia lėta spinduliacinė rekombinacija ($0.7 \times 10^7\,\mathrm{s}^{-1}$) bei sparti interkombinacinė konversija į tripletinius lygmenis ($11 \times 10^7\,\mathrm{s}^{-1}$), kuriuose sužadinimai yra gesinami stiprios nespindulinės vidinės konversijos ($k_{\mathrm{nr}}^{T} = 2.2 \times 10^5\,\mathrm{s}^{-1}$). Nors junginys ir pasižymėjo didele ISC sparta, dėl lėtos spindulinės spartos termiškai aktyvuoto rISC proceso metu sugeneruoti singletiniai sužadinimai buvo ciklišk ai konvertuojami atgal į tripletines būsenas. Kietesnė **3CbzPYR** molekulės konfigūracija sumažino nespindulinius tripletų gesinimo kelius bei paspartino spindulinę singletų rekombinacija kas nulėmė aukštą darinio išeigą su stipria uždelstąja emisija ($\Phi_{\mathrm{TADF}} = 0.33$). Kietesnė molekulės sandara taip pat sumažino konformacinės netvarkos nulemtą raudonąjį spektro poslinkį.

Panaudojant **3CbzPYR** darinį kaip spinduolį OLED prietaise buvo sukurtas našus (EQE= 19.7 %) mėlynas (CIE koordinatės (0.16, 0.23)) šviestukas, kurio elektroliuminescencijos smailės vertė siekė 473 nm. Taigi karbazolų

skaičiaus bei pozicijos keitimas leido optimizuoti TADF emisiją karbazolo-difenilpirimidino dariniuose, kontroliuojant singleto spindulinę bei tripleto nespindulinę spartas, o ne mažinant HOMO ir LUMO sanklotą.

Literatūroje pristatomi dideli OLED išoriniai kvantiniai našumai dažniausiai pasiekiami esant labai mažam šviestuko ryškumui ir staigiai krenta esant intensyviam skaisčiui. Vienas iš būdų sumažinti efektyvumo krytį yra TADF gesimo trukmės trumpinimas, kadangi ilga rekombinacijos trukmė įgalina singleto–tripleto, tripleto–tripleto bei kitus krūvininkų anihiliacijos kelius [89, 98, 112]. Norint sutrumpinti TADF emisijos trukmę modifikacijoms buvo pasirinktas darinys sudarytas iš difenilpirimidino akceptoriaus bei fenoksazino donoro (**PXZ-PYR**). Ši molekulė pasirinkta dėl žinomo gero našumo žaliuose šviestukuose (EQE 19.9 %) bei trumpos uždelstosios fluorescencijos gyvavimo trukmės ($\tau_{\mathrm{TADF}} = 2.56\,\mu\mathrm{s}$) [136]. Siekiant paspartinti rISC procesą darinio akceptoriaus fenilo fragmentai buvo modifikuojami metilo grupėmis *orto* (**PXZ-mdPYR**), *meta* (**PXZ-muPYR**) arba *orto* ir *meta* (**PXZ-2mPYR**) padėtyse, o rezultatai buvo publikuoti [**A4**] straipsnyje.

Fotofizikinė emisijos savybių analizė parodė, jog metilo modifikacijos leido kontroliuoti fluorescencijos spalvą 100 meV intervale nuo 543 nm (smailės pozicija) nemodifikuotam **PXZ-PYR** iki atitinkamai 530, 528 ir 519 nm dariniams **PXZ-muPYR**, **PXZ-mdPYR**ir **PXZ-2mPYR**tolueno tirpaluose. Fosforescencijos spektre buvo stebima vibroninė struktūra, būdinga lokaliai sužadintai būsenai, o jų smailių pozicijos sutapo visuose dariniuose, nors minkščiausio **PXZ-PYR** junginio vibroninė struktūra buvo ganėtinai išplitusi, o smailės susilieję. Taigi, visų darinių fosforecencija kilo iš to pačio donoro fragmento, o įvertintos ΔE_{ST} vertės buvo atitinkamai 10, 70, 150 ir 130 eV dariniams **PXZ-PYR**, **PXZ-muPYR**, **PXZ-mdPYR**ir **PXZ-2mPYR**.

Visų molekulių emisijoje buvo stebima pradinė fluorescencija bei uždelstoji TADF emisija. Atlikus laike–koreliuotos spektroskopijos analizę tolueno tirpaluose buvo pastebėta keltas įdomių savybių:

- Metilo pakaitai *meta* padėtyje (dariniai **PXZ-PYR** ir **PXZ-muPYR**) apribojo donoro fragmento sukimosi galimybes, todėl sumažėjo HOMO–LUMO sanklota kartu paspartinusi TADF emisijos trukmę.

- Atgalinės interkombinacinės konversijos sparta (rISC) buvo mažesnė dariniams su tokiu pačiu donoro minkštumu, tačiau turintiems *orto* metilo grupę, kuri lėmė didesnį energijos tarpą tarp lygmenų ^{1}CT–^{3}LE, t.y. k_{rISC} nukrito nuo 1.8×10^6 iki $0.7 \times 10^6\,\mathrm{s}^{-1}$ molekulėms **PXZ-PYR** ir **PXZ-mdPYR** su lanksčiu donoro fragmentu, o rISC sparta sumažėjo nuo 6.5×10^6 iki $2.5 \times 10^6\,\mathrm{s}^{-1}$ junginiams **PXZ-muPYR** ir **PXZ-2mPYR** su kietesne donorine grupe.

- Pastebėtas rISC spartos išaugimas dariniams su labiau erdviškai fiksuotais donoro fragmentais, mažesne vidinės konversijos sparta ir kartu

mažesne vibronine sąveika tarp ^{3}LE ir ^{3}CT lygmenų (lyginant **PXZ-PYR** su **PXZ-muPYR** arba **PXZ-mdPYR** su **PXZ-2mPYR**). Tokio neįprasto reiškio priežastimi buvo įvardintas sumažėjęs energijos tarpas tarp būsenų ^{3}LE ir ^{3}CT.

- Aukštą darinio **PXZ-muPYR** TADF kvantinę išeigą ($\Phi_{\mathrm{TADF}} = 0.42$) nulėmė sparčiausi ISC ir rISC procesai, tačiau junginyje **PXZ-2mPYR** su ganėtinai lėtesne rISC sparta, kieta molekulės struktūra sumažino nespindulinės vidinės konversijos spartą taip leisdama pasiekti panašią 0.43 TADF išeigą.

- Junginys su *meta* metilo grupe pasižymėjo rekordine TADF trukme kuri siekė 800 ns tolueno tirpale bei 860 ns kietoje 10 wt% DPEPO terpėje. Tokia greita sparta kietoje terpėje buvo pasiekta, dėl sparčios atgalinės interkombinacinės konversijos, kuri sumenkino konformacinės netvarkos padarinius.

Aukštos TADF kvantinės išeigos bei didelė sparta leido sukurti labai našius OLED prietaisus su valdoma elektroliuminescencijos spalva nuo žalios (smailės pozicija ties 536 nm) spinduoliui **PXZ-PYR** iki žydros (smailė ties 502 nm) su *meta* ir *orto* metilais modifikuotu **PXZ-2mPYR** spinduoliu. Buvo pasiekti vieni didžiasių OLED našumų fenoksazino ir pirimidino dariniams: išorinis kvantinis našumas atitinkamai 27.9, 29.1, 27.5 ir 26.3 % dariniams **PXZ-PYR**, **PXZ-muPYR**, **PXZ-mdPYR** ir **PXZ-2mPYR**. Negana to, junginys su *meta* metilo pakaitais bei sparčia TADF fluorescencija išlaikė 20.5 % prietaiso našumą prie aukšto šviesinio 1000 cd/m^2 skaisčio. Aukštos OLED efektyvumo vertės kartu su nedideliu jų kryčiu, esant aukštam emisijos ryškumui, yra konkurencingos su geriausiais šiuo metu žinomais TADF šviestukais.

Išvados

Atliekant darbą buvo padarytos tokios išvados:

1. Dėl TADF specifikos, našiai uždelstajai emisijai yra reikalingas šioks toks molekulės minkštumas, kuris nulemia konformacinę netvarką kietoje aplinkoje, iššaukiant nepageidaujamus efektus: emisijos spektro išplitimą ir slinkimąsi į raudonąją pusę, taip pat, išilgėjusią gesimo trukmę, kas lemia šviestuko efektyvumo krytį prie didesnių šviesinių skaisčių. Visų šių nepalankių efektų galima išvengti standinant molekulės karkasą arba spartinant atgalinę interkombinacinę konversiją.

2. Donoro ir akceptoriaus jungimas hyperkonjuguotu σ jungtuku nulemia labai silpną sąveiką tarp donoro ir akceptoriaus, dėl to žema spindulinės rekombinacijos sparta sunkiai sugeba konkuruoti su nespindulinia-is kanalais bei yra gesinima deguonies, todėl ši molekulės architektūra nėra lengvai taikoma TADF spinduoliams.

3. Donor–akceptorinės molekulės iš karabazolo ir pirimido optimizacija, praplečiant karbazolo donoriškumą *tert*-butilo fragmentais, išsukant fragmentus metilo pagalba bei įterpiant sunkų S atomą, įjungė uždelstąją emisiją nepakeitus tripletinio lygmens energijos. Iš šio spinduolio buvo pagamintas šviestukas su sodriai mėlyna emisija (CIE koordinatės (0.16, 0.12)) ir sąlyginai aukštu išoriniu kvantiniu efektyvumu 8.7 %.

4. Donorinių karbazolų vienetų didinimas bei jungimo pozicijos variacija karbazolo–fenilpirimidino struktūroje leidžia sumažinti ΔE_{ST} tarpą bei uždaro nespindulinius kelius dėl „užgrūstos“ geometrijos. Molekulė su trigubo karbazolo donoru pasižymėjo geru našumu (81 %) ir buvo pritaikyta sukuriant našų (išorinis kvantinis efektyvumas 19.7 %) mėlynos spalvos (elektroliuminescencijos CIE koordinatės (0.16, 0.23)) organinį šviestuką.

5. Modifikuojant fenoksazino–fenilpirimidino struktūrą, mažais metilo fragmentais ties jungiamuoju fenilo žiedu, buvo manipuliuojamos TADF emisijos savybės: elektroliuminescencijos spalva buvo keičiama nuo žalios (smailė ties 536 nm) iki žydros (502 nm); *meta*-metilo modifikacija sumažino ^{1}CT-^{3}LE ir ^{3}CT-^{3}LE energijos tarpus, taip pagreitindama rISC spartą bei kartu leido pasiekti vieną mažiausių TADF gyvavimo trukmių (860 ns) kietoje terpėje. Šis darinys OLED konfiguracijoje demonstravo gerą efektyvumą (išorinis našumas 29.1 %) su mažu našumo kryčiu (20.5 % našumas esant 1000 cd/m^2 šviesiniam skaisčiui).

BIBLIOGRAPHY

[1] T. DeMarse, K. Dockendorf, Adaptive flight control with living neuronal networks on microelectrode arrays, in *Proceedings. 2005 IEEE Int. Jt. Conf. Neural Networks, 2005.* (IEEE, 2005), volume 3, 1548–1551.

[2] N. R. B. Martins, A. Angelica, K. Chakravarthy, Y. Svidinenko, F. J. Boehm, I. Opris, M. A. Lebedev, M. Swan, S. A. Garan, J. V. Rosenfeld, T. Hogg, R. A. Freitas, Human Brain/Cloud Interface, Front. Neurosci. **13**(March) (2019), https://doi.org/10.3389/fnins.2019.00112.

[3] M. Pais-Vieira, M. Lebedev, C. Kunicki, J. Wang, M. A. L. Nicolelis, A Brain-to-Brain Interface for Real-Time Sharing of Sensorimotor Information, Sci. Rep. **3**(1), 1319 (2013), https://doi.org/10.1038/srep01319.

[4] M. Kim, H.-J. Ha, H.-J. Yun, I.-K. You, K.-J. Baeg, Y.-H. Kim, B.-K. Ju, Flexible organic phototransistors based on a combination of printing methods, Org. Electron. **15**(11), 2677–2684 (2014), https://doi.org/10.1016/j.orgel.2014.07.041.

[5] M. J. Coenen, T. M. Slaats, T. M. Eggenhuisen, P. Groen, Inkjet printing the three organic functional layers of two-colored organic light emitting diodes, Thin Solid Films **583**, 194–200 (2015), https://doi.org/10.1016/j.tsf.2015.03.064.

[6] A. Köhler, H. Bässler, *Electronic Processes in Organic Semiconductors* (Wiley-VCH Verlag GmbH & Co. KGaA, Weinheim, Germany, 2015).

[7] M. Pope, H. P. Kallmann, P. Magnante, Electroluminescence in Organic Crystals, J. Chem. Phys. **38**(8), 2042–2043 (1963), https://doi.org/10.1063/1.1733929.

[8] C. W. Tang, S. A. VanSlyke, Organic electroluminescent diodes, Appl. Phys. Lett. **51**(12), 913–915 (1987), https://doi.org/10.1063/1.98799.

[9] J. H. Burroughes, D. D. C. Bradley, A. R. Brown, R. N. Marks, K. Mackay, R. H. Friend, P. L. Burns, A. B. Holmes, Light-emitting diodes based on conjugated polymers, Nature **347**(6293), 539–541 (1990), https://doi.org/10.1038/347539a0.

[10] J. Kido, M. Kimura, K. Nagai, Multilayer White Light-Emitting Organic Electroluminescent Device, Science (80-.). **267**(5202), 1332–1334 (1995), https://doi.org/10.1126/science.267.5202.1332.

[11] M. A. Baldo, D. F. O'Brien, M. E. Thompson, S. R. Forrest, Excitonic singlet-triplet ratio in a semiconducting organic thin film, Phys. Rev. B **60**(20), 14422–14428 (1999), https://doi.org/10.1103/PhysRevB.60.14422.

[12] M. A. Baldo, D. F. O'Brien, Y. You, A. Shoustikov, S. Sibley, M. E. Thompson, S. R. Forrest, Highly efficient phosphorescent emission from

organic electroluminescent devices, Nature **395**(6698), 151–154 (1998), https://doi.org/10.1038/25954.

[13] D. Volz, M. Wallesch, C. Fléchon, M. Danz, A. Verma, J. M. Navarro, D. M. Zink, S. Bräse, T. Baumann, From iridium and platinum to copper and carbon: new avenues for more sustainability in organic light-emitting diodes, Green Chem. **17**(4), 1988–2011 (2015), https://doi.org/10.1039/C4GC02195A.

[14] C. A. Parker, C. G. Hatchard, Triplet-singlet emission in fluid solutions. Phosphorescence of eosin, Trans. Faraday Soc. **57**, 1894 (1961), https://doi.org/10.1039/tf9615701894.

[15] K. Goushi, K. Yoshida, K. Sato, C. Adachi, Organic light-emitting diodes employing efficient reverse intersystem crossing for triplet-to-singlet state conversion, Nat. Photonics **6**(4), 253–258 (2012), https://doi.org/10.1038/nphoton.2012.31.

[16] H. Uoyama, K. Goushi, K. Shizu, H. Nomura, C. Adachi, Highly efficient organic light-emitting diodes from delayed fluorescence, Nature **492**(7428), 234–238 (2012), https://doi.org/10.1038/nature11687.

[17] A. Endo, K. Sato, K. Yoshimura, T. Kai, A. Kawada, H. Miyazaki, C. Adachi, Efficient up-conversion of triplet excitons into a singlet state and its application for organic light emitting diodes, Appl. Phys. Lett. **98**(8), 083302 (2011), https://doi.org/10.1063/1.3558906.

[18] M. Y. Wong, E. Zysman-Colman, Purely Organic Thermally Activated Delayed Fluorescence Materials for Organic Light-Emitting Diodes, Adv. Mater. **29**(22), 1605444 (2017), https://doi.org/10.1002/adma.201605444.

[19] R. K. Konidena, J. Y. Lee, Molecular Design Tactics for Highly Efficient Thermally Activated Delayed Fluorescence Emitters for Organic Light Emitting Diodes, Chem. Rec. **19**(8), 1499–1517 (2019), https://doi.org/10.1002/tcr.201800136.

[20] S. Reindl, A. Penzkofer, Higher excited-state triplet-singlet intersystem crossing of some organic dyes, Chem. Phys. **211**(1-3), 431–439 (1996), https://doi.org/10.1016/0301-0104(96)00191-7.

[21] D. Hu, L. Yao, B. Yang, Y. Ma, Reverse intersystem crossing from upper triplet levels to excited singlet: a 'hot excition' path for organic light-emitting diodes, Philos. Trans. R. Soc. A Math. Phys. Eng. Sci. **373**(2044), 20140318 (2015), https://doi.org/10.1098/rsta.2014.0318.

[22] Y. Liu, Y. Yuan, X. Tian, J. Sun, Theoretical investigation on reverse intersystem crossing from upper triplet to lowest singlet: A "hot exciton" path for blue fluorescent OLEDs, Int. J. Quantum Chem. (July), 1–12 (2020), https://doi.org/10.1002/qua.26399.

[23] D. Y. Kondakov, T. D. Pawlik, T. K. Hatwar, J. P. Spindler, Triplet annihilation exceeding spin statistical limit in highly efficient fluorescent organic light-emitting diodes, J. Appl. Phys. **106**(12), 124510 (2009), https://doi.org/10.1063/1.3273407.

[24] Y. Luo, H. Aziz, Correlation Between Triplet-Triplet Annihilation and Electroluminescence Efficiency in Doped Fluorescent Organic Light-Emitting Devices, Adv. Funct. Mater. **20**(8), 1285–1293 (2010), https://doi.org/10.1002/adfm.200902329.

[25] J. Partee, E. L. Frankevich, B. Uhlhorn, J. Shinar, Y. Ding, T. J. Barton, Delayed Fluorescence and Triplet-Triplet Annihilation in \pi -Conjugated Polymers, Phys. Rev. Lett. **82**(18), 3673–3676 (1999), https://doi.org/10.1103/PhysRevLett.82.3673.

[26] Y. Tao, K. Yuan, T. Chen, P. Xu, H. Li, R. Chen, C. Zheng, L. Zhang, W. Huang, Thermally Activated Delayed Fluorescence Materials Towards the Breakthrough of Organoelectronics, Adv. Mater. **26**(47), 7931–7958 (2014), https://doi.org/10.1002/adma.201402532.

[27] F. B. Dias, T. J. Penfold, A. P. Monkman, Photophysics of thermally activated delayed fluorescence molecules, Methods Appl. Fluoresc. **5**(1), 012001 (2017), https://doi.org/10.1088/2050-6120/aa537e.

[28] T. Hatakeyama, K. Shiren, K. Nakajima, S. Nomura, S. Nakatsuka, K. Kinoshita, J. Ni, Y. Ono, T. Ikuta, Ultrapure Blue Thermally Activated Delayed Fluorescence Molecules: Efficient HOMO-LUMO Separation by the Multiple Resonance Effect, Adv. Mater. **28**(14), 2777–2781 (2016), https://doi.org/10.1002/adma.201505491.

[29] S. Oda, B. Kawakami, R. Kawasumi, R. Okita, T. Hatakeyama, Multiple Resonance Effect-Induced Sky-Blue Thermally Activated Delayed Fluorescence with a Narrow Emission Band, Org. Lett. **21**(23), 9311–9314 (2019), https://doi.org/10.1021/acs.orglett.9b03342.

[30] T.-A. Lin, T. Chatterjee, W.-L. Tsai, W.-K. Lee, M.-J. Wu, M. Jiao, K.-C. Pan, C.-L. Yi, C.-L. Chung, K.-T. Wong, C.-C. Wu, Sky-Blue Organic Light Emitting Diode with 37% External Quantum Efficiency Using Thermally Activated Delayed Fluorescence from Spiroacridine-Triazine Hybrid, Adv. Mater. **28**(32), 6976–6983 (2016), https://doi.org/10.1002/adma.201601675.

[31] X. Gong, C.-h. Lu, W.-k. Lee, P. Li, Y.-h. Huang, Z. Chen, L. Zhan, High-Efficiency Red Thermally Activated Delayed High-Efficiency Red Thermally Activated Delayed Fluorescence Emitters Based on Benzothiophene-Fused Spiro-Acridine Donor, Chem. Eng. J. 126663 (2020), https://doi.org/10.1016/j.cej.2020.126663.

[32] G. Méhes, H. Nomura, Q. Zhang, T. Nakagawa, C. Adachi, Enhanced Electroluminescence Efficiency in a Spiro-Acridine Derivative through Thermally Activated Delayed Fluorescence, Angew. Chemie Int. Ed. **51**(45), 11311–11315 (2012), https://doi.org/10.1002/anie.201206289.

[33] S. Youn Lee, T. Yasuda, H. Nomura, C. Adachi, High-efficiency organic light-emitting diodes utilizing thermally activated delayed fluorescence from triazine-based donor–acceptor hybrid molecules, Appl. Phys. Lett. **101**(9), 093306 (2012), https://doi.org/10.1063/1.4749285.

[34] H. Wang, L. Xie, Q. Peng, L. Meng, Y. Wang, Y. Yi, P. Wang, Novel Thermally Activated Delayed Fluorescence Materials-Thioxanthone Derivatives and Their Applications for Highly Efficient OLEDs, Adv. Mater. **26**(30), 5198–5204 (2014), https://doi.org/10.1002/adma.201401393.

[35] Z. Kuang, G. He, H. Song, X. Wang, Z. Hu, H. Sun, Y. Wan, Q. Guo, A. Xia, Conformational Relaxation and Thermally Activated Delayed Fluorescence in Anthraquinone-Based Intramolecular Charge-Transfer Compound, J. Phys. Chem. C **122**(7), 3727–3737 (2018), https://doi.org/10.1021/acs.jpcc.7b11411.

[36] L. S. Cui, A. J. Gillett, S. F. Zhang, H. Ye, Y. Liu, X. K. Chen, Z. S. Lin, E. W. Evans, W. K. Myers, T. K. Ronson, H. Nakanotani, S. Reineke, J. L. Bredas, C. Adachi, R. H. Friend, Fast spin-flip enables efficient and stable organic electroluminescence from charge-transfer states, Nat. Photonics (2020), https://doi.org/10.1038/s41566-020-0668-z.

[37] Y. Wada, H. Nakagawa, S. Matsumoto, Y. Wakisaka, H. Kaji, Organic light emitters exhibiting very fast reverse intersystem crossing, Nat. Photonics (2020), https://doi.org/10.1038/s41566-020-0667-0.

[38] V. Jankus, C.-J. Chiang, F. Dias, A. P. Monkman, Deep Blue Exciplex Organic Light-Emitting Diodes with Enhanced Efficiency; P-type or E-type Triplet Conversion to Singlet Excitons?, Adv. Mater. **25**(10), 1455–1459 (2013), https://doi.org/10.1002/adma.201203615.

[39] M. Colella, A. Danos, A. P. Monkman, Less Is More: Dilution Enhances Optical and Electrical Performance of a TADF Exciplex, J. Phys. Chem. Lett. **10**(4), 793–798 (2019), https://doi.org/10.1021/acs.jpclett.8b03646.

[40] M. Sarma, K.-T. Wong, Exciplex: An Intermolecular Charge-Transfer Approach for TADF, ACS Appl. Mater. Interfaces **10**(23), 19279–19304 (2018), https://doi.org/10.1021/acsami.7b18318.

[41] M. Chapran, P. Pander, M. Vasylieva, G. Wiosna-Salyga, J. Ulanski, F. B. Dias, P. Data, Realizing 20% External Quantum Efficiency in Electroluminescence with Efficient Thermally Activated Delayed Fluorescence from an Exciplex, ACS Appl. Mater. Interfaces **Under Revi**, acsami.8b18284 (2019), https://doi.org/10.1021/acsami.8b18284.

[42] W. Liu, J.-X. Chen, C.-J. Zheng, K. Wang, D.-Y. Chen, F. Li, Y.-P. Dong, C.-S. Lee, X.-M. Ou, X.-H. Zhang, Novel Strategy to Develop Exciplex Emitters for High-Performance OLEDs by Employing Thermally Activated Delayed Fluorescence Materials, Adv. Funct. Mater. **26**(12), 2002–2008 (2016), https://doi.org/10.1002/adfm.201505014.

[43] Y.-S. Park, S. Lee, K.-H. Kim, S.-Y. Kim, J.-H. Lee, J.-J. Kim, Exciplex-Forming Co-host for Organic Light-Emitting Diodes with Ultimate Efficiency, Adv. Funct. Mater. **23**(39), 4914–4920 (2013), https://doi.org/10.1002/adfm.201300547.

[44] D. Chen, G. Xie, X. Cai, M. Liu, Y. Cao, S.-J. Su, Fluorescent Organic Planar pn Heterojunction Light-Emitting Diodes with Simplified Structure, Extremely Low Driving Voltage, and High Efficiency, Adv. Mater. **28**(2), 239–244 (2016), https://doi.org/10.1002/adma.201504290.

[45] H. Tsujimoto, D.-G. Ha, G. Markopoulos, H. S. Chae, M. A. Baldo, T. M. Swager, Thermally Activated Delayed Fluorescence and Aggregation Induced Emission with Through-Space Charge Transfer, J. Am. Chem. Soc. **139**(13), 4894–4900 (2017), https://doi.org/10.1021/jacs.7b00873.

[46] K. Kawasumi, T. Wu, T. Zhu, H. S. Chae, T. Van Voorhis, M. A. Baldo, T. M. Swager, Thermally Activated Delayed Fluorescence Materials Based on Homoconjugation Effect of Donor-Acceptor Triptycenes, J. Am. Chem. Soc. **137**(37), 11908–11911 (2015), https://doi.org/10.1021/jacs.5b07932.

[47] S. Shao, J. Hu, X. Wang, L. Wang, X. Jing, F. Wang, Blue Thermally Activated Delayed Fluorescence Polymers with Nonconjugated Backbone and Through-Space Charge Transfer Effect, J. Am. Chem. Soc. **139**(49), 17739–17742 (2017), https://doi.org/10.1021/jacs.7b10257.

[48] X. Wang, S. Wang, J. Lv, S. Shao, L. Wang, X. Jing, F. Wang, Through-space charge transfer hexaarylbenzene dendrimers with thermally activated delayed fluorescence and aggregation-induced emission for efficient solution-processed OLEDs, Chem. Sci. **10**(10), 2915–2923 (2019), https://doi.org/10.1039/C8SC04991B.

[49] B. T. Lim, S. Okajima, A. Chandra, E. Lim, Radiationless transitions in electron donor-acceptor complexes: selection rules for S1 $\rightarrow$ T intersystem crossing and efficiency of S1 $\rightarrow$ S0 internal conversion, Chem. Phys. Lett. **79**(1), 22–27 (1981), https://doi.org/10.1016/0009-2614(81)85280-3.

[50] C. M. Marian, Spin-orbit coupling and intersystem crossing in molecules, Wiley Interdiscip. Rev. Comput. Mol. Sci. **2**(2), 187–203 (2012), https://doi.org/10.1002/wcms.83.

[51] T. Ogiwara, Y. Wakikawa, T. Ikoma, Mechanism of Intersystem Crossing of Thermally Activated Delayed Fluorescence Molecules, J. Phys. Chem. A **119**(14), 3415–3418 (2015), https://doi.org/10.1021/acs.jpca.5b02253.

[52] J. Gibson, A. P. Monkman, T. J. Penfold, The Importance of Vibronic Coupling for Efficient Reverse Intersystem Crossing in Thermally Activated Delayed Fluorescence Molecules, ChemPhysChem **17**(19), 2956–2961 (2016), https://doi.org/10.1002/cphc.201600662.

[53] P. L. Santos, J. S. Ward, P. Data, A. S. Batsanov, M. R. Bryce, F. B. Dias, A. P. Monkman, Engineering the singlet–triplet energy splitting in a TADF molecule, J. Mater. Chem. C **4**(17), 3815–3824 (2016), https://doi.org/10.1039/C5TC03849A.

[54] F. B. Dias, K. N. Bourdakos, V. Jankus, K. C. Moss, K. T. Kamtekar, V. Bhalla, J. Santos, M. R. Bryce, A. P. Monkman, Triplet Harvesting with 100% Efficiency by Way of Thermally Activated Delayed Fluorescence in Charge Transfer OLED Emitters, Adv. Mater. **25**(27), 3707–3714 (2013), https://doi.org/10.1002/adma.201300753.

[55] J. S. Ward, R. S. Nobuyasu, A. S. Batsanov, P. Data, A. P. Monkman, F. B. Dias, M. R. Bryce, The interplay of thermally activated delayed fluorescence (TADF) and room temperature organic phosphorescence in sterically-constrained donor-acceptor charge-transfer molecules, Chem. Commun. **52**(12), 2612–2615 (2016), https://doi.org/10.1039/c5cc09645f.

[56] F. B. Dias, J. Santos, D. R. Graves, P. Data, R. S. Nobuyasu, M. A. Fox, A. S. Batsanov, T. Palmeira, M. N. Berberan-Santos, M. R. Bryce, A. P. Monkman, The Role of Local Triplet Excited States and D-A Relative Orientation in Thermally Activated Delayed Fluorescence: Photophysics and Devices, Adv. Sci. **3**(12), 1600080 (2016), https://doi.org/10.1002/advs.201600080.

[57] M. K. Etherington, J. Gibson, H. F. Higginbotham, T. J. Penfold, A. P. Monkman, Revealing the spin-vibronic coupling mechanism of thermally activated delayed fluorescence, Nat. Commun. **7**, 1–7 (2016), https://doi.org/10.1038/ncomms13680.

[58] X.-K. Chen, S.-F. Zhang, J.-X. Fan, A.-M. Ren, Nature of Highly Efficient Thermally Activated Delayed Fluorescence in Organic Light-Emitting Diode Emitters: Nonadiabatic Effect between Excited States, J. Phys. Chem. C **119**(18), 9728–9733 (2015), https://doi.org/10.1021/acs.jpcc.5b00276.

[59] T. J. Penfold, E. Gindensperger, C. Daniel, C. M. Marian, Spin-Vibronic Mechanism for Intersystem Crossing, Chem. Rev. **118**(15), 6975–7025 (2018), https://doi.org/10.1021/acs.chemrev.7b00617.

[60] D. de Sa Pereira, C. Menelaou, A. Danos, C. Marian, A. P. Monkman, Electroabsorption Spectroscopy as a Tool for Probing Charge Transfer and State Mixing in Thermally Activated Delayed Fluorescence Emitters, J. Phys. Chem. Lett. **10**(12), 3205–3211 (2019), https://doi.org/10.1021/acs.jpclett.9b00999.

[61] E. W. Evans, Y. Olivier, Y. Puttisong, W. K. Myers, T. J. H. Hele, S. M. Menke, T. H. Thomas, D. Credgington, D. Beljonne, R. H. Friend, N. C. Greenham, Vibrationally Assisted Intersystem Crossing in Benchmark Thermally Activated Delayed Fluorescence Molecules, J. Phys. Chem. Lett. **9**(14), 4053–4058 (2018), https://doi.org/10.1021/acs.jpclett.8b01556.

[62] T. Serevičius, T. Bučiūnas, J. Bucevičius, J. Dodonova, S. Tumkevičius, K. Kazlauskas, S. Juršėnas, Room temperature phosphorescence vs. thermally activated delayed fluorescence in carbazole–pyrimidine cored compounds, J. Mater. Chem. C **6**(41), 11128–11136 (2018), https://doi.org/10.1039/C8TC02554A.

[63] H. Yersin, L. Mataranga-Popa, R. Czerwieniec, Y. Dovbii, Design of a New Mechanism beyond Thermally Activated Delayed Fluorescence toward Fourth Generation Organic Light Emitting Diodes, Chem. Mater. **31**(16), 6110–6116 (2019), https://doi.org/10.1021/acs.chemmater.9b01168.

[64] R. S. Nobuyasu, J. S. Ward, J. Gibson, B. A. Laidlaw, Z. Ren, P. Data, A. S. Batsanov, T. J. Penfold, M. R. Bryce, F. B. Dias, The influence of molecular geometry on the efficiency of thermally activated delayed fluorescence, J. Mater. Chem. C **7**(22), 6672–6684 (2019), https://doi.org/10.1039/C9TC00720B.

[65] G. Méhes, K. Goushi, W. J. Potscavage, C. Adachi, Influence of host matrix on thermally-activated delayed fluorescence: Effects on emission lifetime, photoluminescence quantum yield, and device performance, Org. Electron. **15**(9), 2027–2037 (2014), https://doi.org/10.1016/j.orgel.2014.05.027.

[66] N. A. Kukhta, A. S. Batsanov, M. R. Bryce, A. P. Monkman, Importance of Chromophore Rigidity on the Efficiency of Blue Thermally Activated Delayed Fluorescence Emitters, J. Phys. Chem. C **122**(50), 28564–28575 (2018), https://doi.org/10.1021/acs.jpcc.8b10867.

[67] T. Northey, J. Stacey, T. J. Penfold, The role of solid state solvation on the charge transfer state of a thermally activated delayed fluorescence emitter, J. Mater. Chem. C **5**(42), 11001–11009 (2017), https://doi.org/10.1039/C7TC04099G.

[68] M. K. Etherington, F. Franchello, J. Gibson, T. Northey, J. Santos, J. S. Ward, H. F. Higginbotham, P. Data, A. Kurowska, P. L. Dos Santos, D. R. Graves, A. S. Batsanov, F. B. Dias, M. R. Bryce, T. J. Penfold, A. P. Monkman, Regio- and conformational isomerization critical to design of efficient thermally-activated delayed fluorescence emitters, Nat. Commun. **8**(1), 14987 (2017), https://doi.org/10.1038/ncomms14987.

[69] M. J. Frisch, G. W. Trucks, H. B. Schlegel, G. E. Scuseria, M. A. Robb, J. R. Cheeseman, G. Scalmani, V. Barone, G. A. Petersson, H. Nakatsuji, X. Li, M. Caricato, A. V. Marenich, J. Bloino, B. G. Janesko, R. Gomperts, B. Mennucci, H. P. Hratchian, J. V. Ortiz, A. F. Izmaylov, J. L. Sonnenberg, D. Williams-Young, F. Ding, F. Lipparini, F. Egidi, J. Goings, B. Peng, A. Petrone, T. Henderson, D. Ranasinghe, V. G. Zakrzewski, J. Gao, N. Rega, G. Zheng, W. Liang, M. Hada, M. Ehara, K. Toyota, R. Fukuda, J. Hasegawa, M. Ishida, T. Nakajima, Y. Honda, O. Kitao, H. Nakai, T. Vreven, K. Throssell, J. A. Montgomery Jr., J. E. Peralta, F. Ogliaro, M. J. Bearpark, J. J. Heyd, E. N. Brothers,

K. N. Kudin, V. N. Staroverov, T. A. Keith, R. Kobayashi, J. Normand, K. Raghavachari, A. P. Rendell, J. C. Burant, S. S. Iyengar, J. Tomasi, M. Cossi, J. M. Millam, M. Klene, C. Adamo, R. Cammi, J. W. Ochterski, R. L. Martin, K. Morokuma, O. Farkas, J. B. Foresman, D. J. Fox, Gaussian 09 Revision C.01 (2016).

[70] Y. Geng, A. D'Aleo, K. Inada, L. Cui, J. U. Kim, H. Nakanotani, C. Adachi, Donor–σ–Acceptor Motifs: Thermally Activated Delayed Fluorescence Emitters with Dual Upconversion, Angew. Chemie Int. Ed. **56**(52), 16536–16540 (2017), https://doi.org/10.1002/anie.201708876.

[71] Y. Kawamura, J. Brooks, J. J. Brown, H. Sasabe, C. Adachi, Intermolecular Interaction and a Concentration-Quenching Mechanism of Phosphorescent Ir(III) Complexes in a Solid Film, Phys. Rev. Lett. **96**(1), 017404 (2006), https://doi.org/10.1103/PhysRevLett.96.017404.

[72] Y. H. Park, Y. Kim, H. Sohn, K.-S. An, Concentration quenching effect of organic light-emitting devices using DCM1-doped tetraphenylgermole, J. Phys. Org. Chem. **25**(3), 207–210 (2012), https://doi.org/10.1002/poc.1893.

[73] K. Masui, H. Nakanotani, C. Adachi, Analysis of exciton annihilation in high-efficiency sky-blue organic light-emitting diodes with thermally activated delayed fluorescence, Org. Electron. **14**(11), 2721–2726 (2013), https://doi.org/10.1016/j.orgel.2013.07.010.

[74] V. Jankus, P. Data, D. Graves, C. McGuinness, J. Santos, M. R. Bryce, F. B. Dias, A. P. Monkman, Highly Efficient TADF OLEDs: How the Emitter-Host Interaction Controls Both the Excited State Species and Electrical Properties of the Devices to Achieve Near 100% Triplet Harvesting and High Efficiency, Adv. Funct. Mater. **24**(39), 6178–6186 (2014), https://doi.org/10.1002/adfm.201400948.

[75] J. R. Lakowicz, *Principles of Fluorescence Spectroscopy* (Springer, Singapore, 2006), third edition.

[76] S. Leyre, E. Coutino-Gonzalez, J. J. Joos, J. Ryckaert, Y. Meuret, D. Poelman, P. F. Smet, G. Durinck, J. Hofkens, G. Deconinck, P. Hanselaer, Absolute determination of photoluminescence quantum efficiency using an integrating sphere setup, Rev. Sci. Instrum. **85**(12), 123115 (2014), https://doi.org/10.1063/1.4903852.

[77] Edinburgh Instruments Ltd, FLS980 Series Reference Guide, https://www.edinst.com/wp-content/uploads/2016/02/FLS980-Series-Reference-Guide-Integrating-Sphere.pdf.

[78] C. Rothe, A. P. Monkman, Triplet exciton migration in a conjugated polyfluorene, Phys. Rev. B **68**(7), 075208 (2003), https://doi.org/10.1103/PhysRevB.68.075208.

[79] C. Grewer, H.-D. Brauer, Mechanism of the Triplet-State Quenching by Molecular Oxygen in Solution, J. Phys. Chem. **98**(16), 4230–4235 (1994), https://doi.org/10.1021/j100067a006.

[80] K. Kawaoka, A. U. Khan, D. R. Kearns, Role of Singlet Excited States of Molecular Oxygen in the Quenching of Organic Triplet States, J. Chem. Phys. **46**(5), 1842–1853 (1967), https://doi.org/10.1063/1.1840943.

[81] J. C. Phys, J. R. Lakowicz, G. Weber, Quenching of Fluorescence by Oxygen . A Probe for Structural Fluctuations in Macromoleculest (2), 4161–4170 (1972), https://doi.org/10.1021/bi00745a020.

[82] L. Patterson, G. Porter, M. Topp, Oxygen quenching of singlet and triplet states, Chem. Phys. Lett. **7**(6), 612–614 (1970), https://doi.org/10.1016/0009-2614(70)87019-1.

[83] G. Kreiza, D. Banevičius, J. Jovaišaitė, K. Maleckaitė, D. Gudeika, D. Volyniuk, J. V. Gražulevičius, S. Juršėnas, K. Kazlauskas, Suppression of benzophenone-induced triplet quenching for enhanced TADF performance, J. Mater. Chem. C **7**(37), 11522–11531 (2019), https://doi.org/10.1039/C9TC02408E.

[84] C. Baleizão, M. N. Berberan-Santos, The Brightest Fullerene: A New Isotope Effect in Molecular Fluorescence and Phosphorescence, ChemPhysChem **12**(7), 1247–1250 (2011), https://doi.org/10.1002/cphc.201100156.

[85] N. Haase, A. Danos, C. Pflumm, A. Morherr, P. Stachelek, A. Mekic, W. Brütting, A. P. Monkman, Kinetic Modeling of Transient Photoluminescence from Thermally Activated Delayed Fluorescence, J. Phys. Chem. C **122**(51), 29173–29179 (2018), https://doi.org/10.1021/acs.jpcc.8b11020.

[86] M. Saigo, K. Miyata, S. Tanaka, H. Nakanotani, C. Adachi, K. Onda, Suppression of Structural Change upon S 1 –T 1 Conversion Assists the Thermally Activated Delayed Fluorescence Process in Carbazole-Benzonitrile Derivatives, J. Phys. Chem. Lett. **10**(10), 2475–2480 (2019), https://doi.org/10.1021/acs.jpclett.9b00810.

[87] Z. Chen, D. Wang, M. Zhang, K. Wang, Y. Shi, J. Chen, W. Tao, C. Zheng, S. Tao, X. Zhang, Optimization on Molecular Restriction for Highly Efficient Thermally Activated Delayed Fluorescence Emitters, Adv. Opt. Mater. **6**(24), 1800935 (2018), https://doi.org/10.1002/adom.201800935.

[88] S.-J. Woo, Y.-H. Ha, Y.-H. Kim, J.-J. Kim, Effect of ortho - biphenyl substitution on the excited state dynamics of a multi-carbazole TADF molecule, J. Mater. Chem. C **8**(35), 12075–12084 (2020), https://doi.org/10.1039/D0TC02627A.

[89] M. Inoue, T. Serevičius, H. Nakanotani, K. Yoshida, T. Matsushima, S. Juršėnas, C. Adachi, Effect of reverse intersystem crossing rate to suppress efficiency roll-off in organic light-emitting diodes with thermally activated delayed fluorescence emitters, Chem. Phys. Lett. **644**, 62–67 (2016), https://doi.org/10.1016/j.cplett.2015.11.042.

[90] D.-G. Chen, T.-C. Lin, Y.-A. Chen, Y.-H. Chen, T.-C. Lin, Y.-T. Chen, P.-T. Chou, Revisiting Dual Intramolecular Charge-Transfer Fluorescence of Phenothiazine-triphenyltriazine Derivatives, J. Phys. Chem. C **122**(23), 12215–12221 (2018), https://doi.org/10.1021/acs.jpcc.8b04395.

[91] K. Wang, C.-J. Zheng, W. Liu, K. Liang, Y.-Z. Shi, S.-L. Tao, C.-S. Lee, X.-M. Ou, X.-H. Zhang, Avoiding Energy Loss on TADF Emitters: Controlling the Dual Conformations of D-A Structure Molecules Based on the Pseudoplanar Segments, Adv. Mater. **29**(47), 1701476 (2017), https://doi.org/10.1002/adma.201701476.

[92] J. Fan, Y. Zhang, Y. Zhou, L. Lin, C.-K. Wang, Excited State Properties of a Thermally Activated Delayed Fluorescence Molecule in Solid Phase Studied by Quantum Mechanics/Molecular Mechanics Method, J. Phys. Chem. C **122**(4), 2358–2366 (2018), https://doi.org/10.1021/acs.jpcc.7b10238.

[93] J. Fan, L. Lin, C.-K. Wang, Excited state properties of non-doped thermally activated delayed fluorescence emitters with aggregation-induced emission: a QM/MM study, J. Mater. Chem. C **5**(33), 8390–8399 (2017), https://doi.org/10.1039/C7TC02541F.

[94] K. Wang, Y.-Z. Shi, C.-J. Zheng, W. Liu, K. Liang, X. Li, M. Zhang, H. Lin, S.-L. Tao, C.-S. Lee, X.-M. Ou, X.-H. Zhang, Control of Dual Conformations: Developing Thermally Activated Delayed Fluorescence Emitters for Highly Efficient Single-Emitter White Organic Light-Emitting Diodes, ACS Appl. Mater. Interfaces **10**(37), 31515–31525 (2018), https://doi.org/10.1021/acsami.8b08083.

[95] D.-G. Chen, T.-C. Lin, C.-L. Chen, Y.-T. Chen, Y.-A. Chen, G.-H. Lee, P.-T. Chou, C.-W. Liao, P.-C. Chiu, C.-H. Chang, Y.-J. Lien, Y. Chi, Optically Triggered Planarization of Boryl-Substituted Phenoxazine: Another Horizon of TADF Molecules and High-Performance OLEDs, ACS Appl. Mater. Interfaces **10**(15), 12886–12896 (2018), https://doi.org/10.1021/acsami.8b00053.

[96] Y. Xiang, Y. Zhao, N. Xu, S. Gong, F. Ni, K. Wu, J. Luo, G. Xie, Z.-H. Lu, C. Yang, Halogen-induced internal heavy-atom effect shortening the emissive lifetime and improving the fluorescence efficiency of thermally activated delayed fluorescence emitters, J. Mater. Chem. C **5**(46), 12204–12210 (2017), https://doi.org/10.1039/C7TC04181K.

[97] A. Kretzschmar, C. Patze, S. T. Schwaebel, U. H. F. Bunz, Development of Thermally Activated Delayed Fluorescence Materials with Shortened Emissive Lifetimes, J. Org. Chem. **80**(18), 9126–9131 (2015), https://doi.org/10.1021/acs.joc.5b01496.

[98] Y. Im, M. Kim, Y. J. Cho, J.-A. Seo, K. S. Yook, J. Y. Lee, Molecular Design Strategy of Organic Thermally Activated Delayed Fluorescence Emitters, Chem. Mater. **29**(5), 1946–1963 (2017), https://doi.org/10.1021/acs.chemmater.6b05324.

[99] R. S. Mulliken, C. A. Rieke, W. G. Brown, Hyperconjugation *, J. Am. Chem. Soc. **63**(1), 41–56 (1941), https://doi.org/10.1021/ja01846a008.

[100] Q. Xie, T. Sun, J. Zhu, T. Sun, J. Zhu, Probing the Strongest Aromatic Cyclopentadiene Ring by Hyperconjugation, Organometallics **37**, 3219–3224 (2018), https://doi.org/10.1021/acs.organomet.8b00571.

[101] J. Mullins, Hyperconjugation: A More Coherent Approach, J. Chem. Educ. **89**(7), 834–836 (2012), https://doi.org/10.1021/ed1011986.

[102] P. L. dos Santos, J. S. Ward, D. G. Congrave, A. S. Batsanov, J. Eng, J. E. Stacey, T. J. Penfold, A. P. Monkman, M. R. Bryce, Triazatruxene: A Rigid Central Donor Unit for a D-A 3 Thermally Activated Delayed Fluorescence Material Exhibiting Sub-Microsecond Reverse Intersystem Crossing and Unity Quantum Yield via Multiple Singlet-Triplet State Pairs, Adv. Sci. **5**(6), 1700989 (2018), https://doi.org/10.1002/advs.201700989.

[103] Y. Qu, P. Pander, A. Bucinskas, M. Vasylieva, Y. Tian, F. Miomandre, F. B. Dias, G. Clavier, P. Data, P. Audebert, Convenient One-Pot Synthesis of 1,2,3,4-Thiatriazoles Towards a Novel Electron Acceptor for Highly-Efficient Thermally-Activated Delayed-Fluorescence Emitters, Chem. – A Eur. J. **25**(10), 2457–2462 (2019), https://doi.org/10.1002/chem.201805358.

[104] Y. Zhang, H. Ma, S. Wang, Z. Li, K. Ye, J. Zhang, Y. Liu, Q. Peng, Y. Wang, Supramolecular Structure-Dependent Thermally-Activated Delayed Fluorescence (TADF) Properties of Organic Polymorphs, J. Phys. Chem. C **120**(35), 19759–19767 (2016), https://doi.org/10.1021/acs.jpcc.6b05537.

[105] K.-L. Woon, C.-L. Yi, K.-C. Pan, M. K. Etherington, C.-C. Wu, K.-T. Wong, A. P. Monkman, Intramolecular Dimerization Quenching of Delayed Emission in Asymmetric D–D'–A TADF Emitters, J. Phys. Chem. C **123**(19), 12400–12410 (2019), https://doi.org/10.1021/acs.jpcc.9b01900.

[106] X. Zhang, M. W. Cooper, Y. Zhang, C. Fuentes-Hernandez, S. Barlow, S. R. Marder, B. Kippelen, Host-Free Yellow-Green Organic Light-Emitting Diodes with External Quantum Efficiency over 20% Based on a Compound Exhibiting Thermally Activated Delayed Fluorescence, ACS Appl. Mater. Interfaces **11**(13), 12693–12698 (2019), https://doi.org/10.1021/acsami.8b18798.

[107] B. L. Cotts, D. G. McCarthy, R. Noriega, S. B. Penwell, M. Delor, D. D. Devore, S. Mukhopadhyay, T. S. De Vries, N. S. Ginsberg, Tuning Thermally Activated Delayed Fluorescence Emitter Photophysics through Solvation in the Solid State, ACS Energy Lett. **2**(7), 1526–1533 (2017), https://doi.org/10.1021/acsenergylett.7b00268.

[108] T. Serevičius, R. Komskis, P. Adomėnas, O. Adomėnienė, G. Kreiza, V. Jankauskas, K. Kazlauskas, A. Miasojedovas, V. Jankus,

A. Monkman, S. Juršėnas, Triplet–Triplet Annihilation in 9,10-Diphenylanthracene Derivatives: The Role of Intersystem Crossing and Exciton Diffusion, J. Phys. Chem. C **121**(15), 8515–8524 (2017), https://doi.org/10.1021/acs.jpcc.7b01336.

[109] Q. Zhang, D. Tsang, H. Kuwabara, Y. Hatae, B. Li, T. Takahashi, S. Y. Lee, T. Yasuda, C. Adachi, Nearly 100% Internal Quantum Efficiency in Undoped Electroluminescent Devices Employing Pure Organic Emitters, Adv. Mater. **27**(12), 2096–2100 (2015), https://doi.org/10.1002/adma.201405474.

[110] T. L. Wu, M. J. Huang, C. C. Lin, P. Y. Huang, T. Y. Chou, R. W. Chen-Cheng, H. W. Lin, R. S. Liu, C. H. Cheng, Diboron compound-based organic light-emitting diodes with high efficiency and reduced efficiency roll-off, Nat. Photonics **12**(4), 235–240 (2018), https://doi.org/10.1038/s41566-018-0112-9.

[111] C. Murawski, K. Leo, M. C. Gather, Efficiency Roll-Off in Organic Light-Emitting Diodes, Adv. Mater. **25**(47), 6801–6827 (2013), https://doi.org/10.1002/adma.201301603.

[112] H. Tanaka, K. Shizu, H. Nakanotani, C. Adachi, Twisted Intramolecular Charge Transfer State for Long-Wavelength Thermally Activated Delayed Fluorescence, Chem. Mater. **25**(18), 3766–3771 (2013), https://doi.org/10.1021/cm402428a.

[113] Z. Liu, F. Cao, T. Tsuboi, Y. Yue, C. Deng, X. Ni, W. Sun, Q. Zhang, A high fluorescence rate is key for stable blue organic light-emitting diodes, J. Mater. Chem. C **6**(29), 7728–7733 (2018), https://doi.org/10.1039/C8TC01471J.

[114] X. Cai, S.-J. Su, Marching Toward Highly Efficient, Pure-Blue, and Stable Thermally Activated Delayed Fluorescent Organic Light-Emitting Diodes, Adv. Funct. Mater. **28**(43), 1802558 (2018), https://doi.org/10.1002/adfm.201802558.

[115] Y. H. Lee, S. Park, J. Oh, S.-J. Woo, A. Kumar, J.-J. Kim, J. Jung, S. Yoo, M. H. Lee, High-Efficiency Sky Blue to Ultradeep Blue Thermally Activated Delayed Fluorescent Diodes Based on Ortho -Carbazole-Appended Triarylboron Emitters: Above 32% External Quantum Efficiency in Blue Devices, Adv. Opt. Mater. **6**(17), 1800385 (2018), https://doi.org/10.1002/adom.201800385.

[116] D. H. Ahn, S. W. Kim, H. Lee, I. J. Ko, D. Karthik, J. Y. Lee, J. H. Kwon, Highly efficient blue thermally activated delayed fluorescence emitters based on symmetrical and rigid oxygen-bridged boron acceptors, Nat. Photonics **13**(8), 540–546 (2019), https://doi.org/10.1038/s41566-019-0415-5.

[117] L. Cui, H. Nomura, Y. Geng, J. U. Kim, H. Nakanotani, C. Adachi, Controlling Singlet–Triplet Energy Splitting for Deep-Blue Thermally Activated Delayed Fluorescence Emitters, Angew. Chemie Int. Ed. **56**(6), 1571–1575 (2017), https://doi.org/10.1002/anie.201609459.

[118] X. Cai, W. Qiu, M. Li, B. Li, Z. Wang, X. Wu, D. Chen, X. Jiang, Y. Cao, S.-J. Su, Nonaromatic Amine Containing Exciplex for Thermally Activated Delayed Fluorescent Electroluminescence, Adv. Opt. Mater. **7**(9), 1801554 (2019), https://doi.org/10.1002/adom.201801554.

[119] Q. Wu, M. Wang, X. Cao, D. Zhang, N. Sun, S. Wan, Y. Tao, Carbazole/α-carboline hybrid bipolar compounds as electron acceptors in exciplex or non-exciplex mixed cohosts and exciplex-TADF emitters for high-efficiency OLEDs, J. Mater. Chem. C **6**(32), 8784–8792 (2018), https://doi.org/10.1039/C8TC02353K.

[120] S.-W. Li, C.-H. Yu, C.-L. Ko, T. Chatterjee, W.-Y. Hung, K.-T. Wong, Cyanopyrimidine–Carbazole Hybrid Host Materials for High-Efficiency and Low-Efficiency Roll-Off TADF OLEDs, ACS Appl. Mater. Interfaces **10**(15), 12930–12936 (2018), https://doi.org/10.1021/acsami.8b02766.

[121] R. Huang, J. Avó, T. Northey, E. Chaning-Pearce, P. L. dos Santos, J. S. Ward, P. Data, M. K. Etherington, M. A. Fox, T. J. Penfold, M. N. Berberan-Santos, J. C. Lima, M. R. Bryce, F. B. Dias, The contributions of molecular vibrations and higher triplet levels to the intersystem crossing mechanism in metal-free organic emitters, J. Mater. Chem. C **5**(25), 6269–6280 (2017), https://doi.org/10.1039/C7TC01958K.

[122] C. Chan, L. Cui, J. U. Kim, H. Nakanotani, C. Adachi, Rational Molecular Design for Deep-Blue Thermally Activated Delayed Fluorescence Emitters, Adv. Funct. Mater. **28**(11), 1706023 (2018), https://doi.org/10.1002/adfm.201706023.

[123] M. Y. Wong, S. Krotkus, G. Copley, W. Li, C. Murawski, D. Hall, G. J. Hedley, M. Jaricot, D. B. Cordes, A. M. Z. Slawin, Y. Olivier, D. Beljonne, L. Muccioli, M. Moral, J.-C. Sancho-Garcia, M. C. Gather, I. D. W. Samuel, E. Zysman-Colman, Deep-Blue Oxadiazole-Containing Thermally Activated Delayed Fluorescence Emitters for Organic Light-Emitting Diodes, ACS Appl. Mater. Interfaces **10**(39), 33360–33372 (2018), https://doi.org/10.1021/acsami.8b11136.

[124] L. Cui, H. Nomura, Y. Geng, J. U. Kim, H. Nakanotani, C. Adachi, Controlling Singlet–Triplet Energy Splitting for Deep-Blue Thermally Activated Delayed Fluorescence Emitters, Angew. Chemie Int. Ed. **56**(6), 1571–1575 (2017), https://doi.org/10.1002/anie.201609459.

[125] W. Zhang, Y.-X. Zhang, X.-Q. Zhang, X.-Y. Liu, J. Fan, L.-S. Liao, Blue thermally activated delayed fluorescence materials based on bi/tricarbazole derivatives, Org. Electron. **58**(January), 238–244 (2018), https://doi.org/10.1016/j.orgel.2018.04.022.

[126] N. Jürgensen, A. Kretzschmar, S. Höfle, J. Freudenberg, U. H. F. Bunz, G. Hernandez-Sosa, Sulfone-Based Deep Blue Thermally Activated Delayed Fluorescence Emitters: Solution-Processed Organic Light-Emitting Diodes with High Efficiency and Brightness, Chem. Mater. **29**(21), 9154–9161 (2017), https://doi.org/10.1021/acs.chemmater.7b02964.

[127] P. Rajamalli, D. Chen, W. Li, I. D. W. Samuel, D. B. Cordes, A. M. Z. Slawin, E. Zysman-Colman, Enhanced thermally activated delayed fluorescence through bridge modification in sulfone-based emitters employed in deep blue organic light-emitting diodes, J. Mater. Chem. C **7**(22), 6664–6671 (2019), https://doi.org/10.1039/C9TC01498E.

[128] C. Chan, L. Cui, J. U. Kim, H. Nakanotani, C. Adachi, Rational Molecular Design for Deep-Blue Thermally Activated Delayed Fluorescence Emitters, Adv. Funct. Mater. **28**(11), 1706023 (2018), https://doi.org/10.1002/adfm.201706023.

[129] J. Liu, K. Zhou, D. Wang, C. Deng, K. Duan, Q. Ai, Q. Zhang, Pyrazine-Based Blue Thermally Activated Delayed Fluorescence Materials: Combine Small Singlet–Triplet Splitting With Large Fluorescence Rate, Front. Chem. **7**(MAY), 1–9 (2019), https://doi.org/10.3389/fchem.2019.00312.

[130] J. Guo, J. Fan, L. Lin, J. Zeng, H. Liu, C. Wang, Z. Zhao, B. Z. Tang, Mechanical Insights into Aggregation-Induced Delayed Fluorescence Materials with Anti-Kasha Behavior, Adv. Sci. **6**(3), 1801629 (2019), https://doi.org/10.1002/advs.201801629.

[131] Y. Liu, H. Huang, T. Zhou, K. Wu, M. Zhu, J. Yu, G. Xie, C. Yang, Boosting photoluminescence quantum yields of triarylboron/phenoxazine hybrids via incorporation of cyano groups and their applications as TADF emitters for high-performance solution-processed OLEDs, J. Mater. Chem. C **7**(16), 4778–4783 (2019), https://doi.org/10.1039/C9TC00538B.

[132] Y. Liu, G. Xie, K. Wu, Z. Luo, T. Zhou, X. Zeng, J. Yu, S. Gong, C. Yang, Boosting reverse intersystem crossing by increasing donors in triarylboron/phenoxazine hybrids: TADF emitters for high-performance solution-processed OLEDs, J. Mater. Chem. C **4**(20), 4402–4407 (2016), https://doi.org/10.1039/C6TC01353H.

[133] J. Lu, Y. Zheng, J. Zhang, Rational design of phenoxazine-based donor–acceptor–donor thermally activated delayed fluorescent molecules with high performance, Phys. Chem. Chem. Phys. **17**(30), 20014–20020 (2015), https://doi.org/10.1039/C5CP02810H.

[134] H. Tanaka, K. Shizu, H. Miyazaki, C. Adachi, Efficient green thermally activated delayed fluorescence (TADF) from a phenoxazine–triphenyltriazine (PXZ–TRZ) derivative, Chem. Commun. **48**(93), 11392 (2012), https://doi.org/10.1039/c2cc36237f.

[135] R. Komatsu, H. Sasabe, K. Nakao, Y. Hayasaka, T. Ohsawa, J. Kido, Unlocking the Potential of Pyrimidine Conjugate Emitters to Realize High-Performance Organic Light-Emitting Devices, Adv. Opt. Mater. **5**(2), 1600675 (2017), https://doi.org/10.1002/adom.201600675.

[136] K. Wu, T. Zhang, L. Zhan, C. Zhong, S. Gong, N. Jiang, Z.-H. Lu, C. Yang, Optimizing Optoelectronic Properties of Pyrimidine-Based

TADF Emitters by Changing the Substituent for Organic Light-Emitting Diodes with External Quantum Efficiency Close to 25 % and Slow Efficiency Roll-Off, Chem. - A Eur. J. **22**(31), 10860–10866 (2016), https://doi.org/10.1002/chem.201601686.

[137] D.-G. Chen, T.-C. Lin, C.-L. Chen, Y.-T. Chen, Y.-A. Chen, G.-H. Lee, P.-T. Chou, C.-W. Liao, P.-C. Chiu, C.-H. Chang, Y.-J. Lien, Y. Chi, Optically Triggered Planarization of Boryl-Substituted Phenoxazine: Another Horizon of TADF Molecules and High-Performance OLEDs, ACS Appl. Mater. Interfaces **10**(15), 12886–12896 (2018), https://doi.org/10.1021/acsami.8b00053.

[138] J. H. Kim, J. H. Yun, J. Y. Lee, Recent Progress of Highly Efficient Red and Near-Infrared Thermally Activated Delayed Fluorescent Emitters, Adv. Opt. Mater. **6**(18), 1800255 (2018), https://doi.org/10.1002/adom.201800255.

[139] A. Köhler, H. Bässler, Triplet states in organic semiconductors, Mater. Sci. Eng. R Reports **66**(4-6), 71–109 (2009), https://doi.org/10.1016/j.mser.2009.09.001.

[140] Y. Liu, C. Li, Z. Ren, S. Yan, M. R. Bryce, All-organic thermally activated delayed fluorescence materials for organic light-emitting diodes, Nat. Rev. Mater. **3**(4), 18020 (2018), https://doi.org/10.1038/natrevmats.2018.20.

CURRICULUM VITAE

Name:	Rokas
Surname:	Skaisgiris
Date of birth:	1991-12-28
Place of birth:	Kaunas, Lithuania
E-mail:	rokas.skaisgiris@gmail.com

Education:

2016 – 2020	Vilnius University, Faculty of Physics *Ph.D. studies.*
2014 – 2016	Vilnius University, Faculty of Physics *Master's degree in Materials Technology.*
2010 – 2014	Vilnius University, Faculty of Physics *Bachelor's degree in Physics.*
2002 – 2010	Kaunas Jonas Jablonskis Gymnasium.

Work experience:

2019-01 – now	Vilnius University, Institute of Photonics and Nanotechnology, *Junior research fellow.*
2016-07 – 2019-01	Vilnius University, Institute of Applied Physics, *Engineer.*
2015-07 – 2015-08	Vilniaus universitetas, Institute of Applied Physics, *Engineer.*
2014-06 – 2014-07	Vilniaus universitetas, Institute of Applied Physics, *Engineer.*
2012-10 – 2013-07	Vilniaus universitetas, Institute of Applied Physics, *Student intern.*

COPIES OF PUBLICATIONS

A1

Emission wavelength dependence on the rISC rate in TADF compounds with large conformational disorder

T. Serevičius, **R. Skaisgiris**, J. Dodonova, L. Jagintavičius, J. Bucevičius, K. Kazlauskas, S. Juršėnas, S.Tumkevičius

Chem. Comm. **55**(13), 1975–1978 (2019)
DOI: 10.1039/C8CC08906J
http://xlink.rsc.org/?DOI=C8CC08906J

Supporting information: http://www.rsc.org/suppdata/c8/cc/c8cc08906j/c8cc08906j1.pdf

ChemComm

COMMUNICATION

View Article Online
View Journal | View Issue

Cite this: *Chem. Commun.*, 2019, 55, 1975

Received 8th November 2018,
Accepted 17th January 2019

DOI: 10.1039/c8cc08906j

rsc.li/chemcomm

Emission wavelength dependence on the rISC rate in TADF compounds with large conformational disorder†

Tomas Serevičius,* [a] Rokas Skaisgiris,[a] Jelena Dodonova,[b] Laimis Jagintavičius,[b] Jonas Bucevičius,[b] Karolis Kazlauskas,[a] Saulius Juršėnas[a] and Sigitas Tumkevičius[b]

Large vibronic coupling between the local and charge-transfer triplet states is required for efficient reverse intersystem crossing in TADF compounds. This is ensured by low steric hindrance between donor and acceptor molecular units. However, flexible molecular cores show large conformational disorder and emission wavelength instability in solid films.

According to the spin statistics, 75% of excitons formed in OLED devices are of non-emissive triplet nature, limiting their efficiency. Thermally activated delayed fluorescence (TADF) is the most promising pathway for triplet harvesting, since TADF compounds are cheaper and much more stable[1] than rare-earth metal based phosphorescent emitters widely used for display applications. Likewise, TADF OLEDs already show pronounced stability[2] and their external quantum efficiency (EQE) reaches exceptional values of about 40%[3] similar to the benchmark devices. All this makes TADF OLEDs perfect candidates to replace expensive phosphorescent OLEDs for applications in flat-panel screens and lighting in near future. The utilization of non-emissive triplet states in TADF emitters is achieved by thermally activated reverse intersystem crossing (rISC),[4] which is possible in molecular compounds with low singlet–triplet energy (ΔE_{ST}) gaps. Although several possible molecular geometries were suggested,[1,5] TADF emitters mostly are constructed from single-bonded donor (D) and acceptor (A) units. In such a geometry donor and acceptor units are twisted to nearly orthogonal angles[4,6] due to a steric hindrance ensuring a low overlap of π-electron orbitals in the HOMO and LUMO and sufficiently low ΔE_{ST}. However, steric hindrance between the D and A fragments should not be too large, as the strong restriction of twisting of the D–A fragments may reduce the vibronic coupling between localized (^{3}LE) and charge transfer (^{3}CT) triplet states, which is mandatory for efficient rISC,[7–9] and reduce the rISC rate. This requirement for a labile molecular core brings several interesting and unexpected effects. In dilute solutions, minor dispersion of D–A twist angles may be observed, having negligible effect on excited state relaxation. However, it becomes especially important in solid films, where molecules are frozen in conformations with a large variation of the molecular geometry. The existence of fixed molecular conformers in solid hosts causes the dispersion of ^{1}CT energies and ΔE_{ST} gaps, which has great importance in TADF properties.[10] There were several reports showing that conformational disorder of a molecular structure in solid hosts causes the temporal shifts of prompt and delayed fluorescence (PF and DF, respectively),[10–13] resulting in multiexponential DF decay with prolonged lifetime. However, the impact of conformational disorder on fluorescence properties, its relation to the rISC rate and methods to reduce the disorder, despite its importance, still are scarcely studied.

In this work we investigate the conformational disorder in solid films of phenothiazine–pyrimidine TADF compounds and its relation to emission properties. Compounds were designed to have different lability of the molecular structure and different reverse intersystem crossing (rISC) rate. A phenothiazine electron-donor unit was selected because of its ability to form several conformations, increasing the number of possible molecular structure arrangements in the solid state. We show that the variation of molecular structure rigidity of phenothiazine-pyrimidine compounds has only minor impact on conformational disorder and emission properties, while the rISC rate was found to have crucial importance in TADF properties.

The molecular structures and synthetic routes of phenothiazine–pyrimidine compounds **PTZ-mPYR**, **PTZ-mPYRCl** and **PTZ-2mPYR** are depicted in Scheme 1. Compounds **PTZ-mPYR** and **PTZ-mPYRCl**, designed to have different ISC and rISC rates by involving a heavy atom effect, were synthesized by Suzuki–Miyaura coupling of 4,6-dichloro-(**1a**) or 2,4,6-trichloropyrimidines (**1b**) with boronic acid **2** in the presence of $Pd(OAc)_2/PPh_3/Na_2CO_3$ as a catalyst system in 79% and 60% yields, respectively. Compound **PTZ-2mPYR**, designed to have a less labile molecular core than **PTZ-mPYR**, was synthesized

[a] *Institute of Photonics and Nanotechnology, Faculty of Physics, Vilnius University, Saulėtekio 3, LT-10257 Vilnius, Lithuania. E-mail: tomas.serevicius@tmi.vu.lt*
[b] *Institute of Chemistry, Faculty of Chemistry and Geosciences, Vilnius University, Saulėtekio 3, LT-10257 Vilnius, Lithuania*

† Electronic supplementary information (ESI) available: Synthesis, DFT calculations, CV data and details of photophysical characterization. See DOI: 10.1039/c8cc08906j

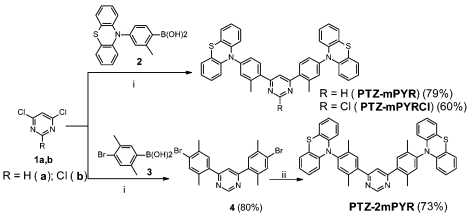

Scheme 1 The synthetic routes of **PTZ-mPYR**, **PTZ-mPYRCl** and **PTZ-2mPYR**. *Reagents and conditions*: (i) $Pd(OAc)_2$ (10 mol%), PPh_3 (20 mol%), Na_2CO_3 aq (6.2 equiv.), glyme/H_2O, Ar, 90 °C, 24 h; (ii) phenothiazine, $Pd(OAc)_2$ (5 mol%), P(*t*-Bu)$_3$·HBF_4 (10 mol%), NaO*t*-Bu (4 equiv.), toluene, Ar, 100 °C, 24 h.

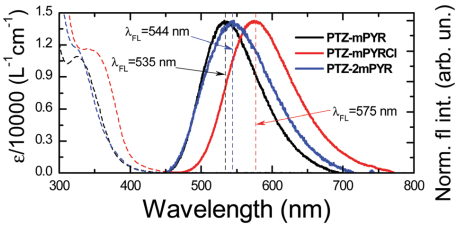

Fig. 1 Absorption and fluorescence spectra of the dominant $^1CT_{QE}$ band of phenothiazine–pyrimidine compounds in dilute toluene solutions. Excitation wavelength was 360 nm.

by a two-step protocol. Firstly, 4,6-dichloropyrimidine **1a** was coupled with boronic acid **3** to afford 4,6-bis(4-bromo-3,5-dimethylphenyl)-pyrimidine (**4**) in 80% yield. Then intermediate **4** was coupled with phenothiazine using the Buchwald–Hartwig amination reaction conditions to give the target **PTZ-2mPYR** in 73% yield. The synthetic details and characterization of the synthesized phenylboronic acids **2** and **3** and target compounds **PTZ-mPYR**, **PTZ-mPYRCl** and **PTZ-2mPYR** are presented in the ESI.†

Cyclic voltammetry analysis revealed that the energies of the HOMO were in the range of about −5.05 to −5.12 eV and those of the LUMO were in the range of −2.46 to −2.79 eV (see Fig. S1 and Table S1 in the ESI† for details).

DFT simulations were employed to optimize the molecular structure and estimate $S_0 \rightarrow S_n/T_n$ transition energies for different phenothiazine orientations (see Fig. S2 and Table S2 in the ESI†). Two main possible molecular conformations of a phenothiazine donor group[14–17] were found, when phenothiazine is oriented perpendicular (quasi-equatorial arrangement, QE) or parallel (quasi-axial arrangement, QA) to the bridging phenyl group. Only the QE conformer state was found for **PTZ-2mPYR** where the rotation of the phenothiazine unit was impeded by additional methyl groups (see Fig. S3 in the ESI†).[18,19] The total potential energies of all possible conformers differed by ~30 meV (see Fig. S4 and Table S3 in the ESI†), thus all arrangements (including mixed QA–QE) may co-exist.[14,19,20] Different π-electron distribution patterns were found for QA, QA–QE and QE conformers. Low overlap of electron density in the HOMO and LUMO was found for QE conformers, while in QA conformations remarkable overlap was observed due to the low twist angle of the phenothiazine unit. QE and QE–QA conformers showed the lowest $S_0 \rightarrow S_1$ transition energies (~2.56–2.98 eV) with negligible oscillator strengths (<0.001), however low ΔE_{ST} gaps up to 20 meV were estimated only for QE-oriented structures. QA conformers showed remarkably larger $S_0 \rightarrow S_1$ absorption energies (~3.23–3.4 eV) with remarkably larger oscillator strengths (~1.01) and ΔE_{ST} gaps of about 440 meV. TADF is expected only from QE conformers, while for QA states a negligible rISC rate is expected.

The absorption and fluorescence spectra of phenothiazine–pyrimidine compounds were analysed in dilute solutions and polymer films. The absorption and emission spectra in toluene are shown in Fig. 1. The absorption spectra showed a broad peak at 320–375 nm (with molar absorption coefficients of about 10^4 mol^{-1} cm^{-1}) of QA conformers (for compounds **PTZ-mPYR** and **PTZ-mPYRCl**) followed by a low intensity absorption band tail in the range of about 400–450 nm of QE states, typically for phenothiazine TADF compounds[14–17] and in-line with the DFT-predictions. The fluorescence spectra of $^1CT_{QE}$ states, after excitation with 360 nm light, peaked in the range of 544–575 nm. Broad and structureless spectra were of intramolecular charge-transfer (ICT) nature. Modification of phenyl fragments with methyl substituents enabled tuning of the FL peak energy for 40 meV due to varying HOMO–LUMO overlap (see Fig. S2 in the ESI†),[21] while the introduction of Cl atom redshifted the FL peak energy of 170 meV up to 575 nm for **PTZ-mPYRCl**.

The presence of different phenothiazine conformations, predicted by DFT simulations, was shown by measuring the fluorescence excitation spectra (see full fluorescence spectra in the log scale in Fig. S5 in the ESI†). Three distinct emission bands were observed for compounds **PTZ-mPYR** and **PTZ-mPYRCl** after excitation with 300–350 nm light: low intensity ^1LE (at about 300–400 nm) and $^1CT_{QA}$ (^1CT fluorescence from QA conformations) at about 400–450 nm together with very intense $^1CT_{QE}$ fluorescence (^1CT fluorescence of QE conformations) at 544–575 nm. Only $^1CT_{QE}$ emission was observed by exciting into the absorption tail at 410–450 nm. Other phenothiazine-based TADF compounds with a similar molecular structure also have shown fluorescence spectra composed of peaks from QA and QE conformers[14–16,22] and dominating $^1CT_{QE}$ emission. In contrast, only ^1LE and $^1CT_{QE}$ fluorescence peaks were observed for **PTZ-2mPYR** for all excitation wavelengths, when the formation of QA conformers was impeded by an extra methyl group.[22]

$^1CT_{QA}$ and $^1CT_{QE}$ emission peaks were also observed in the emission spectra of compounds **PTZ-mPYR** and **PTZ-mPYRCl** embedded in the PMMA host, while only $^1CT_{QE}$ emission was observed for **PTZ-2mPYR** (see Fig. 2a and b and Fig. S6 in the ESI,† black curves). Emission energies were slightly blueshifted in respect of toluene due to the lower dipole moment of PMMA. Singlet–triplet energy gaps between $^1CT_{QE}$ and ^3LE states were estimated to be in the range of 151–187 meV, small enough to observe thermally activated rISC[21] (see Fig. S7 in the ESI†). ΔE_{ST} gaps for QA conformers were too large for triplet upconversion. The presence of TADF was showcased by the temperature activation of delayed fluorescence (see Fig. S8 in the ESI†) and by comparing time-integrated fluorescence (TIFL) spectra in oxygen-sufficient (O_2^+) and deficient (O_2^-) ambient environments (see Fig. 2c and d and

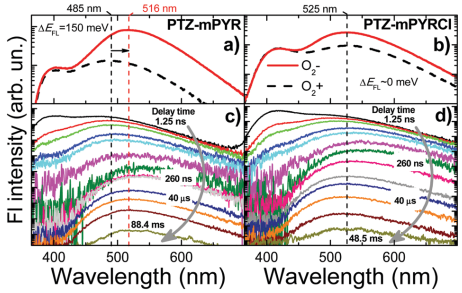

Fig. 2 (a and b) Time-integrated fluorescence spectra of 1 wt% PMMA films of **PTZ-mPYR** and **PTZ-mPYRCl**, respectively, in oxygen-sufficient (O_2^+, black lines) and oxygen-deficient (O_2^-, red lines) surroundings. (c and d) Time-resolved fluorescence spectra of 1 wt% PMMA films of **PTZ-mPYR** (c) and **PTZ-mPYRCl** (d) in O_2^- surrounding. Numbers close to Fl spectra denote delay times (1.25 ns for black lines, 260 ns for yellow lines, 40 µs for dark blue lines and 48.5/88.4 ms for the last spectrum). Vertical lines are guides for eyes.

Fig. S6 in the ESI†). TIFL intensity remarkably increased due to the weakened triplet state quenching by oxygen. Along with that, an unexpected effect was observed. The fluorescence peaks of compounds **PTZ-mPYR** and **PTZ-2mPYR** were redshifted for about 150 meV upon oxygen removal and TADF enhancement, while for **PTZ-mPYRCl** the emission peak energy remained the same.

The nature of such intriguing behaviour was revealed by analysing the temporal evolution of fluorescence spectra (see Fig. 2(c and d) and Fig. S6 in the ESI†). Emission peak energy was found to be time-dependent. Initially, the redshift was observed during the first 250–300 ns, followed by a blueshift later. The observed fluorescence shifts are caused by conformational disorder, the concept of which was elegantly introduced by Northey *et al.*[10] and experimentally observed by others.[11–13] Briefly, flexible donor–acceptor cores of TADF compounds are "frozen" in solid films with different twist angles between donor and acceptor fragments inducing the dispersion of ^{1}CT energies and ΔE_{ST} values. Conformations with the largest ^{1}CT energies have the largest oscillator strengths, and thus are expected to emit first, inducing a gradual redshift of PF. For DF, the opposite trend is observed due to exponential rISC rate dependence on ΔE_{ST}: conformations with the lowest ^{1}CT energies and smallest ΔE_{ST} gaps will emit first, inducing the gradual blueshift of TADF spectra. In our case, only $^1CT_{QE}$ fluorescence with pronounced CT characteristics was affected by conformational disorder. In ambient air (see Fig. S9 in the ESI†), the estimated redshift of the $^1CT_{QE}$ peak varied in the range of 280–380 meV (280 meV, 340 meV and 380 meV for **PTZ-mPYRCl**, **PTZ-mPYR** and **PTZ-2mPYR**, respectively), while the largest blueshift was estimated for **PTZ-mPYRCl** (110 meV) and for the rest of the compounds the blueshift was remarkably lower (40 meV for both **PTZ-mPYR** and **PTZ-2mPYR**). Under O_2^- conditions, the temporal evolution of prompt fluorescence was the same as in ambient air, however the delayed emission showed enhanced intensity at the latest delays (see Fig. S10 in the ESI†) followed by enlarged blueshift. The largest blueshift in ambient O_2^- was estimated for **PTZ-mPYRCl** (130 meV), which was almost the same as in ambient air. For **PTZ-mPYR** and **PTZ-2mPYR**, the blueshift was larger than in ambient O_2^+ (80 meV and 60 meV, respectively), however it still was markedly smaller than for **PTZ-mPYRCl**. In this way, the TIFL spectra of prompt and delayed emission peaked at different wavelengths in ambient O_2^+ and O_2^- for **PTZ-mPYR** and **PTZ-2mPYR**.

To find out why we observe a weaker blueshift for **PTZ-mPYR** and **PTZ-2mPYR** than that for **PTZ-mPYRCl**, fluorescence decay transients were analysed (see Fig. 3). Firstly, O_2^- toluene solutions were analysed in order to estimate the ISC and rISC rates. Double-exponential decay of prompt and delayed fluorescence at the $^1CT_{QE}$ peak was observed. TADF lifetime was comparable for **PTZ-mPYR** and **PTZ-2mPYR** (11 and 6 µs, respectively), while for **PTZ-mPYRCl** it was remarkably shorter, reaching 1.1 µs. Such short TADF lifetime is comparable to the benchmark values.[23] The most rapid TADF decay was followed by the largest delayed fluorescence/prompt fluorescence intensity (DF/PF) ratio of 1.2 for **PTZ-mPYRCl**, while for **PTZ-mPYR** and **PTZ-2mPYR** it was remarkably lower (0.3 and 0.03, respectively). TADF dominated in the emission of **PTZ-mPYRCl** while for **PTZ-mPYR** and **PTZ-2mPYR** the TADF intensity was lower despite almost the same ΔE_{ST} gaps. TADF enhancement in **PTZ-mPYRCl** was promoted by an internal heavy atom effect, enhancing spin–orbit coupling constant, crucial for intersystem crossing (ISC) and rISC.[24] The estimated TADF parameters are listed in Table S4 in the ESI.† The enhanced spin–orbit coupling for **PTZ-mPYRCl** resulted in the most rapid rISC rate, which reached 2×10^6 s^{-1}, about 12–17 times larger than for other compounds. The least efficient TADF for compound **PTZ-2mPYR** could be related to the restricted twisting of the phenothiazine donor fragment, which was shown to be the reason for a negligible rISC rate in similar phenothiazine-based TADF emitters[9] due to decreased coupling of ^{3}LE and ^{3}CT states, crucial for efficient TADF.[7]

Fluorescence decay transients of PMMA films at the dominant $^1CT_{QE}$ peak showed different properties as compared to

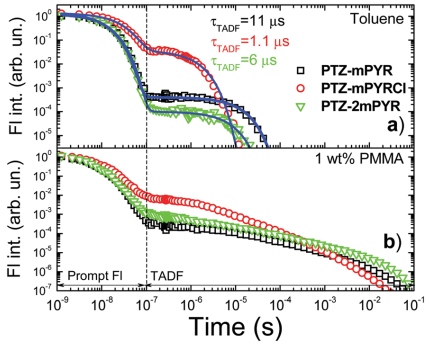

Fig. 3 Normalized $^1CT_{QE}$ fluorescence decay transients of phenothiazine–pyrimidine compounds in toluene (a) and 1 wt% PMMA films (b). Blue lines are biexponential fits.

dilute solutions. The decay of PF was rather typical however the DF decay was multiexponential with remarkably prolonged lifetime due to the conformational disorder. It resulted in tremendously enhanced DF/PF ratios of up to 33.5 (11.8, 8 and 33.5 for **PTZ-mPYR**, **PTZ-mPYRCl** and **PTZ-2mPYR**, respectively). Due to the multiexponential decay profile the TADF decay time and the rISC rate could hardly be correctly evaluated for compounds with such large conformational disorder, however it is clear that **PTZ-mPYRCl** still showed the most rapid TADF decay.

As we can see from the previous results, stable emission in PMMA films was observed for **PTZ-mPYRCl** with the fastest TADF decay. In this case, the TIFL spectra of delayed fluorescence in both ambient O_2^+ and O_2^- were very similar, thus no noticeable shift of the total TIFL spectrum after oxygen removal was observed. In contrast, the latest delayed fluorescence was missing for **PTZ-mPYR** and **PTZ-2mPYR** even under O_2^- conditions, which was completely suppressed by unknown quenchers. The lack of DF from the conformers with the largest ^{1}CT energy disturbed the high-energy shoulder of the TIFL spectrum, resulting in a redshift of its peak. Interestingly, the enhanced rigidity of the **PTZ-2mPYR** molecular core did not reduce the conformational disorder (for all compounds the redshift was rather comparable) and TIFL peak shift. Probably more sophisticated methods should be used to reduce the lability of such phenothiazine–pyrimidine cores. Another possible pathway to achieve low conformational disorder and stable emission wavelength for TADF compounds with slow TADF decay and flexible molecular cores is to use more rigid polymer or small-molecule hosts, impeding the conformation of molecular cores.[13]

In summary, three phenothiazine–pyrimidine TADF compounds with different molecular geometries were synthesized and comprehensively analysed by time-resolved spectroscopy. All compounds showed pronounced conformational disorder governing their emission properties. TADF efficiency and the rISC rate were altered by introducing heavy atoms due to enlarged spin–orbit coupling. A 150 meV redshift of the emission peak in solid films was observed after oxygen removal for compounds with a low rISC rate, while no shift was seen for compounds with rapid rISC. Such unusual behaviour was caused by the quenching of the long-lived DF bearing the largest ^{1}CT energy even in ambient O_2^-, resulting in the loss of the high-energy shoulder of TIFL spectra. Only minor quenching of the latest delayed emission and no noticeable shift of the TIFL spectrum were observed for compounds with rapid rISC. Our results showcase the importance of the large rISC rate in the TADF properties. We have shown that the emission energy of TADF compounds in solid films may depend not only on the conjugation length, but also on some unexpected parameters, such as the rISC rate or molecular core rigidity. This should be taken into account while designing novel TADF compounds.

This research was funded by a grant (No. S-MIP-17-73) from the Research Council of Lithuania. Regimantas Komskis is acknowledged for CV measurements. We are grateful to Dr Alytis Gruodis and High Performance Computing Center "HPC Sauletekis" in Vilnius University Faculty of Physics for total potential energy calculations.

Conflicts of interest

There are no conflicts to declare.

Notes and references

1 Y. Tao, K. Yuan, T. Chen, P. Xu, H. Li, R. Chen, C. Zheng, L. Zhang and W. Huang, *Adv. Mater.*, 2014, **26**, 7931–7958.
2 D. P.-K. Tsang, T. Matsushima and C. Adachi, *Sci. Rep.*, 2016, **6**, 22463.
3 T.-L. Wu, M.-J. Huang, C.-C. Lin, P.-Y. Huang, T.-Y. Chou, R.-W. Chen-Cheng, H.-W. Lin, R.-S. Liu and C.-H. Cheng, *Nat. Photonics*, 2018, **12**, 235–240.
4 H. Uoyama, K. Goushi, K. Shizu, H. Nomura and C. Adachi, *Nature*, 2012, **492**, 234–238.
5 T. Hatakeyama, K. Shiren, K. Nakajima, S. Nomura, S. Nakatsuka, K. Kinoshita, J. Ni, Y. Ono and T. Ikuta, *Adv. Mater.*, 2016, **28**, 2777–2781.
6 P. L. dos Santos, J. S. Ward, D. G. Congrave, A. S. Batsanov, J. Eng, J. E. Stacey, T. J. Penfold, A. P. Monkman and M. R. Bryce, *Adv. Sci.*, 2018, **5**, 1700989.
7 J. Gibson, A. P. Monkman and T. J. Penfold, *ChemPhysChem*, 2016, **17**, 2956–2961.
8 M. K. Etherington, J. Gibson, H. F. Higginbotham, T. J. Penfold and A. P. Monkman, *Nat. Commun.*, 2016, **7**, 13680.
9 J. S. Ward, R. S. Nobuyasu, A. S. Batsanov, P. Data, A. P. Monkman, F. B. Dias and M. R. Bryce, *Chem. Commun.*, 2016, **52**, 2612–2615.
10 T. Northey, J. Stacey and T. J. Penfold, *J. Mater. Chem. C*, 2017, **5**, 11001–11009.
11 G. Méhes, K. Goushi, W. J. Potscavage and C. Adachi, *Org. Electron.*, 2014, **15**, 2027–2037.
12 M. K. Etherington, F. Franchello, J. Gibson, T. Northey, J. Santos, J. S. Ward, H. F. Higginbotham, P. Data, A. Kurowska, P. L. Dos Santos, D. R. Graves, A. S. Batsanov, F. B. Dias, M. R. Bryce, T. J. Penfold and A. P. Monkman, *Nat. Commun.*, 2017, **8**, 14987.
13 T. Serevičius, T. Buciunas, J. Bucevičius, J. Dodonova, S. Tumkevicius, K. Kazlauskas and S. Jursenas, *J. Mater. Chem. C*, 2018, 11128–11136.
14 H. Tanaka, K. Shizu, H. Nakanotani and C. Adachi, *J. Phys. Chem. C*, 2014, **118**, 15985–15994.
15 P. L. dos Santos, J. S. Ward, A. S. Batsanov, M. R. Bryce and A. P. Monkman, *J. Phys. Chem. C*, 2017, **121**, 16462–16469.
16 M. K. Etherington, F. Franchello, J. Gibson, T. Northey, J. Santos, J. S. Ward, H. F. Higginbotham, P. Data, A. Kurowska, P. L. Dos Santos, D. R. Graves, A. S. Batsanov, F. B. Dias, M. R. Bryce, T. J. Penfold and A. P. Monkman, *Nat. Commun.*, 2017, **8**, 14987.
17 R. Huang, J. S. Ward, N. A. Kukhta, J. Avó, J. Gibson, T. Penfold, J. C. Lima, A. S. Batsanov, M. N. Berberan-Santos, M. R. Bryce and F. B. Dias, *J. Mater. Chem. C*, 2018, **6**, 9238–9247.
18 C. Chen, R. Huang, A. Batsanov, P. Pander, Y.-T. Hsu, Z. Chi, F. Dias and M. R. Bryce, *Angew. Chem., Int. Ed.*, 2018, **57**, 16407–16411.
19 K. Wang, C.-J. Zheng, W. Liu, K. Liang, Y.-Z. Shi, S.-L. Tao, C.-S. Lee, X.-M. Ou and X.-H. Zhang, *Adv. Mater.*, 2017, **29**, 1701476.
20 K. Wang, Y.-Z. Shi, C.-J. Zheng, W. Liu, K. Liang, X. Li, M. Zhang, H. Lin, S.-L. Tao, C.-S. Lee, X.-M. Ou and X.-H. Zhang, *ACS Appl. Mater. Interfaces*, 2018, **10**, 31515–31525.
21 R. Komatsu, T. Ohsawa, H. Sasabe, K. Nakao, Y. Hayasaka and J. Kido, *ACS Appl. Mater. Interfaces*, 2017, **9**, 4742–4749.
22 H. F. Higginbotham, C.-L. Yi, A. P. Monkman and K.-T. Wong, *J. Phys. Chem. C*, 2018, **122**, 7627–7634.
23 Y. Im, M. Kim, Y. J. Cho, J.-A. Seo, K. S. Yook and J. Y. Lee, *Chem. Mater.*, 2017, **29**, 1946–1963.
24 Y. Xiang, Y. Zhao, N. Xu, S. Gong, F. Ni, K. Wu, J. Luo, G. Xie, Z.-H. Lu and C. Yang, *J. Mater. Chem. C*, 2017, **5**, 12204–12210.

A2

Origin of dual emission in σ-bridged donor–acceptor TADF compounds

R. Skaisgiris, T. Serevičius, K. Kazlauskas, Y. Geng, C. Adachi, S. Juršėnas

J. Mater. Chem. C. **7**(40), 12601–12609 (2019)
DOI: 10.1039/C9TC03548F
http://xlink.rsc.org/?DOI=C9TC03548F

Supporting information: http://www.rsc.org/suppdata/c9/tc/c9tc03548f/c9tc03548f1.pdf

Journal of
Materials Chemistry C

PAPER

View Article Online
View Journal | View Issue

Cite this: J. Mater. Chem. C, 2019, 7, 12601

Origin of dual emission in σ-bridged donor–acceptor TADF compounds†

Rokas Skaisgiris, [a] Tomas Serevičius, *[a] Karolis Kazlauskas, [a] Yan Geng,[b] Chihaya Adachi *[cd] and Saulius Juršėnas[a]

Received 1st July 2019,
Accepted 20th September 2019

DOI: 10.1039/c9tc03548f

rsc.li/materials-c

The desire to boost the reverse intersystem crossing rate and obtain thermally activated delayed fluorescence with sub-microsecond lifetime fosters the search for novel concepts of molecular geometry. Recently, TADF compounds made of acridine, tetramethylcarbazole and triphenylamine donor and triphenyltriazine acceptor units bound by hyperconjugated spacer units were introduced as having very rapid double TADF decay. Here we present an in-depth time-resolved fluorescence analysis of these intriguing donor–σ–acceptor TADF compounds in various surroundings. Extremely weak coupling of electron-donating and electron-accepting units was found for the σ-bridged TADF compounds, resulting in the coexistence of intramolecular and exciplex fluorescence, whose interplay allowed one to tune the emission properties. The initial fluorescence decay in toluene solutions, previously attributed to rapid TADF, was shown to be prompt intramolecular fluorescence with prolonged fluorescence lifetime, susceptible to molecular oxygen. Only the later delayed fluorescence at the microsecond time-scale, originating from the exciplex states, was attributed to TADF. On the contrary, dominant intramolecular TADF was observed in dilute PMMA films with weaker non-radiative decay. The smooth transition from intramolecular to exciplex TADF was observed by increasing the doping concentration of the polymer films. The DF/PF ratio was found to increase with increasing doping concentration due to the emergence of additional exciplex TADF until a 20 wt% doping load, where concentration quenching emerged at larger doping ratios. The presented findings showcase the unusual fluorescence properties of TADF compounds with weakly bound donor and acceptor units and are important for the future design of novel TADF compounds.

Introduction

Organic light emitting diodes (OLEDs) are highly attractive for lighting and display applications due to their unmatched contrast ratio, lightness and flexibility. The long history of OLED science, dating back to the report by Tang and Van Slyke,[1] mostly was devoted to the improvement of the external quantum efficiency (EQE), which was limited by the dark triplet states. The singlet exciton yield of electrically injected charge carriers for 1st generation fluorescent OLEDs is only 25%, limiting their external quantum efficiency (EQE) to up to about 5%. Later, a new class of phosphorescent emitters employing the internal heavy atom effect was introduced.[2] The involvement of heavy rare-earth atoms, *e.g.*, iridium, resulted in the remarkable enhancement of the spin–orbit coupling, converting all excitons to short-lived triplet ones. This strategy allowed one to reach 100% internal quantum efficiency (IQE) and an EQE of 20% for phosphorescent OLEDs.[3] However, phosphorescent compounds, especially blue emitters, suffer from instability. Moreover, the requirement of rare-earth metals increased the cost of devices and raised concerns over their toxicity. The stability and high-cost issues were solved by introducing 3rd generation all-organic emitters employing thermally activated delayed fluorescence.[4,5] In this case, molecular compounds are designed to have small singlet–triplet energy splitting (ΔE_{ST}), where the triplet excitons are thermally assisted to perform reverse intersystem crossing with internal quantum efficiencies up to 100%.[6,7] Several different approaches for the realization of small ΔE_{ST} were suggested: minimization of the exchange interaction by using donor–acceptor molecular compounds,[5] utilization of multiple resonance effects[8] or by employing the excited-states.[9,10] Yet, the donor–acceptor core still is the mostly used TADF design. In this case efficient reverse

[a] Institute of Photonics and Nanotechnology, Vilnius University, Sauletekio 3, LT-10257, Vilnius, Lithuania. E-mail: tomas.serevicius@tmi.vu.lt
[b] College of Chemistry, Chemical Engineering and Materials Science, Collaborative Innovation Center of Functionalized Probes for Chemical Imaging in Universities of Shandong, Key Laboratory of Molecular and Nano Probes, Ministry of Education, Shandong Normal University, Jinan 250014, P. R. China
[c] Center for Organic Photonics and Electronics Research (OPERA), and International Institute for Carbon Neutral Energy Research (WPI-I^{2}CNER), Kyushu University, Fukuoka 819-0395, Japan. E-mail: adachi@cstf.kyushu-u.ac.jp
[d] Japan Science and Technology Agency ERATO, Adachi Molecular Exciton Engineering Project, Fukuoka 819-0395, Japan

† Electronic supplementary information (ESI) available. See DOI: 10.1039/c9tc03548f

intersystem crossing (rISC) is achieved by minimizing the exchange energy, which is directly proportional to the HOMO–LUMO overlap,[11] and ensuring strong vibronic coupling between the localized (^{3}LE) and charge-transfer (^{3}CT) triplet states.[12,13] Small HOMO–LUMO overlap is attained in compounds constructed of electron-donating (D) and electron-accepting (A) molecular fragments with balanced steric hindrance, having pronounced charge-transfer (CT) character and non-negligible radiative recombination rates.

The same concept based on the minimization of ΔE_{ST} by reducing the HOMO–LUMO overlap was utilized in exciplex emitters,[14,15] composed of electron-donating and electron-accepting molecular materials. Though small ΔE_{ST} in exciplex systems can be realized more easily due to the intermolecular nature of charge transfer and rather efficient exciplex-based OLEDs with EQEs approaching 20% have been presented,[16] the efficiency of exciplex TADF strongly depends on the distance between the donor and acceptor fragments,[17] which is difficult to control. This strongly complicates the applications of exciplex TADF OLEDs. To overcome the shortcomings of exciplex TADF, a novel strategy was suggested. In this case the donor and acceptor units were bound in close proximity (*e.g.* several Å) with conjugated[18] or non-conjugated[19–22] spacers utilizing intermolecular through-space charge transfer. Rather efficient exciplex TADF can be achieved with fluorescence quantum efficiencies (Φ_F) up to about 60% and EQEs up to about 12%. Another promising pathway for similar "fixed" exciplex systems is to employ hyperconjugation,[23,24] which allows one to bind two separated π-conjugated electron systems. Recently, we have suggested a novel donor–σ–acceptor geometry utilizing the hyperconjugation effect to obtain TADF.[25] Several donor units were bound to a triphenyltriazine acceptor fragment by a hexafluoroisopropylidene spacer unit. In this case, the hyperconjugation between the donor and acceptor moieties ensured very small HOMO–LUMO overlap and ΔE_{ST} together with the intramolecular nature of CT. The DFT-estimated oscillator strengths were very low (in the range of 0.0008–0.0054), typical for weakly interacting donor and acceptor systems. Dual TADF decay was observed, one of which was very rapid with a lifetime of only 200–400 ns, which is one of the shortest ever reported.[26] Successful realization of TADF with sub-microsecond lifetime in similar hyperconjugation-based compounds could open new possibilities for realization of highly efficient OLEDs with low roll-off.[27]

Inspired by the intriguing TADF properties of donor–σ–acceptor TADF compounds with sub-microsecond lifetime,[25] here we performed a comprehensive time-resolved fluorescence study of σ-bridged TADF compounds with dual upconversion in various surroundings. The analysis of viscosity, concentration and temperature-dependent fluorescence spectra of the TADF compounds in dilute solutions, and dilute polymer and neat films revealed the interplay of two different CT states, decaying on different time-scales. The molecular concentration and ambient viscosity were shown to tune the emission type, intramolecular or intermolecular CT or even from both types simultaneously. Intramolecular TADF was observed only in dilute polymer films, while the coexisting exciplex emission was shown to be of TADF nature in solutions and films at high doping concentration.

Experimental details

The photophysical properties were measured in 1.2×10^{-5} M toluene solutions, PMMA (poly(methylmethacrylate)) films with variable doping concentration (1–100 wt%) and neat films. The analysis of the CT state was also performed in 1×10^{-4} M toluene solutions. The PMMA films were prepared by dissolving the compound and PMMA at appropriate ratios in toluene and then drop-casting at room temperature on a quartz substrate. The neat films were prepared from 5 mg ml^{-1} toluene solution by spin-coating at 800 rpm for 1 min and finalizing with 8 min of 4000 rpm to accelerate the evaporation of toluene. To modify the viscosity of toluene, PMMA polymer was added into the solution in different proportions.[28] The absorption spectra were measured using a UV-vis-NIR spectrophotometer Lambda 950 (PerkinElmer). Steady-state emission spectra were recorded using a CCD spectrometer PMA-11 (Hamamatsu) coupled with a CW xenon lamp (FWHM < 10 nm). Fluorescence quantum yields (Φ_F) were obtained by using the integrating sphere method.[29] Time-resolved fluorescence spectra, fluorescence decay transients and phosphorescence spectra were obtained by using a nanosecond YAG:Nd^{3+} laser NT 242 with an optical parametric generator (Ekspla, excitation wavelength 300 nm, pulse duration 7 ns, repetition rate 1 kHz, 50 nJ per pulse fluence) and time-gated intensified CCD camera iStar DH340T (Andor) with a spectrograph SR-303i (Shamrock). Phosphorescence spectra were measured at a 10 K temperature after a 100 μs delay with a 890 μs integration time. Fluorescence decay transient measurements were performed by exponentially increasing the delay and integration time as described in ref. 30. This allowed us to record up to 10 orders of magnitude in time and intensity of the photoluminescence decay. Five repetitive freeze–pump–thaw cycles were used to deoxygenate the toluene solutions. The polymer samples were mounted in a closed cycle He cryostat (Cryo Industries 204N) for both oxygen-saturated and oxygen-free (at a 1×10^{-4} Torr pressure) measurements. Temperature dependent measurements were performed in the same closed cycle He cryostat.

Results and discussion

Materials and steady-state spectroscopy analysis of dilute solutions

Three TADF compounds of donor–σ–acceptor structure were analyzed (see Fig. 1). A planar triphenyltriazine fragment was used as an electron-acceptor unit while dihydroacridine (**1**), tetramethylcarbazole (**2**) and triphenylamine (**3**) were selected as electron-donating units with different electron-donating strengths.[31] Hexafluoroisopropylidene was used as a σ-spacer. Synthetic details, initial DFT calculations and a brief analysis of the fluorescence properties were reported elsewhere[25] and are

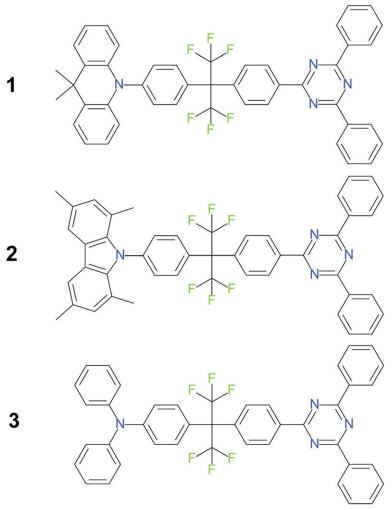

Fig. 1 Chemical structures of donor–σ–acceptor compounds **1–3**.

briefly reported in this chapter, while thorough spectroscopic analysis will be presented in the following chapters.

The absorption spectra peaked below 300 nm with weak absorption of intramolecular charge transfer (ICT) origin at about 300–370 nm, observed for all compounds, in-line with the DFT predictions.[25] Negligible oscillator strengths of 0.0008, 0.0012 and 0.0054 were simulated for compounds **1–3**, respectively. The fluorescence spectra of toluene solutions peaked in the range of 437–463 nm. The broad and structureless spectral lineshape indicated the charge-transfer nature. Locally excited (^{1}LE) state emission at about 360 nm was clearly observed for compound **2**, originating from the tetramethylcarbazole donor unit,[25] while for the rest of the compounds the ^{1}LE intensity was lower. The low-temperature phosphorescence spectra of toluene solutions (LTPh) were of ^{3}LE nature with the lowest energy vibronic replicas peaking at 415–419 nm. Singlet–triplet energy gaps (ΔE_{ST}) of 0.06, 0.07 and 0.18 eV were estimated for compounds **1**, **2** and **3**, respectively.[25]

Excited state relaxation in dilute solutions

The fluorescence decay transients of donor–σ–acceptor compounds **1–3** at the CT emission peak in oxygen-free ($-O_2$) toluene followed a double-exponential decay (see Fig. 2). Initially, the fluorescence decayed with a lifetime of 37–470 ns (τ_{FL1}), followed by later slower decay with a lifetime (τ_{FL2}) of 0.45–10 μs (see Table 1 for details). The presence of oxygen strongly quenched both CT fluorescence bands. Both fluorescence decays in $-O_2$ toluene, the fast and the slower one, were attributed to TADF in the initial analysis.[25] Fluorescence quenching by oxygen and TADF intensity activation with temperature were used as the proof. However, the nature of both decays is more complex.

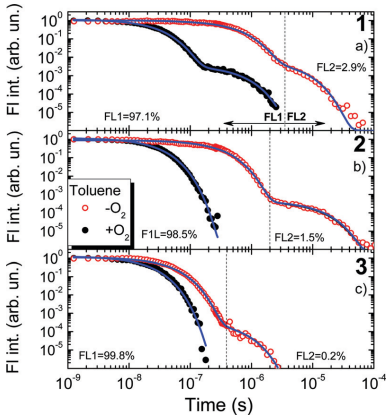

Fig. 2 Normalized fluorescence decay transients of donor–σ–acceptor compounds **1** (a), **2** (b) and **3** (c) in oxygen-saturated ($+O_2$) and oxygen-free ($-O_2$) toluene solutions. Fractional intensities of the initial and delayed fluorescence in $-O_2$ conditions are also noted.

Table 1 Fluorescence data of donor–σ–acceptor compounds **1–3** in oxygen-free toluene

	τ_{FL}[a] (ns)	τ_{TADF}[b] (μs)	DF/PF[c]
1	470	4.5	0.03
2	250	10	0.015
3	37	0.45	0.002

[a] Fluorescence decay time of the initial fluorescence. [b] Fluorescence decay time of the delayed fluorescence. [c] Time-integrated delayed and prompt fluorescence intensity ratio.

The initial decay with a lifetime of 37–470 ns could also be prompt fluorescence. This would not be surprising for weakly coupled D–σ–A compounds with small HOMO–LUMO overlap and negligible oscillator strengths. The lowest oscillator strength was estimated for compound **1** with the largest τ_{FL1} while the lowest τ_{FL1} was for compound **3** with the largest oscillator strength. ΔE_{ST} and the TADF lifetime also depend on the HOMO–LUMO overlap[11] (and thus the oscillator strength) and more rapid TADF decay should be observed for compounds with smaller ΔE_{ST}. The smallest singlet–triplet energy gap was estimated for compounds **1** and **2** (60 and 70 meV, respectively), while for compound **3** it was remarkably larger (180 meV). However, the opposite trend was observed. As we can see, τ_{FL1} was the longest for the compound with the lowest ΔE_{ST} and it was the shortest for the compound with the largest ΔE_{ST}. Such a trend is the opposite of what we would expect for TADF, but in-line with the trend for prompt fluorescence: the longest τ_{FL1} was observed for compound **1** with the strongest dihydroacridine donor unit[25,31] and the lowest oscillator strength, while the shortest τ_{FL1} was observed for compound **3** with the weakest triphenylamine donor unit and the largest oscillator strength. This prompt fluorescence was shown to be susceptible to molecular oxygen. This is rather unusual, however singlet states

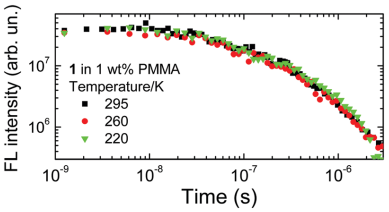

Fig. 3 Initial fluorescence decay transients of 1 wt% PMMA films of compounds **1–3**.

have been shown to be sensitive to molecular oxygen.[32–34] Our donor–σ–acceptor compounds with especially long prompt fluorescence lifetime could be even more prone to quenching by molecular oxygen.

To analyze the nature of the initial fluorescence, temperature-dependent measurements of fluorescence transients were performed in dilute toluene (see Fig. S6 and S7 in ref. 25) and the decrease of τ_{FL1} was observed at larger temperatures, typical for TADF. However, when the compounds were embedded into PMMA polymer films (see Fig. 3), the lifetime and the intensity of the initial decay were insensitive to the temperature. Toluene has a melting point of 178 K, therefore it remained in the liquid state in the temperature range of 300–200 K, thus the variation of the non-radiative recombination rate upon the temperature decrease was not neglected. The impact of non-radiative decay was strongly suppressed in the rigid polymer film, where no thermal activation was observed, typical for prompt fluorescence.

The decay time of the later fluorescence, observed at the microsecond time-scale, was 4.5, 10 and 0.45 μs (an approximate value due to the low emission intensity) for compounds **1**, **2** and **3**, respectively. In this case, the second decay component followed TADF-like behavior: its lifetime was lower for compounds with lower ΔE_{ST} and the DF/PF ratio was larger for compounds with lower ΔE_{ST} (see Table 1).

To conclude, the initial fluorescence decay could hardly be attributed to TADF. The experimental evidence shows its non-TADF nature. Only the later fluorescence, observed at the microsecond time-scale, can be attributed to TADF.

Two charge-transfer states in dilute solutions

The time-integrated fluorescence spectra (TIFL) of compounds **1–3** in toluene[25] showed only one dominating CT fluorescence band with a double-exponential decay profile. On the contrary, time-resolved fluorescence spectra (TRFL) analysis (see Fig. 4) revealed the presence of more complex structure of the emission spectra. Two CT fluorescence spectra were observed at different time-scales. Initially, the first CT fluorescence band ($^1CT_1$) was observed at about 445–465 nm up to about 4 μs, 2 μs and 0.5 μs for compounds **1–3**, respectively. At later delays, the second CT fluorescence band ($^1CT_2$) clearly emerged, peaking at about 475–505 nm (see Fig. S1 in the ESI†). Some long-wavelength shoulders of the fluorescence spectra, extending up to 600–650 nm, were observed for all compounds even at the smallest

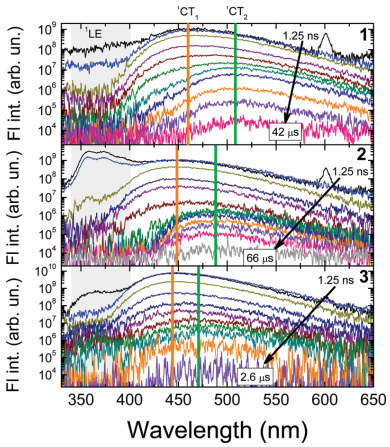

Fig. 4 Time-resolved fluorescence spectra of donor–σ–acceptor compounds **1–3** in oxygen-free toluene at 1.2×10^{-5} M concentration. The numbers in the picture denote the initial and final delay times.

delay times, showing that the weak second CT state probably is formed after the photoexcitation, but is overwhelmed by fluorescence of the $^1CT_1$ state. The $^1CT_2$ emission was more susceptible to oxygen quenching than that of the $^1CT_1$ states (see Fig. S2 in the ESI†). Since the prompt and delayed fluorescence are observed at different wavelengths, the true TADF transients at larger delays are those obtained at the $^1CT_2$ peak (see Fig. S3 in the ESI†). An enhanced TADF intensity was observed (up to about 5–6 times) with the same lifetime.

The nature of both CT states needs further analysis. Clearly, both emission bands are of CT-nature and their peak energies depend on the strength of the donor unit: the stronger the donor, the more redshifted the emission wavelength. The energy difference between the CT bands was 240, 220 and 160 meV for compounds **1–3**, respectively. The second emission band, which becomes clearly evident only at later delays, could originate from, *e.g.*, dynamic molecular conformer states, emerging after the reorganization of the molecular structure,[35] or exciplex states,[36] formed between the donor and acceptor units from separate molecules after diffusion at long time-scales.

To test the nature of the second CT state, the fluorescence decay transients of compound **1** were measured in $-O_2$ toluene solutions with adjustable viscosity (see Fig. 5 and the Experimental section for details). More viscous toluene surrounding had a weak effect on the prompt emission, slightly decreasing its decay time from 470 to 280 ns, while the increased viscosity strongly quenched the TADF, where the DF/PF ratio decreased from 0.15 to 0.003 (see Table 2). The decrease of the prompt fluorescence lifetime could be related with the changes of the non-radiative decay rate. It is clear that the TADF intensity is weakened in viscous surroundings, however still it is not clear whether the quenching of delayed emission was due to the impeded reorganization of the molecular structure or slowed

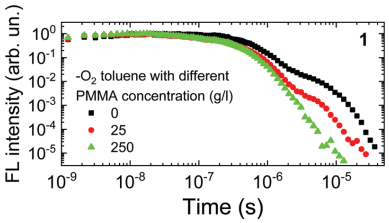

Fig. 5 Normalized fluorescence decay transients of compound **1** at the $^1CT_2$ peak in oxygen-free toluene solutions with different viscosity. The solution viscosity was varied by increasing the PMMA concentration.[28]

Table 2 Photoluminescence decay constants of compound **1** at the $^1CT_2$ peak in toluene with different viscosity

PMMA concentration[a] (g l^{-1})	DF/PF ratio[b]	$\tau_{^1CT_1}$[c] (ns)	$\tau_{^1CT_2}$[d] (μs)
0	0.18	470	4.5
25	0.03	320	2.8
250	0.003	280	1.25

[a] PMMA polymer concentration in oxygen-free toluene. [b] Intensity ratio between the time-integrated delayed and prompt fluorescence spectra. [c] Fluorescence decay time of the CT_1 state (prompt fluorescence). [d] Fluorescence decay time of the CT_2 state (TADF).

molecular diffusion and thus the lower contribution from exciplex states.

The presence of exciplex states was revealed by comparing the TADF properties of 1.2×10^{-5} and 1×10^{-4} M toluene solutions of compound **1** (see Fig. 6). The lineshape of the fluorescence spectra clearly was concentration dependent (see Fig. 6a), where the emission peak was redshifted from 475 nm to 485 nm upon the concentration increase. As we know from the analysis of the time-resolved fluorescence spectra (see Fig. 4), the time-integrated emission spectrum is formed of two distinct

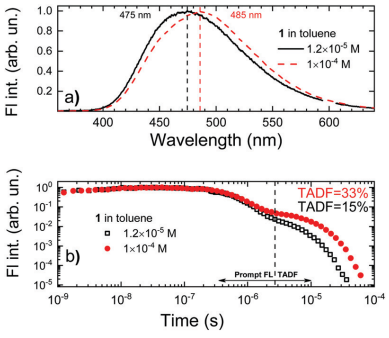

Fig. 6 (a) Normalized time-integrated fluorescence spectra of compound **1** in 1.2×10^{-5} M (solid line) and 10^{-4} M (dashed line) oxygen-free toluene solutions. (b) Fluorescence decay transients of compound **1** in 1.2×10^{-5} M (open symbols) and 10^{-4} M (closed symbols) oxygen-free toluene solutions at the $^1CT_2$ peak.

fluorescence bands of CT_1 and CT_2 states, peaking at about 465 nm and 505 nm (for compound **1**). Increasing the concentration of compound **1** in toluene clearly enhances the emission intensity from the $^1CT_2$ states and, therefore, shifts the peak of the total emission spectrum to longer wavelengths. A similar trend was observed for the fluorescence decay transients, obtained at the $^1CT_2$ emission peak (see Fig. 6b). Here we can see that the increased concentration of compound **1** in toluene solutions enlarged the intensity of the later decay part, attributed to exciplex TADF, increasing the DF/PF ratio from 0.18 to 0.49.

Clearly, viscosity and concentration-dependent measurements of fluorescence spectra support the prediction that the second CT state is of exciplex nature. It may look quite unusual to observe exciplex emission in solutions with concentrations as low as 1×10^{-5} M, however exciplex emission can be successfully observed in various dilute solutions of molecular compounds, especially for those containing large and planar units,[37–40] as in our σ-bonded D–A compounds. Additionally, exceptionally slow fluorescence decay should be beneficial for the observation of exciplex emission in solutions, when the probability of two molecules to meet each other before recombination is greatly enhanced. Obviously, the most intense intermolecular TADF was observed for the compound with the longest intramolecular fluorescence lifetime (see Fig. 2).

Suppression of the exciplex states in polymer films

For the further analysis of exciplex formation, compounds **1–3** were incorporated into a rigid PMMA polymer matrix at low concentration. In this case, emission should originate only from isolated molecules, since molecular diffusion is strongly impeded by the rigid polymer surroundings. The time-integrated fluorescence spectra of 1 wt% PMMA films of compounds **1–3** are shown in Fig. 7a. The emission spectra were very similar to those of the dilute solutions, showing dominating intramolecular CT emission peaking at 460, 455 and 445 nm for compounds **1–3**, respectively. Weak emission, related to the electron-donating unit, was clearly observed for compound **2**.

The fluorescence decay transients of 1 wt% PMMA films of compounds **1–3** are shown in Fig. 7b. The fluorescence decay followed the same trend as in toluene solutions, when two decay components were observed (see Fig. S4 in the ESI†). However, the fluorescence decay profiles were multiexponential, indicating the existence of conformational disorder, typical for TADF compounds.[41–44] Although the exact lifetime of the prompt and delayed emission could not be evaluated due to the multi-exponential nature, it is clear that the prompt fluorescence showed the same trend as in toluene solutions, where the slowest prompt fluorescence decay was observed for compound **1** and the most rapid for compound **3**. For the delayed emission, no clear trend was observed. The delayed fluorescence was quenched by oxygen (see Fig. S5 in the ESI†), typical for TADF. Temperature-dependent fluorescence decay transient measurements also supported our assumptions (see Fig. S6 in the ESI†). The intensity of the initial fluorescence and its lifetime were insensitive to temperature. On the other hand, the delayed emission showed temperature activation, typical for TADF. The TADF intensity was

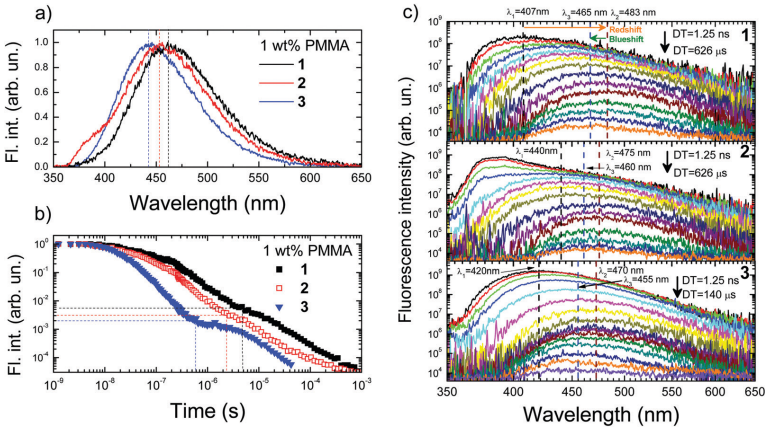

Fig. 7 (a) Normalized time-integrated fluorescence spectra of 1 wt% PMMA films of donor–σ–acceptor compounds **1–3**. Dashed lines are guides for the eye. (b) Normalized fluorescence decay transients of 1 wt% PMMA films of donor–σ–acceptor compounds **1–3** in $-O_2$ conditions. The dashed lines denote the initial intensity of the delayed emission and the delay time when the delayed emission emerges. (c) Time-resolved fluorescence spectra of 1 wt% PMMA films of donor–σ–acceptor compounds **1–3** in $-O_2$ conditions. DT denotes the initial and the latest delay times. λ_1, λ_2 and λ_3 represent the emission peak wavelengths of the initial, the most redshifted and the latest emission spectra, respectively.

remarkably enhanced in the polymer film, where the DF/PF ratios increased up to 1.08, 0.92 and 0.6 for compounds **1**, **2** and **3**, respectively. This was caused by the lowered non-radiative decay in more rigid surroundings and the presence of conformational disorder.[43]

The analysis of the time-resolved fluorescence spectra of compounds **1–3** embedded in 1 wt% PMMA films (see Fig. 7c) revealed the presence of temporal shifts of the emission peak due to the dispersion of ΔE_{ST}, typical for TADF in solid surroundings.[41–44] Initially, a redshift of the CT_1 state of about 210–480 meV was observed for about 0.5–4 μs, while at later delays a blueshift emerged. The blueshift was comparable for all compounds (~100 meV), while the lowest redshift was observed for compound **2** with the sterically-fixed tetramethylcarbazole donor unit. As it was expected, the $^1CT_2$ state was totally suppressed in the polymer films, again confirming its exciplex nature. Both fluorescence decay components, prompt and delayed, originated from the intramolecular $^1CT_1$ state. The non-radiative decay, especially through internal conversion, is remarkably weakened in the rigid polymer surroundings, allowing one to observe the delayed emission from the intramolecular states.

Exciplex states in neat films

In the final stage, the emission properties of neat films of donor–σ–acceptor compounds **1–3** were analyzed (see Fig. 8).

As we can see from Fig. 8a, the time-integrated fluorescence spectra of the neat films of compounds **1–3** were redshifted by about 140–190 meV compared to the 1 wt% PMMA films and by 180–200 meV compared to the 1.2×10^{-5} M toluene solutions and peaked at 495, 482 and 470 nm for compounds **1**, **2** and **3**, respectively. The redshift of the emission wavelength in neat films is a rather frequent effect for both fluorescent and TADF emitters[45,46] and usually occurs due to intermolecular interactions or solid state solvation. However, solid state solvation occurs with smaller magnitude due to the lower rotation ability of molecules and almost exclusively only after the inclusion of additional dopants with large ground-state dipole moments.[42,47,48] Usually the shift of the emission peak with increasing doping concentration occurs due to enhanced intermolecular interactions.[45,49] In our case, the TIFL spectra of the neat films of compounds **1–3** were found to coincide quite well with the fluorescence spectra of the $^1CT_2$ state from the toluene solutions (see the blue and green lines in Fig. 8a), attributed to the emission of exciplex states. The weak exciplex emission observed in toluene solution dominated in the neat films. This is not surprising, since the formation of excimer states should be enforced in the tightly-packed molecular environment of neat films.[24,50] The low-temperature phosphorescence spectra of compounds **1–3** were of different nature. If the LTPh spectra in toluene contained clear vibronic progressions, typical for ^3LE states (see Fig. 2 in ref. 25), the LTPh spectra of the neat films were structureless, indicating the intermolecular CT nature[24] (see Fig. S7 in the ESI†). A ΔE_{ST} of 60 and 90 meV was estimated for compounds **2** and **3**, respectively. Surprisingly, a negative ΔE_{ST} of −40 meV was estimated for **1**, probably due to the impact of the remaining phosphorescence from the intramolecular states.

The time-resolved fluorescence spectra of the neat films of compounds **1–3** are shown in Fig. S8 in the ESI.† The presence of conformational disorder was observed. Initially, the redshift of the emission spectra from about 460 nm to 490–510 nm was observed. No subsequent blueshift of the emission peak was noticed, probably due to the quenching of the latest delayed

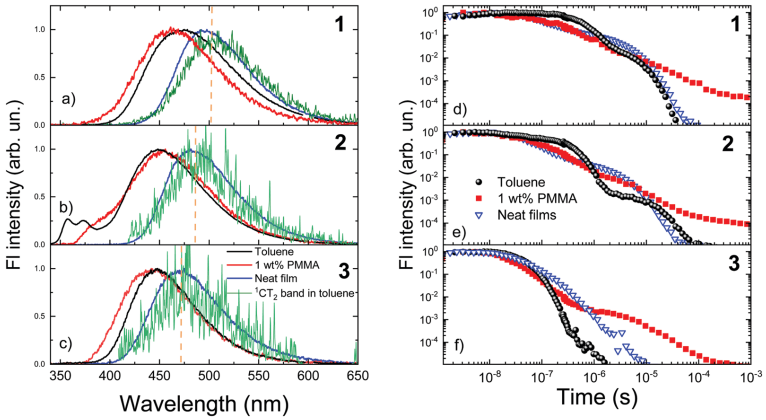

Fig. 8 (a)–(c) Normalized time-integrated fluorescence spectra of 1 wt% PMMA films (red lines), 1.2×10^{-5} M toluene solutions (black lines) and neat films (blue lines) together with fluorescence spectra of the $^1CT_2$ state in toluene solution of donor–σ–acceptor compounds **1–3** in oxygen-free conditions. Vertical lines are guides for the eye. (d)–(f) Normalized fluorescence decay transients of 1 wt% PMMA films (red figures), 1.2×10^{-5} M toluene solutions (black figures) and neat films (blue figures) of donor–σ–acceptor compounds **1–3** in oxygen-free conditions.

emission at the defect sites.[43] The fluorescence decay transients of the neat films of compounds **1–3** at the $^1CT_2$ peak are shown in Fig. 8d–f, along with the emission decay transients of the 1.2×10^{-5} M toluene solutions and 1 wt% PMMA films. A double-multiexponential decay was observed, where the initial decay of the prompt fluorescence resembled that of the 1 wt% PMMA films, while the later decay was rather similar to that of the toluene solutions (except compound **3**). For compound **3**, no clear TADF was observed. As we have already seen, the initial prompt fluorescence was strongly perturbed by conformational disorder, thus its decay was very similar to that of the 1 wt% PMMA films. The later TADF emerged only from the lowest-energy conformer states, where the higher-energy emission was quenched, therefore the TADF decay in the neat films was less perturbed by the conformational disorder and more similar to that in the toluene solutions. The fractional TADF intensity was remarkably enhanced in the neat films (except compound **3**) due to the larger number of TADF-active exciplex states. The DF/PF ratio for the neat films was 1.63 and 1.44 for compounds **1** and **2**, respectively.

The delayed fluorescence of the neat films of compounds **1** and **2** showed strong activation with temperature (see Fig. S9 in the ESI†), typical for TADF. No delayed emission was observed at 10 K, only the decay of phosphorescence after about 10 μs. For compound **3**, the enhancement of the prompt fluorescence lifetime was observed at 10 K, indicating weaker non-radiative losses at 10 K. No TADF was observed at room temperature. Probably the weak TADF observed in the toluene solutions was quenched in the neat films with efficient exciton migration towards defect sites.

Optimization of exciplex TADF

The emergence of the dominating exciplex emission is shown in Fig. 9a and b, where the fluorescence spectra of PMMA films doped with compound **1** at a concentration ranging from 1 to 100 wt% are demonstrated. The fluorescence peaked at about 460 nm at low doping concentration (0.1–2 wt%), where no intermolecular interactions were present, similarly to the emission of the $^1CT_1$ state in toluene. Some mismatch of the emission energies was due to the different polarity of toluene and PMMA (toluene is a more polar environment) and the presence of conformational disorder. The fluorescence peak started to redshift down to about 490 nm for doping concentrations of 5–30 wt% due to the emergence and later increasing number of exciplex states. Almost no further redshift of the emission spectra was observed at larger doping concentrations (30–100 wt%), where the exciplex fluorescence clearly dominated.

The transition from intramolecular TADF to intermolecular TADF from exciplex states was also observed in the fluorescence decay transients of compound **1** doped in PMMA at different concentrations (see Fig. 9c). As we can see, the fluorescence decay transients of the 1 wt% and 5 wt% doped PMMA films were rather similar, where the emission of the $^1CT_1$ states with the strong impact of conformation disorder dominates, however the rise of exciplex TADF is already observed at a 5 wt% concentration. At larger doping concentrations (*e.g.*, 10 wt%), the DF/PF ratio is enhanced (see the inset in Fig. 9) due to the emergence of the additional TADF from exciplex states.[24] The DF/PF ratio peaks at about a 20 wt% doping concentration and later starts to decrease at larger doping loads, due to the enhanced excitation mobility and subsequent quenching of the latest delayed emission at the defect sites[51] (see Fig. S10 in the ESI†). Such behavior was especially evident in the neat films. A similar trend was also observed for the TADF lifetime, which tended to decrease at larger doping concentration due to the quenching of the latest conformer states with the largest fluorescence lifetime.

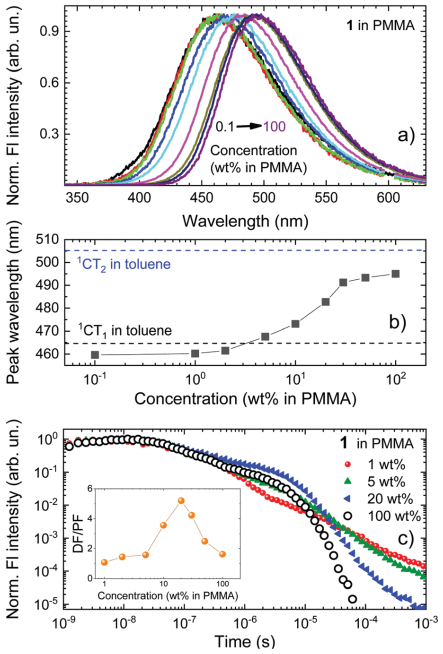

Fig. 9 (a) Normalized time-integrated fluorescence spectra of compound **1** embedded in PMMA surroundings at different concentrations. (b) Fluorescence peak wavelengths of compound **1** embedded in PMMA surroundings at different concentrations. (c) Normalized fluorescence decay transients of compound **1** in PMMA at different doping concentrations. The inset shows the DF/PF ratio at the different doping concentrations.

As we can see, intermolecular TADF is unavoidable in heavily doped polymer films, however the DF/PF ratio can be enhanced by selecting the proper doping concentration.

Conclusions

In summary, we presented a comprehensive analysis of the photophysical properties of a series of donor–σ–acceptor TADF compounds with different donor units. A hyperconjugated hexafluoroisopropylidene spacer unit was selected to reduce the electronic communication between the donor and acceptor units, seeking a negligible singlet–triplet energy gap. However, weak donor–acceptor coupling was observed, leading to remarkably prolonged fluorescence lifetimes and allowing us to observe several unusual effects. Firstly, coexisting intra- and intermolecular fluorescence of different wavelengths was observed at different time-scales even in solutions. Secondly, the initial decay with a remarkably prolonged lifetime was shown to be simple prompt intramolecular CT fluorescence, whose lifetime was shorter for the compounds with weaker electron-donating units. Interestingly, this slow initial fluorescence was susceptible to molecular oxygen. The later delayed fluorescence was shown to be TADF, originating from exciplex states, as proven by concentration and viscosity-dependent fluorescence measurements. In dilute polymer films with weakened non-radiative recombination, both prompt fluorescence and TADF were of intramolecular nature. Rather strong conformational disorder was observed due to the flexible molecular structure, leading to large temporal shifts of the emission peak. With an increasing doping load, a rise of exciplex TADF was observed, which dominated in the neat films at a similar wavelength to that in the solutions. However, the fractional intensity of TADF and its lifetime peaked at about a 20 wt% doping concentration, since the further increase of the doping load enabled excitation migration towards the defect sites and subsequent quenching of the latest TADF.

Our results have shown that weak coupling between donor and acceptor units is not favorable for efficient intramolecular TADF in σ-bridged compounds and the hyperconjugated spacer unit should be carefully designed. In-line, intermolecular interactions should be minimized in order to prevent exciplex emission in highly doped films.

Conflicts of interest

There are no conflicts of interest to declare.

Acknowledgements

SJ and ChA acknowledge funding through the EU Marie Skłodowska-Curie ITN TADFlife grant (GA. 812872). ChA also acknowledges the Japan Science and Technology Agency (JST), ERATO, Adachi Molecular Exciton Engineering Project under JST ERATO Grant Number 436 JPMJER1305, and JSPS KAKENHI Grant Number 437 17H01232.

References

1 C. W. Tang and S. A. VanSlyke, *Appl. Phys. Lett.*, 1987, **51**, 913.
2 M. A. Baldo, D. F. O'Brien, Y. You, A. Shoustikov, S. Sibley, M. E. Thompson and S. R. Forrest, *Nature*, 1998, **395**, 151–154.
3 J.-H. Jou, S. Kumar, A. Agrawal, T.-H. Li and S. Sahoo, *J. Mater. Chem. C*, 2015, **3**, 2974–3002.
4 A. Endo, K. Sato, K. Yoshimura, T. Kai, A. Kawada, H. Miyazaki and C. Adachi, *Appl. Phys. Lett.*, 2011, **98**, 083302.
5 H. Uoyama, K. Goushi, K. Shizu, H. Nomura and C. Adachi, *Nature*, 2012, **492**, 234–238.
6 R. K. Konidena and J. Y. Lee, *Chem. Rec.*, 2018, **18**, 1–20.
7 M. Y. Wong and E. Zysman-Colman, *Adv. Mater.*, 2017, **29**, 1605444.
8 T. Hatakeyama, K. Shiren, K. Nakajima, S. Nomura, S. Nakatsuka, K. Kinoshita, J. Ni, Y. Ono and T. Ikuta, *Adv. Mater.*, 2016, **28**, 2777–2781.

9 M. Mamada, K. Inada, T. Komino, W. J. Potscavage, H. Nakanotani and C. Adachi, *ACS Cent. Sci.*, 2017, **3**, 769–777.
10 Y. Xu, X. Liang, X. Zhou, P. Yuan, J. Zhou, C. Wang, B. Li, D. Hu, X. Qiao, X. Jiang, L. Liu, S. Su, D. Ma and Y. Ma, *Adv. Mater.*, 2019, **31**, 1807388.
11 F. B. Dias, T. J. Penfold and A. P. Monkman, *Methods Appl. Fluoresc.*, 2017, **5**, 012001.
12 J. Gibson, A. P. Monkman and T. J. Penfold, *ChemPhysChem*, 2016, **17**, 2956–2961.
13 M. K. Etherington, J. Gibson, H. F. Higginbotham, T. J. Penfold and A. P. Monkman, *Nat. Commun.*, 2016, **7**, 13680.
14 K. Goushi, K. Yoshida, K. Sato and C. Adachi, *Nat. Photonics*, 2012, **6**, 253–258.
15 M. Colella, P. H. Pander, D. D. S. Pereira and A. P. Monkman, *ACS Appl. Mater. Interfaces*, 2018, **10**, 793–798.
16 M. Sarma and K.-T. Wong, *ACS Appl. Mater. Interfaces*, 2018, **10**, 19279–19304.
17 D. Chen, G. Xie, X. Cai, M. Liu, Y. Cao and S.-J. Su, *Adv. Mater.*, 2016, **28**, 239–244.
18 H. Tsujimoto, D.-G. Ha, G. Markopoulos, H. S. Chae, M. A. Baldo and T. M. Swager, *J. Am. Chem. Soc.*, 2017, **139**, 4894–4900.
19 K. Kawasumi, T. Wu, T. Zhu, H. S. Chae, T. Van Voorhis, M. A. Baldo and T. M. Swager, *J. Am. Chem. Soc.*, 2015, **137**, 11908–11911.
20 S. Shao, J. Hu, X. Wang, L. Wang, X. Jing and F. Wang, *J. Am. Chem. Soc.*, 2017, **139**, 17739–17742.
21 E. Spuling, N. Sharma, I. D. W. Samuel, E. Zysman-Colman and S. Bräse, *Chem. Commun.*, 2018, **54**, 9278–9281.
22 Y.-Z. Shi, K. Wang, X. Li, G.-L. Dai, W. Liu, K. Ke, M. Zhang, S.-L. Tao, C.-J. Zheng, X.-M. Ou and X.-H. Zhang, *Angew. Chem., Int. Ed.*, 2018, **57**, 9480–9484.
23 S.-Y. Qiu, H. Xu, L. Li, H.-T. Xu, L.-K. Meng, H.-S. Pang, C. Tang, Z.-Q. Pang, J. Xiao, X. Wang, S.-H. Ye, Q.-L. Fan and W. Huang, *J. Phys. Chem. C*, 2017, **121**, 9230–9241.
24 D. Zhang, K. Suzuki, X. Song, Y. Wada, S. Kubo, L. Duan and H. Kaji, *ACS Appl. Mater. Interfaces*, 2019, **11**, 7192–7198.
25 Y. Geng, A. D'Aleo, K. Inada, L.-S. Cui, J. U. Kim, H. Nakanotani and C. Adachi, *Angew. Chem., Int. Ed.*, 2017, **52**, 16763–16767.
26 P. L. dos Santos, J. S. Ward, D. G. Congrave, A. S. Batsanov, J. Eng, J. E. Stacey, T. J. Penfold, A. P. Monkman and M. R. Bryce, *Adv. Sci.*, 2018, **5**, 1700989.
27 M. Inoue, T. Serevičius, H. Nakanotani, K. Yoshida, T. Matsushima, S. Juršėnas and C. Adachi, *Chem. Phys. Lett.*, 2016, **644**, 62–67.
28 Z. Kuang, G. He, H. Song, X. Wang, Z. Hu, H. Sun, Y. Wan, Q. Guo and A. Xia, *J. Phys. Chem. C*, 2018, **122**, 3727–3737.
29 J. C. de Mello, H. F. Wittmann and R. H. Friend, *Adv. Mater.*, 1997, **9**, 230–232.
30 C. Rothe and A. P. Monkman, *Phys. Rev. B: Condens. Matter Mater. Phys.*, 2003, **68**, 075208.
31 Y. Im, M. Kim, Y. J. Cho, J.-A. Seo, K. S. Yook and J. Y. Lee, *Chem. Mater.*, 2017, **29**, 1946–1963.
32 A. Köhler and H. Bässler, *Electronic processes in organic semiconductors: an introduction*, Wiley-VCH, Weinheim, 2015.
33 Y. Qu, P. Pander, A. Bucinskas, M. Vasylieva, Y. Tian, F. Miomandre, F. B. Dias, G. Clavier, P. Data and P. Audebert, *Chem. – Eur. J.*, 2019, **25**, 2457–2462.
34 Y. Zhang, H. Ma, S. Wang, Z. Li, K. Ye, J. Zhang, Y. Liu, Q. Peng and Y. Wang, *J. Phys. Chem. C*, 2016, **120**, 19759–19767.
35 K. L. Woon, C.-L. Yi, K.-C. Pan, M. K. Etherington, C.-C. Wu, K.-T. Wong and A. P. Monkman, *J. Phys. Chem. C*, 2019, **123**, 12400–12410.
36 M. Sarma and K.-T. Wong, *ACS Appl. Mater. Interfaces*, 2018, **10**, 19279–19304.
37 P. Valat, V. Wintgens, Y. L. Chow and J. Kossanyi, *Can. J. Chem.*, 1995, **73**, 1902–1913.
38 S. A. Boer, R. P. Cox, M. J. Beards, H. Wang, W. A. Donald, T. D. M. Bell and D. R. Turner, *Chem. Commun.*, 2019, **55**, 663–666.
39 E. V. Bichenkova, A. R. Sardarian, A. N. Wilton, P. Bonnet, R. A. Bryce and K. T. Douglas, *Org. Biomol. Chem.*, 2006, **4**, 367–378.
40 T. C. Barros, S. Brochsztain, V. G. Toscano, P. B. Filho and M. J. Politi, *J. Photochem. Photobiol., A*, 1997, **111**, 97–104.
41 T. Serevičius, T. Bučiūnas, J. Bucevičius, J. Dodonova, S. Tumkevičius, K. Kazlauskas and S. Juršėnas, *J. Mater. Chem. C*, 2018, **6**, 11128–11136.
42 T. Northey, J. Stacey and T. J. Penfold, *J. Mater. Chem. C*, 2017, **5**, 11001–11009.
43 T. Serevičius, R. Skaisgiris, J. Dodonova, L. Jagintavičius, J. Bucevičius, K. Kazlauskas, S. Jursenas and S. Tumkevicius, *Chem. Commun.*, 2019, **55**, 1975–1978.
44 M. K. Etherington, F. Franchello, J. Gibson, T. Northey, J. Santos, J. S. Ward, H. F. Higginbotham, P. Data, A. Kurowska, P. L. Dos Santos, D. R. Graves, A. S. Batsanov, F. B. Dias, M. R. Bryce, T. J. Penfold and A. P. Monkman, *Nat. Commun.*, 2017, **8**, 14987.
45 X. Zhang, M. W. Cooper, Y. Zhang, C. Fuentes-Hernandez, S. Barlow, S. R. Marder and B. Kippelen, *ACS Appl. Mater. Interfaces*, 2019, **11**, 12693–12698.
46 T. Serevičius, R. Komskis, P. Adomėnas, O. Adomėnienė, G. Kreiza, V. Jankauskas, K. Kazlauskas, A. Miasojedovas, V. Jankus, A. P. Monkman and S. Jursenas, *J. Phys. Chem. C*, 2017, **121**, 8515–8524.
47 C. F. Madigan and V. Bulović, *Phys. Rev. Lett.*, 2003, **91**, 247403.
48 B. L. Cotts, D. G. McCarthy, R. Noriega, S. B. Penwell, M. Delor, D. D. Devore, S. Mukhopadhyay, T. S. De Vries and N. S. Ginsberg, *ACS Energy Lett.*, 2017, **2**, 1526–1533.
49 Q. Zhang, D. Tsang, H. Kuwabara, Y. Hatae, B. Li, T. Takahashi, S. Y. Lee, T. Yasuda and C. Adachi, *Adv. Mater.*, 2015, **27**, 2096–2100.
50 M. K. Etherington, N. A. Kukhta, H. F. Higginbotham, A. Danos, A. N. Bismillah, D. R. Graves, P. R. McGonigal, N. Haase, A. Morherr, A. S. Batsanov, C. Pflumm, V. Bhalla, M. R. Bryce and A. P. Monkman, *J. Phys. Chem. C*, 2019, **123**, 11109–11117.
51 M. Colella, A. Danos and A. P. Monkman, *J. Phys. Chem. Lett.*, 2019, **10**, 793–798.

A3

Minimization of solid-state conformational disorder in donor–acceptor TADF compounds

T. Serevičius, **R. Skaisgiris**, J. Dodonova, K. Kazlauskas,
S. Juršėnas, S. Tumkevičius

Phys. Chem. Chem. Phys. **22**(1), 265–272 (2020)
DOI: 10.1039/C9CP05907E
http://xlink.rsc.org/?DOI=C9CP05907E

Supporting information: http://www.rsc.org/suppdata/c9/cp/c9cp05907e/c9cp05907e1.pdf

PCCP

ROYAL SOCIETY OF CHEMISTRY

PAPER

View Article Online
View Journal

Cite this: DOI: 10.1039/c9cp05907e

Minimization of solid-state conformational disorder in donor–acceptor TADF compounds†

Tomas Serevičius, *[a] Rokas Skaisgiris, [a] Jelena Dodonova,[b] Karolis Kazlauskas, [a] Saulius Juršėnas[a] and Sigitas Tumkevičius [b]

Thermally activated delayed fluorescence (TADF) compounds with a flexible donor–acceptor structure suffer from conformational disorder in solid-state, which deteriorates their emission properties as well as OLED performance. Accordingly, TADF materials with predictable solid-state emission properties are highly desirable. In this work, we analyse the relation between the molecular rigidity and solid-state TADF properties. Two TADF compounds, 4,6-bis(2-methyl-4-(10*H*-phenothiazin-10-yl)phenyl)pyrimidine (**PTZ-mPYR**) and 1,2,3,4-tetrakis(carbazol-9-yl)-5,6-dicyanobenzene (**4CzPN**), with similar emission properties in toluene solutions but different rigidity of the molecular structure were systematically studied. The analysis was supplemented by comparison of solid-state TADF properties of **PTZ-mPYR** with its analogue 4,6-bis(4-(10*H*-phenoxazin-10-yl)phenyl)pyrimidine (**PXZ-PYR**), bearing a more sterically constrained planar electron-donor unit. All compounds showed conformational disorder in diluted polymer films; however its extent directly depended on the molecular structure. Large dispersion of singlet–triplet energy gaps resulted in remarkably prolonged TADF lifetime for **PTZ-mPYR** with a less sterically constrained donor unit. In contrast, weakened conformational disorder in rigid **4CzPN** with sterically crowded donor units was shown to ensure rapid TADF decay with only a threefold lower solid-state rISC rate as compared to toluene. Similarly, selection of a more sterically constrained planar electron-donor unit was also shown to be preferable for lowering the conformational disorder. Our findings are important for the future design of compounds with efficient solid-state TADF as well as for the further application in OLEDs with low external quantum efficiency roll-off.

Received 30th October 2019,
Accepted 27th November 2019

DOI: 10.1039/c9cp05907e

rsc.li/pccp

Introduction

The application of thermally activated delayed fluorescence (TADF)[1–3] emitters allows one to boost the external quantum efficiencies (EQE) of organic light emitting diodes (OLEDs) far beyond the typical values for singlet-only emitters.[4,5] The harvesting of triplet states in TADF compounds occurs *via* thermally activated reverse intersystem crossing (rISC). To achieve rapid rISC, generally a small energy gap (ΔE_{ST}) between the charge-transfer singlet (^{1}CT) and the lowest triplet state, usually of local excited triplet (^{3}LE) character, is required. The most usual approach to lower ΔE_{ST} is to minimize the spatial overlap of HOMO and LUMO.[6] This is achieved by decoupling electron-donating (D) and electron-accepting (A) units in highly twisted molecular geometry with strong charge-transfer character. Besides the minimization of ΔE_{ST}, negligible energy splitting between the spin-vibronically coupled ^{3}LE and charge-transfer triplet (^{3}CT) states is also mandatory.[7–10] As it was shown previously, ^{3}CT and ^{3}LE states are coupled through the torsion of the D–A angle,[7–11] thus somewhat rotational flexibility of the D–A bond is required, otherwise the rISC rate would be minimized.[12] On top of that, minimization of the nonradiative internal conversion rate[13] together with decrease of the activation energy barrier for rISC,[14] however, is achieved in compounds with suppressed structural deformation. All those contradictions can be well matched by comprehensive optimization of the molecular structure, and thus a great variety of different highly emissive TADF compounds, constructed of sometimes very different donor and acceptor units bound in diverse molecular geometries, have been presented.[15,16] However, TADF behaviour becomes highly complicated in solid-state and these issues still are very scarcely studied. Regardless of the selected D and A units and their linking patterns, pronounced conformational disorder occurs in solid films.[17–24] TADF molecules in solid polymer or small-molecule host films are "frozen" with a variation of dihedral angles between the D and A units, forming a set of solid molecular conformations, having different HOMO–LUMO overlap and thus different ^{1}CT energies and

[a] *Institute of Photonics and Nanotechnology, Vilnius University, Sauletekio 3, LT-10257 Vilnius, Lithuania. E-mail: tomas.serevicius@tmi.vu.lt*
[b] *Institute of Chemistry, Vilnius University, Naugarduko 24, LT-03225, Vilnius, Lithuania*

† Electronic supplementary information (ESI) available. See DOI: 10.1039/c9cp05907e

singlet–triplet gaps.[22,25] Such conformational disorder in solid state causes temporal shifts of the emission peak and, therefore, results in unwanted effects, like the broadening of the emission spectrum and the prolongation of TADF lifetime.[19,20] All this makes the control of conformational disorder highly important for the successful application of TADF compounds, especially as emitters in OLED devices, since the EQE roll-off of OLEDs at high current densities directly depends on TADF lifetime.[26] Recently it was demonstrated that compounds with large conformational disorder benefited from shortened TADF lifetime.[20] Stable emission was achieved; however TADF decay was still remarkably slower than in solutions. Some control of delayed emission lifetime was also shown by tuning the polarity of the polymer host;[19] however more efficient strategies are still required. As a solution, the enhancement of molecular core rigidity could be applied. Yersin *et al.*[21] recently have demonstrated the benefits of a rigid molecular structure for avoiding the occurrence of prolonged TADF decay; however all the benefits were demonstrated in a rather specific molecular structure with rigid bridges.

In this work, we followed the idea of the necessity of rigid molecular cores for the minimization of unwanted conformational disorder; however typical donor–acceptor TADF compounds with flexible single bonds were investigated. Time-resolved fluorescence was employed for the analysis of conformational disorder in dilute polymer films of two TADF compounds, with similar emission properties in toluene solutions but a completely different molecular structure and stiffness of the molecular core, **PTZ-mPYR** and **4CzPN**. The analysis was supplemented by comparison of solid-state TADF properties of compound **PTZ-mPYR** and its analogue **PXZ-PYR**, bearing a more sterically constrained donor unit. The same trends were observed in both series of compounds, despite remarkable differences in the molecular structure. The rigid **4CzPN** was shown to have almost alike TADF properties in solutions and solid-state due to minimized conformational disorder. Our study has shown that donor–acceptor TADF compounds with a consistently restricted molecular structure could be efficient emitters in both solutions and solid films.

Experimental details

4CzPN was synthesized according to Uoyama *et al.*[3] Synthetic details of **PTZ-mPYR** and **PXZ-PYR** were published elsewhere.[20,27] TADF compounds were analyzed in 1×10^{-5} M toluene solutions and in 1 wt% PMMA films. Polymer films were prepared by dissolving each material and PMMA at appropriate ratios in toluene solutions and then wet-casting the solutions on glass substrates. Time-integrated fluorescence spectra (TIFL), time-resolved fluorescence spectra (TRFL) and fluorescence decay transients were measured using a nanosecond YAG:Nd^{3+} laser NT 242 (Ekspla, τ = 7 ns, pulse energy 200 μJ, λ_{ex} = 350 nm, repetition rate 10–1000 Hz) and time-gated iCCD camera New iStar DH340T (Andor). Time integrated prompt and delayed fluorescence spectra (TIPF and TIDF, respectively) were measured by using 0 ns delay and 200 ns (no prompt fluorescence was observed after 200 ns) exposure time for TIPF and 200 ns delay and 100 ms exposure time for TIDF. Exposure time for TIDF measurement was selected to be longer than TADF lifetime. Fluorescence quantum yields (Φ_F) of the solutions and polymer films in an air atmosphere were estimated with the integrated sphere method[28] by using an integrating sphere (Sphere Optics) connected to the CCD spectrometer PMA-11 (Hamamatsu) *via* an optical fibre. Fluorescence transients were obtained by exponentially increasing delay and integration time. This allows one to record up to 10 orders of magnitude in time and intensity of the fluorescence decay.[29] Solid-state samples were mounted in a closed cycle He cryostat (Cryo Industries 204N) for all measurements (for oxygen-saturated and oxygen-free conditions). Toluene solutions were degassed by using the freeze–pump–thaw method (5 iterations).

Quantum chemical calculations were performed by using density functional theory (DFT) as implemented in the Gaussian 09 software package at the B3LYP/6-31G(d) level.[30] The Polarizable Continuum Model (PCM) was used to estimate the solvation behaviour of toluene surrounding in geometry optimization.

Results and discussion

Material selection

Three TADF compounds were selected to analyse the relation between the molecular geometry and conformational disorder in solid films (see Fig. 1). Compounds **PTZ-mPYR** and **4CzPN** were selected to have completely different molecular geometry but similar TADF properties. **PTZ-mPYR** is composed of a diphenylpyrimidine electron-acceptor unit and two phenothiazine (PTZ) electron-donor fragments with nonplanar geometry, while **4CzPN** is constructed of a dicyanophenyl electron-acceptor fragment, decorated with four adjacent carbazole electron-donating units. The nonplanar PTZ unit is found in two distinct conformer states, namely quasi-axial (QA) and quasi-equatorial (QE) with different corresponding absorption and emission properties.[31,32] However, only the emission from QE states is of TADF nature[20,33] and will be

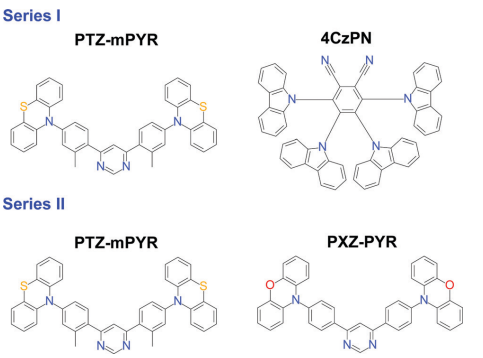

Fig. 1 Molecular structures of TADF compounds **PTZ-mPYR**, **4CzPN** and **PXZ-PYR**.

analysed in this paper. In the second set of compounds, two TADF compounds with a very similar structure were compared, **PTZ-mPYR** and its structural counterpart **PXZ-PYR**, constructed from the almost alike diphenylpyrimidine acceptor fragment but a different donor unit, planar phenoxazine (PXZ). As it was shown earlier, the presence of a methyl unit in the acceptor fragment of **PTZ-mPYR** has almost no effect on solid-state conformational disorder.[20]

Initially, solid-state TADF properties of compounds **PTZ-mPYR** and **4CzPN**, strongly differing in the molecular structure, will be investigated. Lastly, two very similar TADF emitters, **PTZ-mPYR** and **PXZ-PYR**, will be compared to reveal the impact of delicate structural changes on solid-state emission properties.

DFT simulations of PTZ-mPYR and 4CzPN

DFT simulations were performed to analyse the differences in the molecular structure. The optimized geometries of TADF compounds **PTZ-mPYR** and **4CzPN** are shown in Fig. 2. The optimization revealed that the phenothiazine moiety in QE arrangement is almost perpendicular to the phenyl fragment ($\alpha_1 \approx 88.9^\circ$, see Fig. 2); however due to the twisted geometry, the PTZ units also are bent along the C–N bonds,[34] leading to larger rotational flexibility than of planar donor moieties. Both phenyl fragments in the acceptor unit were twisted only for about $\alpha_2 \approx 46^\circ$ with respect to the pyrimidine group due to the weak steric hindrance. Previously, it was shown that such a molecular structure is flexible with large conformational disorder in solid state.[20] For **4CzPN**, carbazole fragments are twisted with respect to the central phenyl moiety for about $\alpha_3 \approx 62$–67°.[35,36] Close proximity of the adjacent carbazole units ensures large steric hindrance and large stiffness of the molecular core.

Ground state dipole moments of 3.08 D and 7.38 D were estimated for **PTZ-mPYR** and **4CzPN**, respectively.

In the context of this paper, molecular rigidity is described as rotational flexibility between the D and A units through C–N bonds. In such case, flexible molecules would have large dispersion of D–A twist angles, while the rigid ones lower dispersion.[21] Differences in the structural rigidity of compounds **PTZ-mPYR** and **4CzPN** with strongly different geometry were assessed by estimating the vibrational frequencies of the lowest vibrational modes in the harmonic approach (see Fig. 3). Ground-state optimized molecular structures were used for vibrational frequency calculations, as the ability of TADF compounds to reorient upon photoexcitation is strongly restricted in the solid films.[34,37] Molecular compounds have a large number of various vibrational modes up to an energy of several thousand cm^{-1}, like symmetric vinyl stretching modes observed at about 1400 cm^{-1}, responsible for vibronic progression in absorption and emission spectra.[38] However, in our case the most important are the lowest energy vibrations, usually arising from the vibration of the loose donor and acceptor molecular units, evidently altering the TADF properties.[7,9–11] D–A twisting motions should occur at the lower energy for more flexible TADF compounds, rather for the rigid ones.[39]

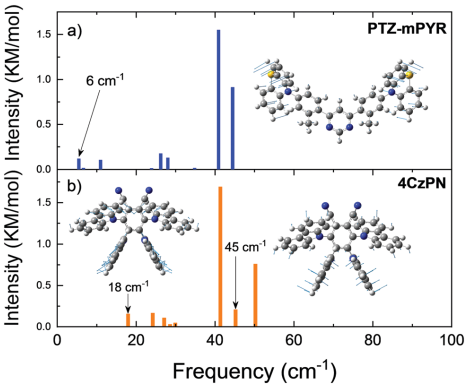

Fig. 3 Calculated frequencies of the lowest vibrational modes (up to 50 cm^{-1}) for compounds **PTZ-mPYR** (a) and **4CzPN** (b). The B3LYP/6-31G(d) method was used. Nuclear displacement vectors, corresponding to the lowest-frequency vibrational normal modes at 6 cm^{-1} (for **PTZ-mPYR**), 18 cm^{-1} and 45 cm^{-1} (for **4CzPN**), are shown.

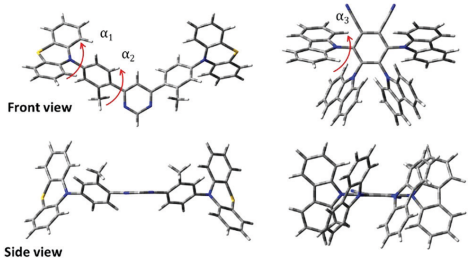

Fig. 2 DFT-optimized molecular geometries of **PTZ-mPYR** and **4CzPN**. Only quasi-equatorial conformation is shown for **PTZ-mPYR**. α_1 is a twist angle between the phenothiazine unit and the phenyl fragment, α_2 is a twist angle between the phenyl fragment and the pyrimidine unit and α_3 represents the twist angle between carbazole and dicyanobenzene acceptor.

Clearly, the lowest vibrational modes of **PTZ-mPYR** and **4CzPN** were of different nature. For **PTZ-mPYR**, the twisting motion of the donor unit was shown to be the lowest vibrational mode at only 6 cm^{-1}, typical for TADF compounds.[9,39] In contrast, the lowest vibrational mode for **4CzPN** was found at the higher energy and was of different nature. The large steric hindrance between the carbazole units suppressed the twisting along the C–N bond, and thus the lowest energy vibration at 18 cm^{-1} was shown to be the waving motion of carbazole units, barely related to conformational disorder in solid state (see Fig. 3b). Only the higher energy vibration mode at 45 cm^{-1} was the twisting motion of the donor units, directly contributing to the rise of conformational disorder in solid state. Supposedly, larger energetic barriers for the twisting motion for donor units for **4CzPN** should result in lower ΔE_{ST} dispersion and lower conformational disorder in solid state.[40,41] Quantum mechanical and experimental analyses of similar to **4CzPN** carbazole-benzonitrile TADF compounds, bearing several adjacent carbazole units,

have also shown the large torsional barriers for twisting of carbazole units, ensuring a rigid molecular structure and subsequent highly efficient TADF.[7,14,35]

TADF properties in solutions: PTZ-mPYR *vs.* 4CzPN

Despite the different molecular structure, compounds **PTZ-mPYR** and **4CzPN** showed similar emission properties in toluene (see Fig. S1 in ESI† and Table 1). Both TADF compounds showed greenish fluorescence, peaking at 535 and 525 nm for **PTZ-mPYR** and **4CzPN**, respectively, with comparable fluorescence lifetimes: the decay time for prompt fluorescence was 10 and 14 ns and TADF lifetimes were 11 and 15.5 μs for **PTZ-mPYR** and **4CzPN**, respectively (see Fig. 5). Energy gaps between the lowest singlet and triplet states were also comparable, 25 meV *vs.* 10 meV, for **PTZ-mPYR** and **4CzPN**, respectively. However, the fluorescence quantum yield of prompt and delayed fluorescence was lower for **PTZ-mPYR** with more rapid non-radiative decay[39] (0.04 and 0.04 *vs.* 0.09 and 0.61, respectively).

TADF properties in polymer films: PTZ-mPYR *vs.* 4CzPN

Although compounds **PTZ-mPYR** and **4CzPN** showed similar properties in toluene, remarkable differences in solid-state emission properties were revealed. Firstly, flexible **PTZ-mPYR** showed strong TADF quantum efficiency enhancement in more rigid PMMA surrounding (0.04 *vs.* 0.32), whereas for rigid **4CzPN** TADF quantum efficiency was rather the same (0.61 *vs.* 0.54). Secondly, typical for TADF compounds temporal shifts of prompt (PF) and delayed (DF) fluorescence spectra[18–20,31] were observed in the time-resolved fluorescence spectra of 1 wt% PMMA films (see Fig. 4a). Initially, the redshift of PF was observed for about 100 ns, followed by the later blueshift of DF. No shift was observed from about 100 ns to 10 μs when emission originated from the conformer states with the lowest ΔE_{ST}.[20] Evident differences in fluorescence shift trends were observed between **PTZ-mPYR** and **4CzPN**. For **PTZ-mPYR** with a more flexible molecular structure, a redshift of 370 meV was observed, followed by 80 meV blueshift. For the rigid **4CzPN**, both red and blueshifts were of the same value, at only about 100 meV (see Table S1 in ESI† for details). Obviously, lower conformational disorder and thus the smaller emission peak shifts for rigid **4CzPN** were mediated by the lower dispersion of ^{1}CT energies. The enhanced rigidity and lowered conformational disorder of **4CzPN** had a remarkable advantage over **PTZ-mPYR** for emission wavelength stability (see Fig. 4b and c). Previously it was shown that the emission of compound **PTZ-mPYR** peaks at different wavelengths in oxygen-free and oxygen-saturated

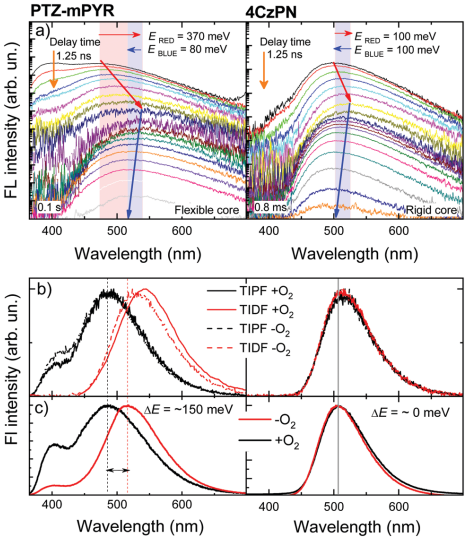

Fig. 4 (a) Time-resolved fluorescence spectra of 1 wt% PMMA films of **PTZ-mPYR** (left picture) and **4CzPN** (right picture). All measurements were performed in oxygen-free surrounding. (b) Time-integrated normalized prompt (TIPF) and delayed fluorescence (TIDF) spectra of 1 wt% PMMA films of **PTZ-mPYR** (left picture) and **4CzPN** (right picture) in oxygen-saturated (+O_2, solid lines) and oxygen-free (−O_2, dashed lines) conditions. Experimental parameters are provided in the Experimental details section. (c) Time-integrated normalized fluorescence spectra of 1 wt% PMMA films of **PTZ-mPYR** (left picture) and **4CzPN** (right picture) in oxygen-saturated (+O_2, black lines) and oxygen-free (−O_2, red lines) conditions.

conditions due to the quenching of the latest delayed emission[20] in oxygen-free conditions. Due to the wide distribution of singlet–triplet energy gaps, the latest emission spectra originate from conformations with very large singlet–triplet energy gaps and prolonged lifetime, which are largely susceptible to quenching by various quenching sites. Quenching of the latest emission with the largest ^{1}CT energy disturbs the high-energy shoulder of the time-integrated delayed fluorescence spectrum in −O_2 conditions, resulting in the redshift of its peak wavelength (see Fig. 4b) and the redshift of the overall time-integrated emission spectrum (see Fig. 4c). A completely different situation was observed for compound **4CzPN** with low conformational disorder. In this case, the stable emission peak wavelength was observed. Due to the rigid

Table 1 TADF properties of **PTZ-mPYR** and **4CzPN** in oxygen-free toluene

	λ_{FL}[a] (nm)	τ_{PR}[b] (ns)	τ_{TADF}[c] (μs)	Φ_{PF}[d]	Φ_{TADF}[e]	k_{ISC}[f] ($\times 10^7$ s^{-1})	k_{rISC}[g] ($\times 10^5$ s^{-1})	ΔE_{ST}[h] (meV)
PTZ-mPYR	535	10	11	0.04	0.04	2.7	1.2	25
4CzPN	525	14	15.5	0.09	0.61	6.5	7.1	10

[a] Fluorescence wavelength. [b] Prompt fluorescence decay time. [c] Delayed fluorescence decay time. [d] Fluorescence quantum yield of prompt fluorescence. [e] Fluorescence quantum yield of delayed fluorescence. [f] Intersystem crossing rate. [g] Reverse intersystem crossing rate. [h] Singlet–triplet energy gap.

molecular core, the latest delayed fluorescence of **4CzPN** originated from the similar conformer states with rather low ΔE_{ST} and rapid rISC in both $+O_2$ and $-O_2$ conditions (see Fig. 4b and c).

Likewise, FWHM values of time-integrated fluorescence spectra of polymer films also were molecular rigidity-dependent. For **4CzPN**, FWHM values in both $+O_2$ and $-O_2$ conditions (400 meV) were only slightly larger than in toluene solution (370 meV). It again evidenced the high rigidity of the molecular structure of **4CzPN**. In contrast, a moderate increase of FWHM of about 15% (from 400 meV in toluene to 460 meV in PMMA) was observed for the solid-state emission spectra of **PTZ-mPYR** in $-O_2$ conditions. However, this was not mediated by small dispersion of ^{1}CT peak energies, as it was for rigid **4CzPN**, but specifically due to the large conformational disorder. **PTZ-mPYR** has large dispersion of ^{1}CT emission energies and singlet–triplet gaps. In $-O_2$ conditions, the latest long-lived delayed emission from the largest-energy conformers is quenched, and thus the emission spectrum mostly consists of the lowest-energy conformers with lower dispersion of ^{1}CT energies. In $+O_2$ conditions, even more delayed emission is quenched (see Fig. S2 in ESI†), and thus the time-integrated emission spectrum contains a larger fraction of prompt fluorescence, formed from nearly all possible conformer states with large dispersion of ^{1}CT emission energies. In the case of $-O_2$ conditions, a 46% increase of FWHM was observed (from 460 meV to 670 meV), and the FWHM of TIFL of polymer films in $+O_2$ conditions was even 68% larger than that of toluene solutions (400 meV *vs.* 670 meV).

The presence of conformational disorder, increasing the spectral linewidth, as well as lower polarity of polymer surrounding resulted in an increase of ΔE_{ST} in polymer films, which represents the average gap of all conformer states (see Fig. S3 in the ESI†). A singlet–triplet gap of 187 meV was observed for **PTZ-mPYR** (with fluorescence spectra obtained in $-O_2$ conditions as a reference) and 140 meV – for **4CzPN** (see Fig. S4 in ESI†).

TADF decay transients: PTZ-mPYR *vs.* 4CzPN

Pronounced differences in emission properties between compounds **4CzPN** and **PTZ-mPYR** with different molecular core rigidity were also observed in solid-state fluorescence decay transients (see Fig. 5). The temporal profiles of emission decay transients in dilute solution and polymer films considerably differed. The presence of conformational disorder, as it was already shown, resulted in the dispersion of ΔE_{ST} values, when the later decaying states had larger singlet–triplet gaps and slower rISC. Compounds with a more flexible molecular core and larger conformational disorder had bigger ΔE_{ST} dispersion and more conformer states with inefficient rISC. It resulted in the extension of TADF lifetime in solid surrounding and the enhancement was remarkably larger for flexible **PTZ-mPYR** as compared to **4CzPN**. This was evident from the comparison of fluorescence decay transients of compounds **PTZ-mPYR** and **4CzPN** in toluene solution and PMMA films (see Fig. 5c and d). TADF lifetime enhancement for **PTZ-mPYR** was followed by subsequent boost of TADF efficiency from 0.04 in toluene to 0.32 in PMMA. The presence of a large number of conformer states with inefficient rISC increased the TADF lifetime and, concomitantly, the average number of ISC/rISC cycles.

In an ideal case with negligible conformational disorder and highly efficient TADF, similar TADF properties should be observed in both surroundings. This was the case for rigid **4CzPN** with similar TADF characteristics in toluene and PMMA films (see Fig. 5). In this case, low conformational disorder resulted only in small dispersion of ΔE_{ST} values, when the TADF lifetime from the conformer states with the largest singlet–triplet gaps was weakly increased. Therefore, rather a simple three-exponential fit of the delayed fluorescence decay allowed one to estimate the average TADF lifetime for **4CzPN** in PMMA film. A three-fold increase of the average TADF lifetime from 15.5 μs to 46 μs was observed, resulting in a slight decrease of the rISC rate from 7.1×10^5 to 2×10^5 s^{-1}. The negligible decrease of the DF/PF ratio in PMMA was due to the lower polarity of polymer surrounding[19] and larger ΔE_{ST}. Certainly, the lower polarity of PMMA also could result in the lowered rISC rate, though the ΔE_{ST} dispersion and the subsequent increase of TADF lifetime still were the main reason. Secondly, fluorescence decay transients of PMMA films of compounds **PTZ-mPYR** and **4CzPN** in $+O_2$ and $-O_2$ conditions followed different pathways (see Fig. 5a and b). A remarkable quenching

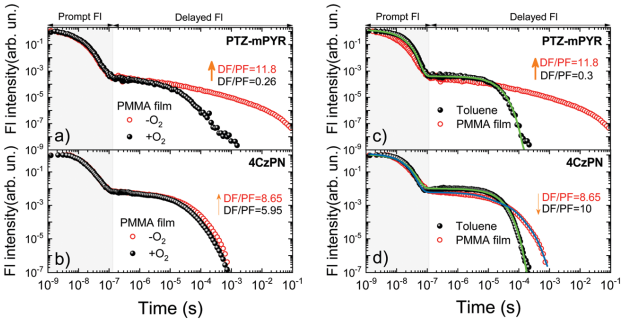

Fig. 5 Fluorescence decay transients of 1 wt% PMMA films of **PTZ-mPYR** and **4CzPN** in oxygen-saturated and oxygen-free conditions (a and b, respectively) and fluorescence decay transients of oxygen-free 1 wt% PMMA films and toluene solutions of **PTZ-mPYR** and **4CzPN** (c and d, respectively). All fluorescence decay transients were normalized. Color lines are multiexponential fits.

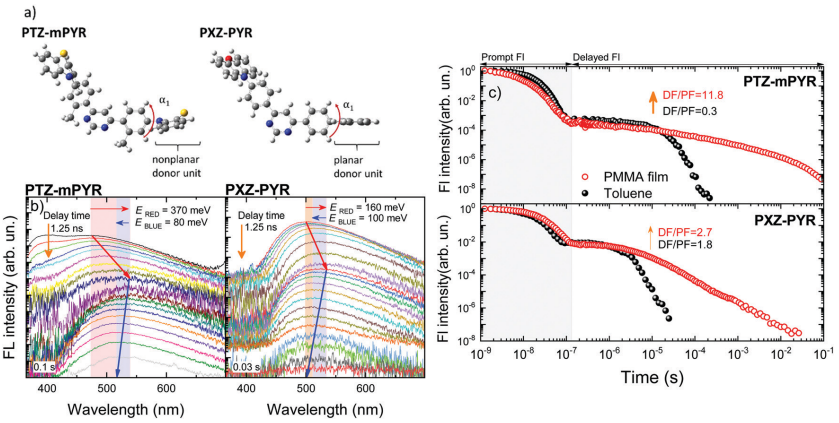

Fig. 6 (a) Optimized molecular structures of compounds **PTZ-mPYR** and **PXZ-PYR**. α_1 is the twist angle between the donor unit and the phenyl spacer. (b) Time-resolved fluorescence spectra of 1 wt% PMMA films of **PTZ-mPYR** (left picture) and **PXZ-PYR** (right picture). (c) Fluorescence decay transients of **PTZ-mPYR** (upper picture) and **PXZ-PYR** (lower picture) in toluene (red open dots) and 1 wt% PMMA films (closed black dots). All measurements were performed in oxygen-free surrounding.

of delayed fluorescence after about 10 μs was observed for compound **PTZ-mPYR**, though the initial TADF from the conformers with the lowest ΔE_{ST} was unquenched even in $+O_2$ conditions. In this way, the intensity ratio of delayed and prompt fluorescence (DF/PF ratio) for **PTZ-mPYR** with large conformational disorder decreased from 11.8 in $-O_2$ conditions to 0.26 in $+O_2$ conditions and enabled the blueshift of the emission peak (see Fig. 4c). The delayed emission of compound **4CzPN** with a rigid molecular core and low ΔE_{ST} dispersion was weakly sensitive to molecular oxygen. Only a modest quenching of the latest delayed emission from conformers with the largest ΔE_{ST} was observed, when the DF/PF ratio decreased about 30% from 8.65 to 5.95. This ensured the stable emission for rigid **4CzPN**.

Phenothiazine *vs.* phenoxazine: the impact of donor planarity

To show the validity of our previous observations for various donor–acceptor TADF systems, the solid-state TADF properties of two compounds with a very similar molecular structure were compared (see Fig. 1, series II). In this case, compounds bearing a diphenylpyrimidine-based electron-acceptor unit, bound with two donor units of different geometry, phenothiazine (**PTZ-mPYR**) and phenoxazine (**PXZ-PYR**), were selected. As it was already mentioned, PTZ is of nonplanar geometry. Such orientation has less steric hindrance, leading to more perturbed TADF properties, especially in solid-state.[42] Those shortcomings could be prevailed by selecting more sterically fixed planar donor units, like PXZ[43,44] (see Fig. 6a), though the expected effect should not be as strong as for highly rigid **4CzPN**.

Despite the different donor unit and different ground-state dipole moment (0.4 D for **PXZ-PYR**), both compounds showed rather similar emission wavelength in toluene (see Fig. S5 in ESI†),[20,27] though **PTZ-mPYR** showed lower prompt and TADF efficiency (0.04 and 0.04 *vs.* 0.15 and 0.27, respectively) together with slower TADF decay (11 *vs.* 1.6 μs, respectively). Simultaneously, rather different solid-state TADF properties were observed. The time-resolved fluorescence spectra of TADF compounds with different donor units in PMMA films are shown in Fig. 6b. As it was shown previously, **PTZ-mPYR** showed a pronounced redshift of the prompt fluorescence peak followed by a remarkably lower blueshift of delayed fluorescence at the larger time-scale, which was even lower in oxygen-saturated conditions. As a result, ambient-dependent emission colour was observed. In contrast, remarkably lower temporal shifts of TRPL spectra were observed for **PXZ-PYR** with a more sterically constrained planar donor unit (160 and 100 meV for redshift and blueshift, respectively). As both temporal shifts were comparable, stable emission colour was observed in both $+O_2$ and $-O_2$ conditions (see Fig. S6 in ESI†). A portion of the latest delayed fluorescence still was quenched, though this share was remarkably lower than for more flexible **PTZ-mPYR**. Lowered conformational disorder was especially beneficial for achieving lower TADF lifetime enhancement in solid-state (see Fig. 6c). Although the exact TADF decay time in PMMA film was unknown, a minor increase of the DF/PF ratio in solid-state indicated low TADF lifetime enhancement. On the contrary to **PTZ-mPYR**, lower dispersion of ΔE_{ST} values in **PXZ-PYR** indicates weaker enhancement on TADF lifetime as well as lower average number of ISC/rISC cycles.

Clearly, the rigid molecular structure is essential for minimization of solid-state conformational disorder, regardless of the selected donor and acceptor pair.

Conclusions

In this work, the importance of molecular rigidity for highly efficient delayed emission in solid-state was highlighted. Two TADF compounds with different molecular core rigidity were

selected to showcase the impact of conformational disorder on solid-state TADF properties. Pronounced conformational disorder with large dispersion of singlet–triplet energy gaps was estimated for **PTZ-mPYR** with a more flexible molecular structure. It had a negative impact on the solid-state TADF properties. Firstly, the large ΔE_{ST} dispersion in polymer films resulted in the emergence of conformer states with large ΔE_{ST} and prolonged TADF lifetime. Secondly, the latest delayed emission with inefficient TADF was strongly quenched. The loss of delayed emission with the largest ^{1}CT energies was the reason for the redshift of the solid-state emission peak in oxygen-free conditions. All the above-mentioned drawbacks were eliminated only by selecting a more rigid molecular structure of **4CzPN**. The second TADF compound was selected to have similar TADF properties in solution but lower rotational flexibility of donor units. Minor conformational disorder was observed in solid-state with stable emission colour. More importantly, only a slight increase of TADF lifetime, as compared to that of solution, was observed. This is especially important for the production of TADF OLEDs with low external quantum efficiency roll-off, which is known to depend on the TADF lifetime. The reliability of the suggested design principle was evaluated in the second set of compounds, when two TADF compounds with an alike acceptor fragment but distinct donor units with different steric hindrance, **PTZ-mPYR** and **PXZ-PYR**, were compared. As it was expected, the minimized conformational disorder was evidenced for the compound with more sterically constrained planar donor unit. Our analysis clearly shows that the design of solid-state efficient TADF compounds requires more delicate approaches, when the stiffness of the molecular structure is as important as efficient separation of HOMO and LUMO overlap and strong coupling between the triplet states.

Conflicts of interest

There are no conflicts to declare.

Acknowledgements

This research has received funding from the Research Council of Lithuania (LMTLT), agreement no. S-MIP-17-73. We are grateful to Dr Alytis Gruodis and High Performance Computing Center "HPC Sauletekis" in Vilnius University Faculty of Physics for vibrational frequency calculations and fruitful discussions. We are also very grateful to the Professor Vytautas Getautis group in Kaunas University of Technology for the synthesis of **4CzPN**.

References

1 A. Endo, M. Ogasawara, A. Takahashi, D. Yokoyama, Y. Kato and C. Adachi, *Adv. Mater.*, 2009, **21**, 4802–4806.
2 A. Endo, K. Sato, K. Yoshimura, T. Kai, A. Kawada, H. Miyazaki and C. Adachi, *Appl. Phys. Lett.*, 2011, **98**, 083302.
3 H. Uoyama, K. Goushi, K. Shizu, H. Nomura and C. Adachi, *Nature*, 2012, **492**, 234–238.
4 T.-A. Lin, T. Chatterjee, W.-L. Tsai, W.-K. Lee, M.-J. Wu, M. Jiao, K.-C. Pan, C.-L. Yi, C.-L. Chung, K.-T. Wong and C.-C. Wu, *Adv. Mater.*, 2016, **28**, 6976–6983.
5 T.-L. Wu, M.-J. Huang, C.-C. Lin, P.-Y. Huang, T.-Y. Chou, R.-W. Chen-Cheng, H.-W. Lin, R.-S. Liu and C.-H. Cheng, *Nat. Photonics*, 2018, **12**, 235–240.
6 F. B. Dias, T. J. Penfold and A. P. Monkman, *Methods Appl. Fluoresc.*, 2017, **5**, 012001.
7 E. W. Evans, Y. Olivier, Y. Puttisong, W. K. Myers, T. J. H. Hele, S. M. Menke, T. H. Thomas, D. Credgington, D. Beljonne, R. H. Friend and N. C. Greenham, *J. Phys. Chem. Lett.*, 2018, **9**, 4053–4058.
8 M. K. Etherington, J. Gibson, H. F. Higginbotham, T. J. Penfold and A. P. Monkman, *Nat. Commun.*, 2016, **7**, 13680.
9 J. Gibson, A. P. Monkman and T. J. Penfold, *ChemPhysChem*, 2016, **17**, 2956–2961.
10 D. de Sa Pereira, C. Menelaou, A. Danos, C. Marian and A. P. Monkman, *J. Phys. Chem. Lett.*, 2019, **10**, 3205–3211.
11 Y. Olivier, J.-C. Sancho-Garcia, L. Muccioli, G. D'Avino and D. Beljonne, *J. Phys. Chem. Lett.*, 2018, **9**, 6149–6163.
12 J. S. Ward, R. S. Nobuyasu, A. S. Batsanov, P. Data, A. P. Monkman, F. B. Dias and M. R. Bryce, *Chem. Commun.*, 2016, **52**, 2612–2615.
13 Z.-P. Chen, D.-Q. Wang, M. Zhang, K. Wang, Y.-Z. Shi, J.-X. Chen, W.-W. Tao, C.-J. Zheng, S.-L. Tao and X.-H. Zhang, *Adv. Opt. Mater.*, 2018, **6**, 1800935.
14 M. Saigo, K. Miyata, S. Tanaka, H. Nakanotani, C. Adachi and K. Onda, *J. Phys. Chem. Lett.*, 2019, **10**, 2475–2480.
15 X. Cai and S.-J. Su, *Adv. Funct. Mater.*, 2018, **28**, 1802558.
16 X. Liang, Z.-L. Tu and Y.-X. Zheng, *Chem. – Eur. J.*, 2019, **25**, 5623–5642.
17 M. K. Etherington, F. Franchello, J. Gibson, T. Northey, J. Santos, J. S. Ward, H. F. Higginbotham, P. Data, A. Kurowska, P. L. Dos Santos, D. R. Graves, A. S. Batsanov, F. B. Dias, M. R. Bryce, T. J. Penfold and A. P. Monkman, *Nat. Commun.*, 2017, **8**, 14987.
18 T. Northey, J. Stacey and T. J. Penfold, *J. Mater. Chem. C*, 2017, **5**, 11001–11009.
19 T. Serevičius, T. Buciunas, J. Bucevičius, J. Dodonova, S. Tumkevicius, K. Kazlauskas and S. Jursenas, *J. Mater. Chem. C*, 2018, 11128–11136.
20 T. Serevičius, R. Skaisgiris, J. Dodonova, L. Jagintavičius, J. Bucevičius, K. Kazlauskas, S. Jursenas and S. Tumkevicius, *Chem. Commun.*, 2019, **55**, 1975–1978.
21 H. Yersin, L. Mataranga-Popa, R. Czerwieniec and Y. Dovbii, *Chem. Mater.*, 2019, **31**, 6110–6116.
22 G. Méhes, K. Goushi, W. J. Potscavage and C. Adachi, *Org. Electron.*, 2014, **15**, 2027–2037.
23 R. S. Nobuyasu, J. S. Ward, J. Gibson, B. A. Laidlaw, Z. Ren, P. Data, A. S. Batsanov, T. J. Penfold, M. R. Bryce and F. B. Dias, *J. Mater. Chem. C*, 2019, **7**, 6672–6684.
24 S. Weissenseel, N. A. Drigo, L. G. Kudriashova, M. Schmid, T. Morgenstern, K.-H. Lin, A. Prlj, C. Corminboeuf, A. Sperlich, W. Brütting, M. K. Nazeeruddin and V. Dyakonov, *J. Phys. Chem. C*, 2019, **123**, 27778–27784.
25 T. Northey, J. Stacey and T. J. Penfold, *J. Mater. Chem. C*, 2017, **5**, 11001–11009.

26 M. Inoue, T. Serevičius, H. Nakanotani, K. Yoshida, T. Matsushima, S. Juršėnas and C. Adachi, *Chem. Phys. Lett.*, 2016, **644**, 62–67.
27 K. Wu, T. Zhang, L. Zhan, C. Zhong, S. Gong, N. Jiang, Z.-H. Lu and C. Yang, *Chem. – Eur. J.*, 2016, **22**, 10860–10866.
28 J. C. de Mello, H. F. Wittmann and R. H. Friend, *Adv. Mater.*, 1997, **9**, 230–232.
29 C. Rothe and A. P. Monkman, *Phys. Rev. B: Condens. Matter Mater. Phys.*, 2003, **68**, 075208.
30 M. J. Frisch, G. W. Trucks, H. B. Schlegel, G. E. Scuseria, M. A. Robb, J. R. Cheeseman, G. Scalmani, V. Barone, B. Mennucci, G. A. Petersson, H. Nakatsuji, M. Caricato, X. Li, H. P. Hratchian, A. F. Izmaylov, J. Bloino, G. Zheng, J. L. Sonnenberg, M. Hada, M. Ehara, K. Toyota, R. Fukuda, J. Hasegawa, M. Ishida, T. Nakajima, Y. Honda, O. Kitao, H. Nakai, T. Vreven, J. A. Montgomery, Jr., J. E. Peralta, F. Ogliaro, M. Bearpark, J. J. Heyd, E. Brothers, K. N. Kudin, V. N. Staroverov, T. Keith, R. Kobayashi, J. Normand, K. Raghavachari, A. Rendell, J. C. Burant, S. S. Iyengar, J. Tomasi, M. Cossi, N. Rega, J. M. Millam, M. Klene, J. E. Knox, J. B. Cross, V. Bakken, C. Adamo, J. Jaramillo, R. Gomperts, R. E. Stratmann, O. Yazyev, A. J. Austin, R. Cammi, C. Pomelli, J. W. Ochterski, R. L. Martin, K. Morokuma, V. G. Zakrzewski, G. A. Voth, P. Salvador, J. J. Dannenberg, S. Dapprich, A. D. Daniels, O. Farkas, J. B. Foresman, J. V. Ortiz, J. Cioslowski and D. J. Fox, *Gaussian 09, Revision C.01*, Gaussian, Inc., Wallingford CT, 2010.
31 M. K. Etherington, F. Franchello, J. Gibson, T. Northey, J. Santos, J. S. Ward, H. F. Higginbotham, P. Data, A. Kurowska, P. L. Dos Santos, D. R. Graves, A. S. Batsanov, F. B. Dias, M. R. Bryce, T. J. Penfold and A. P. Monkman, *Nat. Commun.*, 2017, **8**, 14987.
32 H. Tanaka, K. Shizu, H. Nakanotani and C. Adachi, *J. Phys. Chem. C*, 2014, **118**, 15985–15994.
33 C. Chen, R. Huang, A. S. Batsanov, P. Pander, Y.-T. Hsu, Z. Chi, F. B. Dias and M. R. Bryce, *Angew. Chem., Int. Ed.*, 2018, **57**, 16407–16411.
34 D.-G. Chen, T.-C. Lin, Y.-A. Chen, Y.-H. Chen, T.-C. Lin, Y.-T. Chen and P.-T. Chou, *J. Phys. Chem. C*, 2018, **122**, 12215–12221.
35 Q. Peng, D. Fan, R. Duan, Y. Yi, Y. Niu, D. Wang and Z. Shuai, *J. Phys. Chem. C*, 2017, **121**, 13448–13456.
36 S. Wang, Y. Zhang, W. Chen, J. Wei, Y. Liu and Y. Wang, *Chem. Commun.*, 2015, **51**, 11972–11975.
37 H. F. Higginbotham, C.-L. Yi, A. P. Monkman and K.-T. Wong, *J. Phys. Chem. C*, 2018, **122**, 7627–7634.
38 F. C. Spano, *Acc. Chem. Res.*, 2010, **43**, 429–439.
39 G. Kreiza, D. Banevičius, J. Jovaišaitė, K. Maleckaitė, D. Gudeika, D. Volyniuk, J. V. Gražulevičius, S. Juršėnas and K. Kazlauskas, *J. Mater. Chem. C*, 2019, **7**, 11522–11531.
40 J. Fan, Y. Zhang, Y. Zhou, L. Lin and C.-K. Wang, *J. Phys. Chem. C*, 2018, **122**, 2358–2366.
41 J. Fan, L. Lin and C.-K. Wang, *J. Mater. Chem. C*, 2017, **5**, 8390–8399.
42 K. Wang, C.-J. Zheng, W. Liu, K. Liang, Y.-Z. Shi, S.-L. Tao, C.-S. Lee, X.-M. Ou and X.-H. Zhang, *Adv. Mater.*, 2017, **29**, 1701476.
43 K. Wang, Y.-Z. Shi, C.-J. Zheng, W. Liu, K. Liang, X. Li, M. Zhang, H. Lin, S.-L. Tao, C.-S. Lee, X.-M. Ou and X.-H. Zhang, *ACS Appl. Mater. Interfaces*, 2018, **10**, 31515–31525.
44 D.-G. Chen, T.-C. Lin, C.-L. Chen, Y.-T. Chen, Y.-A. Chen, G.-H. Lee, P.-T. Chou, C.-W. Liao, P.-C. Chiu, C.-H. Chang, Y.-J. Lien and Y. Chi, *ACS Appl. Mater. Interfaces*, 2018, **10**, 12886–12896.

A4

Achieving Submicrosecond Thermally Activated Delayed Fluorescence Lifetime and Highly Efficient Electroluminescence by Fine-Tuning of the Phenoxazine-Pyrimidine Structure

T. Serevičius, **R. Skaisgiris**, J. Dodonova, L. Jagintavičius, D. Banevičius, K. Kazlauskas, S. Tumkevičius, S. Juršėnas

ACS Appl. Mater. Interfaces **12**(9), 10727–10736 (2020)
DOI: 10.1021/acsami.9b21394
https://pubs.acs.org/doi/10.1021/acsami.9b21394

Supporting information: https://pubs.acs.org/doi/suppl/10.1021/acsami.9b21394/suppl_file/am9b21394_si_001.pdf

ACS APPLIED MATERIALS & INTERFACES

www.acsami.org

Research Article

Achieving Submicrosecond Thermally Activated Delayed Fluorescence Lifetime and Highly Efficient Electroluminescence by Fine-Tuning of the Phenoxazine–Pyrimidine Structure

Tomas Serevičius,* Rokas Skaisgiris, Jelena Dodonova, Laimis Jagintavičius, Dovydas Banevičius, Karolis Kazlauskas, Sigitas Tumkevičius, and Saulius Juršėnas

Cite This: *ACS Appl. Mater. Interfaces* 2020, 12, 10727–10736

Read Online

ACCESS | Metrics & More | Article Recommendations | Supporting Information

ABSTRACT: Thermally activated delayed fluorescence (TADF) materials, combining high fluorescence quantum efficiency and short delayed emission lifetime, are highly desirable for application in organic light-emitting diodes (OLEDs) with negligible external quantum efficiency (EQE) roll-off. Here, we present the pathway for shortening the TADF lifetime of highly emissive 4,6-bis[4-(10-phenoxazinyl)phenyl]pyrimidine derivatives. Tiny manipulation of the molecular structure with methyl groups was applied to tune the singlet–triplet energy-level scheme and the corresponding coupling strengths, enabling the boost of the reverse intersystem crossing (rISC) rate (from 0.7 to 6.5) × 10^6 s^{-1} and shorten the TADF lifetime down to only 800 ns in toluene solutions. An almost identical TADF lifetime of roughly 860 ns was attained also in solid films for the compound with the most rapid TADF decay in toluene despite the presence of inevitable conformational disorder. Concomitantly, the boost of fluorescence quantum efficiency to near unity was achieved in solid films due to the weakened nonradiative decay. Exceptional EQE peak values of 26.3–29.1% together with adjustable emission wavelength in the range of 502–536 nm were achieved in TADF OLEDs. Reduction of EQE roll-off was demonstrated by lowering the TADF lifetime.

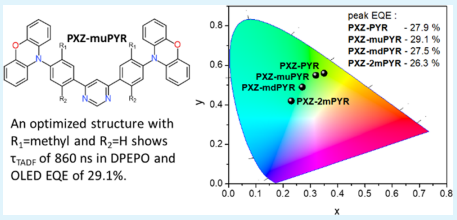

KEYWORDS: *TADF, pyrimidine, phenoxazine, conformational disorder, rISC, OLEDs*

INTRODUCTION

Thermally activated delayed fluorescence (TADF) is an elegant way to employ the "dark" triplet states in organic light-emitting diode (OLED) devices and to achieve nearly 100% internal quantum efficiency[1,2] without the usage of expensive and rare heavy metals, for example, iridium.[3,4] The recent progress in design of TADF materials[5−7] and understanding the processes behind the reverse intersystem crossing (rISC)[8−15] led to the realization of green and sky-blue TADF OLEDs with external quantum efficiency (EQE) values approaching 40%.[16,17] However, large EQE values usually are demonstrated only at low luminance, and pronounced EQE roll-off at larger luminance usually is observed due to the emergence of triplet–triplet, singlet–triplet, and similar annihilation pathways.[18,19] Boosting the rISC rate has been shown to be the successful strategy for lowering the EQE roll-off;[19−21] however, shortening the TADF lifetime is rather a difficult task,[22,23] requiring the minimization of energy gaps between the coupled singlet and triplet states.[8,23] This is achieved by selecting the appropriate electron-donating (D) and electron-accepting (A) units and bounding them in an appropriate molecular geometry.[21] Among the wide variety of possible donor fragments, phenoxazine (PXZ) was shown to be a good candidate for achieving the short TADF lifetime together with a high fluorescence quantum yield[24−32] due to the strong enough electron-donating properties and ability to show large steric hindrance to acceptor units.[21,33] However, being noncontinuously conjugated, phenoxazine is found in two forms, planar and crooked conformation, and only the planar form shows strong TADF.[34,35] This issue can be solved by weakening the interaction between the phenoxazine and the electron-accepting part of the TADF molecule by introducing the spacer unit, minimizing the population of crooked conformations, and enhancing the number of TADF-active planar orientations.[28,36] The application of such molecular design by using phenoxazine D and suitable pyrimidine (PYR) electron-acceptor (A) together with phenyl spacer units (s) in a D-s-A-s-D layout allowed to achieve highly efficient single-band fluorescence with a TADF lifetime of 2.56 μs together with an EQE value of 19.9%.[24] The later modification of a

Received: November 25, 2019
Accepted: February 5, 2020
Published: February 5, 2020

Scheme 1. Synthesis of 4,6-Bis[4-(10-phenoxazinyl)phenyl]pyrimidines PXZ-PYR, PXZ-muPYR, PXZ-mdPYR, and PXZ-2mPYR[a]

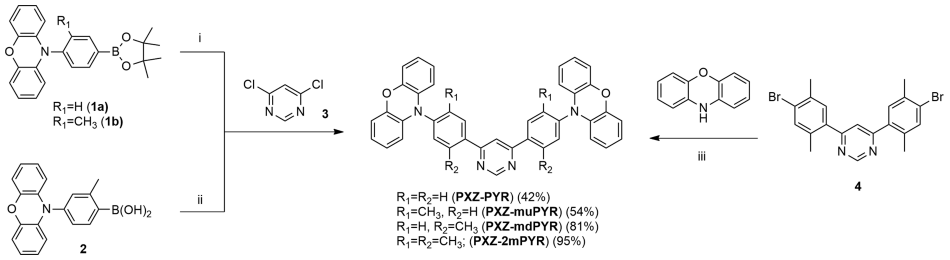

[a]Reagents and conditions: (i) boronic ester **1a** or **1b** (2.2 equiv), $Pd(PPh_3)_4$ (10 mol %), aq. K_2CO_3 (15 equiv), glyme, 80 °C, 24 h; (ii) boronic acid **2** (2.5 equiv), $Pd(OAc)_2$ (10 mol %), PPh_3 (20 mol %), aq. Na_2CO_3 (6.2 equiv), glyme, 90 °C, 24 h; (iii) phenoxazine (2.2 equiv), Pd_2dba_3 (5 mol %), P(*t*-Bu)$_3$·HBF_4 (10 mol %), NaO*t*-Bu (3 equiv), toluene, Ar, 110 °C, 24 h.

promising phenoxazine−pyrimidine structure by different aryl and methyl moieties at the pyrimidine unit resulted in subsequent lowering of the TADF decay time down to 1.99 μs while preserving a high emission yield.[24,25] Further substantial shortening of the TADF lifetime down to 1.32 μs for the analogous phenoxazine−pyrimidine compounds was achieved by introducing Cl or Br atoms and enhancing both ISC and rISC rates due to internal heavy-atom effect, simultaneously preserving a high fluorescence quantum yield. This strategy also allowed to increase peak EQE values up to 25.3%.[26] However, boosting the rISC rate by halogenation results in the redshift of the emission wavelength,[26,37,38] which is beneficiary while seeking the green-to-yellow emission, however other approaches are needed for blue TADF.

Inspired by the potential of pyrimidine−phenoxazine TADF compounds for achieving rapid and highly efficient TADF, we performed the further modification of the 4,6-bis[4-(10-phenoxazinyl)phenyl]pyrimidine molecular structure aiming the additional shortening of the TADF lifetime. Tiny alteration of the molecular structure was performed by inserting methyl units at the different positions of the phenylpyrimidine fragment, changing the geometry and rigidity of the molecular structure. The comprehensive analysis of time-resolved fluorescence spectra revealed the remarkable impact of methyl substitution pattern to energy-level alignment and fluorescence decay rate constants. An optimum molecular geometry was revealed with a balanced ratio between the singlet−triplet energy splittings and corresponding coupling strengths, showing the submicrosecond solid-state TADF lifetime and high emission yield. The optimized TADF compounds were employed in optimized OLED devices as emitters with tunable emission color. Outstanding peak EQE values of 26.3−29.1% were obtained with minimized EQE roll-off.

EXPERIMENTAL SECTION

Reagents and solvents were purchased directly from commercial suppliers; solvents were purified by known procedures. Melting points were determined in open capillaries with a digital melting point IA9100 series apparatus (Thermo Fisher Scientific) and were not corrected. Thin layer chromatography was performed using TLC aluminum sheets with silica gel (Merck 60 F254). Visualization was accomplished by UV light. Column chromatography was performed using silica gel 60 (0.040−0.063 mm) (Merck). NMR spectra were recorded on a Bruker Ascend 400 (400 and 100 MHz for ^{1}H and ^{13}C, respectively). ^{1}H NMR and ^{13}C NMR spectra were referenced to residual solvent peaks. High-resolution mass spectrometry (HRMS) analyses were carried out on microTOF-Q II or microTOF-Q III mass spectrometers (Bruker). DSC curves were measured by Mettler Toledo DSC1 apparatus using aluminum crucibles under N_2 flow. Sample mass was around 8−10 mg, and heating and cooling rates were 10 K/min. TADF compounds were analyzed in 1 × 10^{-5} M toluene solutions, 1 wt % PMMA, and 10 wt % DPEPO films. Solid-state films were prepared by dissolving each material and host at appropriate ratios in toluene solutions and then wet-casting the solutions on quartz substrates. Absorption spectra were measured using a Lambda 950 UV/Vis spectrophotometer (PerkinElmer). Time-integrated fluorescence spectra (TIFL), time-resolved fluorescence spectra (TRFL), phosphorescence spectra and fluorescence decay transients were measured using a nanosecond YAG:Nd^{3+} laser NT 242 (Ekspla, τ = 7 ns, pulse energy 200 μJ, λ_{ex} = 300 nm, repetition rate = 1 kHz) and time-gated iCCD camera New iStar DH340T (Andor). Fluorescence transients were obtained by exponentially increasing delay and integration time. This allows to record up to 10 orders of magnitude in time and intensity of the fluorescence decay.[39] Fluorescence quantum yields (Φ_F) within the ±5% error of the solutions and polymer films in ambient air were estimated by the integrated sphere method[40] using an integrating sphere (Sphere Optics) connected to the CCD spectrometer PMA-12 (Hamamatsu) via optical fiber. Solid-state samples were mounted in a closed-cycle He cryostat (Cryo Industries 204 N) for all measurements (for oxygen-saturated (+O_2) and oxygen-free (−O_2) conditions). Toluene solutions were degassed by using the freeze−pump−thaw method. OLED devices were fabricated on precleaned indium-tin oxide (ITO)-coated glass substrates. The small-molecule and cathode layers were thermally evaporated using a vacuum evaporation apparatus (Vacuum Systems and Technologies Ltd) at <6 × 10^{-6} Torr pressure and deposition rate of about 1 Å/s. OLED devices were encapsulated with a clear glass cover to prevent the interaction with ambient atmosphere. Device current−voltage (I−V) characteristics and electroluminescence properties were measured using a calibrated integrating sphere (Orb Optronics) and CCD spectrometer PMA-11 (Hamamatsu), powered by a 2601A power supply unit (Keithley).

RESULTS AND DISCUSSION

Molecular Design. Four TADF compounds, bearing phenoxazine electron-donor and diphenylpyrimidine electron-acceptor units, were synthesized and comprehensively analyzed. 4,6-Bis[4-(10-phenoxazinyl)phenyl]pyrimidine (**PXZ-PYR**) was taken as a starting point for further optimization due to the high solid-state fluorescence efficiency

https://dx.doi.org/10.1021/acsami.9b21394
ACS Appl. Mater. Interfaces 2020, 12, 10727−10736

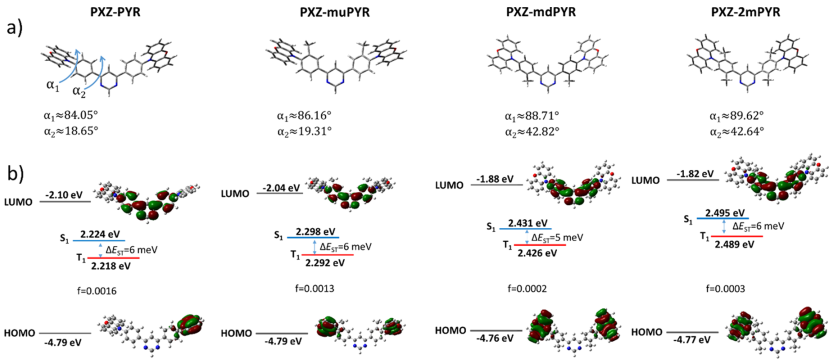

Figure 1. (a) DFT-optimized molecular geometries of TADF compounds **PXZ-PYR**, **PXZ-muPYR**, **PXZ-mdPYR**, and **PXZ-2mPYR**. α_1 and α_2 are dihedral angles between phenyl−phenoxazine and phenyl−pyrimidine units, respectively. (b) HOMO and LUMO energies, $S_0 \rightarrow S_1/T_1$ absorption energies with corresponding transition oscillator strengths and $S_1 - T_1$ energy gaps (ΔE_{ST}) and π-electron density distribution in the HOMO and LUMO of compounds **PXZ-PYR**, **PXZ-muPYR**, **PXZ-mdPYR**, and **PXZ-2mPYR**.

(0.88) and rapid TADF decay (2.56 μs).[24] Various modifications of the **PXZ-PYR** structure were demonstrated,[24,26] seeking for the shortening of the TADF lifetime; however, either the effect was rather low (from 2.56 to 1.99 μs[24]) or the modification resulted in usually unwanted narrowing of the bandgap.[26] As a solution, molecular structure modification of similar D-s-A-s-D TADF compounds bearing acridine donor units by methyl units for the minimization of τ_{TADF} without the emission redshift was suggested by Komatsu et al.[41] The presented strategy allowed to widen the energy gap and observe the blueshift of the emission peak. Such a strategy was also successfully applied for different TADF compounds.[42−46] Inspired by such observations and our previous findings,[37] we designed three new phenoxazine−pyrimidine TADF compounds with methyl units introduced into the acceptor unit. In contrast to Komatsu et al.,[41] we tuned the twist angles not only between the pyrimidine and phenyl units but also between the phenyl units and phenoxazine, seeking for more pronounced alteration of TADF properties and a molecular rigidity increase. Namely, compound **PXZ-muPYR** was modified with *meta*-methyl units, **PXZ-mdPYR** by *ortho*-methyl moieties, and **PXZ-2mPYR** by both *meta*- and *ortho*-methyl units at the phenyl spacers (see Scheme 1).

Synthesis and Thermal Properties. Synthetic routes of the designed molecules **PXZ-PYR**, **PXZ-mdPYR**, **PXZ-muPYR**, and **PXZ-2mPYR** are outlined in Scheme 1. 4,6-Bis[4-(10-phenoxazinyl)phenyl]pyrimidine (**PXZ-PYR**)[24] and 4,6-bis[3-methyl-4-(10-phenoxazinyl)phenyl]pyrimidine (**PXZ-muPYR**) were synthesized by the Suzuki−Miyaura cross-coupling reaction of 4,6-dichloropyrimidine (**3**) with corresponding 4-(10-pheoxazinyl)phenyl boronates (**1a,b**) in the presence of $Pd(PPh_3)_4$ as a catalyst. Coupling of boronic acid **2** with 4,6-dichloropyrimidine (**3**) using $Pd(OAc)_2/PPh_3$ as a catalyst system gave **PXZ-mdPYR** in a good yield (81%). Compound **PXZ-2mPYR** bearing two methyl groups in a phenyl spacer between pyrimidine and phenoxazine moieties was obtained in an excellent yield (95%) by reacting 4,6-bis(4-bromo-2,5-dimethylphenyl)pyrimidine (**4**), previously reported by us,[37] with phenoxazine under the palladium-catalyzed amination reaction conditions. For clarity, methyl groups in the phenyl spacer will be hereinafter referred to as follows: 2-methyl group in compounds **PXZ-mdPYR** and **PXZ-2mPYR** as *ortho*-methyl group and 3-methyl group in **PXZ-muPYR** and 5-methyl group in **PXZ-2mPYR** as *meta*-methyl groups. The synthetic details and characterization data of the synthesized 4-(10-phenoxazinyl)phenylboronic acid esters **1a,b**, boronic acid **2**, and target compounds **PXZ-PYR**, **PXZ-muPYR**, **PXZ-muPYR**, and **PXZ-2mPYR** are presented in the Supporting Information.

Differential scanning calorimetry analysis (see Figure S21 in the Supporting Information) revealed that all phenoxazine−pyrimidine compounds were molecular glasses with glass transition temperatures ranging from 109 to 137 °C, typically for similar phenoxazine−pyrimidine TADF materials.[24,26]

DFT Simulations. Quantum chemical calculations were performed by using density functional theory (DFT) as implemented in the Gaussian 09 software package at the B3LYP/6-31G(d) level.[47] Polarizable continuum model (PCM) was used to estimate the solvation behavior of the toluene surrounding.

The synthesized phenoxazine−pyrimidine TADF compounds **PXZ-PYR**, **PXZ-muPYR**, **PXZ-mdPYR**, and **PXZ-2mPYR** were optimized at the ground-state molecular geometry and π-electron density distribution in the HOMO and LUMO, and $S_0 \rightarrow S_1/T_1$ transition energies with corresponding oscillator strengths were calculated (see Figure 1). DFT analysis revealed that the lowest-energy molecular conformations were those with a planar (quasi-equatorial) orientation of the PXZ unit[28,34] (see Figure S22 in the Supporting Information for the detailed analysis). The phenoxazine fragment was nearly perpendicular in all compounds with minor variations of the twist angle (angle α_1 in Figure 1). The modification of the molecular structure with *ortho*-methyl groups had a pronounced effect on the twist angle between phenyl and pyrimidine units (angle α_2 in Figure 1). Both phenyls were weakly twisted with respect to the pyrimidine fragment in **PXZ-PYR** and **PXZ-muPYR**; however, α_2 angle increased from about 19° to nearly 43° after the introduction of the *ortho*-methyl group due to the enhanced

https://dx.doi.org/10.1021/acsami.9b21394
ACS Appl. Mater. Interfaces 2020, 12, 10727−10736

steric hindrance. It had an evident effect on the energies of LUMO, which increased from about −2.04 to −2.10 eV for compounds **PXZ-PYR** and **PXZ-muPYR**, respectively, and from −1.82 to −1.88 eV for compounds **PXZ-mdPYR** and **PXZ-2mPYR**, respectively, weakening the electron-accepting ability and enlarging the bandgap, while the HOMO energies were almost the same (from −4.76 to −4.79 eV). All phenoxazine−pyrimidine compounds showed charge-transfer (CT) character when the electron density in the HOMO mostly was distributed over the phenoxazine unit, while in the LUMO, the π-electron density was localized over the diphenylpyrimidine moiety. Molecular structure modification also had the pronounced effect on singlet and triplet transition energies and the corresponding oscillator strengths. $S_0 \rightarrow S_1$ transition energies ranged at 2.224−2.298 eV for **PXZ-PYR** and **PXZ-muPYR** with an oscillator strength of 0.0013−0.0016. The enlarged $S_0 \rightarrow S_1$ transition energies up to about 2.495 eV with an oscillator strength of 0.0002−0.0003 were observed for *ortho*-methyl modified compounds **PXZ-mdPYR** and **PXZ-2mPYR** with the lowest electron cloud overlap in the HOMO and LUMO and the weakest electron-acceptor. The same trend was also estimated for $S_0 \rightarrow T_1$ transition, when the transition energies of <2.3 eV were estimated for compounds **PXZ-PYR** and **PXZ-muPYR** and >2.4 eV for **PXZ-mdPYR** and **PXZ-2mPYR** with corresponding singlet−triplet gaps of only 5−6 meV. Such a negligible splitting shows the possibility of highly efficient TADF with controllable emission properties.

Absorption and Emission Properties. The impact of molecular core modifications for absorption and fluorescence properties of phenoxazine−pyrimidine compounds was revealed by analyzing absorption and emission spectra in toluene solutions (see Figure 2 and Table 1).

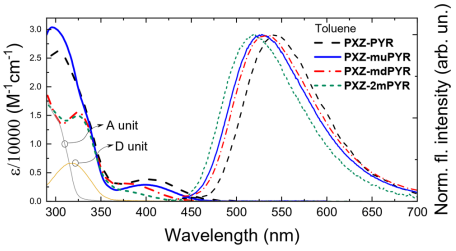

Figure 2. Absorption and fluorescence spectra of compounds **PXZ-PYR**, **PXZ-muPYR**, **PXZ-mdPYR**, and **PXZ-2mPYR** in toluene. Absorption spectra of diphenylpyrimidine A and phenoxazine D units are also shown.

Two regions can be discerned in the absorption spectra, peaking at about 300−320 and 380−400 nm (with absorption tail until about 500 nm). The absorption peaks at the higher energies were the composition of the absorption of individual phenoxazine and phenylpyrimidine units. Since no absorption of donor or acceptor units extended beyond ∼375 nm, the lower energy absorption band was attributed to the absorption of charge-transfer states.[24,26,28] Larger molar absorption values (up to about 3900 M^{-1} cm^{-1}) were observed for compounds **PXZ-PYR** and **PXZ-muPYR**, in line with DFT predictions. Fluorescence spectra of compounds **PXZ-PYR**, **PXZ-muPYR**, **PXZ-mdPYR**, and **PXZ-2mPYR** peaked at 519−543 nm in toluene solutions, typically for phenoxazine-based TADF compounds.[24−29] The introduction of methyl groups into the phenyl spacer unit allowed us to tune the CT emission wavelength for 100 meV when the fluorescence of the unmodified **PXZ-PYR** peaked at 543 nm and blueshifted up to 519 nm for **PXZ-2mPYR**. This was achieved by the manipulating the electron density overlap in the HOMO and LUMO and the strength of donor unit, as shown by DFT calculations. Fluorescence quantum yields (Φ_F) of TADF compounds in toluene solutions ranged from 0.1 to 0.15 and were larger for compounds without the *meta*-methyl fragments (see Table 1).

To reveal the nature of Φ_F variation, radiative (k_r) and nonradiative (k_{nr}) fluorescence decay rates of phenoxazine−pyrimidine compounds were estimated (see Table 1). Compounds **PXZ-PYR** and **PXZ-muPYR** with the largest oscillator strength showed the most rapid radiative decay; however, k_r was almost twice lower for **PXZ-muPYR**, resulting in Φ_F decrease. Simultaneously, both **PXZ-PYR** and **PXZ-muPYR** with the most flexible molecular structure showed the fastest nonradiative decay due to the pronounced excited-state relaxation (and/or, probably, different ISC rates), though the introduction of the *meta*-methyl unit lowered the nonradiative decay for about 17%. The further modification of the molecular structure with *ortho*-methyl units weakened the HOMO−LUMO overlap and lowered the radiative decay rate. Despite that, compounds **PXZ-mdPYR** and **PXZ-2mPYR** benefited from the more rigid molecular structure, leading to about 60% lowered nonradiative decay rate.[48,49] The weaker nonradiative decay, despite the lowered radiative decay rate, resulted in enhanced Φ_F for compound **PXZ-mdPYR**, almost the same as for **PXZ-PYR** with the largest k_r.

The nonradiative decay was further suppressed by embedding phenoxazine−pyrimidine compounds in solid polymer films. In this case, the emission peaked at 498−513 nm, slightly blueshifted with respect to toluene solutions due to weaker solid-state solvation in the PMMA surrounding[50] (see Figure S23 in the Supporting Information). Same as in

Table 1. Absorption and Emission Data of Compounds PXZ-PYR, PXZ-muPYR, PXZ-mdPYR, and PXZ-2mPYR in Toluene Solutions

compounds	λ_{ABS} (nm)[a]	ε (M^{-1} cm^{-1})[b]	λ_{FL} (nm)[c]	Φ_F[d]	k_{FL} ($\times 10^7$ s^{-1})[e]	k_r ($\times 10^6$ s^{-1})[f]	k_{nr} ($\times 10^7$ s^{-1})[g]
PXZ-PYR	402	3880	543	0.15	7.5	11.3	6.4
PXZ-muPYR	401	2880	530	0.1	6.1	6.1	5.5
PXZ-mdPYR	375	3100	528	0.14	4.0	5.6	3.4
PXZ-2mPYR	-*	below 2000*	519	0.1	4.2	4.2	3.8

[a]Peak wavelength of the lowest energy absorption band. *, no clear absorption peak. [b]Molar absorption coefficient of the lowest energy absorption band. *, approximate value. [c]Peak wavelength of the fluorescence spectrum. [d]Fluorescence quantum yield. [e]Fluorescence decay rate. [f]Radiative fluorescence decay rate ($k_{FL} \times \Phi_{FL}$). [g]Nonradiative fluorescence decay rate ($k_{FL} \times (1 - \Phi_{FL})$).

https://dx.doi.org/10.1021/acsami.9b21394
ACS Appl. Mater. Interfaces 2020, 12, 10727−10736

toluene, unmodified **PXZ-PYR** peaked at the longest wavelengths, while compounds modified with *ortho*-methyl units peaked at the shortest wavelengths. Fluorescence quantum yields of compounds in PMMA films were enhanced due to the largely minimized nonradiative decay. Φ_F were 0.26, 0.16, 0.19, and 0.13 for **PXZ-PYR**, **PXZ-muPYR**, **PXZ-mdPYR**, and **PXZ-2mPYR**, respectively (see Figure S24 in the Supporting Information for the estimation of Φ_F for polymer films). A more pronounced increase in Φ_F was estimated for less rigid compounds.

Phosphorescence (PH) properties of phenoxazine−pyrimidine compounds were investigated by analyzing low-temperature spectra of 1 wt % PMMA films (see Figure 3). Clear

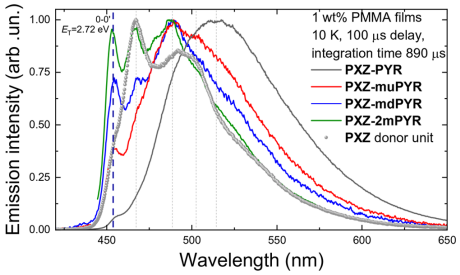

Figure 3. Normalized emission spectra of 1 wt % PMMA films of compounds **PXZ-PYR**, **PXZ-muPYR**, **PXZ-mdPYR**, and **PXZ-2mPYR** and the phenoxazine (**PXZ**) donor unit at 10 K. Spectra were obtained after 100 μs delay with 890 μs integration time.

vibronic progression was observed, typically for localized-excited state (^{3}LE) emission. Vibronic bands of more rigid compounds **PXZ-muPYR**, **PXZ-mdPYR**, and **PXZ-2mPYR** peaked at the same wavelengths as that of the phenoxazine donor fragment, and the intensity of the 0th vibronic band was the largest for the most rigid **PXZ-2mPYR**, indicating negligible reorganization of the molecular structure in the excited state. On the other hand, those strongly overlapped and broadened lower energy vibronic bands clearly dominated in the phosphorescence spectrum of the least sterically constrained **PXZ-PYR**, though the weak 0th vibronic band still was visible. Therefore, all phosphorescence spectra originate from the phenoxazine electron-donor unit with the same T_1 energy of 2.72 eV. These results contradicts with other reports of similar D-s-A-s-D phenoxazine−pyrimidine materials and even the report of same compound **PXZ-PYR**[24] when the T_1 states were shown to be at the lower energies.[24−26] The estimated singlet−triplet energy gaps of phenoxazine−pyrimidine compounds in PMMA films (calculated by subtracting the energy of phosphorescence's 0th vibronic peak from the onset energy of fluorescence spectra) were in the range of 10−150 meV (10, 70, 150, and 130 meV for **PXZ-PYR**, **PXZ-muPYR**, **PXZ-mdPYR**, and **PXZ-2mPYR**, respectively; see Figure S25 in the Supporting Information). The lowest ΔE_{ST} was estimated for compounds **PXZ-PYR** and **PXZ-muPYR**, while the compounds with the lowered HOMO−LUMO overlap showed enlarged ΔE_{ST}.

To sum up, the introduction of methyl groups to the bridging phenyl unit enabled the significant reduction of k_{nr}; however, it also decreased k_r and enlarged the singlet−triplet energy gaps. Later, it will be shown to have the crucial impact to TADF properties.

TADF Properties. In this section, solution and solid-state TADF properties of phenoxazine−phenylpyrimidine compounds will be discussed. All materials showed delayed fluorescence of TADF nature in both toluene solutions and PMMA films, as demonstrated by its temperature activation (see Figure S26 in the Supporting Information) and quenching by molecular oxygen (see Figures S27 and S28 in the Supporting Information). The fluorescence intensity of toluene solutions was strongly enhanced upon the oxygen removal for compounds **PXZ-muPYR** and **PXZ-2mPYR** (for 5.2−5.3 times), while for **PXZ-PYR** and **PXZ-mdPYR**, the enhancement was lower (for 2.7−2.8 times). Although Φ_F was rather similar for all compounds in $-O_2$ toluene (0.38−0.53), fluorescence quantum yields of delayed fluorescence (Φ_{DF}) were markedly larger for **PXZ-muPYR** and **PXZ-2mPYR** than those for **PXZ-PYR** and **PXZ-mdPYR** (~0.42 vs ~0.25), together with remarkably enhanced DF/PF ratios (~4.3 vs ~1.8).

The TADF lifetime of phenoxazine−pyrimidine compounds in toluene solutions (see Figure 4a and Table 2) was rather fast

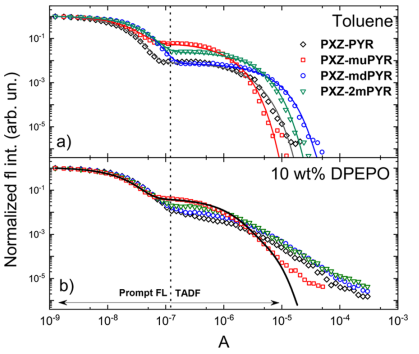

Figure 4. Normalized fluorescence decay transients of phenoxazine−pyrimidine TADF compounds in (a) $-O_2$ toluene and (b) 10 wt % DPEPO films. Color lines are biexponential fits, while the black line in (b) is a triexponential fit.

for compounds **PXZ-PYR**, **PXZ-mdPYR**, and **PXZ-2mPYR** with the lifetime ranging from 1.6 to 4.0 μs, while for **PXZ-muPYR**, the TADF decay time decreased down to 0.8 μs. This value was among the lowest reported for solutions,[20,22,28,38,51] though the low TADF lifetime in solutions with Φ_F of only ~0.5 could also be affected by the nonradiative fluorescence recombination.[52] Clearly, the molecular structure had a direct effect on TADF properties, altering the rates of ISC and rISC in toluene solutions (see Table 2). According to Gibson et al.,[8] efficient ISC and rISC require the combination of large spin-orbit coupling between ^{1}CT and ^{3}LE states and large vibronic coupling between ^{3}LE and ^{3}CT states (via the torsion of D-A angle), together with small corresponding energy gaps (^{1}CT-^{3}LE and ^{3}LE-^{3}CT, respectively).

In our case, we obviously tune the rotational flexibility of PXZ unit and alter the ^{1}CT-^{3}LE gap by changing the HOMO−LUMO overlap. Likewise, ^{3}LE-^{3}CT gaps may also be different,

https://dx.doi.org/10.1021/acsami.9b21394
ACS Appl. Mater. Interfaces 2020, 12, 10727−10736

Table 2. TADF Properties of Compounds PXZ-PYR, PXZ-muPYR, PXZ-mdPYR, and PXZ-2mPYR in $-O_2$ Toluene[a]

compounds	Φ_F[b]	$\frac{DF}{PF}$[c]	Φ_{ISC}[d]	τ_{PF} (ns)[e]	τ_{TADF} (μs)[f]	k_{IC} (10^6 s^{-1})[g]	k_{ISC} (10^7 s^{-1})[h]	k_{rISC} (10^6 s^{-1})[i]
PXZ-PYR	0.15/0.27/0.42	1.8	0.64	13.3	1.6	16.0	4.8	1.8
PXZ-muPYR	0.1/0.42/0.52	4.2	0.81	16.4	0.8	5.6	4.9	6.5
PXZ-mdPYR	0.14/0.24/0.38	1.7	0.63	25.0	4.0	9.2	2.5	0.7
PXZ-2mPYR	0.1/0.43/0.53	4.3	0.81	23.8	2.1	3.7	3.4	2.5

[a]Calculations were carried out according to Dias et.al.[55] [b]Fluorescence quantum yield of prompt, delayed, and total fluorescence, respectively. [c]Delayed fluorescence/prompt fluorescence intensity ratio. [d]Triplet yield. It was estimated according to ref 53 using PH lifetime from Figure S29 in the Supporting Information. [e]Fluorescence decay time. [f]TADF decay time. [g]Internal conversion rate. [h]Intersystem crossing rate. [i]Reverse intersystem crossing rate. Alike k_{rISC} values, we also obtained accordingly to the model for compounds with $k_r \approx k_{rISC}$; see Table S1 in the Supporting Information.

while the spin-orbit coupling constants should be similar for compounds with a similar molecular structure.[53] All this resulted in changes of the ISC rate (from 4.8 to 4.9) × 10^7 s^{-1} for compounds **PXZ-PYR** and **PXZ-muPYR**, respectively, and (from 2.5 to 3.4) × 10^7 s^{-1} for **PXZ-mdPYR** and **PXZ-2mPYR**, respectively, together with more pronounced variation of the rISC rate from 6.5 × 10^6 s^{-1} (for **PXZ-muPYR**) to 0.7 × 10^6 s^{-1} (**PXZ-mdPYR**). Both rates were clearly lower for compounds with larger ^{1}CT-^{3}LE splittings but the same rotational flexibility of PXZ unit (e.g., **PXZ-PYR** vs **PXZ-mdPYR** and **PXZ-muPYR** vs **PXZ-2mPYR**). Here, the decrease in ISC and rISC rates mostly was caused by the enhancement of ^{1}CT-^{3}LE gaps. Surprisingly, the increase in both rates was found for compounds with more sterically constrained PXZ units, lowered IC rates, and, supposedly, weakened vibronic coupling between ^{3}LE and ^{3}CT states[54] (**PXZ-PYR** vs **PXZ-muPYR** and **PXZ-mdPYR** vs **PXZ-2mPYR**). In this case, the decrease in ^{3}LE-^{3}CT gaps for *meta*-methyl modified compounds **PXZ-muPYR** and **PXZ-2mPYR** probably was the cause of enhanced ISC and rISC rates,[11] though the exact mechanism still is debatable. The largest rISC rate (6.5 × 10^{-6} s^{-1}) and, therefore, the most rapid TADF decay (0.8 μs) was estimated for **PXZ-muPYR** together with one of the largest Φ_{TADF} (0.42) due to the largest k_{rISC}/k_{IC} ratio. On the other hand, the weakened IC rate for **PXZ-2mPYR** allowed us to achieve the same TADF quantum yield together with a large enough rISC rate of 2.5 × 10^{-6} s^{-1} as for **PXZ-muPYR** having 45% more rapid radiative decay. However, the nonradiative decay still was strong for all compounds, resulting in Φ_F way below 1.

The boost of the fluorescence quantum yield was achieved by embedding the TADF compounds into the solid PMMA polymer matrix in $-O_2$ conditions. Although the rotational flexibility of the molecular structure already was reduced by the introduction of methyl groups, the additional suppression of structural relaxation in a more rigid surrounding eliminated the remaining nonradiative decay. Near-unity Φ_F were observed for compounds **PXZ-PYR**, **PXZ-muPYR**, and **PXZ-mdPYR** (0.92, 0.94, and 0.95, respectively). A somewhat lower Φ_F of 0.72 was estimated for **PXZ-2mPYR** with the largest ΔE_{ST}.[41] For further solid-state TADF analysis, small-molecule host DPEPO (bis(2-(diphenylphosphino)phenyl) ether oxide) was selected due to the large triplet energy and larger polarity.[56] Similar to those of PMMA Φ_F values were obtained for 10 wt % DPEPO (bis(2-(diphenylphosphino)phenyl) ether oxide) films, when, for example, a Φ_F of 0.84 was estimated for **PXZ-muPYR**, comparable to that in PMMA within the measurement error. The more polar DPEPO surrounding favored more pronounced stabilization of CT energies, though the emission energies were slightly redshifted with respect to PMMA films (λ_{FL} = 515−542 nm; see Figure S30 in the Supporting Information).^{1}CT-^{3}LE gaps were also reduced to nearly zero for **PXZ-PYR** and **PXZ-muPYR** and 50−100 meV for **PXZ-mdPYR** and **PXZ-2mPYR**, respectively (see Figure S30 in the Supporting Information). Prompt fluorescence decay transients of 10 wt % DPEPO films of compounds **PXZ-PYR**, **PXZ-muPYR**, **PXZ-mdPYR**, and **PXZ-2mPYR** in the $-O_2$ surrounding (see Figure 4b) were similar to toluene solutions; however, the TADF decay was strongly multiexponential for compounds **PXZ-muPYR**, **PXZ-mdPYR**, and **PXZ-2mPYR** due to the presence of conformational disorder (see Figure S31 in the Supporting Information for time-resolved spectra, showing temporal shifts of the emission peak).[37,52,56−61] Although no exact TADF lifetime and decay rates could be estimated, still the slowest TADF decay could be attributed for **PXZ-2mPYR**. On the contrary, an approximate three-exponential fit of fluorescence decay transient was successfully applied for **PXZ-muPYR** with the most rapid rISC in toluene,[37] though the latest DF decay tail (from about 10^{-5} to about 10^{-4} s) still was impossible to fit. Roughly, a solid-state TADF lifetime of only 860 ns was obtained, being one of the lowest among the ever reported for various TADF compounds[7,21,51,62] and especially for pyrimidine derivatives (see Table S2 in the Supporting Information).

To sum up, molecular structure modification by small methyl units is a powerful strategy for tunning of TADF properties. Later, the enhanced TADF decay rate together with a large fluorescence quantum yield will be shown to be essential for achieving highly efficient electroluminescence with low EQE roll-off.

Electroluminescence Properties. At the final stage, electroluminescence properties of phenoxazine−pyrimidine compounds **PXZ-PYR**, **PXZ-muPYR**, **PXZ-mdPYR**, and **PXZ-2mPYR** were elucidated (see Figure 5 and Table 3). Typical for similar phenoxazine−pyrimidine TADF compounds OLED structure was used:[24−26] indium tin oxide (ITO)/1,1-bis[(di-4-tolylamino)phenyl]cyclohexane (TAPC) (30 nm)/4,4′,4″-tri(*N*-carbazolyl)triphenylamine (TCTA) (5 nm)/10 wt % TADF emitter:DPEPO (bis(2-(diphenylphosphino)phenyl) ether oxide) (15 nm)/1,3,5-tri(*m*-pyridin-3-yl-phenyl)benzene (TmPyPB) (65 nm)/lithium fluoride (LiF) (0.8 nm)/Al (100 nm). However, contrary to the reports of similar phenoxazine−pyrimidine compounds,[24−26] the high triplet energy host DPEPO (E_T = 3.3 eV[25]) was used rather than CBP with lower triplet energy (E_T = 2.6 eV[25]) to efficiently confine triplet excitons (T_1 = 2.72 eV) in the emissive layer. Neighboring compounds TCTA and

https://dx.doi.org/10.1021/acsami.9b21394
ACS Appl. Mater. Interfaces 2020, 12, 10727−10736

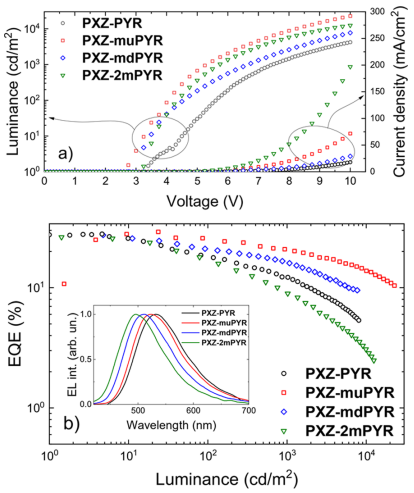

Figure 5. (a) Voltage−current density and voltage−luminance curves of the OLEDs. (b) External quantum efficiency dependence on the luminance of the OLEDs. Inset: electroluminescence spectra of devices at a driving voltage of 9 V.

TmPyPB were also selected to have larger T_1 energies than of emitting compounds to assist the exciton confinement.[63,64]

Electroluminescence (EL) spectra of all OLED devices (see the inset in Figure 5b) showed the emission only from the TADF emitter with no additional peaks from the host or neighboring materials. EL spectra peaked in the range of 502−536 nm. The alteration of the molecular structure allowed us to tune the EL peak wavelength from green, peaking at 536 nm for **PXZ-PYR** (CIE color coordinates of (0.35, 0.56)) to cyan for **PXZ-2mPYR**, peaking at 502 nm (CIE color coordinates of (0.23, 0.42)). EL turn-on voltages were in the range of 2.5−3.3 V, typically for OLEDs with a weakly electroactive DPEPO host.[65,66] The estimated peak values of power efficiency and luminance were in the range of 53.3−84.1 lm/W and 4214−22,730 cd/m^2. Very high external quantum efficiency (EQE) values were obtained, being among the highest values for pyrimidine compounds (see Table S3 in the Supporting Information). Compound **PXZ-muPYR** with the most rapid rISC and near-unity fluorescence quantum yield showed a peak EQE of 29.1% for green electroluminescence without introducing any outcoupling enhancement technique, consistent with high Φ_F values and considering a light extraction yield of 0.2−0.3[67] (though the presence of molecular alignment of rod-like molecules, enhancing the outcoupling, still is possible[59,68]). A weak EQE roll-off of about 30% was observed when the EQE decreased down to 20.5% at the practical luminance of 1000 cd/m^2. A low EQE roll-off was achieved due to the short TADF lifetime of only 860 ns, weakening the EQE quenching by triplet−triplet and singlet−triplet annihilation at high luminance.[19,20] The combination of submicrosecond solid-state TADF lifetime and near 30% OLED EQE puts compound **PXZ-muPYR** among the most efficient TADF emitters (see Table S3 in the Supporting Information). Further optimization of EQE roll-off probably could be achieved by selecting a high T_1 host layer with larger carrier drift mobilities.[69] Also, very large EQE values were obtained for compounds **PXZ-PYR** and **PXZ-mdPYR** with similar near-unity Φ_F values, reaching 27.9 and 27.5%, respectively, though EQE roll-off was markedly larger due to the slower TADF decay. The lowest, though still large, peak EQE of 26.3% of cyan EL was estimated for compound **PXZ-2mPYR** with the lowest solid-state Φ_F; however, the EQE roll-off was rather large (an EQE of 8.9% at the luminance of 1000 cd/m^2) due to the largest TADF lifetime. Therefore, all the OLEDs with phenoxazine−phenylpyrimidine TADF emitters showed high EQE values, ranging from 26.3 to 29.1%, differing mainly by EQE roll-off, which was determined by the TADF lifetime.

CONCLUSIONS

In summary, we presented the synthesis, comprehensive analysis, and device application of a series of TADF compounds based on the phenoxazine−phenylpyrimidine structure with high TADF efficiency and rapid delayed fluorescence decay. The modification of the molecular structure with methyl groups at the acceptor unit was employed to tune the acceptor properties and donor−acceptor interaction, which were shown to have a significant effect on emission properties of TADF compounds. First, the introduction of *ortho*-methyl units was found to reduce the acceptor strength, resulting in enlarged ^{1}CT-^{3}LE energy gap and lowered rISC rate together with lowered TADF efficiency. On the contrary, the modification of the molecular structure with *meta*-methyl fragments was shown to be beneficial for enhancing the rISC rate up to 6.5 × 10^6 s^{-1} and shortening the TADF lifetime to 800 ns in toluene solutions. Lowering the ^{3}LE-^{3}CT energy gap was attributed as the nature of TADF enhancement. The modification of the phenoxazine−phenylpyrimidine molecular structure by introduction of both *ortho*- and *meta*-methyl units into the phenyl moiety was shown to lower the rISC rate and prolong TADF lifetime due to the

Table 3. Electroluminescence Properties of Phenoxazine−Pyrimidine TADF Compounds PXZ-PYR, PXZ-muPYR, PXZ-mdPYR, and PXZ-2mPYR

compounds	λ_{EL} (nm)[a]	V_{ON} (V)[b]	EQE[c]	PE_{MAX} (lm/w)[d]	L_{MAX} (cd/m^2)[e]	CIE (x, y)[f]
PXZ-PYR	536	3.3	27.9/18.0/12.3	84.1	4214	(0.35, 0.56)
PXZ-muPYR	529	2.7	29.1/25.0/20.5	74.1	22730	(0.32, 0.55)
PXZ-mdPYR	514	2.5	27.5/21.0/16.0	75.2	7702	(0.27, 0.49)
PXZ-2mPYR	502	2.9	26.3/16.9/8.9	53.3	12476	(0.23, 0.42)

[a]Electroluminescence peak wavelength. [b]Electroluminescence turn-on voltage. [c]External quantum yield. The order of measured values: maximum/at 100 cd/m^2/at 1000 cd/m^2. [d]Peak values of power efficiency. [e]Peak values of luminance. [f]Commission Internationale de l'Eclairage coordinates recorded at 9 V.

https://dx.doi.org/10.1021/acsami.9b21394
ACS Appl. Mater. Interfaces 2020, 12, 10727−10736

enlarged ^{1}CT-^{3}LE energy gap; however, the weakened IC rate allowed us to achieve a very large TADF quantum yield. An enhanced fluorescence quantum yield, reaching near unity, was achieved after the insertion of compounds in solid films and elimination of remaining nonradiative decay, though the solid-state Φ_F was slightly lower for compounds with both *ortho*- and *meta*-methyl units. Despite the Φ_F enhancement, the unwanted conformational disorder appeared in solid films, resulting in multiexponential TADF decay transients, though the TADF decay of the *meta*-methyl modified compound was successfully approximated with the three-exponential model, and a decay time of only about 860 ns was estimated, being one of the lowest reported for TADF compounds. Although no solid-state TADF lifetime was possible to evaluate for the rest of compounds, still it was evident that the slowest decay was for the compound with both methyl units. Highly efficient green electroluminescence with weak EQE roll-off was obtained when the external quantum efficiency of OLEDs made of the compound with the shortest TADF lifetime peaked at 29.1%, and an EQE of 20.5% was observed at a practical luminance of 1000 cd/m^2. Slightly lower peak EQE values of 27.1−27.5% with more pronounced EQE roll-off were obtained for compounds with slower TADF decay. Cyan EL with peak EQE of 26.3% was observed for *ortho*- and *meta*-methyl modified compounds with the shortest conjugation length, though the EQE roll-off was rather large due to the prolonged TADF decay.

Our results show that the fine-tuning of the TADF emitter structure by methyl groups enable the adjustment of the rISC rate, which directly controls the OLED performance at high current densities and enlarges the bandgap, which is favorable for the design of blue TADF emitters. Our insights, we believe, would be important for the optimization of TADF with compounds with diverse molecular structures.

■ ASSOCIATED CONTENT

Supporting Information

The Supporting Information is available free of charge at https://pubs.acs.org/doi/10.1021/acsami.9b21394.

Synthetic methods with NMR identification, DSC thermograms, DFT calculations of PXZ conformers, and detailed fluorescence properties (PDF)

■ AUTHOR INFORMATION

Corresponding Author

Tomas Serevičius − *Institute of Photonics and Nanotechnology, Vilnius University, LT-10257 Vilnius, Lithuania;* orcid.org/0000-0003-1319-7669; Email: tomas.serevicius@tmi.vu.lt

Authors

Rokas Skaisgiris − *Institute of Photonics and Nanotechnology, Vilnius University, LT-10257 Vilnius, Lithuania*

Jelena Dodonova − *Institute of Chemistry, Vilnius University, LT-03225 Vilnius, Lithuania*

Laimis Jagintavičius − *Institute of Chemistry, Vilnius University, LT-03225 Vilnius, Lithuania*

Dovydas Banevičius − *Institute of Photonics and Nanotechnology, Vilnius University, LT-10257 Vilnius, Lithuania*

Karolis Kazlauskas − *Institute of Photonics and Nanotechnology, Vilnius University, LT-10257 Vilnius, Lithuania;* orcid.org/0000-0001-7900-0465

Sigitas Tumkevičius − *Institute of Chemistry, Vilnius University, LT-03225 Vilnius, Lithuania*

Saulius Juršėnas − *Institute of Photonics and Nanotechnology, Vilnius University, LT-10257 Vilnius, Lithuania*

Complete contact information is available at: https://pubs.acs.org/10.1021/acsami.9b21394

Author Contributions

The manuscript was written through contributions of all authors. All authors have given approval to the final version of the manuscript.

Notes

The authors declare no competing financial interest.

■ ACKNOWLEDGMENTS

This project has received funding from the European Social Fund (project no. 09.3.3-LMT-K-718-01-0026) under grant agreement with the Research Council of Lithuania (LMTLT). Regimantas Komskis is acknowledged for DSC measurements. We are grateful for Dr. Alytis Gruodis and High Performance Computing Center "HPC Sauletekis" in Vilnius University Faculty of Physics for total potential energy calculations.

■ REFERENCES

(1) Endo, A.; Ogasawara, M.; Takahashi, A.; Yokoyama, D.; Kato, Y.; Adachi, C. Thermally Activated Delayed Fluorescence from Sn4+-Porphyrin Complexes and Their Application to Organic Light Emitting Diodes - A Novel Mechanism for Electroluminescence. *Adv. Mater.* **2009**, *21*, 4802−4806.

(2) Uoyama, H.; Goushi, K.; Shizu, K.; Nomura, H.; Adachi, C. Highly Efficient Organic Light-Emitting Diodes from Delayed Fluorescence. *Nature* **2012**, *492*, 234−238.

(3) Baldo, M. A.; O'Brien, D. F.; You, Y.; Shoustikov, A.; Sibley, S.; Thompson, M. E.; Forrest, S. R. Highly Efficient Phosphorescent Emission from Organic Electroluminescent Devices. *Nature* **1998**, *395*, 151−154.

(4) Adachi, C.; Baldo, M. A.; Thompson, M. E.; Forrest, S. R. Nearly 100% Internal Phosphorescence Efficiency in an Organic Light-Emitting Device. *J. Appl. Phys.* **2001**, *90*, 5048.

(5) Wong, M. Y.; Zysman-Colman, E. Purely Organic Thermally Activated Delayed Fluorescence Materials for Organic Light-Emitting Diodes. *Adv. Mater.* **2017**, *29*, 1605444.

(6) Liang, X.; Tu, Z.-L.; Zheng, Y.-X. Thermally Activated Delayed Fluorescence Materials: Towards Realization of High Efficiency Through Strategic Small Molecular Design. *Chem. − Eur. J.* **2019**, *25*, 5623−5642.

(7) Konidena, R. K.; Lee, J. Y. Molecular Design Tactics for Highly Efficient Thermally Activated Delayed Fluorescence Emitters for Organic Light Emitting Diodes. *Chem. Rec.* **2019**, *19*, 1499−1517.

(8) Gibson, J.; Monkman, A. P.; Penfold, T. J. The Importance of Vibronic Coupling for Efficient Reverse Intersystem Crossing in Thermally Activated Delayed Fluorescence Molecules. *ChemPhysChem* **2016**, *17*, 2956−2961.

(9) Etherington, M. K.; Gibson, J.; Higginbotham, H. F.; Penfold, T. J.; Monkman, A. P. Revealing the Spin−Vibronic Coupling Mechanism of Thermally Activated Delayed Fluorescence. *Nat. Commun.* **2016**, *7*, 13680.

(10) Chen, X.-K.; Kim, D.; Brédas, J.-L. Thermally Activated Delayed Fluorescence (TADF) Path toward Efficient Electroluminescence in Purely Organic Materials: Molecular Level Insight. *Acc. Chem. Res.* **2018**, *51*, 2215−2224.

(11) Noda, H.; Nakanotani, H.; Adachi, C. Excited State Engineering for Efficient Reverse Intersystem Crossing. *Sci. Adv.* **2018**, *4*, eaao6910.

(12) Saigo, M.; Miyata, K.; Tanaka, S.; Nakanotani, H.; Adachi, C.; Onda, K. Suppression of Structural Change upon S_1 −T_1 Conversion

Assists the Thermally Activated Delayed Fluorescence Process in Carbazole-Benzonitrile Derivatives. *J. Phys. Chem. Lett.* **2019**, *10*, 2475−2480.
(13) de Sa Pereira, D.; Menelaou, C.; Danos, A.; Marian, C.; Monkman, A. P. Electroabsorption Spectroscopy as a Tool for Probing Charge Transfer and State Mixing in Thermally Activated Delayed Fluorescence Emitters. *J. Phys. Chem. Lett.* **2019**, *10*, 3205−3211.
(14) Xue, L.; Cui, B.; Xie, S.; Yin, S. Influence of the Length of the Donor−Acceptor Bridge on Thermally Activated Delayed Fluorescence. *J. Phys. Chem. Lett.* **2019**, *10*, 302−308.
(15) Evans, E. W.; Olivier, Y.; Puttisong, Y.; Myers, W. K.; Hele, T. J. H.; Menke, S. M.; Thomas, T. H.; Credgington, D.; Beljonne, D.; Friend, R. H.; Greenham, N. C. Vibrationally Assisted Intersystem Crossing in Benchmark Thermally Activated Delayed Fluorescence Molecules. *J. Phys. Chem. Lett.* **2018**, *9*, 4053−4058.
(16) Lin, T.-A.; Chatterjee, T.; Tsai, W.-L.; Lee, W.-K.; Wu, M.-J.; Jiao, M.; Pan, K.-C.; Yi, C.-L.; Chung, C.-L.; Wong, K.-T.; Wu, C.-C. Sky-Blue Organic Light Emitting Diode with 37% External Quantum Efficiency Using Thermally Activated Delayed Fluorescence from Spiroacridine-Triazine Hybrid. *Adv. Mater.* **2016**, *28*, 6976−6983.
(17) Wu, T.-L.; Huang, M.-J.; Lin, C.-C.; Huang, P.-Y.; Chou, T.-Y.; Chen-Cheng, R.-W.; Lin, H.-W.; Liu, R.-S.; Cheng, C.-H. Diboron Compound-Based Organic Light-Emitting Diodes with High Efficiency and Reduced Efficiency Roll-Off. *Nat. Photonics* **2018**, *12*, 235−240.
(18) Murawski, C.; Leo, K.; Gather, M. C. Efficiency Roll-Off in Organic Light-Emitting Diodes. *Adv. Mater.* **2013**, *25*, 6801−6827.
(19) Inoue, M.; Serevičius, T.; Nakanotani, H.; Yoshida, K.; Matsushima, T.; Juršėnas, S.; Adachi, C. Effect of Reverse Intersystem Crossing Rate to Suppress Efficiency Roll-off in Organic Light-Emitting Diodes with Thermally Activated Delayed Fluorescence Emitters. *Chem. Phys. Lett.* **2016**, *644*, 62−67.
(20) Tanaka, H.; Shizu, K.; Nakanotani, H.; Adachi, C. Twisted Intramolecular Charge Transfer State for Long-Wavelength Thermally Activated Delayed Fluorescence. *Chem. Mater.* **2013**, *25*, 3766−3771.
(21) Im, Y.; Kim, M.; Cho, Y. J.; Seo, J.-A.; Yook, K. S.; Lee, J. Y. Molecular Design Strategy of Organic Thermally Activated Delayed Fluorescence Emitters. *Chem. Mater.* **2017**, *29*, 1946−1963.
(22) Geng, Y.; D'Aleo, A.; Inada, K.; Cui, L.-S.; Kim, J. U.; Nakanotani, H.; Adachi, C. Donor-σ-Acceptor Motifs: Thermally Activated Delayed Fluorescence Emitters with Dual Upconversion. *Angew. Chem., Int. Ed.* **2017**, *56*, 16536−16540.
(23) dos Santos, P. L.; Ward, J. S.; Congrave, D. G.; Batsanov, A. S.; Eng, J.; Stacey, J. E.; Penfold, T. J.; Monkman, A. P.; Bryce, M. R. Triazatruxene: A Rigid Central Donor Unit for a D-A_3 Thermally Activated Delayed Fluorescence Material Exhibiting Sub-Microsecond Reverse Intersystem Crossing and Unity Quantum Yield via Multiple Singlet-Triplet State Pairs. *Adv. Sci.* **2018**, *5*, 1700989.
(24) Wu, K.; Zhang, T.; Zhan, L.; Zhong, C.; Gong, S.; Jiang, N.; Lu, Z.-H.; Yang, C. Optimizing Optoelectronic Properties of Pyrimidine-Based TADF Emitters by Changing the Substituent for Organic Light-Emitting Diodes with External Quantum Efficiency Close to 25% and Slow Efficiency Roll-Off. *Chem. − Eur. J.* **2016**, *22*, 10860−10866.
(25) Komatsu, R.; Sasabe, H.; Nakao, K.; Hayasaka, Y.; Ohsawa, T.; Kido, J. Unlocking the Potential of Pyrimidine Conjugate Emitters to Realize High-Performance Organic Light-Emitting Devices. *Adv. Opt. Mater.* **2017**, *5*, 1600675.
(26) Xiang, Y.; Zhao, Y.; Xu, N.; Gong, S.; Ni, F.; Wu, K.; Luo, J.; Xie, G.; Lu, Z.-H.; Yang, C. Halogen-Induced Internal Heavy-Atom Effect Shortening the Emissive Lifetime and Improving the Fluorescence Efficiency of Thermally Activated Delayed Fluorescence Emitters. *J. Mater. Chem. C* **2017**, *5*, 12204−12210.
(27) Kitamoto, Y.; Namikawa, T.; Ikemizu, D.; Miyata, Y.; Suzuki, T.; Kita, H.; Sato, T.; Oi, S. Light Blue and Green Thermally Activated Delayed Fluorescence from 10H-Phenoxaborin-Derivatives and Their Application to Organic Light-Emitting Diodes. *J. Mater. Chem. C* **2015**, *3*, 9122−9130.
(28) Chen, D.-G.; Lin, T.-C.; Chen, C.-L.; Chen, Y.-T.; Chen, Y.-A.; Lee, G.-H.; Chou, P.-T.; Liao, C.-W.; Chiu, P.-C.; Chang, C.-H.; Lien, Y.-J.; Chi, Y. Optically Triggered Planarization of Boryl-Substituted Phenoxazine: Another Horizon of TADF Molecules and High-Performance OLEDs. *ACS Appl. Mater. Interfaces* **2018**, *10*, 12886−12896.
(29) Liu, Y.; Huang, H.; Zhou, T.; Wu, K.; Zhu, M.; Yu, J.; Xie, G.; Yang, C. Boosting Photoluminescence Quantum Yields of Triarylboron/Phenoxazine Hybrids *via* Incorporation of Cyano Groups and Their Applications as TADF Emitters for High-Performance Solution-Processed OLEDs. *J. Mater. Chem. C* **2019**, *7*, 4778−4783.
(30) Guo, J.; Fan, J.; Lin, L.; Zeng, J.; Liu, H.; Wang, C.-K.; Zhao, Z.; Tang, B. Z. Mechanical Insights into Aggregation-Induced Delayed Fluorescence Materials with Anti-Kasha Behavior. *Adv. Sci.* **2019**, *6*, 1801629.
(31) Xiang, Y.; Zhu, Z.-L.; Xie, D.; Gong, S.; Wu, K.; Xie, G.; Lee, C.-S.; Yang, C. Revealing the New Potential of an Indandione Unit for Constructing Efficient Yellow Thermally Activated Delayed Fluorescence Emitters with Short Emissive Lifetimes. *J. Mater. Chem. C* **2018**, *6*, 7111−7118.
(32) Chen, Z.; Wu, Z.; Ni, F.; Zhong, C.; Zeng, W.; Wei, D.; An, K.; Ma, D.; Yang, C. Emitters with a Pyridine-3,5-Dicarbonitrile Core and Short Delayed Fluorescence Lifetimes of about 1.5 Ms: Orange-Red TADF-Based OLEDs with Very Slow Efficiency Roll-Offs at High Luminance. *J. Mater. Chem. C* **2018**, *6*, 6543−6548.
(33) Cai, X.; Su, S.-J. Marching Toward Highly Efficient, Pure-Blue, and Stable Thermally Activated Delayed Fluorescent Organic Light-Emitting Diodes. *Adv. Funct. Mater.* **2018**, *28*, 1802558.
(34) Wang, K.; Zheng, C.-J.; Liu, W.; Liang, K.; Shi, Y.-Z.; Tao, S.-L.; Lee, C.-S.; Ou, X.-M.; Zhang, X.-H. Avoiding Energy Loss on TADF Emitters: Controlling the Dual Conformations of D-A Structure Molecules Based on the Pseudoplanar Segments. *Adv. Mater.* **2017**, *29*, 1701476.
(35) Chen, C.; Huang, R.; Batsanov, A. S.; Pander, P.; Hsu, Y.-T.; Chi, Z.; Dias, F. B.; Bryce, M. R. Intramolecular Charge Transfer Controls Switching Between Room Temperature Phosphorescence and Thermally Activated Delayed Fluorescence. *Angew. Chem.* **2018**, *57*, 16407−16411.
(36) Wang, K.; Shi, Y.-Z.; Zheng, C.-J.; Liu, W.; Liang, K.; Li, X.; Zhang, M.; Lin, H.; Tao, S.-L.; Lee, C.-S.; Ou, X.-M.; Zhang, X.-H. Control of Dual Conformations: Developing Thermally Activated Delayed Fluorescence Emitters for Highly Efficient Single-Emitter White Organic Light-Emitting Diodes. *ACS Appl. Mater. Interfaces* **2018**, *10*, 31515−31525.
(37) Serevičius, T.; Skaisgiris, R.; Dodonova, J.; Jagintavičius, L.; Bucevičius, J.; Kazlauskas, K.; Juršėnas, S.; Tumkevičius, S. Emission Wavelength Dependence on rISC Rate in TADF Compounds with Large Conformational Disorder. *Chem. Commun.* **2019**, *55*, 1975−1978.
(38) Kretzschmar, A.; Patze, C.; Schwaebel, S. T.; Bunz, U. H. F. Development of Thermally Activated Delayed Fluorescence Materials with Shortened Emissive Lifetimes. *J. Org. Chem.* **2015**, *80*, 9126−9131.
(39) Rothe, C.; Monkman, A. P. Triplet Exciton Migration in a Conjugated Polyfluorene. *Phys. Rev. B* **2003**, *68*, No. 075208.
(40) de Mello, J. C.; Wittmann, H. F.; Friend, R. H. An Improved Experimental Determination of External Photoluminescence Quantum Efficiency. *Adv. Mater.* **1997**, *9*, 230−232.
(41) Komatsu, R.; Ohsawa, T.; Sasabe, H.; Nakao, K.; Hayasaka, Y.; Kido, J. Manipulating the Electronic Excited State Energies of Pyrimidine-Based Thermally Activated Delayed Fluorescence Emitters To Realize Efficient Deep-Blue Emission. *ACS Appl. Mater. Interfaces* **2017**, *9*, 4742−4749.
(42) Cui, L.-S.; Nomura, H.; Geng, Y.; Kim, J. U.; Nakanotani, H.; Adachi, C. Controlling Singlet-Triplet Energy Splitting for Deep-Blue Thermally Activated Delayed Fluorescence Emitters. *Angew. Chem., Int. Ed.* **2017**, *56*, 1571−1575.

https://dx.doi.org/10.1021/acsami.9b21394
ACS Appl. Mater. Interfaces 2020, 12, 10727−10736

(43) Oh, C. S.; Han, S. H.; Lee, J. Y. Molecular Design of Thermally Activated Delayed Fluorescent Emitters for Blue-Shifted Emission by Methoxy Substitution. *J. Mater. Chem. C* **2017**, *5*, 9106−9114.
(44) Huang, W.; Einzinger, M.; Maurano, A.; Zhu, T.; Tiepelt, J.; Yu, C.; Chae, H. S.; Van Voorhis, T.; Baldo, M. A.; Buchwald, S. L. Large Increase in External Quantum Efficiency by Dihedral Angle Tuning in a Sky-Blue Thermally Activated Delayed Fluorescence Emitter. *Adv. Opt. Mater.* **2019**, *7*, 1900476.
(45) Wu, T.-L.; Lo, S.-H.; Chang, Y.-C.; Huang, M.-J.; Cheng, C.-H. Steric Switching for Thermally Activated Delayed Fluorescence by Controlling the Dihedral Angles between Donor and Acceptor in Organoboron Emitters. *ACS Appl. Mater. Interfaces* **2019**, *11*, 10768−10776.
(46) Woo, S.-J.; Kim, Y.; Kwon, S.-K.; Kim, Y.-H.; Kim, J.-J. Phenazasiline/Spiroacridine Donor Combined with Methyl-Substituted Linkers for Efficient Deep Blue Thermally Activated Delayed Fluorescence Emitters. *ACS Appl. Mater. Interfaces* **2019**, *11*, 7199−7207.
(47) Frisch, M. J.; Trucks, G. W.; Schlegel, H. B.; Scuseria, G. E.; Robb, M. A.; Cheeseman, J. R.; Scalmani, G.; Barone, V.; Mennucci, B.; Petersson, G. A.; Nakatsuji, H.; Caricato, M.; Li, X.; Hratchian, H. P.; Izmaylov, A. F.; Bloino, J.; Zheng, G.; Sonnenberg, J. L.; Hada, M.; Ehara, M.; Toyota, K.; Fukuda, R.; Hasegawa, J.; Ishida, M.; Nakajima, T.; Honda, Y.; Kitao, O.; Nakai, H.; Vreven, T.; Montgomery, Jr., J. A.; Peralta, J. E.; Ogliaro, F.; Bearpark, M.; Heyd, J. J.; Brothers, E.; Kudin, K. N.; Staroverov, V. N.; Keith, T.; Kobayashi, R.; Normand, J.; Raghavachari, K.; Rendell, A.; Burant, J. C.; Iyengar, S. S.; Tomasi, J.; Cossi, M.; Rega, N.; Millam, J. M.; Klene, M.; Knox, J. E.; Cross, J. B.; Bakken, V.; Adamo, C.; Jaramillo, J.; Gomperts, R.; Stratmann, R. E.; Yazyev, O.; Austin, A. J.; Cammi, R.; Pomelli, C.; Ochterski, J. W.; Martin, R. L.; Morokuma, K.; Zakrzewski, V. G.; Voth, G. A.; Salvador, P.; Dannenberg, J. J.; Dapprich, S.; Daniels, A. D.; Farkas, O.; Foresman, J. B.; Ortiz, J. V.; Cioslowski, J.; Fox, D. J. *Gaussian 09*; Revision C.01, Gaussian, Inc.: Wallingford CT, 2010.
(48) Peng, Q.; Fan, D.; Duan, R.; Yi, Y.; Niu, Y.; Wang, D.; Shuai, Z. Theoretical Study of Conversion and Decay Processes of Excited Triplet and Singlet States in a Thermally Activated Delayed Fluorescence Molecule. *J. Phys. Chem. C* **2017**, *121*, 13448−13456.
(49) Wang, L.; Cai, X.; Li, B.; Li, M.; Wang, Z.; Gan, L.; Qiao, Z.; Xie, W.; Liang, Q.; Zheng, N.; Liu, K.; Su, S.-J. Achieving Enhanced Thermally Activated Delayed Fluorescence Rates and Shortened Exciton Lifetimes by Constructing Intramolecular Hydrogen Bonding Channels. *ACS Appl. Mater. Interfaces* **2019**, *11*, 45999−46007.
(50) Cotts, B. L.; McCarthy, D. G.; Noriega, R.; Penwell, S. B.; Delor, M.; Devore, D. D.; Mukhopadhyay, S.; De Vries, T. S.; Ginsberg, N. S. Tuning Thermally Activated Delayed Fluorescence Emitter Photophysics through Solvation in the Solid State. *ACS Energy Lett.* **2017**, *2*, 1526−1533.
(51) Kim, J. H.; Yun, J. H.; Lee, J. Y. Recent Progress of Highly Efficient Red and Near-Infrared Thermally Activated Delayed Fluorescent Emitters. *Adv. Opt. Mater.* **2018**, *6*, 1800255.
(52) Kreiza, G.; Banevičius, D.; Jovaišaitė, J.; Maleckaitė, K.; Gudeika, D.; Volyniuk, D.; Gražulevičius, J. V.; Juršėnas, S.; Kazlauskas, K. Suppression of Benzophenone-Induced Triplet Quenching for Enhanced TADF Performance. *J. Mater. Chem. C* **2019**, *7*, 11522−11531.
(53) Köhler, A.; Bässler, H. Triplet States in Organic Semiconductors. *Mater. Sci. Eng. R Rep.* **2009**, *66*, 71−109.
(54) Ward, J. S.; Nobuyasu, R. S.; Batsanov, A. S.; Data, P.; Monkman, A. P.; Dias, F. B.; Bryce, M. R. The Interplay of Thermally Activated Delayed Fluorescence (TADF) and Room Temperature Organic Phosphorescence in Sterically-Constrained Donor−Acceptor Charge-Transfer Molecules. *Chem. Commun.* **2016**, *52*, 2612−2615.
(55) Dias, F. B.; Penfold, T. J.; Monkman, A. P. Photophysics of Thermally Activated Delayed Fluorescence Molecules. *Methods Appl. Fluoresc.* **2017**, *5*, No. 012001.
(56) Serevičius, T.; Bučiūnas, T.; Bucevičius, J.; Dodonova, J.; Tumkevičius, S.; Kazlauskas, K.; Juršėnas, S. Room Temperature Phosphorescence *vs.* Thermally Activated Delayed Fluorescence in Carbazole−Pyrimidine Cored Compounds. *J. Mater. Chem. C.* **2018**, *6*, 11128−11136.
(57) Etherington, M. K.; Franchello, F.; Gibson, J.; Northey, T.; Santos, J.; Ward, J. S.; Higginbotham, H. F.; Data, P.; Kurowska, A.; Dos Santos, P. L.; Graves, D. R.; Batsanov, A. S.; Dias, F. B.; Bryce, M. R.; Penfold, T. J.; Monkman, A. P. Regio- and Conformational Isomerization Critical to Design of Efficient Thermally-Activated Delayed Fluorescence Emitters. *Nat. Commun.* **2017**, *8*, 14987.
(58) Northey, T.; Stacey, J.; Penfold, T. J. The Role of Solid State Solvation on the Charge Transfer State of a Thermally Activated Delayed Fluorescence Emitter. *J. Mater. Chem. C.* **2017**, *5*, 11001−11009.
(59) Weissenseel, S.; Drigo, N. A.; Kudriashova, L. G.; Schmid, M.; Morgenstern, T.; Lin, K.-H.; Prlj, A.; Corminboeuf, C.; Sperlich, A.; Brütting, W.; Nazeeruddin, M. K.; Dyakonov, V. Getting the Right Twist: Influence of Donor−Acceptor Dihedral Angle on Exciton Kinetics and Singlet−Triplet Gap in Deep Blue Thermally Activated Delayed Fluorescence Emitter. *J. Phys. Chem. C* **2019**, *123*, 27778−27784.
(60) Wada, Y.; Kubo, S.; Kaji, H. Adamantyl Substitution Strategy for Realizing Solution-Processable Thermally Stable Deep-Blue Thermally Activated Delayed Fluorescence Materials. *Adv. Mater.* **2018**, *30*, 1705641.
(61) Wada, Yoshimasa; Nakagawa, H.; Matsumoto, S.; Wakisaka, Y.; Kaji, H. Molecular Design Realizing Very Fast Reverse Intersystem Crossing in Purely Organic Emitter. 2019, *ChemRxiv*: doi.org/10.26434/chemrxiv.9745289.v1 ChemRxiv.org e-Print archive preprint. https://chemrxiv.org/articles/Molecular_Design_Realizing_Very_Fast_Reverse_Intersystem_Crossing_in_Purely_Organic_Emitter/9745289/1 (accessed Nov. 21, 2019).
(62) Liu, Y.; Li, C.; Ren, Z.; Yan, S.; Bryce, M. R. All-Organic Thermally Activated Delayed Fluorescence Materials for Organic Light-Emitting Diodes. *Nat. Rev. Mater.* **2018**, *3*, 18020.
(63) Tsai, Y.-S.; Hong, L.-A.; Juang, F.-S.; Chen, C.-Y. Blue and White Phosphorescent Organic Light Emitting Diode Performance Improvement by Confining Electrons and Holes inside Double Emitting Layers. *J. Lumin.* **2014**, *153*, 312−316.
(64) Srivastava, R.; Joshi, L. R. The Effect of Substituted 1,2,4-Triazole Moiety on the Emission, Phosphorescent Properties of the Blue Emitting Heteroleptic Iridium(III) Complexes and the OLED Performance: A Theoretical Study. *Phys. Chem. Chem. Phys.* **2014**, *16*, 17284−17294.
(65) Chatterjee, T.; Wong, K.-T. Perspective on Host Materials for Thermally Activated Delayed Fluorescence Organic Light Emitting Diodes. *Adv. Opt. Mater.* **2019**, *7*, 1800565.
(66) Zhang, J.; Ding, D.; Wei, Y.; Xu, H. Extremely Condensing Triplet States of DPEPO-Type Hosts through Constitutional Isomerization for High-Efficiency Deep-Blue Thermally Activated Delayed Fluorescence Diodes. *Chem. Sci.* **2016**, *7*, 2870−2882.
(67) Gather, M. C.; Reineke, S. Recent Advances in Light Outcoupling from White Organic Light-Emitting Diodes. *J. Photon. Energy* **2015**, *5*, No. 057607.
(68) Liu, M.; Komatsu, R.; Cai, X.; Hotta, K.; Sato, S.; Liu, K.; Chen, D.; Kato, Y.; Sasabe, H.; Ohisa, S.; Suzuri, Y.; Yokoyama, D.; Su, S.-J.; Kido, J. Horizontally Orientated Sticklike Emitters: Enhancement of Intrinsic Out-Coupling Factor and Electroluminescence Performance. *Chem. Mater.* **2017**, *29*, 8630−8636.
(69) Ihn, S.-G.; Lee, N.; Jeon, S. O.; Sim, M.; Kang, H.; Jung, Y.; Huh, D. H.; Son, Y. M.; Lee, S. Y.; Numata, M.; Miyazaki, H.; Gómez-Bombarelli, R.; Aguilera-Iparraguirre, J.; Hirzel, T.; Aspuru-Guzik, A.; Kim, S.; Lee, S. An Alternative Host Material for Long-Lifespan Blue Organic Light-Emitting Diodes Using Thermally Activated Delayed Fluorescence. *Adv. Sci.* **2017**, *4*, 1600502.

A5

Achieving efficient deep-blue TADF in carbazole-pyrimidine compounds

T. Serevičius, **R. Skaisgiris**, I. Fiodorova, V. Steckis,
J. Dodonova, D. Banevičius, K. Kazlauskas, S. Juršėnas
S. Tumkevičius

Org. Electon. **82**, 105723 (2020)
DOI: 10.1016/j.orgel.2020.105723
https://linkinghub.elsevier.com/retrieve/pii/S1566119920301099

Supporting information: https://ars.els-cdn.com/content/image/1-s2.0-S1566119920301099-mmc1.docx

Organic Electronics 82 (2020) 105723

Contents lists available at ScienceDirect

Organic Electronics

journal homepage: http://www.elsevier.com/locate/orgel

Achieving efficient deep-blue TADF in carbazole-pyrimidine compounds

Tomas Serevičius [a,*], Rokas Skaisgiris [a], Irina Fiodorova [b], Vytautas Steckis [b], Jelena Dodonova [b], Dovydas Banevičius [a], Karolis Kazlauskas [a], Saulius Juršėnas [a], Sigitas Tumkevičius [b]

[a] Institute of Photonics and Nanotechnology, Vilnius University, Sauletekio 3, LT-10257, Vilnius, Lithuania
[b] Institute of Chemistry, Vilnius University, Naugarduko 24, LT-03225, Vilnius, Lithuania

ARTICLE INFO

Keywords:
TADF
OLED
Deep blue fluorescence
Pyrimidine
Carbazole
rISC

ABSTRACT

An approach for achieving deep blue thermally activated delayed fluorescence (TADF) is presented. A simple carbazole-pyrimidine compound **Cbz-PYR** with near-UV emission and simultaneous room-temperature phosphorescence (RTP) was selectively modified by lowering the singlet state energy, simultaneously preserving high triplet energy. The modified compound **tCbz-mPYRs** was shown to be efficient TADF emitter with 0.5 solid-state emission yield and peak wavelength of 428 nm. When used in OLED device, **tCbz-mPYRs** based OLED showed electroluminescence with 8.7% external quantum efficiency (EQE) and Commission Internationale de l'Eclairage (CIE) coordinates of (0.16; 0.12).

1. Introduction

TADF is an attractive way to achieve 100% internal fluorescence quantum yield without involving any expensive heavy atoms by converting all excitations to singlet ones by thermal activation [1]. Usually, this is achieved by constructing TADF compounds from electron-donating (D) and –accepting (A) units, decreasing the spatial overlap of electron density distribution in highest occupied molecular orbital (HOMO) and lowest unoccupied molecular orbitals (LUMO), resulting in narrowing the singlet-triplet energy gap (ΔE_{ST}) up to values, comparable to thermal energy at room temperature [1,2]. The successful optimization of TADF compounds led to the realization of TADF OLEDs with external quantum EQE approaching 40% without applying any additional EQE enhancement techniques (only spontaneous molecular orientation) [3] and more than 60% with those techniques applied [4]. However, TADF efficiency is remarkably lower for deep-blue emission ($CIE_y < 0.1$), which is necessary for successful TADF OLED application in full-colour displays [5]. In this case, EQE of the most efficient deep-blue TADF OLEDs usually approaches 20% and only very rarely exceeds 20% [6–8]. It is rather difficult to find suitable D and A units with limited conjugation length and high triplet energy and bound them in a suitable architecture [5]. Among the all candidates, 9,10-dihydroacridine derivatives together with carbazole usually are used as D units while sulphone and nitrogen-containing moieties, like triazine, frequently are used as A fragments for constructing deep-blue TADF compounds [5]. However, not all D and A units are stable enough. Usually, nitrogen-containing donor and acceptor fragments, like carbazole, triazine or benzonitrile are considered as more stable [9]. As an example, the combined phenyl-carbazole-phenyl electron-donating group with electron-accepting oxadiazole or nitrile units were shown to be efficient deep-blue TADF emitters with high device lifetime [10–13]. However, pyridine/pyrimidine-carbazole compounds, even with noticeable TADF activity, are less explored as deep-blue emitters, though they are successfully used as high triplet energy hosts [14,15].

Seeing the potential of carbazole-pyrimidine pair for achieving efficient deep-blue TADF, we performed the design, synthesis, photophysical characterization as well as application in OLED devices of deep-blue TADF emitter **tCbz-mPYRs**. Our approach for deep blue TADF started from a simple carbazole-pyrimidine-carbazole (**Cbz-PYR**) compound (see Scheme 1). **Cbz-PYR** was selected as suitable starting compound due to high triplet energy and potentially suitable energy level scheme for achieving triplet upconversion, evidenced by the presence of weak room-temprature phosphoresence (RTP) [16]. To shift the emission wavelength of **Cbz-PYR** from ultraviolet towards the deep-blue and narrow the singlet-triplet gap, the following design steps were applied: 3,6-di-*tert*-butyl units were introduced to increase the electron-donating properties of D units; methyl group at the 5th position of pyrimidine unit was introduced to lower the electron density overlap in HOMO and LUMO; sulphur atom was introduced to enhance the ISC and rISC rates and additionally redshift the emission peak [17–20]. The thorough

* Corresponding author.
E-mail address: tomas.serevicius@tmi.vu.lt (T. Serevičius).

https://doi.org/10.1016/j.orgel.2020.105723
Received 17 January 2020; Received in revised form 9 March 2020; Accepted 18 March 2020
Available online 23 March 2020

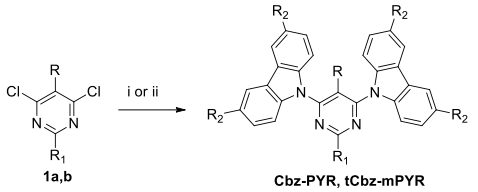

R=R_1=R_2=H (**1a**, **Cbz-PYR**)
R=Me, R_1=SMe, R_2=*t*-Bu (**1b**, **tCbz-mPYR**)

Scheme 1. Synthesis of **Cbz-PYR** and **tCbz-mPYRs**. *Reagents and conditions:* i-carbazole (2.06 equiv.), Cs_2CO_3, DMF, 100 °C; 24 h; ii – 3,6-di-*tert*-butylcarbazole (1.4 equiv.), Pd_2dba_3 (5 mol%), P(*t*-Bu)$_3$*HBF_4 (10 mol%), NaO*t*Bu (1.5 equiv.), toluene, 150 °C, 24 h.

analysis of photophysical and electroluminescence properties highlighted the significance of the adapted design principles for achieving efficient deep-blue TADF with emission yield of 0.5 and the corresponding OLED device performance of 8.7%.

2. Experimental section

2.1. General methods

Reagents and solvents were purchased directly from commercial suppliers; solvents were purified by known procedures. Melting points were determined in open capillaries with a digital melting point IA9100 series apparatus (ThermoFischer Scientific) and were not corrected. Thin layer chromatography was performed using TLC-aluminum sheets with silica gel (Merck 60 F254). Visualization was accomplished by UV light. Column chromatography was performed using Silica gel 60 (0.040–0.063 mm) (Merck). NMR spectra were recorded on a Bruker Ascend 400 (400 MHz and 100 MHz for ^{1}H and ^{13}C, respectively). ^{1}H NMR and ^{13}C NMR spectra were referenced to residual solvent peaks. High Resolution Mass Spectrometry (HRMS) analyses were carried out on microTOF-Q II or microTOF-Q III mass spectrometers (Bruker). Thermogravimetric analysis (TGA) curves were measured by PerkinElmer STA6000 set-up, using aluminium oxide crucibles under N_2 flow with heating rate of 10 K/min. Differential scanning calorimetry (DSC) curves were measured by Metler Toledo DSC1 aparatus, using aluminium crucibles under N_2 flow (DSC). Sample mass was around 8–10 mg, heating and cooling rates were 10 K/min. TADF compounds were analysed in 1×10^{-5} M toluene solutions, 1 wt% PMMA and 10 wt % DPEPO films. Solid-state films were prepared by dissolving each material and host at appropriate ratios in toluene solutions and then wet-casting the solutions on quartz substrates. Absorption spectra were measured using Lambda 950 UV/Vis spectrophotometer (PerkinElmer). Time-integrated fluorescence spectra (TIFL), phosphorescence, time-resolved fluorescence spectra (TRFL) and fluorescence decay transients were measured using nanosecond YAG:Nd^{3+} laser NT 242 (Ekspla, $\tau = 7$ ns, pulse energy 200 μJ, $\lambda_{ex} = 300$ nm, repetition rate 0.01–1 kHz) and time-gated iCCD camera New iStar DH340T (Andor). Fluorescence transients were obtained by exponentially increasing delay and integration time [21]. Fluorescence quantum yields (Φ_F) of the solutions and polymer films in air ambient were estimated using the integrated sphere method [22] by integrating sphere (Sphere Optics) connected to the CCD spectrometer PMA-12 (Hamamatsu) via optical fibre. Solid-state samples were mounted in closed cycle He cryostat (Cryo Industries 204 N) for all measurements (for oxygen-saturated and oxygen-free conditions). Toluene solutions were degassed by using freeze-pump-thaw method. OLED device were fabricated on precleaned indium-tin oxide (ITO)--coated glass substrates. The small-molecule and cathode layers were thermally evaporated using vacuum evaporation apparatus (Vacuum Systems and Technologies Ltd) at $<6 \times 10^{-6}$ Torr pressure and deposition rate of about 1 Å/s. OLED devices were encapsulated with a clear glass cover to prevent the interaction with ambient. Device current-voltage (*I-V*) characteristics and electroluminescence properties were measured using calibrated integrating sphere (Orb Optronics) and CCD spectrometer PMA-11 (Hamamatsu), powered by 2601 A power supply unit (Keithley).

Quantum chemical calculations were performed by using density functional theory (DFT) as implemented in the Gaussian 09 software package at the B3LYP/6-31G(d) level [23]. Polarizable Continuum Model (PCM) was used to estimate the solvation behaviour of toluene surrounding.

2.2. Material synthesis

2.2.1. 4,6-Di(9H-carbazol-9-yl)pyrimidine (Cbz-PYR)

To a screw-cap vial with magnetic stirrer 2 mL of dry *N,N*-dimethylformamide, 50 mg (0.34 mmol) of 4.6-dichloropyrimidine (**1a**), 118 mg (0.70 mmol) of 9*H*-carbazole and 344 mg (1.06 mmol) of Cs_2CO_3 were placed and flushed with argon for 0.5 h. Reaction mixture was heated at 100 °C for 24 h. Then, the mixture was cooled down to room temperature, poured into water and extracted with chloroform (3 × 25 mL). Chloroform solution was dried with Na_2SO_4 and concentrated under reduced pressure to dryness. Residue was purified by column chromatography (eluent – petroleum ether: $CHCl_3$, 1:2) to afford 72 mg (53%) of **Cbz-PYR**, mp 264–266 °C. ^{1}H NMR (400 MHz, $CDCl_3$), *δ*, ppm: 7.42 (4H, t, $J = 7.5$ Hz, Cbz); 7.54 (4H, t, $J = 7.5$ Hz, Cbz); 8.00 (1H, s, Pyr); 8.15 (4H, d, $J = 7.7$ Hz, Cbz), 8.20 (4H, d, $J = 7.7$ Hz, Cbz), 9.37 (1H, s, Pyr). ^{13}C NMR (100 MHz, $CDCl_3$), *δ*, ppm: 105.5; 112.6; 120.4; 122.5; 125.5; 126.8; 138.8; 159.7; 160.1. HRMS-ESI: *m/z* calcd. for $[M+H]^+$ ($C_{28}H_{19}N_4$): 411.1604, found: 411.1606.

2.2.2. 4,6-Bis(3,5-di-tert-butyl-9H-carbazol-9-yl)-5-methyl-2-methylthiopyrimidine (tCbz-mPYRs)

4,6-Dichloro-5-methyl-2-methylthiopyrimidine (**1b**) (120.0 mg, 0.574 mmol, 0.7 equiv.), 3,6-di-*tert*-butylcarbazole (228.9 mg, 0.820 mmol, 1 equiv.), $Pd_2(dba)_3$ (26.3 mg, 0.0287 mmol, 5 mol%), P(*t*-Bu)$_3$·HBF_4 (16.7 mg, 0.0574 mmol, 10 mol%), NaO*t*-Bu (82.7 mg, 0.0861 mmol, 1.5 equiv.) and toluene (3 mL) were placed in a screw-cap vial equipped with a magnetic stir bar. The reaction mixture was stirred at 150 °C for 24 h under argon atmosphere. After completion of the reaction, toluene was removed by distillation under reduced pressure, water (40 mL) was added to a residue and the aqueous solution was extracted with chloroform (4 × 25 mL). The combined extract was dried with anhydrous Na_2SO_4, filtered and chloroform was removed by distillation under reduced pressure. Purification by column chromatography (eluent - petroleum ether: $CHCl_3$, 2:1) and recrystallization from 2-propanol gave 120 mg (42%) of **tCbz-mPYRs,** $T_{95\%}$ 368 °C (dec.). ^{1}H NMR (400 MHz, $CDCl_3$), *δ*, ppm: 1.52 (36H, s, *t*-Bu), 1.86 (3H, s, CH_3), 2.65 (3H, s, SCH_3), 7.50 (4H, d, $J = 8.6$ Hz, Cbz), 7.61 (4H, dd, $J = 8.6$ Hz, $J = 1.8$ Hz, Cbz), 8.16 (4H, d, $J = 1.8$ Hz, Cbz). ^{13}C NMR (100 MHz, $CDCl_3$), *δ*, ppm: 14.4, 14.9, 32.0, 34.8, 111.0, 115.4, 116.5, 124.0, 124.6, 137.7, 144.5, 160.0, 170.7. HRMS-ESI: *m/z* calcd. for $[M+H]^+$ ($C_{46}H_{55}N_4S$): 695.4142, found: 695.4144.

3. Results and discussion

3.1. Synthesis and thermal characterization

Synthesis of **Cbz-PYR** with carbazole was accomplished by heating **1a** and carbazole in DMF at 100 °C in the presence of Cs_2CO_3 (see Scheme 1). However, attempts to obtain **tCbz-mPYRs** by the reaction of **1b** with 3,6-di-*tert*-butylcarbazole under similar reaction conditions failed. The reaction proceeded with the formation of a complex inseparable mixture of compounds and tars. The reason, most probably, is rather high reactivity of methylthio group at the 2nd position of

pyrimidine ring toward various nucleophiles in S_NAr reactions [24–26]. Therefore, **tCbz-mPYRs** was obtained by palladium-catalyzed Buchwald-Hartwig cross-coupling reaction of 4,6-dichloro-5-methyl-2-methylthiopyrimidine (**1b**) with 3,6-di-*tert*-butylcarbazole in the presence of Pd_2dba_3 and $P(t\text{-}Bu)_3{\cdot}HBF_4$ as a catalyst system and NaO*t*-Bu as a base. Better yields of **tCbz-mPYRs** were obtained when a slight excess of dichloropyrimidine **1b** was used in the reaction. ^1H and ^{13}C NMR spectroscopy and HRMS were employed to confirm the structures of **Cbz-PYR** and **tCbz-mPYRs** (see Fig. S1-Fig. S4 in the supplementary information). **tCbz-mPYRs** showed good thermal stability with decomposition and glass transition temperatures of 368 °C and 159 °C, respectively (see Fig. S5 in the supplementary information).

3.2. DFT calculations

DFT calculations (see Fig. 1 and Table S1 in the supplementary information) revealed, that the introduction of 5-methyl group at the 5th position of pyrimidine ring clearly increased the twisting angle between the D and A units, as it was expected. This, as well as the introduction of *tert*-butyl fragments, had strong effect to electron density distribution in LUMO and only minor effect to distribution in HOMO, decreasing the electron density overlap in HOMO-LUMO, preferably for lowering the lowest energy singlet-triplet energy gap (ΔE_{ST}). This was evidenced by the decreased oscillator strength for **tCbz-mPYRs** (0.558 *vs* 0.394) and, concomitantly, lowered ΔE_{ST} (540 meV *vs* 289 meV). This was achieved by selectively altering only the energy of S_1 (3.69 eV *vs* 3.43 eV), keeping the energy of the lowest triplet states almost unaltered (3.15 eV *vs* 3.14 eV). Five higher-energy triplet states, situated between T_1 and S_1, were found for compound **Cbz-PYR** and three - for **tCbz-mPYRs** (see Table S2 in the supplementary information). Some of $S_0 \rightarrow T_n$ transitions were assigned to more LE-type transitions (*e.g.* $S_0 \rightarrow T_1$ and $S_0 \rightarrow T_2$ for **Cbz-PYR** and **tCbz-mPYRs**, respectively), while several of transitions were found with more CT character (*e.g.* $S_0 \rightarrow T_3$ for both **Cbz-PYR** and **tCbz-mPYRs**). Such energy level scheme, where CT and LE triplet states are lying close to each other, is highly preferable for ensuring the non-zero spin-vibronic coupling and, therefore, efficient rISC [2,16].

3.3. Optical properties

The applied molecular modifications clearly had the strong impact to optical properties of **Cbz-PYR** and **tCbz-mPYRs** (see Fig. 2 and Table S3 in the supplementary information).

Absorption spectra in toluene peaked at 336 nm and 339 nm with corresponding molar absorption coefficients of about 41,600 and 22,000 M^{-1} cm^{-1} for **Cbz-PYR** and **tCbz-mPYRs**, respectively, in line with DFT calculations, predicting stronger CT character for **tCbz-mPYRs**. Fluorescence spectra of toluene solutions peaked at about 379 nm for **Cbz-PYR** and at about 423 nm for **tCbz-mPYRs** with

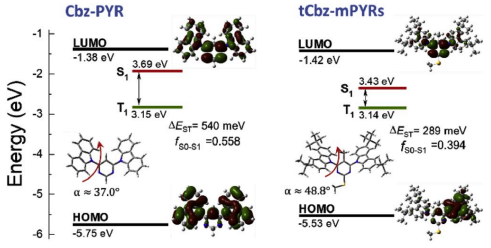

Fig. 1. HOMO and LUMO energies, $S_0 \rightarrow S_1/T_1$ absorption energies with corresponding transition oscillator strengths and S_1-T_1 energy gaps (ΔE_{ST}), optimized molecular structure and π-electron density distribution in HOMO and LUMO of compounds **Cbz-PYR** and **tCbz-mPYRs**.

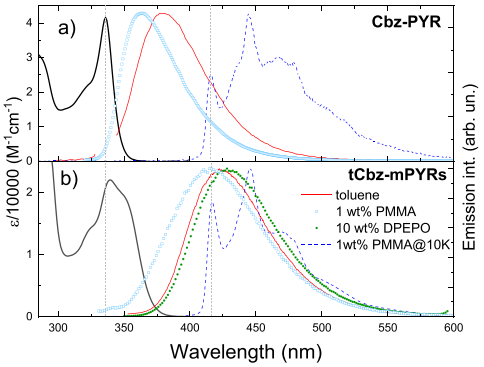

Fig. 2. Absorption (black lines) and emission (red and blue lines, blue and green figures) spectra of **Cbz-PYR** (a) and **tCbz-mPYRs** (b) in dilute toluene, 1 wt% PMMA and 10 wt% DPEPO films. (For interpretation of the references to colour in this figure legend, the reader is referred to the web version of this article.)

intentionally extended conjugation length. When embedded in solid polymer films (1 wt% PMMA), emission spectra peaked at 364 nm and 415 nm due to weaker solid-state solvation (SSS) in polymer surrounding [27]. However, fluorescence of **tCbz-mPYRs** peaked at about 428 nm in 10 wt% DPEPO films, even at higher wavelength than in toluene, probably due to the more pronounced SSS and different conformational disorder [28]. Phosphorescence, originating from the donor fragment (see Fig. S6 in the supplementary information), peaked at similar wavelength for both compounds (416 nm and 417 nm for **Cbz-PYR** and **tCbz-mPYRs**, respectively), resulting in lower ΔE_{ST} for **tCbz-mPYRs**, especially when embedded in DPEPO host (290 meV). Such value is comparable to that of other deep-blue TADF compounds [10,11].

Fluorescence quantum yields (Φ_F) of toluene solutions were similar for both **Cbz-PYR** and **tCbz-mPYRs**, 0.1 and 0.07, respectively. Somewhat decrease of Φ_F for **tCbz-mPYRs** was related with the changes of radiative (k_r) and nonradiative (k_{nr}) fluorescence decay rates (see Table 1). Though the compound **tCbz-mPYRs** showed 2.6-time lower k_r due to more pronounced CT character, more restricted molecular backbone, as well as different energy level scheme, lead to 1.8 times slower nonradiative decay, resulting in only minor Φ_F decrease. Despite the partially lowered k_{nr}, no TADF were observed in toluene even for **tCbz-mPYRs**, quite typically for deep-blue TADF emitters in solutions [10,11] (see Fig S7 and Fig S8 a and c in the supplementary information). However, TADF emerged in 1 wt% PMMA films of **tCbz-mPYRs**, where the nonradiative decay was remarkably lowered, as it was evidenced by fluorescence intensity enhancement in oxygen-free surrounding (Fig. S8 d in the supplementary information) and temperature

Table 1
Fluorescence data of **Cbz-PYR** and **tCbz-mPYRs** in oxygen-free toluene.

	Φ_{PF}[a]	Φ_{DF}[b]	k_{PF} (× 10^8 s^{-1})[c]	k_r (× 10^8 s^{-1})[d]	k_{nr} (× 10^8 s^{-1})[e]
Cbz-PYR	0.1	–	4.57	0.46	4.11
tCbz-mPYRs	0.07	–	2.50	0.18	2.33

[a] Prompt fluorescence quantum yield.
[b] Delayed fluorescence quantum yield.
[c] Prompt fluorescence decay rate.
[d] Radiative promt fluorescence decay rate (k_{FL}*Φ_{FL}).
[e] Non-radiative prompt fluorescence decay rate (k_{FL}*(1-Φ_{FL})).

activation of delayed fluorescence (Fig. S9 in the supplementary information). The increase of Φ_F up to 0.44 followed the emergence of TADF. Both prompt and delayed fluorescence decayed with multiexponential temporal profile due to the conformational disorder (see Fig. S7 in the supplementary information), therefore decay constants were difficult to estimate [28]. On the other hand, weak RTP was observed in oxygen-free conditions for **Cbz-PYR** at later delays probably due to the rather efficient ISC (see Fig. S10 in the supplementary information), though no triplets were able to upconvert back to singlets due to too large ΔE_{ST}.

The further boost of TADF yield was achieved by embedding **tCbz-mPYRs** in DPEPO (bis[2-(diphenylphosphino)phenyl] ether oxide) host with enhanced SSS at 10 wt% doping load (see Fig. 3 and Fig. S7 in the supplementary information). Fluorescence quantum yield increased up to 0.5, when TADF accounted for 0.42. Although the fluorescence decay still was multiexponential for both prompt and delayed fluorescence, TADF decay evidently was more rapid. Moderate conformational disorder was observed (see Fig. S11 in the supplementary information), when the redshift of temporal emission shift was comparable with the blueshift [29]. Due to the enhanced TADF, approximate fluorescence time-constants were estimated by multiexponential fitting of both PF and DF transients (see Fig. 3). Fluorescence decay rate was found rather high ($k_{PF} \approx 1 \times 10^8\ s^{-1}$), as well as radiative fluorescence decay ($k_r \approx 8 \times 10^6\ s^{-1}$), probably due to only moderate CT character of singlet emission, evidenced by quite large oscillator strength [17,30]. Intersystem crossing (ISC) was shown to be the dominant singlet excited state deactivation pathway ($k_{ISC} \approx 9 \times 10^7\ s^{-1}$) with yield of 0.84, in-line with DFT-predicted suitable energy level scheme [16]. Roughly, about half of triplet excitons were successfully upconverted back to the singlet states via rISC with the approximate rISC rate of $k_{rISC} \approx 3 \times 10^4\ s^{-1}$, comparable to some of other deep-blue TADF emitters [6]. TADF lifetime was estimated of about 143 μs, also comparable to other reports for deep-blue TADF emitters [5].

3.4. Electroluminescence properties

The potential of carbazole-pyrimidine derivative **tCbz-mPYRs** as deep-blue TADF emitter was also shown in OLED devices. Before doing that, HOMO and LUMO energies were estimated to evaluate the energetic compatibility between **tCbz-mPYRs** and host DPEPO, selected due to its high triplet energy [30] (see Fig. S12 in the supplementary information). The energy of emitter HOMO and LUMO were found larger than of host (−5.08 eV *vs.* −6.1 eV for HOMO and −1.77 eV *vs.* −2 eV for LUMO, respectively) [30]. This mismatch of LUMO energies may lead to poorer charge balance in OLED device, however DPEPO host still was one of the best candidates.

The device structure was the following: ITO/TAPC (30 nm)/TcTa (5 nm)/10 wt% **tCbz-mPYRs**:DPEPO (20 nm)/DPEPO (5 nm)/TmPyPb (50 nm)/LiF (0.8 nm)/Al (100 nm), see Fig. 4 and Fig. S13 in the supplementary information. The device showed deep-blue electroluminescence (EL) with turn-on voltage of about 4.5 V, peaking at about 441 nm with CIE colour coordinates of (0.16; 0.12) and large peak EQE of 8.7%. The estimated EQE of deep-blue OLED was comparable with those of other efficient deep-blue OLEDs (see Table S4 in the supplementary information). However, rather strong EQE roll-off was observed, probably due to rather slow TADF decay [31] and low electroactivity of DPEPO host, though this problem is rather frequent for deep-blue TADF OLEDs [12].

4. Conclusions

In summary, an approach for deep-blue TADF in carbazole-pyrimidine compounds was presented. High-triplet-energy carbazole-pyrimidine-carbazole compound with near-UV emission was used for the molecular structure optimization. The enhancement of electron-donating properties of carbazole, the increase of D and A twisting angle as well as inclusion of sulphur heteroatom was shown to shift the emission towards deep-blue together with lowering the singlet-triplet gap, resulting in rather high emission yield of 0.5 and emergence of TADF with the average delayed fluorescence lifetime of 143 μs. The optimized TADF compound showed an efficient deep-blue electroluminescence with peak EQE of 8.7% and emission CIE colour coordinates of (0.16; 0.12). Our simple molecular design steps were shown to be the successful strategy for achieving deep-blue TADF in highly promising carbazole-pyrimidine compounds. Further optimization of carbazole-pyrimidine molecular design, as well as OLED design, we believe, should enhance the TADF efficiency and boost the electroluminescence properties.

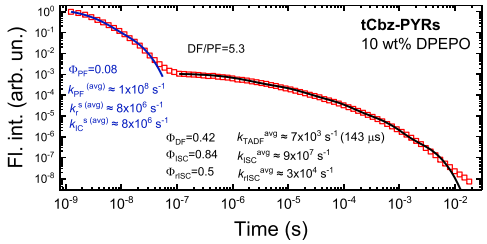

Fig. 3. Fluorescence decay transient of 10 wt% DPEPO film of **tCbz-PYRs** in oxygen-free ambient. Photophysical data, estimated according to Ref. [29], are included. Grey lines are multiexponential fits.

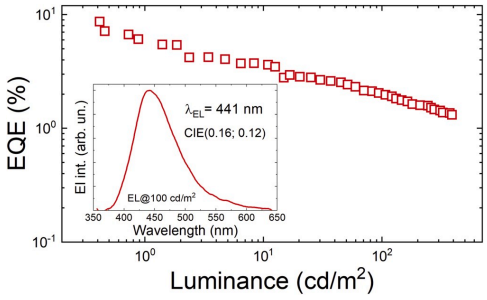

Fig. 4. External quantum efficiency values of OLED device with **tCbz-mPYRs** emitter at different values of luminance. The inset shows electroluminescence spectrum of the device at luminance of 100 cd/cm^2.

Declaration of competing interest

The authors declare that they have no known competing financial interests or personal relationships that could have appeared to influence the work reported in this paper.

Acknowledgements

This research has received funding from the Research Council of Lithuania (LMTLT), agreement No S-MIP-17-73. We are also very thankful for Regimantas Komskis, Milita Vagner and dr. Egidijus Kamarauskas for DSC, TGA and ionization potential measurements, respectively.

Appendix A. Supplementary data

Supplementary data to this article can be found online at https://doi.

org/10.1016/j.orgel.2020.105723.

References

[1] H. Uoyama, K. Goushi, K. Shizu, H. Nomura, C. Adachi, Highly efficient organic light-emitting diodes from delayed fluorescence, Nature 492 (2012) 234–238, https://doi.org/10.1038/nature11687.

[2] M.K. Etherington, J. Gibson, H.F. Higginbotham, T.J. Penfold, A.P. Monkman, Revealing the spin–vibronic coupling mechanism of thermally activated delayed fluorescence, Nat. Commun. 7 (2016), 13680, https://doi.org/10.1038/ncomms13680.

[3] T.-L. Wu, M.-J. Huang, C.-C. Lin, P.-Y. Huang, T.-Y. Chou, R.-W. Chen-Cheng, H.-W. Lin, R.-S. Liu, C.-H. Cheng, Diboron compound-based organic light-emitting diodes with high efficiency and reduced efficiency roll-off, Nat. Photon. 12 (2018) 235–240, https://doi.org/10.1038/s41566-018-0112-9.

[4] T.-A. Lin, T. Chatterjee, W.-L. Tsai, W.-K. Lee, M.-J. Wu, M. Jiao, K.-C. Pan, C.-L. Yi, C.-L. Chung, K.-T. Wong, C.-C. Wu, Sky-blue organic light emitting diode with 37% external quantum efficiency using thermally activated delayed fluorescence from spiroacridine-triazine hybrid, Adv. Mater. 28 (2016) 6976–6983, https://doi.org/10.1002/adma.201601675.

[5] X. Cai, S.-J. Su, Marching toward highly efficient, pure-blue, and stable thermally activated delayed fluorescent organic light-emitting diodes, Adv. Funct. Mater. 28 (2018), 1802558, https://doi.org/10.1002/adfm.201802558.

[6] L.-S. Cui, H. Nomura, Y. Geng, J.U. Kim, H. Nakanotani, C. Adachi, Controlling singlet-triplet energy splitting for deep-blue thermally activated delayed fluorescence emitters, Angew. Chem. Int. Ed. 56 (2017) 1571–1575, https://doi.org/10.1002/anie.201609459.

[7] D.H. Ahn, S.W. Kim, H. Lee, I.J. Ko, D. Karthik, J.Y. Lee, J.H. Kwon, Highly efficient blue thermally activated delayed fluorescence emitters based on symmetrical and rigid oxygen-bridged boron acceptors, Nat. Photon. 13 (2019) 540–546, https://doi.org/10.1038/s41566-019-0415-5.

[8] Y.H. Lee, S. Park, J. Oh, S.-J. Woo, A. Kumar, J.-J. Kim, J. Jung, S. Yoo, M.H. Lee, High-efficiency sky blue to ultradeep blue thermally activated delayed fluorescent diodes based on *ortho* -Carbazole-Appended triarylboron emitters: above 32% external quantum efficiency in blue devices, Adv. Opt. Mater. 6 (2018), 1800385, https://doi.org/10.1002/adom.201800385.

[9] Y. Im, M. Kim, Y.J. Cho, J.-A. Seo, K.S. Yook, J.Y. Lee, Molecular design strategy of organic thermally activated delayed fluorescence emitters, Chem. Mater. 29 (2017) 1946–1963, https://doi.org/10.1021/acs.chemmater.6b05324.

[10] M.Y. Wong, S. Krotkus, G. Copley, W. Li, C. Murawski, D. Hall, G.J. Hedley, M. Jaricot, D.B. Cordes, A.M.Z. Slawin, Y. Olivier, D. Beljonne, L. Muccioli, M. Moral, J.-C. Sancho-Garcia, M.C. Gather, I.D.W. Samuel, E. Zysman-Colman, Deep-blue oxadiazole-containing thermally activated delayed fluorescence emitters for organic light-emitting diodes, ACS Appl. Mater. Interfaces 10 (2018) 33360–33372, https://doi.org/10.1021/acsami.8b11136.

[11] Z. Li, W. Li, C. Keum, E. Archer, B. Zhao, A.M.Z. Slawin, W. Huang, M.C. Gather, I. D.W. Samuel, E. Zysman-Colman, 1,3,4-Oxadiazole-based deep blue thermally activated delayed fluorescence emitters for organic light emitting diodes, J. Phys. Chem. C 123 (2019) 24772–24785, https://doi.org/10.1021/acs.jpcc.9b08479.

[12] C. Chan, L. Cui, J.U. Kim, H. Nakanotani, C. Adachi, Rational molecular design for deep-blue thermally activated delayed fluorescence emitters, Adv. Funct. Mater. 28 (2018), 1706023, https://doi.org/10.1002/adfm.201706023.

[13] M. Kim, S.K. Jeon, S.-H. Hwang, J.Y. Lee, Stable blue thermally activated delayed fluorescent organic light-emitting diodes with three times longer lifetime than phosphorescent organic light-emitting diodes, Adv. Mater. 27 (2015) 2515–2520, https://doi.org/10.1002/adma.201500267.

[14] Q. Wu, M. Wang, X. Cao, D. Zhang, N. Sun, S. Wan, Y. Tao, Carbazole/α-carboline hybrid bipolar compounds as electron acceptors in exciplex or non-exciplex mixed cohosts and exciplex-TADF emitters for high-efficiency OLEDs, J. Mater. Chem. C. 6 (2018) 8784–8792, https://doi.org/10.1039/C8TC02353K.

[15] S.-W. Li, C.-H. Yu, C.-L. Ko, T. Chatterjee, W.-Y. Hung, K.-T. Wong, Cyanopyrimidine–carbazole hybrid host materials for high-efficiency and low-efficiency roll-off TADF OLEDs, ACS Appl. Mater. Interfaces 10 (2018) 12930–12936, https://doi.org/10.1021/acsami.8b02766.

[16] R. Huang, J. Avó, T. Northey, E. Chaning-Pearce, P.L. dos Santos, J.S. Ward, P. Data, M.K. Etherington, M.A. Fox, T.J. Penfold, M.N. Berberan-Santos, J.C. Lima, M.R. Bryce, F.B. Dias, The contributions of molecular vibrations and higher triplet levels to the intersystem crossing mechanism in metal-free organic emitters, J. Mater. Chem. C. 5 (2017) 6269–6280, https://doi.org/10.1039/C7TC01958K.

[17] Y. Xiang, Y. Zhao, N. Xu, S. Gong, F. Ni, K. Wu, J. Luo, G. Xie, Z.-H. Lu, C. Yang, Halogen-induced internal heavy-atom effect shortening the emissive lifetime and improving the fluorescence efficiency of thermally activated delayed fluorescence emitters, J. Mater. Chem. C. 5 (2017) 12204–12210, https://doi.org/10.1039/C7TC04181K.

[18] G. Baryshnikov, B. Minaev, H. Ågren, Theory and calculation of the phosphorescence phenomenon, Chem. Rev. 117 (2017) 6500–6537, https://doi.org/10.1021/acs.chemrev.7b00060.

[19] L. Skardziute, J. Dodonova, A. Voitechovicius, J. Jovaisaite, R. Komskis, A. Voitechoviciute, J. Bucevicius, K. Kazlauskas, S. Jursenas, S. Tumkevicius, Dyes Pigments 118 (2015) 118–128, https://doi.org/10.1016/j.dyepig.2015.03.008.

[20] T. Serevičius, R. Skaisgiris, J. Dodonova, L. Jagintavičius, J. Bucevičius, K. Kazlauskas, S. Juršėnas, Sigitas Tumkevičius, Chem Commun. 55 (2019) 1975–1978, https://doi.org/10.1039/c8cc08906j.

[21] C. Rothe, A.P. Monkman, Triplet exciton migration in a conjugated polyfluorene, Phys. Rev. B 68 (2003), https://doi.org/10.1103/PhysRevB.68.075208.

[22] J.C. de Mello, H.F. Wittmann, R.H. Friend, An improved experimental determination of external photoluminescence quantum efficiency, Adv. Mater. 9 (1997) 230–232, https://doi.org/10.1002/adma.19970090308.

[23] M. J. Frisch, G. W. Trucks, H. B. Schlegel, G. E. Scuseria, M. A. Robb, J. R. Cheeseman, G. Scalmani, V. Barone, B. Mennucci, G. A. Petersson, H. Nakatsuji, M. Caricato, X. Li, H. P. Hratchian, A. F. Izmaylov, J. Bloino, G. Zheng, J. L. Sonnenberg, M. Hada, M. Ehara, K. Toyota, R. Fukuda, J. Hasegawa, M. Ishida, T. Nakajima, Y. Honda, O. Kitao, H. Nakai, T. Vreven, J. A. Montgomery, Jr, J. E. Peralta, F. Ogliaro, M. Bearpark, J. J. Heyd, E. Brothers, K. N. Kudin, V. N. Staroverov, T. Keith, R. Kobayashi, J. Normand, K. Raghavachari, A. Rendell, J. C. Burant, S. S. Iyengar, J. Tomasi, M. Cossi, N. Rega, J. M. Millam, M. Klene, J. E. Knox, J. B. Cross, V. Bakken, C. Adamo, J. Jaramillo, R. Gomperts, R. E. Stratmann, O. Yazyev, A. J. Austin, R. Cammi, C. Pomelli, J. W. Ochterski, R. L. Martin, K. Morokuma, V. G. Zakrzewski, G. A. Voth, P. Salvador, J. J. Dannenberg, S. Dapprich, A. D. Daniels, O. Farkas, J. B. Foresman, J. V. Ortiz, J. Cioslowski, D. J. Fox, Gaussian 09, Revision C.01.

[24] S. Rostamizadeh, M. Nojavan, R. Aryan, Synthesis of N2-arylaminopyrimidine-5-carbonitrile derivatives via SNAr amination reaction, Chin. Chem. Lett. 26 (2015) 152–156, https://doi.org/10.1016/j.cclet.2014.10.007.

[25] V. Jakubkiene, V. Cepla, M.M. Burbuliene, P. Vainilavicius, Synthesis and functionalization of 8-methyl-2 h -pyrimido [2,1- c][1,2,4]triazine-3,6(1 h ,4 h)-dione: synthesis and functionalization of 8-methyl-2H-pyrimido[2,1-c] 3[1,2,4] triazine-3,6(1H,4H)-dione, J. Heterocycl. Chem. 49 (2012) 737–741, https://doi.org/10.1002/jhet.844.

[26] V. Jakubkiene, J. Zurba, M.M. Burbuliene, Synthesis of some aryl (pyrimidin-3-yl) methyl ureas, hydrazones and semicarbazones, Arkivoc (Part 3) (2016) 374–386, https://doi.org/10.3998/ark.5550190.p009.620.

[27] B.L. Cotts, D.G. McCarthy, R. Noriega, S.B. Penwell, M. Delor, D.D. Devore, S. Mukhopadhyay, T.S. De Vries, N.S. Ginsberg, Tuning thermally activated delayed fluorescence emitter photophysics through solvation in the solid state, ACS Energy Lett. 2 (2017) 1526–1533, https://doi.org/10.1021/acsenergylett.7b00268.

[28] T. Serevičius, R. Skaisgiris, J. Dodonova, K. Kazlauskas, S. Jursenas, S. Tumkevicius, Minimization of solid - state conformational disorder in donor – acceptor TADF compounds, Phys. Chem. Chem. Phys. 22 (2020) 265–272, https://doi.org/10.1039/C9CP05907E.

[29] F.B. Dias, T.J. Penfold, A.P. Monkman, Photophysics of thermally activated delayed fluorescence molecules, Methods Appl. Fluoresc. 5 (2017), 012001, https://doi.org/10.1088/2050-6120/aa537e.

[30] G. Kreiza, D. Banevičius, J. Jovaišaitė, K. Maleckaitė, D. Gudeika, D. Volyniuk, J. V. Gražulevičius, S. Juršėnas, K. Kazlauskas, Suppression of benzophenone-induced triplet quenching for enhanced TADF performance, J. Mater. Chem. C. 7 (2019) 11522–11531, https://doi.org/10.1039/C9TC02408E.

[31] M. Inoue, T. Serevičius, H. Nakanotani, K. Yoshida, T. Matsushima, S. Juršėnas, C. Adachi, Effect of reverse intersystem crossing rate to suppress efficiency roll-off in organic light-emitting diodes with thermally activated delayed fluorescence emitters, Chem. Phys. Lett. 644 (2016) 62–67, https://doi.org/10.1016/j.cplett.2015.11.042.

A6

Optimization of the carbazole–pyrimidine linking pattern for achieving efficient TADF

T. Serevičius, J. Dodonova, **R. Skaisgiris**, D. Banevičius, K. Kazlauskas, S. Juršėnas and S. Tumkevičius

J. Mater. Chem. C **8**(32), 11192–11200 (2020)
DOI: 10.1039/D0TC02194F
http://xlink.rsc.org/?DOI=D0TC02194F

Supporting information: http://www.rsc.org/suppdata/d0/tc/d0tc02194f/d0tc02194f1.pdf

Journal of Materials Chemistry C

ROYAL SOCIETY OF CHEMISTRY

PAPER

View Article Online
View Journal

Cite this: DOI: 10.1039/d0tc02194f

Optimization of the carbazole–pyrimidine linking pattern for achieving efficient TADF†

Tomas Serevičius, *[a] Jelena Dodonova,[b] Rokas Skaisgiris,[a] Dovydas Banevičius,[a] Karolis Kazlauskas,[a] Saulius Juršėnas[a] and Sigitas Tumkevičius[b]

Received 5th May 2020,
Accepted 26th June 2020

DOI: 10.1039/d0tc02194f

rsc.li/materials-c

A high fluorescence quantum yield is essential for achieving a high OLED efficiency. Due to their typically strong charge-transfer (CT) character, thermally activated delayed fluorescence (TADF) compounds usually have a lower prompt fluorescence efficiency, and therefore the boosting of the total emission yield (Φ_{PL}) mostly relies on the enhancement of the delayed fluorescence efficiency. In this paper, we present a less frequently used approach for achieving a high Φ_{PL} by maximising both prompt and delayed emission yields of carbazole–pyrimidine compounds. Strong decoupling of HOMO and LUMO and the subsequent emergence of TADF were achieved by introducing four carbazole units at both *meta* positions of the phenyl unit, though Φ_{PL} was low due to the prominent nonradiative triplet decay rate. Crowding the relatively loose carbazole units together at the *para* position and both *meta* positions, conversely, was shown to diminish the nonradiative decay, enhance the radiative decay rate and subsequently boost the fluorescence yield. Efficient blue electroluminescence with a nearly 20% yield was demonstrated for the optimized compound.

Introduction

Thermally activated delayed fluorescence provides an elegant way to retrieve "dark" triplet excitons and attain exceptional external quantum efficiencies (EQEs) of OLED devices reaching nearly 30–40%.[1–6] A breakthrough in TADF materials research is expected to advance the large-area ultrathin display and lighting technologies, where OLEDs are nearly unbeatable due to their exceptional emission properties as well as low production cost, pronounced flexibility and high power efficiency.[7] A high emission yield of TADF compounds is achieved by recovering triplet states by lowering the singlet–triplet energy splitting (ΔE_{ST}) towards the values low enough for thermal upconversion.[1,8,9] As ΔE_{ST} depends on the spatial overlap of HOMO and LUMO, lowered singlet–triplet energy gaps are achieved by constructing TADF materials from loosely bound donor and acceptor units with enhanced HOMO–LUMO decoupling. Unfortunately, the enlarged spatial separation of electron density in HOMO and LUMO concomitantly diminishes the radiative fluorescence decay rate, which may be outcompeted by nonradiative decay, leading to a low prompt fluorescence quantum yield (Φ_{PF}). In line with that, the prolonged prompt fluorescence lifetime often leads to a low Φ_F.[10] Recently, it has been shown that a low fluorescence decay rate is harmful for TADF OLEDs, as the increasing singlet exciton density in the light-emitting layer boosts the rate of unwanted singlet–singlet annihilation, increasing the molecular decomposition rate.[11] Therefore, the delicate balance between the minimization of the HOMO–LUMO overlap and the preservation of a high enough fluorescence yield should be maintained. As an alternative solution, highly efficient TADF can be achieved by minimizing the rate of competing nonradiative decay. As an example, a remarkable TADF efficiency has recently been demonstrated for compounds with large ΔE_{ST} values and low rISC rates, when the competing nonradiative decay of triplet states, occurring mostly through molecular vibration modes, was suppressed.[12,13]

The management of singlet radiative and nonradiative quenching rates could also be used as a pathway for seeking efficient TADF.[14–16] Such an approach, relying on the simultaneous maximization of prompt and delayed fluorescence efficiency, is presented in this paper. Three carbazole–pyrimidine compounds were synthesized and comprehensively analysed. The alteration of the donor–acceptor linking pattern was shown to lower the singlet–triplet energy gap and subsequently modify the ratio between the radiative and nonradiative emission decay rates. An optimized carbazole–pyrimidine structure was revealed with minimized ΔE_{ST} and a high yield of prompt and delayed fluorescence. An OLED device with the optimized

[a] Institute of Photonics and Nanotechnology, Vilnius University, Sauletekio 3, LT-10257 Vilnius, Lithuania. E-mail: tomas.serevicius@tmi.vu.lt
[b] Institute of Chemistry, Vilnius University, Naugarduko 24, LT-03225, Vilnius, Lithuania

† Electronic supplementary information (ESI) available. See DOI: 10.1039/d0tc02194f

compound in the light-emitting layer showed blue electroluminescence with a high emission yield.

Experimental section

Reagents and solvents were purchased directly from commercial suppliers; solvents were purified by known procedures. Melting points were determined in open capillaries with IA9100 series digital melting point apparatus (Thermo Fisher Scientific) and were not corrected. Thin layer chromatography was performed using TLC-aluminum sheets with silica gel (Merck 60 F254). Visualization was accomplished using UV light. Column chromatography was performed using Silica gel 60 (0.040–0.063 mm) (Merck). NMR spectra were recorded on a Bruker Ascend 400 (400 MHz and 100 MHz for ^{1}H and ^{13}C, respectively). ^{1}H NMR and ^{13}C NMR spectra were referenced to residual solvent peaks. Mass spectrometry (HRMS) analyses were carried out on a quadrupole time-of-flight mass spectrometer (micrOTOF-Q II, Bruker Daltonics GmbH, Bremen, Germany) or on a Dual-ESI Q-TOF 6520 (Agilent Technologies) mass spectrometer. MALDI mass spectra were acquired on a Bruker MALDI-TOF Autoflex Speed operating in linear mode, and *trans*-2-[3-(4-*tert*-butylphenyl)-2-methyl-2-propenylidene] malononitrile was chosen as the matrix. DSC curves were measured using Mettler Toledo DSC1 apparatus with aluminum crucibles under N_2 flow. The sample mass was around 8–10 mg, and the heating and cooling rates were both 10 K min^{-1}. TADF compounds were analysed in 1×10^{-5} M toluene solutions and 1 wt% PMMA and 10 wt% DPEPO films. Solid-state films were prepared by dissolving each material and host in appropriate ratios in toluene solutions and then wet-casting the solutions on quartz substrates. Absorption spectra were measured using a Lambda 950 UV/Vis spectrophotometer (PerkinElmer). Time-integrated fluorescence (TIFL) spectra, time-resolved fluorescence (TRFL) spectra, low-temperature phosphorescence (PH) and fluorescence decay transients were measured using an NT 242 nanosecond YAG:Nd^{3+} laser (Ekspla, τ = 7 ns, pulse energy = 200 μJ, repetition rate = 1 kHz) and a New iStar DH340T time-gated iCCD camera (Andor). Fluorescence transients were obtained by exponentially increasing the delay and integration time.[17] Fluorescence quantum yield values (Φ_F, ±5% error) of the solutions and polymer films in ambient air were estimated by the integrated sphere method[18] using an integrating sphere (Sphere Optics) connected to a PMA-12 CCD spectrometer (Hamamatsu) *via* an optical fibre. Partially unquenched TADF, existing in solid films in ambient air, was excluded from the Φ_F values.[19,20] Solid-state samples were mounted in a closed cycle He cryostat (Cryo Industries 204N) for all measurements (for oxygen-saturated and oxygen-free conditions). Toluene solutions were degassed by using the freeze–pump–thaw method. OLED devices were fabricated on precleaned indium-tin oxide (ITO)-coated glass substrates. The small-molecule and cathode layers were thermally evaporated using vacuum evaporation apparatus (Vacuum Systems and Technologies Ltd) at a pressure $< 6 \times 10^{-6}$ Torr and a deposition rate of about 1 Å s^{-1}. The OLED devices were encapsulated with a clear glass cover to prevent their interaction with the ambient atmosphere. Device current–voltage (*I*–*V*) characteristics and electroluminescence properties were measured using a calibrated integrating sphere (Orb Optronics) and a PMA-11 CCD spectrometer (Hamamatsu), powered by a 2601A power supply unit (Keithley).

Quantum chemical calculations were performed by using density functional theory (DFT) as implemented in the Gaussian 09 software package at the B3LYP/6-31G(d) level.[21] The polarizable continuum model (PCM) was used to estimate the solvation behaviour of the surrounding toluene.

Results and discussion

Materials design and synthesis

Three carbazole–pyrimidine compounds, differing by the linking pattern of carbazole units, were synthesized and analysed (see Scheme 1). The first compound in this series, **1CbzPYR** (4,6-bis[4-(9-carbazolyl)phenyl]pyrimidine), despite the evident ΔE_{ST}, was selected due to its large bandgap, suitable for achieving blue TADF, and proven intersystem crossing activity.[19,22] The compounds **2CbzPYR** (4,6-bis[3,5-di(9-carbazolyl)phenyl] pyrimidine) and **3CbzPYR** (4,6-bis[3,4,5-tri(9-carbazolyl)phenyl] pyrimidine) were selected to have different numbers and linking patterns of electron-donating carbazole units, seeking TADF turn-on and further maximization of emission yield. Two carbazole units were incorporated at both *meta* positions of the phenyl fragment, as a similar strategy was shown to be successful for narrowing ΔE_{ST}.[23,24] Further modification of the **2CbzPYR** structure with additional *para* carbazole units was performed (compound **3CbzPYR**), as a similar molecular structure with closely crowded carbazole units was shown to minimize the deformation of molecular structure and, as expected, lower the rate of nonradiative decay as well as minimize the unwanted conformational disorder.[20,25] Efficient TADF was already achieved in compounds with a similar molecular structure, but a stronger triazine acceptor unit[26–28] or other acceptor units[29–31] were used; however, the authors used them to analyse other aspects of TADF performance than in our study.

Synthesis of the designed emitters **1CbzPYR**, **2CbzPYR** and **3CbzPYR** was carried out *via* the Suzuki–Miyaura cross-coupling reaction of 4,6-dichloropyrimidine (**1**) with a slight excess of 4-(9-carbazolyl)- (**2a**), 3,5-di(9-carbazolyl)phenylboronic acids (**2b**) or 3,4,5-tri(9-carbazolyl)phenylboronate (**2c**) in the presence of $Pd(OAc)_2/PPh_3$ or $Pd(PPh_3)_4$ as a catalyst, respectively (see Scheme 1). The synthetic details, characterization data and spectroscopic analysis data of the synthesized carbazolyl substituted phenylboronic acids **2a**,**b**, phenylboronate **2c** and target compounds **1CbzPYR**, **2CbzPYR** and **3CbzPYR** are presented in the ESI.†

DFT analysis

Quantum chemical simulations were used to assess the structural and electronic properties of carbazole–pyrimidine compounds **1CbzPYR–3CbzPYR**. Ground-state molecular geometry, $S_0 \rightarrow S_1$/T_1 transition energies and π-electron density distribution of the

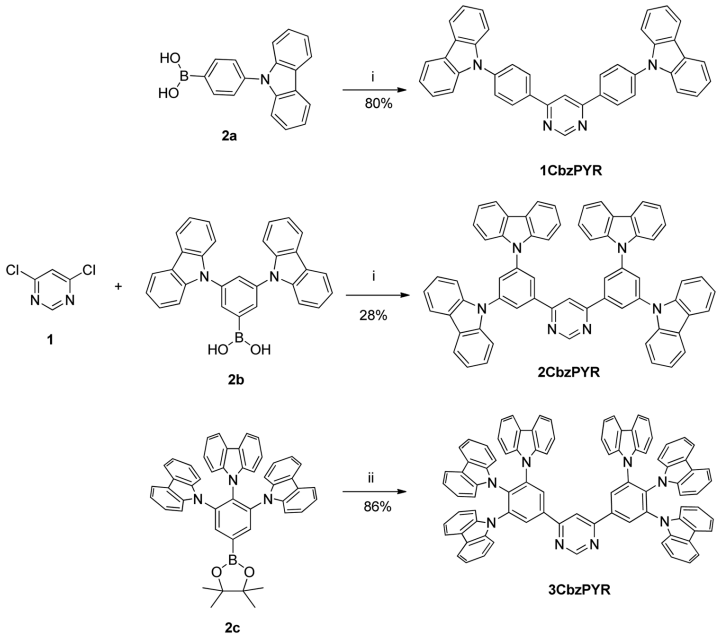

Scheme 1 Synthesis of the **1CbzPYR**, **2CbzPYR** and **3CbzPYR** emitters. *Reagents and conditions*: (i) boronic acid (2.2 equiv.), $Pd(OAc)_2$ (5 mol%), PPh_3 (10 mol%), aq. Na_2CO_3 (3.1 equiv.), glyme, 90 °C, 24 h; (ii) boronic ester (2.2 equiv.), $Pd(PPh_3)_4$ (10 mol%), aq. K_2CO_3 (15 equiv.), glyme, 80 °C, 24 h.

HOMO and LUMO are shown in Fig. 1, and Fig. S8 and S9 in the ESI.† Molecular structure optimization (see Fig. 1a) revealed that the phenyl-pyrimidine unit is rather flat with a dihedral twist angle (α_1) in the range of 14.5–16.5°. The α_1 twist angle was slightly lower for compounds with more bulky donor fragments. Electron-donating carbazole units, on the other hand, were more perpendicular, with twist angle (α_2) ranging from about 52° for **1CbzPYR** to 56.5–67.8° for **3CbzPYR** (slightly larger α_2 values were estimated for both *meta* carbazoles). An increase of the α_2 angle was observed for compounds with more sterically crowded carbazole units.[32] HOMO energies were found to be rather similar for all compounds, ranging from −5.49 to −5.52 eV, comparable with that of sole carbazole,[6] while the LUMO energies varied from −1.99 eV for **1CbzPYR** to −2.37 eV for **3CbzPYR**, in line with the DFT-predicted decrease of α_1 angle, altering the conjugation length of the donor unit[33] (see Fig. 1b). The π-electron density distribution was similar for all compounds in the LUMO (although a portion of π-conjugation extends over the nitrogen atom in the *para*-carbazole unit), while the π-electrons in the HOMO tended to localize over the carbazole fragments rather than over the spacing phenyl unit, resulting in a lower HOMO–LUMO overlap for compounds with a more localized HOMO. This was evidenced by the decreasing oscillator strength of the $S_0 \rightarrow S_1$ transition (f) for compounds with more carbazole units, typically for compounds with stronger CT character,[34,35] though f was slightly larger for **3CbzPYR** with an additional *para*-carbazole unit due to the somewhat enlarged HOMO–LUMO coupling.

The different architectures of the carbazole–pyrimidine compounds had a direct effect on the $S_0 \rightarrow S_1/T_1$ transition energies (see Fig. 1b). Compound **1CbzPYR** showed the largest $S_0 \rightarrow S_1$ transition energy of 3.04 eV. Increasing the number of electron-donating carbazole units lowered the transition energy to 2.82 eV for compound **2CbzPYR** and later to 2.7 eV for compound **3CbzPYR**. Since the energy of the first triplet state was almost the same for compounds **1CbzPYR** and **2CbzPYR** (2.75 and 2.72 eV, respectively) and only slightly lower for compound **3CbzPYR**, the calculated ΔE_{ST} gaps gradually decreased from 290 meV for **1CbzPYR** to 100 and 140 meV for compounds **2CbzPYR** and **3CbzPYR**, respectively. Several higher-energy triplet states were found to have a lower energy compared to S_1, the number of which was larger for compounds with more carbazole units[36,37] (see Fig. S8 in the ESI†). One higher-energy triplet state at 2.79 eV was found for **1CbzPYR**, three states were found for **2CbzPYR** and four states were found for **3CbzPYR**. In contrast to the $S_0 \rightarrow S_1$ transition, which was of almost pure CT character, a few $S_0 \rightarrow T_n$ transitions had some localized excited state (LE) character (*e.g.* $S_0 \rightarrow T_1/T_2$ transitions for compound **3CbzPYR**), while other transitions were nearly pure CT transitions (*e.g.* $S_0 \rightarrow T_3/T_4$ transitions for compound **3CbzPYR**; see Fig. S9 in the ESI†). Such an energy-level scheme

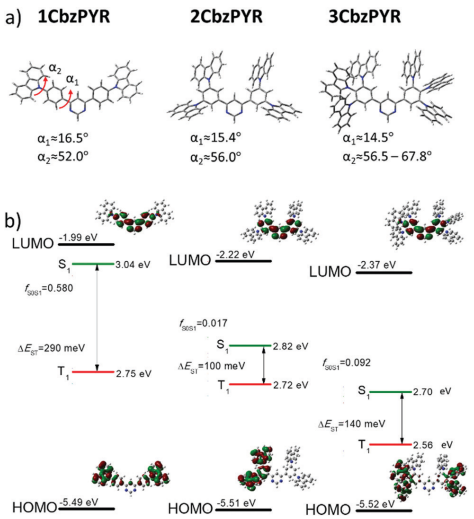

Fig. 1 (a) Optimized geometries of carbazole–pyrimidine TADF compounds. The α_1 angle is the twisting angle between pyrimidine and phenyl units, while α_2 is the twisting angle between the phenyl and carbazole units. (b) Energies of HOMO and LUMO as well as energies of $S_0 \rightarrow S_1/T_1$ transitions. The calculated oscillator strengths of the $S_0 \rightarrow S_1$ transition and energy gaps between the lowest singlet and triplet states are also denoted.

with a high density of closely lying vibronically-coupled excited states with different LE/CT character was shown to be mandatory for a large rISC rate and efficient TADF.[9,36–40]

Absorption and emission properties

The absorption and emission spectra of the variously substituted carbazole–pyrimidine compounds in solution and solid state are shown in Fig. 2 and the details are presented in Table 1. The selective control of absorption and emission peak energies in all surroundings was achieved by increasing the number of carbazole units. A direct charge transfer absorption band was observed at about 355–375 nm, whereby the absorption peaked at larger wavelengths for the more conjugated compounds, in line with DFT predictions (see Fig. S10 in the ESI† for the detailed analysis). Molar absorption coefficient (ε) values were in line with the DFT-estimated oscillator strength (f). The lowest ε was observed for the *meta*-substituted compound **2CbzPYR** ($\varepsilon < 5000$ M^{-1} cm^{-1}) with the strongest HOMO–LUMO decoupling and, therefore, the lowest f (0.017). In contrast, the largest ε of about 30 000 M^{-1} cm^{-1} was measured for **1CbzPYR** with weak CT character and a high f of 0.58. **3CbzPYR**, bearing three carbazole units, showed only a slightly lower ε than that of **1CbzPYR** (about 23 000 M^{-1} cm^{-1}) due to the somewhat enhanced HOMO–LUMO coupling through *para*-carbazole (see Fig. 1b), in line with the rather high f of 0.092. The molar absorption coefficients of **1CbzPYR** and **3CbzPYR** were rather high, which was likely due to the enhanced mixing of π–π* and n–π* states in the partially twisted carbazole units.[41,42] Similar large ε values were also observed for the analogous carbazole–triazine compounds.[26,27] The same trend was also observed for the fluorescence spectra. The introduction of more carbazole donor units allowed us to tune the fluorescence wavelength for 370 meV, from 408 nm for **1CbzPYR** to 464 nm for **3CbzPYR**. Similarly, the fluorescence peaked at 408–446 nm for compounds embedded in 1 wt% PMMA films. A slight blueshift of fluorescence wavelength for compound **3CbzPYR** was probably caused by the lower solid-state solvation (SSS) in the PMMA surrounding[43] and the minor conformational disorder of the rigid **3CbzPYR** structure, in contrast to the less sterically constrained **1CbzPYR** and **2CbzPYR**, where the lowered SSS was outcompensated by the more pronounced conformational disorder[19,20] (the peculiarities of the conformational disorder will be analysed later in the text). In contrast, a 220 meV redshift of fluorescence peak was

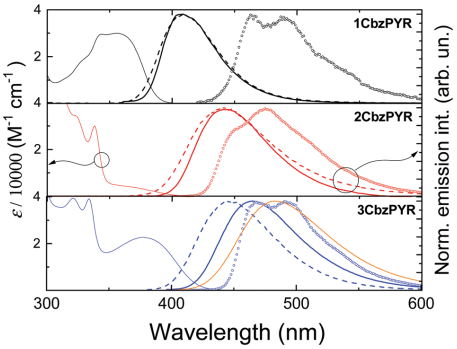

Fig. 2 Absorption, fluorescence and phosphorescence spectra of carbazole–pyrimidine compounds: **1CbzPYR** (a), **2CbzPYR** (b) and **3CbzPYR** (c). Absorption spectra were obtained in toluene (solid thin lines) and fluorescence spectra were obtained in toluene (thin solid lines), 1 wt% PMMA films (dashed lines) and 10 wt% DPEPO films (orange line for **3CbzPYR**). Phosphorescence spectra (open dots) were obtained in 1 wt% PMMA films at 10 K with a 100 μs delay.

Table 1 Absorption and emission data of carbazole–pyrimidine compounds. Fluorescence onsets, used for ΔE_{ST} calculations, are shown in Table S1 in the ESI

	Toluene				1 wt% PMMA films		
	λ_{ABS}[a] (nm)	ε[b] (L mol^{-1} cm^{-1})	λ_{PL}[c] (nm)	ΔE_{ST}[d] (meV)	λ_{PL}[c] (nm)	λ_{PH}[e] (nm)	ΔE_{ST}[d] (meV)
1CbzPYR	355	30 000	408	440	408	440	480
2CbzPYR	—	Below 5000	442	180	440	427	270
3CbzPYR	378	22 750	464	190	446	445	320

[a] Peak wavelength of the high-energy absorption band. "—" indicates that no peak could be estimated. [b] Extinction coefficient of the high-energy absorption band. [c] Peak wavelength of the fluorescence spectra. [d] Energy gap between the onset of fluorescence and 1 wt% PMMA phosphorescence spectra at 10 K. [e] Onset wavelength of the phosphorescence spectra of 1 wt% PMMA films at 10 K.

observed in the 10 wt% DPEPO solid host with more pronounced solid-state solvation.[19] The low-temperature phosphorescence spectra of 1 wt% PMMA films of carbazole–pyrimidine compounds peaked at 427–445 nm with similar ^{3}LE peak wavelengths for compounds **1CbzPYR** and **3CbzPYR**, while the lowest-energy vibronic peak for **2CbzPYR** was observed at a slightly higher energy and with a different vibronic pattern. Singlet–triplet energy gaps gradually decreased in both toluene and 1 wt% PMMA films for the compounds with more carbazole units (although ΔE_{ST} was slightly larger for **3CbzPYR** due to the somewhat boosted HOMO–LUMO coupling through the *para*-carbazole), though a larger ΔE_{ST} was observed in the polymer surrounding due to the lower SSS and conformational disorder.[20] ΔE_{ST} was further lowered down to 110 meV for compound **3CbzPYR** when embedded in the more polar 10 wt% DPEPO host.

Temporal fluorescence properties

Further investigation of differently substituted carbazole–pyrimidine compounds was carried out by analysing the time-resolved fluorescence properties. The fluorescence decay transients of carbazole–pyrimidine compounds in solution and solid surroundings are shown in Fig. 3. Typically, prompt fluorescence was observed for the initial 100–200 ns, later followed by long-lived delayed fluorescence, though it was absent for **1CbzPYR** with the largest ΔE_{ST}.

The prompt fluorescence decay rate (k_{fl}) in toluene solutions systematically decreased for compounds with more carbazole units (see Table 2). A rather large k_{fl} was obtained for **1CbzPYR** (26×10^7 s^{-1}), which is typical for compounds with pronounced LE fluorescence.[44] Lower k_{fl} values were estimated for compounds **2CbzPYR** and **3CbzPYR** with more pronounced CT character. To reveal the processes behind the variation of k_{fl}, the rates of radiative and nonradiative decay processes were assessed. Before doing that, prompt fluorescence quantum yield values were determined (Φ_{PF}). Φ_{PF} followed a different trend compared to k_{fl}: it was the largest for compounds **1CbzPYR** (0.8) and **3CbzPYR** (0.43), while it was remarkably lower (0.057) for compound **2CbzPYR**. As Φ_{PF} for **1CbzPYR** with pronounced LE emission is quite typical, a rather high emission yield was also determined for **3CbzPYR** with stronger CT character. Unsurprisingly, the trend of the radiative decay rate (k_r) was in line with those of oscillator strength and molar absorption coefficient: the lowest k_r was estimated for **2CbzPYR**, while for **3CbzPYR**, k_r was 4.1 times larger, and for **1CbzPYR**, it was even 32 times larger. Surprisingly, the nonradiative decay rate (k_{nr}), on the other hand, also followed the same trend. Rather similar k_{nr} values were estimated for both **1CbzPYR** and **3CbzPYR**, while for **2CbzPYR**, the k_{nr} rate was 2.2–2.9 times larger. The combination of a low k_r (0.7×10^7 s^{-1}) and a pronounced non-radiative decay rate (11×10^7 s^{-1}) resulted in a low Φ_{PF} of 0.057 for **2CbzPYR**. In contrast, a rapid k_r (2.9×10^7 s^{-1}), one of the largest for TADF compounds,[45] and an only moderate k_{nr} (3.8×10^7 s^{-1}) ensured an exceptional prompt fluorescence yield of 0.43 for **3CbzPYR**. Almost no changes of Φ_{PF} and k_{nr} were observed after embedding the compounds in partially rigid PMMA films. As the k_{nr} values were almost the same in both surroundings, the nonradiative decay rate of the singlet states, mostly occurring through vibrations of the molecular core, could be neglected and the dominating nonradiative decay pathway could be assigned to intersystem crossing (ISC) to triplet states.[12,13,25,46]

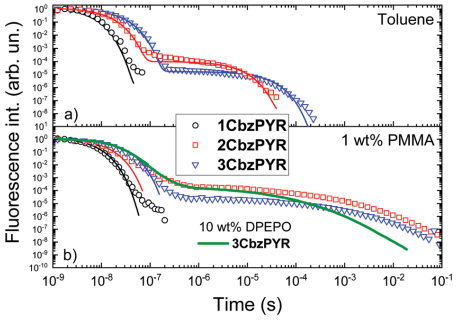

Fig. 3 Normalized fluorescence decay transients of carbazole–pyrimidine TADF compounds in toluene (a) and 1 wt% PMMA films (b) under oxygen-free conditions. The fluorescence decay transient of the 10 wt% DPEPO film of compound **3CbzPYR** is also shown in (b) (thick dark green line). Thin color lines are exponential fits.

The delayed fluorescence, observed only for compounds **2CbzPYR** and **3CbzPYR**, was found to be TADF. The total fluorescence intensities of both compounds were enhanced after oxygen removal in both dilute solutions and solid films (see Fig. S11 in the ESI†), when oxygen mostly quenched the delayed fluorescence, though some minor quenching of prompt fluorescence was also observed in toluene solutions[10,47] (see Fig. S12 and S13 in the ESI†). Similarly, the lowered temperature also eliminated the delayed fluorescence, which is typical for TADF (see Fig. S14 in the ESI†). No delayed fluorescence was observed for **1CbzPYR** in both oxygen-free surroundings due to the rather high ΔE_{ST},[48] though weak room-temperature phosphorescence at 450–550 nm was observed in PMMA films (see Fig. S15 in the ESI†), related to the negligible quenching of triplet states.[19] The TADF parameters are presented in Table 2. Similar trends were observed for both prompt and delayed fluorescence, as compound **3CbzPYR** with a larger prompt fluorescence yield also showed a more efficient delayed fluorescence. In the case of prompt fluorescence, a high radiative decay rate ensured a pronounced Φ_{PF} for **3CbzPYR**, while the combination of a slower radiative decay and boosted nonradiative quenching yielded a low Φ_{PF} for **2CbzPYR**. Similarly, **2CbzPYR** with a more flexible molecular structure also yielded a low Φ_{DF} due to the enhanced nonradiative triplet quenching rate (k_{nr}^T),[13] which was 3.8 times larger for **2CbzPYR** (2.2×10^5 s^{-1} and 0.6×10^5 s^{-1} for compounds **2CbzPYR** and **3CbzPYR**, respectively). As both compounds showed a similar rISC rate (k_{rISC}) of 1.2×10^4 s^{-1} and 1.9×10^4 s^{-1}, the triplet quenching rate was around 18 times larger than k_{rISC} for **2CbzPYR**. This was the reason for the negligible Φ_{DF} and enhanced TADF decay rate for **2CbzPYR** in toluene. Despite the high ISC yield (Φ_{ISC} = 0.94), only 5 triplet states out of 100 were upconverted for

Table 2 Prompt and delayed fluorescence decay constants of carbazole–pyrimidine compounds under $-O_2$ conditions. The parameters of exponential fits, shown in Fig. 3, are presented in Table S2 in the ESI. TADF parameters were assessed according to Kreiza *et al.*;[25] see Table S3 in the ESI

	Toluene			1 wt% PMMA	
	PF	TADF		PF	TADF
	$k_{fl}/k_r/k_{nr}{}^a$ ($\times 10^7$ s^{-1})	$k_{TADF}/k_{ISC}/k_{rISC}/k_{nr}^T{}^b$ ($\times 10^7$ s^{-1})	$\Phi_{PF}/\Phi_{DF}/\Phi_{ISC}/\Phi_{rISC}{}^c$	$k_{fl}/k_r/k_{nr}{}^a$ ($\times 10^7$ s^{-1})	$\Phi_{PF}/\Phi_{DF}{}^c$
1CbzPYR	26.0/21.0/5.1	—/5.1/—/—	0.8/—/0.2/—	24.0/16.0/8.3	0.66/—
2CbzPYR	11.0/0.7/11.0	2.2^d/11.0/1.2^e/2.2^d	0.057/0.003/0.94/0.05	14.0/0.8/13.0	0.06/0.16
3CbzPYR	7/2.9/3.8	0.7^d/3.8/1.9^e/0.6^d	0.43/0.07/0.57/0.25	7.9/3.8/4.1	0.48/0.33

[a] Fluorescence, radiative and nonradiative fluorescence decay rates, respectively. [b] TADF, ISC, rISC and nonradiative triplet quenching rates, respectively. [c] Prompt fluorescence quantum, delayed fluorescence quantum, ISC and rISC yields, respectively. [d] $\times 10^5$. [e] $\times 10^4$.

compound **2CbzPYR** (Φ_{rISC} = 0.05). As the ISC rate was evidently larger than that of radiative decay ($k_{ISC} = 11 \times 10^7$ s^{-1} *vs.* $k_r = 0.7 \times 10^7$ s^{-1}), the majority of the singlet states were repeatedly converted back to triplet states and *vice versa*, subsequently leading to a poor Φ_{DF} value of only 0.003 and Φ_{PL} of 0.06. A different result was observed for **3CbzPYR** having closely arranged carbazole units. In this case, the nonradiative triplet decay rate was remarkably lower (0.6×10^5 s^{-1}), only about 3 times larger than k_{rISC}, in line with the enhanced rigidity of the molecular structure. Due to the evidently enhanced k_{rISC}/k_{nr}^T ratio, more triplet states were upconverted (Φ_{rISC} = 0.25), where around half of the singlet states decayed radiatively. The combination of weakened triplet quenching and a rapid k_r allowed enlargement of the delayed fluorescence yield up to 0.07 and Φ_{PL} up to 0.5 for compound **3CbzPYR**.

The increase of Φ_{DF} was achieved by embedding compounds **2CbzPYR** and **3CbzPYR** in the PMMA surrounding. In contrast to prompt fluorescence, the restricted molecular deformation in the polymer surrounding weakened the nonradiative triplet quenching and increased the TADF yield up to 0.16 and 0.33 and the Φ_{PL} up to 0.22 and 0.81 for **2CbzPYR** and **3CbzPYR**, respectively. Despite the decreased k_{nr}^T and remarkably boosted Φ_{DF}, the performance of **2CbzPYR** was still low due to the poor prompt fluorescence yield. On the other hand, the enlarged radiative decay rate together with the minimized nonradiative decay rate ensured the excellent performance of **3CbzPYR**. The TADF decay rates of compounds embedded in polymer films, however, were difficult to estimate due to the highly nonexponential fluorescence decay profiles, mediated by the solid-state conformational disorder,[19,20,49–51] though k_{TADF} was clearly lower. A typical improvement of the TADF decay rate was observed for **3CbzPYR** embedded in the more polar 10 wt% DPEPO films,[19] though the decay was still multiexponential. To evaluate the conformational disorder (CD) in carbazole–pyrimidine TADF compounds, the time-resolved fluorescence spectra of 1 wt% PMMA (see Fig. 4) and 10 wt% DPEPO (see Fig. S16 in the ESI†) films were obtained. Larger CD was observed for compounds with larger temporal shifts of emission peaks,[51] usually estimated as the redshift of the prompt fluorescence, as the latest delayed fluorescence mostly was quenched in TADF compounds with a prolonged lifetime.[20,51] As expected, a larger temporal shift of 380 meV was observed for **2CbzPYR**, while for **3CbzPYR**, the redshift was only 240 meV. A further decrease in conformational disorder, evidenced by the lowered redshift of about 200 meV, was observed for **3CbzPYR** in the DPEPO surrounding due to enhanced solid-state solvation,[19] leading to an enhanced k_{TADF}. Interestingly, larger conformational disorder was observed for compound **2CbzPYR** with more rapid nonradiative decay of triplet states. As both processes, in general, share a similar nature, related with the deformation of the molecular structure, reasonably enlarged stiffness of the molecular structure may help weaken both the unwanted processes, conformational disorder and nonradiative emission decay, and enhance the TADF yield,[9,13,52,53] as evidenced in compound **3CbzPYR**.

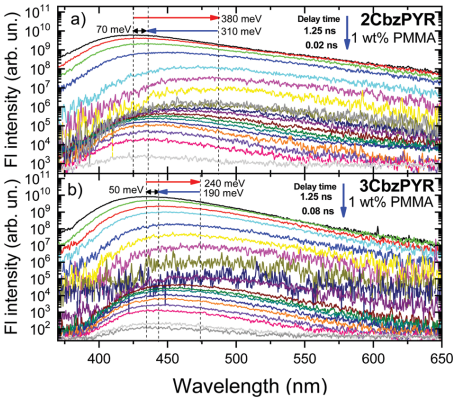

Fig. 4 Time-resolved fluorescence spectra of 1 wt% PMMA films of compounds **2CbzPYR** (a) and **3CbzPYR** (c) under $-O_2$ conditions. Red lines show the size of the redshift of the fluorescence peak, while blue lines represent the size of the blueshift. The initial and latest delay times are also shown.

Electroluminescence properties

Lastly, the highly-emissive carbazole–pyrimidine compound **3CbzPYR** was utilized as a blue emitter in an OLED device. Before that, the thermal properties were evaluated. Exceptionally high glass transition (T_g = 279 °C) and melting (T_m = 516 °C) temperatures were determined for **3CbzPYR** (see Fig. S17 in the ESI†). Such high thermal stability is preferable to ensure high device operation stability.[26,27] The OLED device was designed with the following structure: indium tin oxide (ITO)/1,1-bis[(di-4-tolylamino)phenyl]-cyclohexane (TAPC) (30 nm)/4,4′,4″-tri(*N*-carbazolyl)triphenylamine (TCTA) (5 nm)/10 wt% TADF

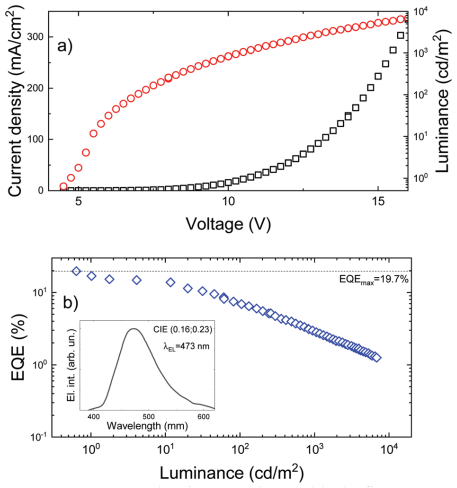

Fig. 5 (a) Current density–voltage (black figures) and luminance–voltage (red figures) curves of the OLED device. (b) EQE dependence on luminance. The inset shows the electroluminescence spectrum at 10 V (850 cd m^{-2}).

emitter: DPEPO (bis(2-(diphenylphosphino)phenyl)ether oxide) (15 nm)/1,3,5-tri(*m*-pyridin-3-yl-phenyl)benzene (TmPyPB) (65 nm)/lithium fluoride (LiF) (0.8 nm)/Al (100 nm). ITO and Al acted as the anode and cathode, whereas TCTA and TAPC acted as the hole injection and transport layers, and LiF and TmPyPB acted as the electron injection and transport layers, respectively. DPEPO was selected as the host material due to its high triplet energy (E_{T1} of about 3.0 eV) and pronounced solid-state solvation, leading to a lowered solid-state TADF lifetime (see Fig. 3b). OLED characterization data are shown in Fig. 5. The OLED device showed blue electroluminescence, occurring at a turn-on voltage of about 4.5 V and peaking at 473 nm, corresponding to the CIE colour coordinates of (0.16, 0.23). An exceptional peak EQE of 19.7% was achieved, in line with a large fluorescence quantum yield and a 20–30% outcoupling efficiency, excluding weakly probable spontaneous molecular orientation.[54,55] Some EQE roll-off was observed at larger luminance due to the average solid-state TADF lifetime of **3CbzPYR** and the weak electroactivity of the DPEPO host,[56] though this issue could be solved by further optimization of the OLED architecture.

Overall, the high electroluminescence efficiency nicely evidenced compound **3CbzPYR** as an efficient blue TADF emitter, utilizing nearly equally efficient prompt and delayed emission.

Conclusions

In summary, we presented an approach to achieve efficient TADF by combining high prompt and delayed fluorescence yields through the selective optimization of emission decay constants. This approach was evidenced on a series of differently substituted carbazole–pyrimidine compounds. Singlet energies systematically decreased as more carbazoles were introduced, keeping triplet energies just weakly altered. The initial compound with one *para*-carbazole, despite the too large singlet–triplet gap, showed efficient prompt fluorescence as well as evident room-temperature phosphorescence activity. The singlet–triplet energy gap was sufficiently low for TADF in the compound with two *meta* carbazoles as well as its derivative with an additional *para* substituted donor unit. Prompt and delayed fluorescence properties, on the other hand, were drastically different for both compounds. Strong HOMO–LUMO decoupling in the *meta*-substituted compound **2CbzPYR** drastically lowered the radiative decay rate, resulting in a low prompt fluorescence yield, as the radiative decay was outcompeted by the rapid intersystem crossing. Even with a pronounced ISC rate, **2CbzPYR** showed a low TADF yield as the majority of triplets were quenched by the rapid nonradiative decay, promoted by the rather flexible molecular structure. All the drawbacks of compound **2CbzPYR** were eliminated simply by introducing an additional *para*-carbazole unit. The enlarged radiative decay rate of about 3×10^7 s^{-1} as well as the minimized nonradiative decay rate boosted the prompt fluorescence yield up to 0.43 for **3CbzPYR**. On the other hand, the lowered rate of triplet quenching, achieved by enlarging the stiffness of the molecular structure by crowding the carbazole units, concomitantly boosted the TADF yield up to 0.33 and Φ_{PL} up to 0.81 in the solid state. The compound **3CbzPYR** with the optimized donor–acceptor architecture was used as a blue emitter in an OLED device. Highly efficient electroluminescence with a peak EQE of 19.7% and colour coordinates of (0.16, 0.23) was achieved.

Our findings, highlighting the parrallel way to achieve a high TADF yield, we believe, will be important for further advancing the design of TADF compounds with diverse molecular structures.

Conflicts of interest

There are no conflicts of interest to declare.

Acknowledgements

This research has received funding from the Research Council of Lithuania (LMTLT) (Agreement No. S-MIP-17-73). We are grateful to Dr Regimantas Komskis for conducting the thermal analysis.

References

1 H. Uoyama, K. Goushi, K. Shizu, H. Nomura and C. Adachi, *Nature*, 2012, **492**, 234–238.
2 T.-L. Wu, M.-J. Huang, C.-C. Lin, P.-Y. Huang, T.-Y. Chou, R.-W. Chen-Cheng, H.-W. Lin, R.-S. Liu and C.-H. Cheng, *Nat. Photonics*, 2018, **12**, 235–240.
3 T.-A. Lin, T. Chatterjee, W.-L. Tsai, W.-K. Lee, M.-J. Wu, M. Jiao, K.-C. Pan, C.-L. Yi, C.-L. Chung, K.-T. Wong and C.-C. Wu, *Adv. Mater.*, 2016, **28**, 6976–6983.

4 X. Cai and S.-J. Su, *Adv. Funct. Mater.*, 2018, **28**, 1802558.
5 M. Y. Wong and E. Zysman-Colman, *Adv. Mater.*, 2017, **29**, 1605444.
6 Y. Im, M. Kim, Y. J. Cho, J.-A. Seo, K. S. Yook and J. Y. Lee, *Chem. Mater.*, 2017, **29**, 1946–1963.
7 C.-H. Oh, H.-J. Shin, W.-J. Nam, B.-C. Ahn, S.-Y. Cha and S.-D. Yeo, *SID Int. Symp. Dig. Tech. Pap.*, 2013, **44**, 239–242.
8 A. Endo, M. Ogasawara, A. Takahashi, D. Yokoyama, Y. Kato and C. Adachi, *Adv. Mater.*, 2009, **21**, 4802–4806.
9 M. K. Etherington, J. Gibson, H. F. Higginbotham, T. J. Penfold and A. P. Monkman, *Nat. Commun.*, 2016, **7**, 13680.
10 R. Skaisgiris, T. Serevičius, K. Kazlauskas, Y. Geng, C. Adachi and S. Juršėnas, *J. Mater. Chem. C*, 2019, **7**, 12601–12609.
11 Z. Liu, F. Cao, T. Tsuboi, Y. Yue, C. Deng, X. Ni, W. Sun and Q. Zhang, *J. Mater. Chem. C*, 2018, **6**, 7728–7733.
12 T. Hosokai, H. Nakanotani, S. Santou, H. Noda, Y. Nakayama and C. Adachi, *Synth. Met.*, 2019, **252**, 62–68.
13 H. Noda, H. Nakanotani and C. Adachi, *Chem. Lett.*, 2019, **48**, 126–129.
14 J.-A. Seo, Y. Im, S. H. Han, C. W. Lee and J. Y. Lee, *ACS Appl. Mater. Interfaces*, 2017, **9**, 37864–37872.
15 X. Cai, B. Gao, X.-L. Li, Y. Cao and S.-J. Su, *Adv. Funct. Mater.*, 2016, **26**, 8042–8052.
16 L. Yu, Z. Wu, G. Xie, C. Zhong, Z. Zhu, H. Cong, D. Ma and C. Yang, *Chem. Commun.*, 2016, **52**, 11012–11015.
17 C. Rothe and A. P. Monkman, *Phys. Rev. B: Condens. Matter Mater. Phys.*, 2003, **68**, 075208.
18 J. C. de Mello, H. F. Wittmann and R. H. Friend, *Adv. Mater.*, 1997, **9**, 230–232.
19 T. Serevičius, T. Bučiūnas, J. Bucevičius, J. Dodonova, S. Tumkevičius, K. Kazlauskas and S. Juršėnas, *J. Mater. Chem. C*, 2018, **6**, 11128–11136.
20 T. Serevičius, R. Skaisgiris, J. Dodonova, K. Kazlauskas, S. Jursenas and S. Tumkevicius, *Phys. Chem. Chem. Phys.*, 2020, **22**, 265–272.
21 M. J. Frisch, G. W. Trucks, H. B. Schlegel, G. E. Scuseria, M. A. Robb, J. R. Cheeseman, G. Scalmani, V. Barone, B. Mennucci, G. A. Petersson, H. Nakatsuji, M. Caricato, X. Li, H. P. Hratchian, A. F. Izmaylov, J. Bloino, G. Zheng, J. L. Sonnenberg, M. Hada, M. Ehara, K. Toyota, R. Fukuda, J. Hasegawa, M. Ishida, T. Nakajima, Y. Honda, O. Kitao, H. Nakai, T. Vreven, J. A. Montgomery, Jr., J. E. Peralta, F. Ogliaro, M. Bearpark, J. J. Heyd, E. Brothers, K. N. Kudin, V. N. Staroverov, T. Keith, R. Kobayashi, J. Normand, K. Raghavachari, A. Rendell, J. C. Burant, S. S. Iyengar, J. Tomasi, M. Cossi, N. Rega, J. M. Millam, M. Klene, J. E. Knox, J. B. Cross, V. Bakken, C. Adamo, J. Jaramillo, R. Gomperts, R. E. Stratmann, O. Yazyev, A. J. Austin, R. Cammi, C. Pomelli, J. W. Ochterski, R. L. Martin, K. Morokuma, V. G. Zakrzewski, G. A. Voth, P. Salvador, J. J. Dannenberg, S. Dapprich, A. D. Daniels, O. Farkas, J. B. Foresman, J. V. Ortiz, J. Cioslowski and D. J. Fox, *Gaussian 09, Revision C.01*, Gaussian, Inc., Wallingford, CT, 2010.
22 L. Skardziute, J. Dodonova, A. Voitechovicius, J. Jovaisaite, R. Komskis, A. Voitechoviciute, J. Bucevicius, K. Kazlauskas, S. Jursenas and S. Tumkevicius, *Dyes Pigm.*, 2015, **118**, 118–128.
23 S.-J. Su, C. Cai and J. Kido, *Chem. Mater.*, 2011, **23**, 274–284.
24 T. H. Ha, E.-H. Cho, C. W. Lee, H. J. Choi, O. Y. Kim and B. D. Chin, *J. Korean Phys. Soc.*, 2019, **74**, 1059–1066.
25 G. Kreiza, D. Banevičius, J. Jovaišaitė, K. Maleckaitė, D. Gudeika, D. Volyniuk, J. V. Gražulevičius, S. Juršėnas and K. Kazlauskas, *J. Mater. Chem. C*, 2019, **7**, 11522–11531.
26 M. Kim, S. K. Jeon, S.-H. Hwang and J. Y. Lee, *Adv. Mater.*, 2015, **27**, 2515–2520.
27 D. R. Lee, M. Kim, S. K. Jeon, S.-H. Hwang, C. W. Lee and J. Y. Lee, *Adv. Mater.*, 2015, **27**, 5861–5867.
28 C. S. Oh, H. L. Lee, S. H. Han and J. Y. Lee, *Chem. – Eur. J.*, 2019, **25**, 642–648.
29 J. Yoon, C. Lee, S. H. Park, D. W. Kang, H. Kim, J.-E. Jeong, H. Y. Woo, C. S. Hong, S. Park, M. J. Cho and D. H. Choi, *J. Mater. Chem. C*, 2020, **8**, 2196–2204.
30 C. Y. Kim, C. Lee, H. J. Kim, J. Hwang, M. Godumala, J.-E. Jeong, H. Y. Woo, M. J. Cho, S. Park and D. H. Choi, *J. Mater. Chem. C*, 2020, **8**, 6780–6787, DOI: 10.1039/D0TC01144D.
31 M. Xu, M. Liu, M. Shi, M. U. Ali, S. Jiao, W. Cao, Y.-C. Wu and H. Meng, *J. Mater. Chem. C*, 2019, **7**, 13754–13758.
32 X. Zheng, R. Huang, C. Zhong, G. Xie, W. Ning, M. Huang, F. Ni, F. B. Dias and C. Yang, *Adv. Sci.*, 2020, 1902087.
33 T. Serevičius, R. Skaisgiris, J. Dodonova, L. Jagintavičius, D. Banevičius, K. Kazlauskas, S. Tumkevičius and S. Juršėnas, *ACS Appl. Mater. Interfaces*, 2020, **12**(9), 10727–10736, DOI: 10.1021/acsami.9b21394.
34 S. Hirata, Y. Sakai, K. Masui, H. Tanaka, S. Y. Lee, H. Nomura, N. Nakamura, M. Yasumatsu, H. Nakanotani, Q. Zhang, K. Shizu, H. Miyazaki and C. Adachi, *Nat. Mater.*, 2015, **14**, 330–336.
35 K. Shizu, H. Tanaka, M. Uejima, T. Sato, K. Tanaka, H. Kaji and C. Adachi, *J. Phys. Chem. C*, 2015, **119**, 1291–1297.
36 P. L. dos Santos, J. S. Ward, D. G. Congrave, A. S. Batsanov, J. Eng, J. E. Stacey, T. J. Penfold, A. P. Monkman and M. R. Bryce, *Adv. Sci.*, 2018, **5**, 1700989.
37 J. Eng, J. Hagon and T. J. Penfold, *J. Mater. Chem. C*, 2019, **7**, 12942–12952.
38 T. J. Penfold, E. Gindensperger, C. Daniel and C. M. Marian, *Chem. Rev.*, 2018, **118**, 6975–7025.
39 D. de Sa Pereira, C. Menelaou, A. Danos, C. Marian and A. P. Monkman, *J. Phys. Chem. Lett.*, 2019, **10**, 3205–3211.
40 E. W. Evans, Y. Olivier, Y. Puttisong, W. K. Myers, T. J. H. Hele, S. M. Menke, T. H. Thomas, D. Credgington, D. Beljonne, R. H. Friend and N. C. Greenham, *J. Phys. Chem. Lett.*, 2018, **9**, 4053–4058.
41 S. Izumi, H. F. Higginbotham, A. Nyga, P. Stachelek, N. Tohnai, P. de Silva, P. Data, Y. Takeda and S. Minakata, *J. Am. Chem. Soc.*, 2020, **142**, 1482–1491.
42 P. L. dos Santos, J. S. Ward, A. S. Batsanov, M. R. Bryce and A. P. Monkman, *J. Phys. Chem. C*, 2017, **121**, 16462–16469.
43 B. L. Cotts, D. G. McCarthy, R. Noriega, S. B. Penwell, M. Delor, D. D. Devore, S. Mukhopadhyay, T. S. De Vries and N. S. Ginsberg, *ACS Energy Lett.*, 2017, **2**, 1526–1533.

44 T. Serevičius, P. Adomėnas, O. Adomėnienė, K. Karpavičius, J. Bucevičius, R. Komskis, G. Kreiza, V. Jankauskas, K. Kazlauskas and S. Juršėnas, *Dyes Pigm.*, 2015, **122**, 147–159.
45 J. Liu, K. Zhou, D. Wang, C. Deng, K. Duan, Q. Ai and Q. Zhang, *Front. Chem.*, 2019, **7**, 312.
46 T. Serevičius, R. Komskis, P. Adomėnas, O. Adomėnienė, G. Kreiza, V. Jankauskas, K. Kazlauskas, A. Miasojedovas, V. Jankus, A. P. Monkman and S. Jursenas, *J. Phys. Chem. C*, 2017, **121**, 8515–8524.
47 N. Notsuka, H. Nakanotani, H. Noda, K. Goushi and C. Adachi, *J. Phys. Chem. Lett.*, 2020, **11**, 562–566.
48 Y. Tan, B. Rui, J. Li, Z. Zhao, Z. Liu, Z. Bian and C. Huang, *Opt. Mater.*, 2019, **94**, 103–112.
49 T. Northey, J. Stacey and T. J. Penfold, *J. Mater. Chem. C*, 2017, **5**, 11001–11009.
50 S. Weissenseel, N. A. Drigo, L. G. Kudriashova, M. Schmid, T. Morgenstern, K.-H. Lin, A. Prlj, C. Corminboeuf, A. Sperlich, W. Brütting, M. K. Nazeeruddin and V. Dyakonov, *J. Phys. Chem. C*, 2019, **123**, 27778–27784.
51 T. Serevičius, R. Skaisgiris, J. Dodonova, L. Jagintavičius, J. Bucevičius, K. Kazlauskas, S. Jursenas and S. Tumkevicius, *Chem. Commun.*, 2019, **55**, 1975–1978.
52 J. S. Ward, R. S. Nobuyasu, A. S. Batsanov, P. Data, A. P. Monkman, F. B. Dias and M. R. Bryce, *Chem. Commun.*, 2016, **52**, 2612–2615.
53 M. Saigo, K. Miyata, S. Tanaka, H. Nakanotani, C. Adachi and K. Onda, *J. Phys. Chem. Lett.*, 2019, **10**, 2475–2480.
54 M. Tanaka, H. Noda, H. Nakanotani and C. Adachi, *Appl. Phys. Lett.*, 2020, **116**, 023302.
55 M. Liu, R. Komatsu, X. Cai, K. Hotta, S. Sato, K. Liu, D. Chen, Y. Kato, H. Sasabe, S. Ohisa, Y. Suzuri, D. Yokoyama, S.-J. Su and J. Kido, *Chem. Mater.*, 2017, **29**, 8630–8636.
56 S.-G. Ihn, N. Lee, S. O. Jeon, M. Sim, H. Kang, Y. Jung, D. H. Huh, Y. M. Son, S. Y. Lee, M. Numata, H. Miyazaki, R. Gómez-Bombarelli, J. Aguilera-Iparraguirre, T. Hirzel, A. Aspuru-Guzik, S. Kim and S. Lee, *Adv. Sci.*, 2017, **4**, 1600502.

NOTES

NOTES

NOTES

Vilnius University Press
Saulėtekio al. 9, LT-10222 Vilnius
e-mail: info@leidykla.vu.lt,
www.leidykla.vu.lt
Print run copies 20